INVESTIGATING THE ROLE OF INNATE LYMPHOID CELLS IN SECONDARY LYMPHOID TISSUE

By

EMMA CHRISTINE MACKLEY

A thesis submitted to the University of Birmingham

For the Degree of DOCTOR OF PHILOSOPHY

School of Immunity and Infection

College of Medical and Dental Sciences

University of Birmingham

September 2015

ABSTRACT

Innate lymphoid cells (ILCs) are an emerging family of cells which have been well-characterised within the gut and peripheral tissues. Despite being implicated in shaping adaptive immune responses, relatively little is known about their function within lymph nodes (LNs), important sites for the generation of this type of response. The aim of this investigation was to characterise ILC populations within a range of different LNs, both at steady state and using a draining LN model to understand their role in an immune response. Mice in which a subset of ILC, or key functional molecules, are deficient will be used to better understand their function within LNs, with a focus on adaptive immune responses.

My results reveal that ILCs are present in all LNs analysed, however, differences in the ILC composition of mucosal tissue and peripheral tissue-draining LNs indicate site-specific requirements for these cells. Differing dependencies on CCR7 for ILC entry into LNs were observed, consistent with migration of these cells into these secondary lymphoid tissues. Within LNs, group 3 ILCs were found to express major-histocompatibility complex class-II and specifically locate to sites where adaptive immune responses are initiated and maintained. Notably, ILCs accumulated in draining LNs following immunisation and whilst their roles here remain unclear they are unlikely to be involved in the priming of naïve $CD4^+$ T cells. In summary, I show that subsets of ILC3 are enriched in LNs which drain mucosal sites and can be found to locate to crucial sites within LNs following their entry by a CCR7-dependent mechanism. These data support a role for ILC3 in adaptive immune responses.

ACKNOWLEDGEMENTS

First and foremost, I would like to thank Dr. David Withers for being a brilliant supervisor, and for his patience and enthusiasm. I realised from a very early stage that I had been extremely fortunate in my choice of PhD, both for the excellent help, support and guidance provided by Dave and because the project itself was extremely interesting – and for that I can thank the newly-emerging family of ILCs for emerging when they did.

Thank you as well to my co-supervisors, Professor Graham Anderson and Professor Peter Lane and to everyone within their research groups. It has been a pleasure to work closely with everyone within the Withers and Lane labs, but I would like especially to thank Clare Marriott, Emily Halford, Emma Dutton, Fabrina Gaspal, Fiona McConnell and Maher Nawaf for their help and advice over the last four years and for leaving me with so many fond memories of this time. The fourth floor IBR has been an incredibly friendly place to work; with special thanks to Emily, Clare, Emma and Pete Hart for making me so sad to leave.

Finally, I would like to thank all of my amazing family, friends and especially James Goss for keeping me going whenever things got tough and I hope they all realise just how important their support has been.

TABLE OF CONTENTS

LIST OF FIGURES

LIST OF TABLES

LIST OF ABBREVIATIONS

-/-	knockout
µg	microgram
µl	microliter
µm	micrometre
aLN	axillary LN
alum	aluminium hydroxide
alum-ppt	aluminium hydroxide-precipitated
APC	antigen-presenting cell
bLN	brachial LN
BMC	bone marrow chimera
BSA	bovine serum albumin
CCR	Chemokine receptor
CCL	Chemokine ligand
CD	cluster of differentiation
CSF	colony stimulating factor
CXCR	CXC chemokine receptor
CXCL	CXC chemokine ligand
DAPI	4,6-diamidino-2-phenylindole
DC	dendritic cell
dLN	draining LN
DT	diphtheria toxin
FACS	fluorescence activated cell sorting
FBS	fetal bovine serum
FoxP3	forkhead box P3
FRCs	fibroblastic reticular cells
GATA-3	GATA transcription factor
HBSS	Hank's balanced salt solution
HEV	high endothelial venule

ICOS	inducible T cell co-stimulator
IFN-γ	interferon-γ
IL-7Rα	interleukin-7 receptor α
IL	interleukin
ILC	innate lymphoid cell
ILC1	group 1 ILC
ILC2	group 2 ILC
ILC3	group 3 ILC
ILF	isolated lymphoid follicle
iLN	inguinal LN
i.p	intraperitoneally
i.v	intravenously
KLRG-1	killer cell lectin-like receptor subfamily G member 1
LEC	lymphatic endothelial cell
Lin	lineage
LN	lymph node
LT	lymphotoxin
LTβR	lymphotoxon β receptor
LTi	lymphoid tissue inducer
M	molar
mM	millimolar
medLN	mediastinal LN
MFI	median fluorescence intensity
MHC	major histocompatibility complex
MHCI	major histocompatibility complex class I
MHCII	major histocompatibility complex class II
ml	millilitre
mLN	mesenteric LN
MRC	marginal reticular cell
mRNA	messenger RNA

NCR	natural cytotoxity receptor
ndLN	non-draining LN
NK	natural killer
nm	nanometre
nM	nanomolar
ns	non-significant
OVA	ovalbumin
PAMP	pathogen associated molecular pattern
PBS	phosphate buffered saline
p.i	post-immunisation
pLN	peripheral LN
popLN	popliteal LN
PPs	Peyer's patches
PRR	pattern recognition receptor
RA	retinoic acid
RAG	recombination activating gene
RORγt	retinoid-related orphan receptor γt
SA	streptavidin
SI	small intestine
SILP	small intestine lamina propria
T-bet	T-box transcription factor
TCR	T cell receptor
TGF-β	transforming growth factor β
Th	T helper
TLR	Toll-like receptor
TLRL	Toll-like receptor ligand
TNF	tumour necrosis factor
Treg	T regulatory
WT	wildtype
ZAP-70	Zeta-chain-associated protein kinase 70

CHAPTER 1. INTRODUCTION

1.1 THE IMMUNE SYSTEM

Our immune system protects us from agents which can cause disease, known as pathogens, in a variety of different ways; from maintaining the physical barriers which prevent pathogen entry, to efficiently eliminating pathogens should these barriers be breached. The vast number and variation of pathogens is reflected in the complexity of the immune system, which has evolved to defend us against a wide range of different threats. The effectiveness of the immune system is largely due to the complex interplay of many different immune cells which, to aid understanding, have been grouped into two distinct arms; the innate immune system and the adaptive.

Cells of the innate immune system provide rapid but broad protection in the initial stages of immunological challenge, limiting damage to the host whilst the slower-acting adaptive immune system mounts a tailored, pathogen-specific defence. Although adaptive immunity is more evolutionarily advanced (Cooper and Alder, 2006) the innate immune system which pre-dates it is nonetheless highly conserved, thus highlighting the importance of both. Innate lymphoid cells (ILCs), a newly-emerging family of cells at the cutting-edge of immunological research, epitomise this interplay. Described as cells which 'blur' the lines between innate and adaptive immunity (Lanier, 2013) ILCs have the ability to respond rapidly to immunological challenge as cells of the innate immune system, yet possess many of the effector functions commonly associated with adaptive immunity.

This introduction will provide a description of key aspects of the ability of the immune system to prevent disease caused by pathogens; beginning with the physical barriers

which exclude these agents from the internal milieu, to the response of the immune system in the event of a breach. The differences between both arms of the immune system will be discussed, with an emphasis on the importance of cells of the innate immune system in shaping the adaptive immune response. ILCs will be introduced and their far-reaching and crucial contributions to both innate and adaptive immune responses discussed.

1.2 BARRIER SURFACES

The first line of host defence are the physical barriers which prevent access of pathogens to internal tissues. The epithelial cells which form these surfaces are highly specialised, first and foremost to actively prevent the invasion of potentially pathogenic microorganisms, but also to alert cells of the innate immune system to a threat should a breach occur. Three crucial barrier sites are the skin, and surfaces of the respiratory and gastrointestinal tracts. In addition to fulfilling the functional requirements of each site, the epithelium at these barrier surfaces is tailored to deal with commonly encountered immunological challenges.

The skin, for example, is formed of multiple layers of tightly joined or cornified cells which act as a robust barrier to common insults which could result in infection, such as wounding or insect bites (Heath and Carbone, 2013). By comparison, the barrier which lines the gastrointestinal tract consists of only a single layer of cells to facilitate the absorption of nutrients from food. Given that inflammation or infection at this site in healthy individuals is rare, in spite of the large number of microorganisms which colonise the gut, it is clear that this barrier is nonetheless highly effective (Peterson and Artis, 2014). Internal membranes, such as those which line the gastrointestinal and respiratory

tracts, are referred to as mucosal membranes due to their ability to produce mucin proteins. Mucus secretion helps to prevent the adherence of microorganisms to the epithelial cell surface, therefore restricting their ability to inflict damage and cause infection, as is demonstrated by the increase in intestinal inflammation and membrane damage in mice which lack these proteins (Van der Sluis et al., 2006).

The exposure to and colonisation of these surfaces by a large number of microorganisms is unavoidable and can be of benefit to the host. Microorganisms which reside symbiotically on these surfaces are known as the commensal microbiota and benefit the host in a number of different ways. In the gut these bacteria help to digest certain food molecules and facilitate absorption of nutrients by the host (Brestoff and Artis, 2013), whilst at all surfaces the presence of these microbes actually prevents colonisation by more harmful, pathogenic strains (Kamada et al., 2013). These commensal microbes can however cause tissue damage and spread systemically if barrier surfaces are impaired (Sonnenberg et al., 2012), demonstrating how important it is that these barriers are properly maintained and quickly healed upon damage. Despite the highly effective exclusion of the majority of pathogens, there are occasions when these barriers are breached and it falls to cells of the innate immune system to control the spread of the infection. Patrolling the inner side of these membranes are innate cells which are capable of ingesting and destroying pathogens, and an additional function of epithelial cells is to release immunogenic molecules upon damage to alert these cells to the threat (Heath and Carbone, 2013, Peterson and Artis, 2014).

1.3 INNATE IMMUNITY

On occasions when these barriers are breached it is vital that a protective immune response is rapidly initiated to restrict the growth and spread of the pathogen; and this is one of the functions of cells of the fast-acting innate immune system.

Epithelial cells at barrier surfaces have been shown to be immunologically competent, and capable of secreting immunological molecules upon damage or infection. Upon recognition of pathogenic stimuli, epithelial cells in the skin have been shown to produce soluble signalling molecules, known as cytokines and chemokines, which recruit innate cells to the skin (Heath and Carbone, 2013), whilst similar is true of epithelial cells in the gut (Peterson and Artis, 2014). Tissue-resident mononuclear phagocytes, such as macrophages and dendritic cells (DCs) are amongst the first innate cells to respond. These cells recognise pathogens through broadly-specific receptors, known as pathogen recognition receptors (PRRs), that can bind elements commonly found on the surface of foreign organisms, known as pathogen-associated molecular patterns (PAMPs) (Akira et al., 2006). This interaction triggers a complex program of signalling events, which results in the activation of the innate cell. In addition to phagocytosing and destroying the pathogen these activated cells also release cytokines and chemokines, amplifying the response of the damaged epithelia and resulting in further innate cell recruitment (Mogensen, 2009).

1.3.1 Inflammation

Cytokines are glycoproteins which can induce signalling events in those cells which possess a corresponding receptor, and play important roles at many different stages of an immune response. Chemokines are a distinct family of cytokines with chemoattractive

properties. Binding of a chemokine to its receptor induces the migration of that cell towards the source (Griffith et al., 2014). Release of pro-inflammatory cytokines induces inflammation at the site of infection. Inflammation results in the cytokine-induced upregulation of adhesion molecules on the endothelial cells of the blood vessels, enabling immune cells to leave the blood and enter the inflamed tissue; attracted to the site by the presence of chemokines (Garrood et al., 2006). Early in an immune response these cells include neutrophils and natural killer (NK) cells, which are specialised to kill pathogenic microorganisms and infected cells using cytotoxic mechanisms (Basset et al., 2003). The innate immune system therefore plays an important role in creating an environment which is unfavourable for the pathogen and preventing further spread, whilst also recruiting cells to the site which can limit pathogen growth. Sometimes, however, this non-specific innate response is insufficient to eliminate the pathogen entirely and it is necessary to engage cells of the adaptive immune system.

1.3.2 Role in activating adaptive immune responses

In the event that a pathogen cannot be eliminated by the innate immune system alone the adaptive immune system must be alerted. Cells of the adaptive immune response, known as lymphocytes, are capable of producing effector molecules which are highly specific to the invading pathogen and as a result highly effective at clearing infection. Their activation also results in the generation of a population of memory cells, which survive long past the primary infection is cleared but remain poised to act should the pathogen be encountered again (Sprent, 1997). Despite their importance, however, lymphocytes are rarely found at common sites of infection. Instead, and for reasons which will become apparent, large numbers of lymphocytes reside within secondary lymphoid tissues, such

as the lymph nodes and spleen, and it is the responsibility of the innate immune system to educate cells of the adaptive immune system to the presence and nature of a threat.

This function is carried out by antigen-presenting cells (APCs) expressing major-histocompatibility complex (MHC), such as dendritic cells (DCs), which are known to be highly important in this process (Sallusto and Lanzavecchia, 1999). DCs carry both MHC class I (MHCI) and MHC class II (MHCII), receptors, which are capable of binding many different pathogenic peptides and presenting them on the cell surface (Villadangos and Schnorrer, 2007). In doing so, DCs are activated and instructed to transport pathogenic peptides to local secondary lymphoid organs where they can be presented to lymphocytes (Sallusto et al., 1998). The importance of APCs in this step can be highlighted by the fact that T lymphocytes of the adaptive immune system can only recognise antigen carried in the context of MHC molecules (Zinkernagel and Doherty, 1974), therefore the innate immune system plays an crucial role in initiating the adaptive.

Whilst cells of the innate immune system possess receptors which are broadly-specific for elements commonly found on foreign microorganisms, lymphocytes recognise specific antigens. There are a vast number of different potential antigens and correspondingly many lymphocytes of different specificities. However, as lymphocytes of each specificity are extremely rare the chances of the dendritic cell meeting this cell are seemingly small. Lymph nodes and other secondary lymphoid tissues provide the solution, however, by providing an organised microenvironment through which lymphocytes can re-circulate and which confines the necessary components required for the initiation of an adaptive immune response to one area; thus increasing the probability of the interaction of antigen-specific T lymphocytes with their cognate antigen (von Andrian and Mempel,

2003). Lymph nodes are situated at sites where lymphatic vessels converge and are highly numerous in humans (Willard-Mack, 2006). Lymphatic fluid containing both antigen and antigen-presenting cells drains from the inflamed site of infection to the local lymph node, thus bringing antigenic peptides into contact with lymph node-resident cells (von Andrian and Mempel, 2003). Lymph nodes which drain the peripheral tissues and skin are termed peripheral lymph nodes, whereas those which drain the gut, airway and other mucosal tissues are known as mucosal lymph nodes; and the presence of local lymphoid tissue can be important in the generation of a targeted tissue-specific immune response (Kraal et al., 2006).

Naïve lymphocytes will circulate through lymph nodes at different sites via the blood and are thought to spend less than a day within the lymph node before moving on (von Andrian and Mempel, 2003), thereby providing a mechanism by which T cells of many different specificities can come into contact with an antigen which they recognise and mount a response. In one study it was reported that, in lymph nodes in the absence of antigen, at least five hundred different $CD8^+$ T cells came into contact with each DC analysed within an hour (Bousso and Robey, 2003).

1.4 ADAPTIVE IMMUNITY

The adaptive immune system is comprised of T and B lymphocytes. Following their development in primary lymphoid tissues, naïve T and B cells enter the blood and recirculate through different secondary lymphoid tissue until they encounter their cognate antigen. Both T and B lymphocytes carry somatically rearranged antigen receptors, rather than the germline encoded receptors expressed by innate cells, which accounts for their vastly different antigen specificities (Nishana and Raghavan, 2012).

This process depends upon the proteins expressed by recombination-activating genes 1 and 2 (RAG-1 and RAG-2 proteins), which are essential for recombinase activity, and expression of a somatically rearranged T cell (TCR) or B cell receptor is essential for the cell's survival, which is demonstrated by the lack of all B and T lymphocytes in $RAG^{-/-}$ mice (Mombaerts et al., 1992).

1.4.1 T cells

Multiple populations of T cells have been described. T cell populations can first be separated by the type of TCR that they express. The majority of T cells possess a TCR formed from an α-chain and a β-chain, and are therefore known as αβ T cells; whilst a small population expresses an alternative receptor formed from γ and δ chains (Girardi, 2006). γδ T cells, unlike their αβ TCR^{+} counterparts, often reside in peripheral organs and at barrier surfaces (Girardi, 2006). In either case this TCR is expressed on the surface of cells in association with CD3, forming what is known as the TCR-CD3 complex, and both elements are required for antigen-induced signalling events within the T cell (Wucherpfennig et al., 2010). Two main groups of αβ T cells exist, $CD4^{+}$ 'helper' T cells and $CD8^{+}$ 'killer' T cells, although other non-conventional cells such as invariant natural killer T cells (iNKT) and NKT cells have been recognised. $CD8^{+}$ T cells are restricted to recognising peptide presented by APCs in the context of MHCI, whilst $CD4^{+}$ T cells recognise peptide presented in the context of MHCII. Intracellular-derived peptides are loaded onto MHCI molecules and, as a result, the presence of endogenous pathogens, such as intracellular bacteria or viruses, will often trigger a $CD8^{+}$ killer T cell response. MHCII, by contrast, binds peptides which have been acquired by APCs from the external milieu (Vyas et al., 2008), although such exogenous peptides can also be presented in MHCI through a process known as cross-presentation (Kurts et al., 2010). Whilst the cytotoxic

activity of T cells is important in the clearance of many infections, this investigation will focus primarily on the functions of $CD4^+$ T cells.

1.4.2 $CD4^+$ T cell activation

$CD4^+$ T cells continuously sample antigens presented by DCs in secondary lymphoid tissue. Upon coming across an antigen which they recognise the $CD4^+$ T cell and APC form an immunological synapse (Monks et al., 1998); with the T cell TCR binding to peptide:MHCII on the surface of the APC in an interaction stabilised by the presence of CD4 (Madrenas et al., 1997). Although this interaction is indispensable for T cell activation, it alone is insufficient (Mueller et al., 1989). T cells require additional signalling through co-stimulatory receptors expressed by professional APCs in order to become activated. This secondary activation signal ensures that $CD4^+$ T cells do not become activated inadvertently in the absence of infection, which could result in damaging immune-mediated pathologies. In the event that such inappropriate activation does occur T cells will become unresponsive to further stimuli, rendering them anergic (Schwartz, 2003). Co-stimulatory molecule signalling is complex, however the most well-characterised interactions occur between CD28 on the T cell and ligands of the B7 family, CD80 and CD86, on the professional APC (Chen and Flies, 2013). Recognition of antigen and appropriate co-stimulation results in the activation and clonal expansion of the T cell, and T cell proliferation is markedly reduced in mice where T cells lack CD28 (Green et al., 1994). Activated $CD4^+$ T helper cells can then activate other cells to become involved in the immune response, for example by providing co-stimulation to B cells, and directly target the pathogen through production of highly tailored effector molecules.

1.4.3 T helper cell subsets

The immune system has the capacity to deal with a wide range of different pathogens, from intracellular bacteria and viruses to extracellular bacteria, fungi and parasites. Given the differences in the mechanisms of infection of these pathogens the immune system often has to mount a highly tailored and pathogen-specific immune response to clear them, and this is in part carried out by different subsets of $CD4^+$ T helper cells. Following activation, T helper cells can develop different pathogen-specific effector functions, depending on signals which they receive following activation and the gene expression programs which these promote. Given that T cells are activated in secondary lymphoid organs and not at the site of infection, it is the job of the antigen-presenting cell to provide these signals; educating the T helper cell to the nature of the threat and eliciting the appropriate response (Walsh and Mills, 2013). For example, intracellular bacteria and viruses require what is commonly known as a type 1 immune response, characterised by phagocytic activity, whilst expulsion of extracellular parasite infections requires a type 2 immune response. $CD4^+$ T helper cells can be induced to acquire these effector functions through a process called differentiation, and differentiated cells can be assigned to four main subsets based on their expression of transcription factors and cytokines; T helper 1 (Th1), Th2, Th17 and T regulatory cells (Treg) (Zhu et al., 2010).

Th1 and Th2 cells were first discovered as populations of $CD4^+$ T cells which could produce vastly different effector cytokines, yet arose from the same murine $CD4^+$ T cell clone (Mosmann et al., 1986, Killar et al., 1987), a principle which could also be applied in parts to $CD4^+$ T cells from humans (Umetsu et al., 1988). Two further subsets, Th17 (Park et al., 2005, Harrington et al., 2005) and Treg (Chen et al., 2003) cells were later identified; with a fifth group, the T follicular helper (Tfh) cells now also known to exist (Vinuesa et

al., 2005). The phenotype of each T helper cell results from its decision to upregulate the expression of known master transcription factors which, with the help of activator of transcription (STAT) proteins, induce the expression of the molecules associated with each subset.

Th1 cells express the transcription factor T-bet and the cytokines IFN-γ, IL-2 and TNF-α. IFN-γ expression has been shown to correlate to, and depend upon, expression of T-bet (Szabo et al., 2000). Th1 cells form in the presence of the cytokines IFN-γ and IL-12 and are important in defence against so-called type 1 immune responses; those involving intracellular bacteria and viruses. Th2 cells express GATA-3 (Zhu et al., 2004) and secrete the cytokines IL-4, IL5 and IL-13 which help in the expulsion of parasites and contribute to allergic inflammatory responses. The presence of TGF-β and IL-6 or IL-21 results in $CD4^+$ T cell expression of the transcription factor RORγt and differentiation into Th17 cells (Korn et al., 2009). Th17 cells are primarily known for their ability to release the cytokine IL-17A and have been implicated in inflammatory immune responses to extracellular bacteria and fungi (Korn et al., 2009). A reciprocal relationship exists between Th17 cells and regulatory T cells. Similarly to Th17 cells, differentiation of naïve $CD4^+$ T cells into Tregs requires signalling by TGF-β, but in this case in the absence of IL-6 and IL-21. There are two types of regulatory T cell: natural Tregs, which develop in the thymus, and those which are induced from naïve $CD4^+$ T cells in the periphery (Liston and Gray, 2014). Activation and exposure of peripheral naïve $CD4^+$ T cells to TGF-β, in the absence of IL-6 and IL-21, results in their expression of the transcription factor FoxP3 (Chen et al., 2003) and differentiation into cells with immunosuppressive functions, which serve to dampen potentially damaging autoimmune and inflammatory immune responses. Interestingly in addition to similarities in requirements for their differentiation, there have also been

reports of plasticity between Th17 cells and Tregs. Th17 cells have been shown to 'transdifferentiate' into cells with a regulatory capacity during an immune response (Gagliani et al., 2015), whilst there have been reports of Tregs expressing RORγt (Yang et al., 2015). Once the $CD4^+$ T helper cell has acquired its specific effector functions, it can target the invading pathogen by modifying the effector functions of other immune cells and expressing homing molecules which enable it to migrate directly to the site of infection (Butcher and Picker, 1996, von Andrian and Mempel, 2003).

1.4.4 Innate immunity shapes adaptive immune responses

Dendritic cells have previously been described as 'converter stations'; cells which recognise input signals from pathogens and innate cells, then convert these into output signals which can be communicated to the adaptive immune system (Walsh and Mills, 2013). Input signals can come from direct interaction with pathogens, through binding of dendritic cell PRRs to pathogenic proteins, and signalling from other cells, such as neutrophils, NK cells and even cells of the damaged epithelia. The output signals, in addition to the initial presentation of pathogenic antigens and provision of co-stimulatory signals, are primarily the production of APC-derived cytokines which influence the polarisation of naïve $CD4^+$ T cells (Walsh and Mills, 2013). Therefore although it is the cytokine milieu which surrounds the $CD4^+$ T cells in the secondary lymphoid tissue which ultimately dictates its differentiation, this has been influenced by the innate immune system and pathogen itself.

For these reasons a better understanding of cells which make up the innate immune system is vital, particularly in regards to their potential as therapeutic targets. It is also therefore unsurprising that the recent discovery of a number of new and under-

appreciated innate cell types has garnered substantial interest. This new family of cells, named the innate lymphoid cells (ILCs) (Spits et al., 2013), respond rapidly to immunological challenge, as cells of the innate immune system, and have found to be enriched at barrier surfaces. However, strikingly these cells possess effector functions which are more commonly associated with T helper subsets and as such many have fittingly been branded as 'innate helper cells'.

1.5 INNATE LYMPHOID CELLS (ILCs)

Innate lymphoid cells have been separated into three distinct groups based on their expression of transcription factors and cytokines, in a similar manner to that discussed above for T helper subsets (Figure 1.1). This family now includes a range of different cells, including those previously known, such as conventional NK cell populations and a previously defined population of lymphoid tissue inducer (LTi) cells. Their ability to rapidly respond to immunological challenge without specific interaction with cognate antigen marks these cells as part of the innate immune system, however their functional properties have up until now been associated primarily with T helper cells (Walker et al., 2013). These cells have already been implicated in a number of important roles in the immune system at steady state and during disease, and these are discussed in more detail below. Nonetheless, as with most immune cells, if control mechanisms break down subsets of ILCs can be participants in immune-mediated pathologies, such as chronic inflammation in the gut (Buonocore et al., 2010, Geremia et al., 2011). For this reason it is vital that we better understand these cells, in the hope that they will provide valuable new therapeutic targets both to strengthen immune responses or, alternatively, to restrict them.

A uniform nomenclature has been established (Spits et al., 2013), segregating groups of ILCs based on the transcription factors and cytokines that they express, in a similar manner to that described for T helper subsets. Although separated into three distinct groups, all ILCs can be characterised by their lack of expression of lineage markers which are associated with other cell populations—most importantly the lack of a somatically rearranged antigen-specific receptor (Walker et al., 2013)—and, in the most part, on their reliance on signalling through IL-7 for survival (Vonarbourg and Diefenbach, 2012) and consequent high levels of IL-7Rα.

1.5.1 Group 1 ILCs

Group 1 ILCs, like Th1 cells, express the transcription factor T-bet and secrete IFNγ and TNF (Klose et al., 2014). Included within this group are conventional NK cells and a distinct population of cells referred to as ILC1 (Spits et al., 2013). Although often included in this group, conventional NK cells have recently been found to be developmentally distinct from ILC1 (Klose et al., 2014), and unlike other ILCs, do not depend upon GATA-3 expression during development (Yagi et al., 2014, Serafini et al., 2014), nor IL-7 signalling for survival (Satoh-Takayama et al., 2010). It has therefore been proposed that those ILCs which express IL-7Rα and lack cytotoxic function be classed as 'helper-like ILCs' (Klose et al., 2014), thereby excluding conventional NK cells, and it is these cell types which will be focused on in this investigation.

Although considered a distinct cell type, studies into the plasticity of ILCs has revealed that cells within a different group of ILC can, under certain circumstances, closely resemble ILC1s (Klose et al., 2013). Defining cells within this group is therefore often

challenging (Klose et al., 2014, Spits et al., 2013) and it is not yet clear whether ILC1 represent a distinct cell type or simply a transition state of group 3 ILCs.

1.5.2 Group 2 ILCs

ILC2, like Th2 cells, secrete cytokines associated with a type 2 immune response, including IL-4, IL-5, IL-9 and IL-13 (Artis and Spits, 2015). ILC2 were first identified as innate sources of type 2 cytokines which did not express markers associated with commonly-known cell lineages (Fort et al., 2001, Hurst et al., 2002), however were better characterised in three, almost simultaneous, seminal publications. Cells which expressed type 2 cytokines but lacked lineage markers were found to be present in a number of different tissues, and to increase in number substantially upon administration of the type-2-immunity inducing cytokines IL-25 and IL-33 (Neill et al., 2010, Price et al., 2010, Moro et al., 2010). These cells were still present in $RAG^{-/-}$ and $ROR\gamma t^{-/-}$ mice, indicating that they did not belong to the adaptive immune system and were not members of the already known population of lineage negative LTi cells, despite obvious similarities (Neill et al., 2010, Moro et al., 2010). Similar cells which responded to IL-25 and IL-33 were also identified within human tissue (Mjosberg et al., 2011, Monticelli et al., 2011) and are now widely known as ILC2 (Spits et al., 2013).

Again with notable similarity to Th2 $CD4^+$ T cells, ILC2 were shown to express high levels of the transcription factor GATA-3 in both mice (Hoyler et al., 2012) and humans (Mjosberg et al., 2012). GATA-3 has been shown to be essential for the development of not only ILC2 (Hoyler et al., 2012), but all subsets of helper-like ILCs (Serafini et al., 2014, Yagi et al., 2014), however only ILC2 require GATA-3 for homeostatic survival despite this transcription factor being expressed at low levels by group 3 ILCs (Hoyler et al., 2012).

Although ILC3 expressing low levels of GATA-3 do not make type 2 cytokines there is a report of ILC2 being able to make Th17-associated cytokines under certain circumstances (Huang et al., 2015), suggesting some degree of plasticity between the subsets.

In addition to transcription factors and cytokines ILC2 can also be defined by the surface markers that they express. Like all helper-like ILCs they express IL-7Rα, and their expression of receptors for IL-25 and IL-33 is well established (Neill et al., 2010). ILC2 can also be identified using their high levels of the co-stimulatory molecule ICOS and the IL-2 receptor CD25, and Sca-1 (Walker and McKenzie, 2013). Expression of KLRG-1 has also been reported on intestinal ILC2 and proposed to be a marker of ILC2 maturation (Hoyler et al., 2012) and high level expression of this molecule has been reported on a specific subset of ILC2, described as 'inflammatory' ILC2 (Huang et al., 2015).

1.5.3 Group 3 ILCs

The final group of ILCs include those which secrete IL-17 and IL-22 and express the transcription factor RORγt, which is essential for their development (Eberl et al., 2004), and therefore in many ways resemble Th17 cells. Members of this group include the prototypic lymphoid tissue inducer (LTi) cell. The presence of LTi cells during embryonic development is essential for the development of lymph nodes and Peyer's patches in the gut. In RORγt$^{-/-}$ mice, where the transcription factor RORγt is absent from all cells, LTi cells fail to develop and as a result lymph nodes and Peyer's patches do not form (Sun et al., 2000, Eberl et al., 2004).

RORγt^{+} ILCs can be further divided by their expression of the chemokine receptor CCR6, distinguishing two distinct cell lineages although both depend upon expression of RORγt to develop (Klose et al., 2013). Those ILC3 which express CCR6 most closely resemble

classical LTi cells; they develop from a common lymphoid progenitor in the bone marrow, can be found in the fetal small intestine during embryonic development and express both IL-17 and IL-22. CCR6$^-$ ILC3 on the other hand can only be detected in significant numbers postnatally, increasing in number in the small intestine with age, in a process which required proliferation (Klose et al., 2013).

Arising from this CCR6$^-$ population (Klose et al., 2013), is a subset of ILC3 which express the natural cytotoxicity receptor (NCR) NKp46, most commonly found on NK cells, the transcription factor RORγt and produce IL-22. These NCR$^+$ ILC3 develop from NCR$^-$ ILC3 but not NK cells (Vonarbourg et al., 2010) and their phenotype and function depends upon gradients of the transcription factors which they express. T-bet expression had been detected by NKp46$^+$ ILC3 in the gut (Sciume et al., 2012), whilst Klose et al (2013) showed that expression of T-bet by CCR6$^-$ NKp46$^-$ RORγt$^+$ ILC3 enabled these cells to upregulate NKp46 and express the type 1 cytokine IFNγ. Accordingly, although CCR6$^-$ ILC3 could be detected in T-bet$^{-/-}$ mice, NCR$^+$ ILC3 were absent (Klose et al., 2013). Upregulation of T-bet by ILC3 was found to be dependent upon the presence of commensal microbiota (Klose et al., 2013), and NCR$^+$ ILC3 numbers were reduced in germ-free mice (Sanos et al., 2009). Similar IL-22 producing cells have also been identified in humans (Cella et al., 2009, Cupedo et al., 2009). Strikingly, studies have shown that in addition to upregulating expression of T-bet, CCR6$^-$ ILC3 are capable of downregulating their expression of RORγt. These so-called 'ex-RORγt' ILCs can express IFN-γ and have a diminished ability to express IL-22, and as a result in many ways resemble ILC1 (Vonarbourg et al., 2010, Klose et al., 2013). Plasticity was also detected within subsets of human NCR$^+$ ILC3 (Cella et al., 2010).

1.6 FUNCTIONS OF ILCs

Given their similarity to subsets of $CD4^+$ T helper cells yet ability to respond rapidly as members of the innate immune system, there has been a great deal of interest in what previously unappreciated roles cells of this family could be playing in the immune system at steady state and during immune responses. Similar to T helper cell subsets, innate helper-like ILCs have been implicated in both direct and indirect immunity to infection by a range of different pathogens, and ILCs have been found to be enriched at barrier sites which are susceptible to colonisation or invasion by microorganisms.

1.6.1 Gut

Secretion of cytokines by ILCs in the intestine has been shown to aid defence against bacterial and parasite colonisation. Secretion of IFN-γ by $CD127^+$ 'helper-like' ILCs— including ILC1 and those $NKp46^+$ $T\text{-}bet^+$ ILCs which expressed low levels of, or had previously expressed, RORγt— has been shown to be important in the defence against *S. Typhimurium* infection. IFN-γ produced in this context has been found to stimulate epithelial cells to produce mucin proteins, which prevent bacterial adherence and colonisation, and $CD127^+$ ILCs were found to be the main source of this cytokine following infection (Klose et al., 2013). Absence of type 2 cytokines early in an immune response to helminth infection has been associated with impaired ability to expel parasites. Provision of these cytokines, most importantly IL-13, by lineage negative innate cells may contribute to the induction of mucus production by intestinal epithelial cells and muscle contractility which promotes expulsion of the worms (Oliphant et al., 2014). Secretion of IL-22 by ILCs was also found to be crucial in defence against infection with the extracellular bacterium *C. rodentium* in the colon. $CD4^+$ LTi-like ILC3 were found to be key producers of this cytokine in this infection, prior to the involvement of IL-22 producing

cells of the adaptive immune system (Sonnenberg et al., 2011). IL-22 in the context of this infection was shown to induce the production of antimicrobial proteins by colonic epithelial cells, resulting in a more effective defence during this infection (Zheng et al., 2008).

IL-22 was also shown to be important in maintaining intestinal homeostasis at steady state, after IL-22 producing ILCs were detected in the intestinal tissues of healthy mice, and depletion of ILCs in $Rag^{-/-}$ mice resulted in dissemination of an otherwise contained commensal bacteria species to the spleen and liver (Sonnenberg et al., 2012). In addition, production of IL-22 and expression of lymphotoxin (LT) by ILC3 promotes the fucosylation of epithelial cells in mice, disruption of which resulted in an increased susceptibility of mice to infection by *S. Typhimurium* (Goto et al., 2014).

Besides these roles in protecting the integrity of the intestinal barrier and preventing pathogen colonisation, ILCs have been shown to influence other immune cells. Given the intestinal tissues exposure to a wide range of commensal bacterial and food antigens, in addition to those of harmful pathogens, it is vital that immune responses at this surface are highly regulated as inappropriate immune responses can result in immune-mediated pathologies (Pabst and Mowat, 2012). ILCs, in particular ILC3s, have been shown to interact with cells of the adaptive immune system to promote a tolerogenic state, and thus maintain this fine balance in a number of direct and indirect ways. ILC3 have been shown to produce colony stimulating factor (CSF) -2 in response to signals from mononuclear phagocytes (MNP), such as dendritic cells and macrophages, which in turn promotes MNP support of intestinal Tregs (Mortha et al., 2014). Although this demonstrates an indirect involvement in regulating adaptive immune responses, a key discovery in the field was

the discovery that subsets of ILC could express the molecule MHCII and process and present peptide; thus giving them a clear mechanism by which to interact directly with $CD4^+$ T cells. MHCII was reported to be expressed on ILC2 (Neill et al., 2010) and ILC3 (Hepworth et al., 2013), although there have been indications that expression of this molecule by ILC2s differs between tissues (Oliphant et al., 2014). Despite being shown to express functional MHCII and present peptide to $CD4^+$ T cells *in vitro*, it was reported that ILC3 do not express the co-stimulatory molecules required to provide further signals to $CD4^+$ T cells (Hepworth et al., 2013). Classically it is thought that provision of antigen without further stimulation through CD28 by co-stimulatory molecules on the APC results in T cell anergy rather than activation (Schwartz, 2003). Certainly when the function of MHCII on ILC3 was investigated *in vivo*, using mice where MHCII was specifically deleted on ILC3 only, $CD4^+$ T cell responses to commensal bacteria were found to be expanded, supporting the notion that these cells promote tolerance to commensal bacteria in the intestine (Hepworth et al., 2013). It has subsequently been shown that ILC3 are capable of inducing T cell apoptosis in a MHCII-dependent manner (Hepworth et al., 2015), and therefore are likely to contribute to the deletion of commensal bacteria-specific $CD4^+$ T cells in the gut. It is possible, however, that the roles performed by $MHCII^+$ ILC3 are dependent upon location, following reports that ILC3 derived from the spleen can express CD80 and CD86 (von Burg et al., 2014).

ILC2 can also express MHCII, and $MHCII^+$ ILC2 have been implicated in immune responses to helminth infections in the gut (Oliphant et al., 2014). A type 2 immune response is most effective at expelling parasites and the production of type 2 cytokines by Th2 cells and innate cells, such as eosinophils and alternatively activated macrophages in response to helminth infection has been established (Anthony et al., 2007). ILC2 were found to be key

producers of IL-13 early in immune responses to the helminth *N. Brasiliensis*, and ILC2-derived IL-13 was found to contribute to the expulsion of these parasites (Neill et al., 2010, Price et al., 2010). Further investigation revealed that the induction of IL-13 production was in fact dependent upon cross-talk with $CD4^+$ T cells via MHCII expressed on the surface of ILC2. Both murine and human ILC2 have been shown to be capable of presenting antigen to $CD4^+$ T cells in an interaction which resulted in the proliferation of the T cells *in vitro* (Oliphant et al., 2014); made possible by their expression of CD80 and CD86, whose expression has been contentious on ILC3 (Hepworth et al., 2013, von Burg et al., 2014). In the context of *N. Brasiliensis* infection, MHCII-expression by ILC2 and interaction with T cells is required for efficient IL-13 induced worm expulsion (Oliphant et al., 2014).

1.6.2 Lung

ILCs in the lung have been previously assigned protective roles, from ILC2 enhancing tissue repair following viral infection (Monticelli et al., 2011) to ILC3-derived IL-22 limiting allergic inflammation (Taube et al., 2011), however they have also been shown to take a pro-inflammatory role. Group 2 ILCs were found to promote airway hyper-responsitivity in mice following infection with *H3N1 influenza virus* (Chang et al., 2011). Their expression of type 2 related cytokines has been found to exacerbate pro-inflammatory responses within the lung (Barlow et al., 2012) and to influence adaptive immune responses in allergic inflammation through signalling to DCs. Following intranasal treatment with papain, ILC2-derived IL-13 was found to be important for the differentiation of $CD4^+$ T cells into those with a Th2 phenotype. Further investigation revealed that this was through promoting trafficking of DCs to the draining LN where they activated naïve $CD4^+$ T cells which then contributed to allergic responses (Halim et al.,

2014). In accordance with a role in allergic inflammation in humans, patients with chronic rhinosinusitis have elevated numbers of ILC2 (Mjosberg et al., 2011).

1.6.3 Skin

Recent publications have also identified group 2 and 3 ILCs in the skin. Group 2 ILCs have been detected in the skin of both humans and mice, and found to be enriched in number in lesions of patients with atopic dermatitis, where they are suspected to contribute to the inappropriately activated pro-inflammatory type 2 immune response (Salimi et al., 2013). The presence of ILC2 in the skin has also been confirmed in healthy mice (Roediger et al., 2013), and these cells have been shown to cluster and interact with basophils during cutaneous inflammation (Kim et al., 2014). Group 3 ILCs in the skin, along with populations of γδ T cells, were found to be key producers of IL-17A, IL-17F and IL-22, rather than the Th17 cells with which these cytokines are commonly associated. Loss of expression of these cytokines in mice resulted in a reduction in the severity of an induced form of psoriasis, therefore providing a link between these cells and inflammatory skin conditions (Pantelyushin et al., 2012). Additionally, study of skin and peripheral blood of patients with psoriasis revealed populations of NKp44^{+} ILC3, the frequency of which was increased when compared to healthy controls (Villanova et al., 2014).

1.6.4 Secondary lymphoid tissue

ILCs have also been detected in a range of different secondary lymphoid organs. The essential role of RORγt-expressing ILCs in the development of lymph nodes and Peyer's patches (PPs) was established over a decade ago. Lymphoid tissue inducer cells, now considered a member of the group 3 ILCs, can first be detected within the embryo at embryonic day 12.5, where they provide signals which are essential for the development

of lymph nodes (Eberl et al., 2004). During the formation of lymph nodes provision of LTα1β2 signals to LTβR^{+} stromal cells is essential for the subsequent recruitment of hematopoietic cells and development of these structures (Mebius, 2003). Signalling to LTβR^{+} stromal cells results in their expression of chemokines—including CCL19, CCL21 and CXCL13—which attract lymphocytes and adhesion molecules which then retain these cells within the anlagen (Mebius, 2003). LTi cells, initially characterised as cells which expressed CD4 but not CD3 (Kelly and Scollay, 1992), were found to be some of the first hematopoietic cells to enter these areas and shown to express LTα1β2 (Mebius et al., 1997, Cupedo et al., 2002). The observation that these cells were absent from mice which had impairments in lymphoid tissue organogenesis, those which lacked Id2 (Yokota et al., 1999) and later RORγt (Sun et al., 2000), clearly demonstrated their importance to this process. LTi cells were found to be the only RORγt expressing cells during mouse fetal life (Eberl et al., 2004) and their absence in RORγt$^{-/-}$ mice corresponded with a lack of lymph nodes and PPs, but no effect on the development of the spleen (Sun et al., 2000). Furthermore, transfer of fetal CD4^{+} CD3^{-} cells into neonatal mice which lacked Peyer's patches was sufficient to induce Peyer's patch formation (Finke et al., 2002).

Cells with a comparable phenotype were later described within adult mouse lymph nodes (Kim et al., 2003) and found to play a role in repairing secondary lymphoid tissue, which appeared in some ways related to their lymphoid tissue inducing functions (Scandella et al., 2008). For example, cells which resembled LTi cells in secondary lymphoid tissues of mice were found to aid the repair of lymphoid tissues damaged by viral infection in a LTβR-dependent manner (Scandella et al., 2008). There have, however, also been a number of studies into the role of these cells in providing support to cells of the adaptive

immune system, given the importance of secondary lymphoid tissue for adaptive immune responses. $CD4^+$ $CD3^-$ cells identified in adult mice were shown to share many gene transcripts with neonatal $CD4^+CD3^-$ cells, but additionally expressed the co-stimulatory molecules OX40L and CD30L (Kim et al., 2006, Kim et al., 2005), signalling by which has been shown to be important for the generation of $CD4^+$ T cell-dependent memory antibody responses (Kim et al., 2003, Gaspal et al., 2005). Persistence of a memory $CD4^+$ T cell population has been shown to be dependent upon these cells, with mice in which LTi cells are depleted using a bone chimera method demonstrating that LTi cells are a key RORγt-expressing cell type required for $CD4^+$ memory cell maintenance (Withers et al., 2012). This study however focused only on immune responses in the spleen, with there being inherent difficulties in studying the absence of these cells in lymph nodes given the role of LTi cells in their formation.

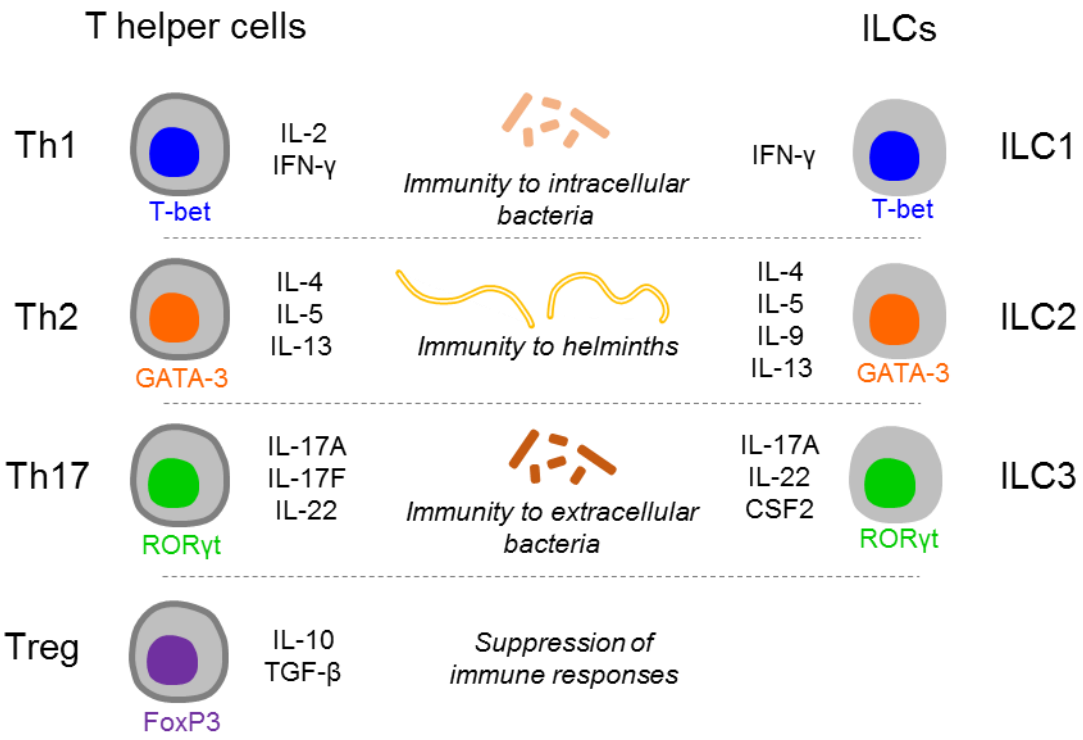

Figure 1.1 Comparison of T helper subsets and ILCs

Figure showing simplistically some of the similarities and shared effector functions of T helper cells and ILCs, with a focus on the roles of these cells in infection (Zhu et al., 2010, Artis and Spits, 2015). Transcription factors and signature cytokines which each cell type can express are shown. ILC subsets shown are restricted to so-called helper-like ILCs. ILC3 here focuses on those RORγt^{+} ILCs which express CCR6. T cells surrounded by grey outline to represent the presence of a TCR

1.7 AIMS OF THIS INVESTIGATION

The overall aim of this investigation was to characterise subsets of ILCs in secondary lymphoid tissue with a particular focus on lymph nodes. Investigations up until this point have primarily focused on the role of these cells in peripheral tissues and at barrier sites, with comparatively less known about their function in adult lymph nodes. Nonetheless, these cells are increasingly being implicated in influencing adaptive immune responses, the mounting of which takes place primarily within secondary lymphoid tissue, therefore it is vital that we understand the behaviour of ILCs better at these sites.

In this investigation we sought to:

1. Characterise ILC populations within a range of different lymph nodes and investigate whether differences can be detected between those which drain different sites.
2. Investigate the behaviour of ILC populations in draining lymph nodes following immunisation, with an emphasis on determining whether they could influence an immune response.
3. Begin to understand the mechanisms by which these cells enter lymph nodes in the first place to determine whether or not they are consistent to trafficking from mucosal and peripheral tissues, and to provide an insight into their possible roles within secondary lymphoid tissue.

CHAPTER 2. MATERIALS AND METHODS

2.1 MICE

Mice were used in accordance with Home Office guidelines and maintained at the [redacted] Wildtype (WT) mice were either bred and maintained in the [redacted] or sourced from an external supplier (Harlan or Charles River), whilst all transgenic mice were bred and maintained in the [redacted] Externally sourced WT mice were female, but [redacted] derived mice used were of both genders. Efforts were made to ensure that mice used were age and sex-matched within experiments, and [redacted]-derived transgenic mice were compared to [redacted] derived controls. All mice used in this investigation were on a C57BL/6 background and can be found in Table 2.1.

Table 2.1 Mouse strains used in this investigation

Strain	CD45 allotype	Phenotype	Source
B6.SJL-*Ptprc*^{a} *Pepc*^{b}/BoyJ (BoyJ)	CD45.1	WT	[redacted]
C57BL/6	CD45.2	WT	[redacted] or external suppliers
C57BL/6 x BoyJ	CD45.1 CD45.2	WT	[redacted]
Ccr7$^{-/-}$	CD45.2	Deficiency in expression of the chemokine receptor CCR7. Results in impaired ability of cells to respond to the chemokines CCL19 and CCL21.	A kind gift from Prof. A Rot, University of York.
Cd80$^{-/-}$*Cd86*$^{-/-}$	CD45.2	No expression of co-stimulatory ligands CD80 or CD86. Mice are unable to provide co-stimulation to T cells via these ligands resulting in an impaired T cell response.	The Jackson Laboratory.

Strain	CD45 allotype	Phenotype	Source
OTII	CD45.2	OTII mice with high numbers of $CD4^+$ T cells specific for $OVA_{323-339}$ (Barnden et al., 1998).	[redacted] OTII mice a kind gift from Prof. W Heath and Prof. F Carbone.
Rag$^{-/-}$	CD45.2	Impaired ability for lymphocytes to undergo somatic recombination and consequent failure to survive. No mature T or B lymphocytes (Mombaerts et al., 1992).	[redacted]
Rag$^{-/-}$ x OTII	CD45.1 and/or CD45.2	OTII mice with high numbers of $CD4^+$ T cells specific for $OVA_{323-339}$ (Barnden et al., 1998) were crossed onto a *Rag*$^{-/-}$ background to generate mice with OTII T cells but no other lymphocytes.	[redacted] OTII mice a kind gift from Prof. W Heath and Prof. F Carbone.
Rag$^{-/-}$ x SM1	CD45.1 and/or CD45.2	SM1 mice with high numbers of $CD4^+$ T cells specific for a peptide of flagellin, (427-441)-I-A^b (McSorley et al., 2002), were crossed onto a *Rag*$^{-/-}$ background to generate mice with SM1 $CD4^+$ T cells but no other lymphocytes.	[redacted] a kind gift from Prof. S McSorley.
Rorc(γt)$^{-/-}$	CD45.2	Deficiency in RORγt expression results in impaired survival of thymocytes and absence of cell types which require this transcription factor for development. This includes LTi cells and populations of RORγt$^+$ T cells. Absence of LTi cells abrogates the formation of LNs or Peyer's patches in these mice (Sun et al., 2000).	[redacted] a kind gift from Prof. D Littman.
Rorc(γt) cre x *Rosa26 eYFP*	CD45.2	Fate mapping mice in which expression of Cre recombinase in cells which express *Rorc(γt)*, resulting in the removal of a floxed STOP sequence and expression of eYFP by those cells.	Rosa26 eYFP mice a kind gift from [redacted]
Zap70$^{-/-}$	CD45.2	Deficiency in expression of the protein tyrosine kinase ZAP-70 results in impaired T cell development and absence of $CD4^+$ or $CD8^+$ mature T cells (Negishi et al., 1995).	[redacted]

2.2 MEDIUM AND REAGENTS

2.2.1 Medium

Table 2.2 Culture medium for overnight culture of cells

Medium and additives	Final Concentration	Supplier
RPMI 1640 with L-glutamine		Gibco
Heat inactivated fetal bovine serum (FBS)	10%	Sigma-Aldrich
L-glutamine	1%	Sigma-Aldrich
Penicillin and Streptomycin	1%	Sigma-Aldrich

Table 2.3 Staining buffer for flow cytometry

Medium and additives	Final Concentration	Supplier
DPBS		Gibco
Ethylenedinitrilotetraacetic acid (EDTA)	2.5mM	Sigma-Aldrich
Heat inactivated FBS	2%	Sigma-Aldrich

Table 2.4 Staining solution for immunofluorescence microscopy

Medium and additives	Final Concentration	Supplier
PBS		Sigma-Aldrich
Bovine serum albumin (BSA)	1%	Sigma-Aldrich

2.2.2 Gey's solution

Gey's solution red blood cell lysis buffer was made within the laboratory from the solutions detailed below. Stock solutions A-C were made to 1L final volume with distilled water and autoclaved prior to use. Gey's solution was made by mixing 10ml Solution A, 2.5ml Solution B, 2.5ml Solution C and 35ml of distilled water and kept at 4°C.

Table 2.5 Solution A

Component	Amount
Gelatin	25g
Glucose	5g
KCl	1.85g
KH_2PO_4	0.119g
$Na_2HPO_4.12H_2O$	1.5g
NH_4Cl	35g
1% Phenol red	1.5ml

Table 2.6 Solution B

Component	Amount
$CaCl_2$	3.4g
$MgCl_2.6H_2O$	4.2g
$MgSO_4.7H_2O$	1.4g

Table 2.7 Solution C

Component	Amount
$NaHCO_5$	22.5g

2.3 PREPARATION OF CELL SUSPENSIONS

2.3.1 Lymph nodes

Lymph nodes were isolated from mice and placed in small petri dishes (Nunclon, Thermo Scientific) with RPMI. Any fat lining the outside of the LN was removed under a microscope using forceps. Forceps were then used to tease the LNs apart and release the cells. LN tissue was then incubated, in a standing incubator for 25 minutes at 37°C, in RPMI with 250µg/ml Collagenase-Dispase (Roche) and 25µg/ml DNase I, before the reaction was stopped with 10mM EDTA (Sigma-Aldrich). Tissue was then crushed through a 70µm cell strainer (Falcon, Corning), resulting in a single cell suspension, and both petri dish and cell strainer were washed with medium to retrieve maximum cell

yields. The cell suspension was then centrifuged to form a cell pellet and facilitate removal of the supernatant before cells were re-suspended in appropriate medium. Centrifugation took place for 6 minutes at 394rcf and at 4°C, unless otherwise stated. Preparation of cells for overnight culture or injection into mice took place in a flume hood using only sterile reagents, whilst preparation of cells for flow cytometry took place under non-sterile conditions.

2.3.2 Spleen

Spleens were isolated from mice and placed in RPMI. Those spleens used for ILC analysis were first either teased using forceps or cut into small sections using scissors and then digested as outlined above, with the exception that digestion was for 30 minutes rather than 25. Spleen tissue was then crushed through a 70μm cell strainer to extract a single cell suspension. Following centrifugation, cell pellets were re-suspended in Gey's solution red blood cell lysis buffer and incubated for 5 minutes on ice. 10ml of RPMI was added to dilute the lysis buffer prior to centrifugation. Splenocytes were re-suspended in appropriate medium and re-filtered prior to use.

2.3.3 Bone marrow

Skin and muscle was removed from the legs of mice before the bones (femur and tibia) were transferred into small petri dishes with RPMI. Bone marrow was extracted by forcing RPMI through the centre of the bone using a syringe and crushed through a 70μm cell strainer to yield a single cell suspension. Following centrifugation bone marrow cells were lysed using Gey's solution and re-filtered as above.

2.3.4 Small intestine

Small intestine (from the end of the stomach to the cecum) was isolated and fat and Peyer's patches (PPs) removed. Tissue was cut into approximately 0.5cm sections and washed in HBSS (Sigma-Aldrich) with 2% FBS. Between each step the liquid was filtered through nylon mesh to retrieve the tissue. HBSS and HBSS with 2mM EDTA was pre-warmed in a 37°C water bath. Tissue was placed in warm HBSS with 2mM EDTA and incubated in a 37°C shaking incubator for 20 minutes. Following the removal of liquid, tissue was manually shaken for 10 seconds in HBSS before the previous incubation in HBSS with 2mM EDTA was repeated. Tissue was washed three times by manually shaking in HBSS before being placed in culture media plus 1mg/ml Collagenase VIII (Sigma-Aldrich) in a shaking incubator at 37°C for 15 minutes, shaking manually after the first 10 minutes had passed. Cells were passed through 100μm and 70μm cell strainers, and strainers rinsed with staining buffer. The resulting cell suspension was centrifuged, re-suspended in staining buffer and placed on ice.

2.4 CELL CULTURE

Cells were cultured overnight at 37°C in 1ml culture media (Table 2.2) in a 12 well plate in a final volume of 1ml. Pam3CSK4 (Invivogen) TLR1/2 agonist was added to selected samples at a final concentration of 1μg/ml, whilst IL-7 (Peprotech) was added to others at a final concentration of 100ng/ml. The following day cells were retrieved and analysed by flow cytometry as outlined below.

2.5 FLOW CYTOMETRY

All antibodies used for flow cytometric analysis in this investigation are listed in Tables 2.8 and 2.9. Gut samples and accompanying experimental tissues were stained with an

APC eFluor 780 viability dye (1:1000, eBioscience) in PBS for 20 minutes on ice prior to antibody staining. Surface antibody staining was carried out in 96-well plates (Thermo Scientific) in 50µl or 100µl staining buffer (Table 2.3) for 25-30 minutes on ice, unless otherwise stated. CXCR5 staining was carried out at room temperature for 1 hour, and antibodies to CCR7 were incubated with cells for 30 minutes at 37°C. Antibodies to lineage markers were either included individually or collectively with the same fluorochrome. 96-well plates were centrifuged at 394rcf for 2 minutes to pellet cells, unless otherwise stated. Following each incubation step 100-150µl staining buffer was added before centrifugation. Cell pellets were then washed with 200µl staining buffer and centrifuged prior to next staining step. Biotinylated antibodies were typically incubated with cells in an additional staining step prior to the addition of the main antibody cocktail, which would then include a fluorochrome-conjugated streptavidin.

Intracellular staining was carried out in those experiments where transcription factors were analysed. Cells were stained with surface antibodies before being fixed and permeabilised using the FoxP3 fixation and permeabilisation buffers (eBioscience), with the exception of experiments where YFP was present within cells, where Cytofix/Cytoperm Plus (BD Biosciences) was used instead. Both kits were used in accordance with manufacturer's instructions. Cells were incubated in 100µl of fixation buffer for at least 30 minutes on ice prior to addition of 100µl of permeabilisation buffer and centrifugation. Cells were washed twice more in 200µl permeabilisation buffer prior to intracellular labelling. Antibodies to intracellular antigens were then incubated with cells, in 50-100µl of appropriate buffer, for 25-30 minutes on ice. To remove unbound antibody following incubation, 100µl of permeabilisation buffer was added and the cells centrifuged. Cell pellets were washed with a further 200µl of permeabilisation buffer

before plates were centrifuged and cells re-suspended in 200-300µl staining buffer for analysis.

Appropriate isotype controls, cells from knockout ($^{-/-}$) mice or fluorescence minus one controls were used where required to identify negative populations. Single fluorochrome controls were used to set fluorochrome compensation parameters, and these were typically WT splenocytes labelled alongside experimental samples. The amount of cells labelled depended upon the tissue and cell types being analysed. Prior to analysis Spherotech Accucount blank particles (Spherotech) were added to enable calculation of cell frequencies.

Flow cytometric analysis was performed on a Fortessa X-20 or LSRII analyser (BD Biosciences), with data analysed using FlowJo (Tree Star). During analysis, pre-gating on forward and side scatter of cells enabled the exclusion of dead cells and debris. Individual mLN numbers were calculated by dividing total cells by 5 to account for multiple constituent LNs, unless otherwise stated.

Table 2.8 Antibodies used during flow cytometry

Specificity (anti-)	Clone	Conjugate	Working dilution	Supplier
γδ TCR	UC7-13D5	FITC	1:100	eBioscience
B220	RA3-6B2	FITC PECy7 Alexa Fluor 700 efluor 450	1:300 1:300 1:100 1:200	eBioscience eBioscience BioLegend eBioscience
CCR6	29-2L17	BV 421 BV 605	1:100 1:100	BioLegend BioLegend
CCR7	4B12	PECy7	1:100	eBioscience
CD3	145-2C11	FITC PECy7 Alexa Fluor 700 BV 650 PE	1:100 1:100 1:100 1:200 1:500	eBioscience eBioscience eBioscience BioLegend eBioscience

Specificity (anti-)	Clone	Conjugate	Working dilution	Supplier
CD4	RM4-5	BV 785 BV 711 V500	1:300 1:200 1:300	Biolegend Biolegend BD Biosciences
CD5	53-7.3	FITC PECy7	1:100 1:100	eBioscience eBioscience
CD11b	M1/70	FITC APC eFluor 780 eFluor 450	1:300 1:100 1:200	eBioscience eBioscience eBioscience
CD11c	N418	FITC PECy7 eFluor 450 BV 785	1:300 1:300 1:200 1:100	eBioscience eBioscience eBioscience Biolegend
CD25	PC61	BV 650	1:200	Biolegend
CD44	1M7	PECy7 BV 785 A700	1:800 1:200 1:100	eBioscience BD Biosciences eBioscience
CD45.1	A20	BV 421 PE APC eFluor 780	1:100 1:200 1:100	Biolegend eBioscience eBioscience
CD45.2	104	BV 510 PerCP-Cy5.5	1:100 1:200	Biolegend eBioscience
CD62L	MCL-14	PE	1:400	eBioscience
CD80	16-10AI	BV 605	1:100	BioLegend
CD86	GL1	APC	1:100	eBioscience
CD103	2E7	PE	1:200	eBioscience
CXCR5	2G8	Biotin	1:25	BD Biosciences
FoxP3	FJK-16s	FITC	1:100	eBioscience
GATA-3	TWAJ	PerCP eFluor 710	1:50	eBioscience
I-Ab	M5/114.15.2	A700 BV 510	1:100 1:500	eBioscience Biolegend
ICOS	15F9	PerCP eFluor 710	1:100	eBioscience
IL-7Rα	A7R34	Alexa eFluor 660 BV 421 PECy7	1:200 1:100 1:100	eBioscience Biolegend eBioscience
Ki-67	SolA15	PECy7	1:300	eBioscience
NKp46	29A1.4	PECy7 BV 605 BV711	1:100 1:200 1:200	eBioscience Biolegend Biolegend
RORγt	AFKJS-9	PE	1:50	Bioscience
T-bet	eBio4B10	Alexa eFluor 660	1:25	eBioscience
Vβ5.1/2 TCR	MR9-4	PerCP eFluor 710	1:200	eBioscience

Table 2.9 Streptavidin used to detect biotinylated antibodies

Streptavidin (SA)	Supplier
SA-Alexa fluor 647	Invitrogen
SA-PerCP efluor 710	eBioscience

2.6 CHEMOKINE CAPTURE ASSAY

Biotinylated CCL19 was pre-incubated with streptavidin-647 (SA-647) at room temperature and in the dark for 45 minutes prior to the start of the assay. WT and CCR7$^{-/-}$ mLN cells were incubated with 90ng of pre-conjugated CCL19 at a final concentration of 1.8ng/µl in a 96-well plate for 1 hour at 37°C. Secondary antibody controls were incubated with SA-647 only. Samples were stained for cell surface markers and analysed on the flow cytometer.

2.7 TRANSMIGRATION ASSAY

100µl RPMI containing 2 x10^6 cells from WT or CCR7$^{-/-}$ mLN were loaded into transwell inserts (Corning Transwell Permeable Supports, 3421, Sigma-Aldrich; 6.5mm diameter, pore size of 5µm). Inserts were placed into wells containing RPMI with 2% FBS +/- 20nM CCL21. Plates were incubated at 37°C for 3 hours, before the addition of 5.5mM EDTA to the bottom well and transfer of plate to ice for 10 minutes (Mackley et al., 2015). Migrated (output) cells and those in the insert (input) were analysed by flow cytometry. Samples were analysed in triplicate, with the exception of CCR7$^{-/-}$ controls which were analysed in duplicate, and average values displayed on graphs. Percentages of each cell type that had migrated are as a proportion of the total of each cell type retrieved from both input and output wells, as shown in the equation below:

$$\%\ total\ cells\ migrated = \left(\frac{total\ cells\ in\ output}{\left[total\ cells\ in\ output + total\ cells\ in\ input \right]} \right) x\ 100$$

2.8 IMMUNOFLUORESCENCE MICROSCOPY

2.8.1 Sectioning of frozen tissues

Tissues for immunofluorescence microscopy analysis were rapidly frozen on dry ice and stored at -80°C. Lymph nodes were mounted in optimal cutting temperature (OCT) compound prior to freezing to aid cutting. 6µm tissues were cut using a cryostat and mounted onto 4 spot glass slides (Hendley-Essex). Dry tissue sections were fixed in cold acetone (Baker) at 4°C for 20 minutes, air dried for at least 10 minutes and stored at -20°C prior to use.

2.8.2 Immunolabelling of tissue

Slides were air dried for at least 30 minutes before being placed in a PBS (Sigma-Aldrich) bath for 10 minutes to hydrate tissue. Staining solution was made from 1% bovine serum albumin (BSA) in PBS, as detailed in Table 2.4. Sections were incubated with 75µl 10% horse serum in staining solution for 15 minutes to block non-specific protein binding sites, before this solution was aspirated from slides. Primary antibodies mixes, made up in staining solution, were incubated with tissue for 1 hour at room temperature in a dark, humidified chamber. Subsequent staining steps were carried out for only 30 minutes, and slides washed in PBS for 10 minutes in between each.

Detection of the transcription factors RORγt and GATA-3 required multiple signal amplification steps. Purified rat antibodies against RORγt or GATA-3 (primary) were detected using donkey anti-rat-IgG FITC (secondary), then rabbit anti-FITC-AF488 (tertiary) and finally donkey anti-rabbit-IgG-AF488 (quaternary), as detailed in Tables 2.10 and 2.11. Other FITC-conjugated antibodies were often amplified using tertiary and

quaternary antibodies. To prevent broad binding of secondary anti-rat antibodies to all antibodies derived from rat hosts, rat antibodies other than RORγt or GATA-3 were included after the donkey anti-rat-IgG FITC amplification stage, and a 10-15 minute blocking step in 10% rat serum introduced to prevent unwanted binding. Prior to use, secondary, tertiary and quaternary antibodies were cross-absorbed in a final volume of 100µl 10% mouse serum for 30 minutes, then diluted with staining solution to reach the required final concentration. Biotinylated antibodies were detected using streptavidin-conjugated fluorochromes. Following the completion of staining steps sections were counterstained with 4',6-diamidino-2-phenylindole (DAPI) and mounted with ProLong Gold (Invitrogen). Clear nail varnish was used to seal slides which were left to dry in the dark overnight at room temperature, then stored at 4°C until analysis.

2.8.3 Analysis of slides

Slides were analysed on a Zeiss 780 Zen microscope (Zeiss). Tilescanned images were automatically stitched by the Zen software (Zeiss) following acquisition. Percentage of RORγt^{+} IL-7Rα^{hi} cells within interfollicular areas which were CD3^{-} ILC3 was quantified using the Zen software (Zeiss).

Table 2.10 Primary antibodies for immunofluorescence microscopy

Specificity (anti-)	Clone	Conjugate	Working dilution	Supplier
CD3	eBio500A2 145-2C11	Biotin FITC	1:50 1:100	eBioscience eBioscience
CD31	390	Biotin	1:200	eBioscience
CD169	3D6.112	FITC	1:800	AbD Serotec
F4/80	BM8	Alexa Fluor 647	1:50	eBioscience
GATA-3	TWAJ	N/A	1:25	eBioscience
ICOS	C398.4A	Alexa Fluor 647	1:25	BioLegend
IgM		Rhodamine Red	1:200	Jackson ImmunoResearch
IL-7Rα	A7R34	eFluor 660	1:25	eBioscience
KLRG-1	2F1	APC	1:50	eBioscience
RANKL	IK22/5	Biotin	1:50	eBioscience
RORγt	AFKJS-9	N/A	1:25	eBioscience
MadCAM-1	MECA-367	Biotin	1:100	eBioscience

Table 2.11 Additional antibodies and streptavidin for immunofluorescence microscopy

Antibody	Type	Working dilution	Supplier
Streptavidin-AF555	Secondary	1:500	Life Technologies
Donkey anti-rat-IgG-FITC	Secondary	1:150	Jackson ImmunoResearch
Rabbit anti-FITC-AF488	Tertiary	1:200	Life Technologies
Donkey anti-rabbit-IgG-AF488	Quarternary	1:200	Life Technologies

2.9 *IN VIVO* EXPERIMENTS

2.9.1 Bone marrow chimeras

Host mice were given Baytril antibiotic in drinking water by [redacted] staff for several days prior to irradiation, and this treatment was continued for at least a week following bone marrow transfer. Bone marrow was prepared from donor mice, as previously described and with aseptic techniques, then filtered and re-suspended in sterile PBS for injection. 4-5 million bone marrow cells were transferred in total, and mice left for sufficient time for cells to become reconstituted within the periphery.

RORγt$^{+/-}$:WT and RORγt$^{+/-}$:RORγt$^{-/-}$ chimeras were lethally irradiated with 2 x 450rad irradiation on consecutive days before receiving either WT or RORγt$^{-/-}$ bone marrow intravenously (i.v). Approximately 3-4 weeks post-transfer, RORγt$^{+/-}$:RORγt$^{-/-}$ chimeras were treated with two 1mg doses of anti-CD90.2 antibody (generated at University of Birmingham) intraperitoneally (i.p), and mice analysed approximately three weeks later. WT:WT and WT:RORγt$^{-/-}$ chimeras were generated from WT hosts which received 2 x 600rad irradiation on consecutive days prior to transfer of WT or RORγt$^{-/-}$ bone marrow i.v. WT:RORγt$^{-/-}$ mice were further treated with two 1mg doses of anti-CD90.2 antibody i.p, whilst WT:WT chimeras received 1mg control rat IgG (Sigma-Aldrich) and mice were analysed approximately 6-12 weeks post-antibody treatment. CCR7$^{-/-}$:WT and CCR7$^{-/-}$:RORγt$^{-/-}$ chimeras were lethally irradiated with 2 x 600rad irradiation on consecutive days prior to intravenous bone marrow transfer and analysed approximately 5-9 weeks later.

Mixed bone marrow chimera hosts were lethally irradiated with 2 x 600rad irradiation on consecutive days before a 1:1 mix of CD45.1^{+} WT and either CD45.2^{+} WT (WT:WT) or CD45.2^{+} CCR7$^{-/-}$ (WT:CCR7$^{-/-}$) bone marrow was transferred intravenously. The mixed bone marrow was analysed by flow cytometry to ensure that the ratio of transferred cells was approximately 1:1. Mice were analysed approximately 6-8 weeks post-bone marrow transfer. Analysis of mixed bone marrow chimeras generated in CD45.1^{+}CD45.2^{+} WT hosts required the exclusion of irradiation resistant host cells at the time of tissue analysis. Percentage of each cell population (X) which were CD45.1^{+} or CD45.2^{+} was calculated from donor cells only, with CD45.1^{+}CD45.2^{+} host cells excluded as shown below:

$$\%\ of\ X = \left(\frac{CD45.1^{+}CD45.2^{-}X\ or\ CD45.1^{-}CD45.2^{+}X}{\left[Total\ X - CD45.1^{+}CD45.2^{+}X\right]}\right) x\ 100$$

2.9.2 Adoptive transfer of TCR transgenic T cells

Cells for transfer were isolated from selected LNs and spleen from RAG$^{-/-}$ SM1, RAG$^{-/-}$ OTII or OTII mice. Cells were prepared under sterile conditions and were not enzymatically digested. A small sample of cells was analysed by flow cytometry prior to transfer to calculate the percentage of total cells which were either SM1 or OTII T cells, and therefore to ensure the accurate and consistent transfer of either 10^4 or 10^5 TCR transgenic CD4$^+$ T cells to each mouse. Cells were re-suspended in sterile PBS and filtered prior to intravenous injection into the tail vein of experimental mice. The day following adoptive transfer, mice were immunised with the appropriate cognate antigen as described below.

2.9.3 Immunisation

Mice were immunised in the front or hind paw pad with 10^6 *actA*-deficient *L. monocytogenes* expressing FliC$_{427\text{-}441}$ peptide (Lm-FliC, a kind gift from Dr. Sing Sing Way), the target antigen of SM1 T cells (McSorley et al., 2002). Lm-FliC was grown from frozen stocks on Luria-Bertani (LB) chloramphenicol-treated agar plates at 37°C overnight. Chloramphenicol-selective agar plates were made within the laboratory to a final chloramphenicol concentration of 20µg/ml agar. To prepare for injection, a single colony of Lm-FliC was grown overnight in a shaking 37°C incubator in LB broth supplemented with 20µg/ml chloramphenicol. The following day bacteria was subcultured and grown under the same conditions until the OD_{600}=0.1, as calculated using a spectrophotometer. 1ml aliquots of Lm-FliC were centrifuged at 9300rcf for 10 minutes at room temperature,

then cell pellets washed twice with sterile PBS. The OD_{600} of the washed bacteria was re-calculated and Lm-FliC was diluted in sterile PBS to a final concentration of 10^6 Lm-FliC per 20µl sterile PBS for injection.

Mice were immunised in the front paw pad with 10-20µg of aluminium hydroxide precipitated (alum ppt) FliC peptide or NP-OVA protein, or with 100µg alum-ppt FliC peptide i.p. To alum ppt antigen 500µg of FliC peptide or NP-OVA protein was diluted in PBS to a final volume of 150µl and added to 150µl of 9% Aluminium sulphate. For alum ppt FliC experiments 7µl of 10M sodium hydroxide (NaOH) was added to this solution, and in the case of NP-OVA precipitation NaOH was added dropwise until the correct pH, represented by a yellow colouring, was achieved (between 7.5-9µl NaOH). The solution was mixed and incubated at room temperature for 30 minutes, before being thoroughly washed 3 times with 500µl of sterile PBS. The alum precipitated antigen was then diluted to the required concentration in sterile PBS for injection. A final volume of 20µl alum-ppt antigen or 100µl alum-ppt antigen in PBS was injected in the paw pads or i.p respectively.

2.10 STATISTICAL ANALYSIS

Numerical data was analysed using Microsoft Excel (Microsoft) and graphs were generated using GraphPad Prism 6 (GraphPad). Statistical significance was determined using Mann-Whitney non-parametric, two-tailed tests and significance set at $P<0.05$, unless otherwise stated.

CHAPTER 3. CHARACTERISING ILCS IN LYMPH NODES

3.1 INTRODUCTION

Although well characterised in non-lymphoid tissues, in particular the gut where ILCs are enriched, comparatively little is known about ILCs within secondary lymphoid tissues, such as lymph nodes (LNs). The detection of group 3 ILCs within regions of lymph nodes which are important sites of interaction during immune responses and the sites of lymphocyte recirculation is indicative of an important role (Withers et al., 2012). Given that previous investigations within our research group have focused on the role of members of this family within the spleen (Withers et al., 2012), this investigation will focus primarily on subsets of ILCs found in lymph nodes.

Lymph nodes provide an environment within which interactions between cells of the adaptive immune system and antigen-presenting cells (APCs) are facilitated. Antigen and activated APCs enter the lymph at the site of infection and are transported through a system of lymphatic vessels to the local lymph node, known as the draining lymph node (dLN) (Braun et al., 2011). Here APCs presenting antigenic peptides are kept in close proximity to naïve lymphocytes, facilitating the initiation of a primary adaptive immune response. Lymph nodes are highly organised, segregated structures which provide separate areas for B and T lymphocytes. Each lymph node is surrounded by a capsule beneath which lies the sub-capsular sinus, where lymph from the peripheral organs enters. Within these layers, but lining the lymph node exterior sit the B cell follicles, whilst T cells reside deeper within an area known as the paracortex (Willard-Mack, 2006). The location of these two types of lymphocytes is dictated by their interaction with

chemokines secreted by distinct stromal cell populations that form the framework of each area. B cells express CXCR5 that binds the chemokine CXCL13, which is highly expressed within the B cell follicles (Ansel et al., 2000), whilst T cells express CCR7, which binds to the chemokines CCL19 and CCL21 and attracts T cells to the paracortical zone (Worbs et al., 2007). $CD4^+$ T cells, however, upon activation will downregulate expression of CCR7 and upregulate CXCR5, thus facilitating their movement to the interface between the B cell follicles and T cell area, the B-T interface. Some activated $CD4^+$ T cells will then enter the follicle as T follicular helper cells (Ansel et al., 1999, Ma et al., 2012). In order to sample as many antigens as possible, naïve lymphocytes will continuously recirculate through lymphoid tissues until they encounter their cognate antigen. Entry of these naïve lymphocytes into the lymph node is through high endothelial venules (HEVs) located in the paracortical zones and interfollicular areas, whilst cells will leave through the efferent lymph (von Andrian and Mempel, 2003).

It is within the regions between LN follicles and near the B-T interface that RORγt-expressing LTi cells have previously been documented in mouse mesenteric LNs (Withers et al., 2012). Their resulting proximity to recirculating naïve and memory lymphocytes in part led to the hypothesis that LTi cells might support $CD4^+$ T cell responses. Although not found to be important for primary $CD4^+$ T cell responses within the spleen, the presence of LTi cells within this tissue was found to be important for the survival of populations of memory $CD4^+$ T cells (Withers et al., 2012).

The roles of ILCs in lymph nodes has not been widely explored. ILCs have been studied within the mesenteric LN, in part due to its ease of isolation and size. Whether or not any or all subsets reside within other lymph nodes is unknown. Given that investigations have

identified these cells within tissues such as the skin and lung in addition to the gut, we hypothesised that the differences in immune requirements at each site might be reflected in the cells which reside in local draining lymph nodes. Therefore this chapter will investigate the presence and phenotype of different subsets of ILCs in a range of different peripheral and mucosal tissue draining lymph nodes at steady state.

3.2 IDENTIFICATION OF ILCS IN LYMPH NODES

3.2.1 All groups of ILC reside within lymph nodes

As has been previously reported, a distinct population of ILCs which lacked common lineage (Lin) defining markers which would mark them out as T cells, B cells or DCs, and expressed high levels of the receptor for IL-7 (IL-7Rα) could be detected within the small intestine (SI) of WT mice by flow cytometry (Figure 3.1a). This population was also evident within mesenteric LNs (mLN) which drain tissues of the gut, albeit in lower numbers than seen in the comparatively ILC-enriched SI (Figure 3.1a,d). In focusing on those Lin^- cells which expressed IL-7Rα, we excluded populations of conventional NK cells commonly associated with cytotoxic activity. Thus throughout this investigation the ILCs analysed were those which depend upon IL-7 for survival and are described in recent publications as 'helper' ILCs (Artis and Spits, 2015).

As has been described in the literature, different subsets of ILCs could be distinguished from this population based on their expression of the transcription factors GATA-3, RORγt and T-bet (Figure 3.1a-c), which have previously been associated with $CD4^+$ T cell subsets. As such, it was crucial that T cells could confidently be excluded from our Lin^- IL-7Rα$^+$ gate, and steps were taken to ensure that this was the case. By excluding those cells which express CD3-epsilon (CD3)—a molecule which is expressed on the surface of a T cell in

Figure 3.1 All subsets of ILC can be detected in the mLN

Cells were isolated from naïve WT mouse small intestine lamina propria (SI) as specified in methods. mLNs were taken alongside and cells isolated as normal. Both SI and mLN samples were analysed using Live/Dead viability dye and anti-CD45 antibody in addition to normal markers. Samples were analysed by flow cytometry and absolute numbers calculated.

All bars shown on graphs represent the median value. Data representative of (a-c) or pooled from (d) 2 independent experiments. Statistical test used is Mann-Whitney non-parametric, two-tailed test. **P*<0.05, ***P*<0.01, ****P*<0.001 and *****P*<0.0001.

a) FACS plots showing gating on subsets of Lin^- IL-7Rα^+ ILCs in WT SI (top) and mLN (bottom). R^-G^- is RORγt^- GATA-3^- cells. Lin is CD3/CD5 B220/CD11b/CD11c.

b) FACS plots showing T-bet intracellular staining on RORγt^-GATA-3^- (R^-G^-) ILCs in SI and mLN tissue, as gated in (a). R^-G^- T-bet^+ cells labelled as ILC1.

c) Histogram showing T-bet expression by R^-G^- (blue line) ILCs compared to GATA-3^+ ILC2 (filled grey) from WT mLN, as defined in (a). Y axis is normalised to mode.

d) Graph showing the total number of Lin^- IL-7Rα^+ ILCs in whole WT mLN tissue (here not taking into account individual constituent LNs) or whole SI tissue. (n=6,6).

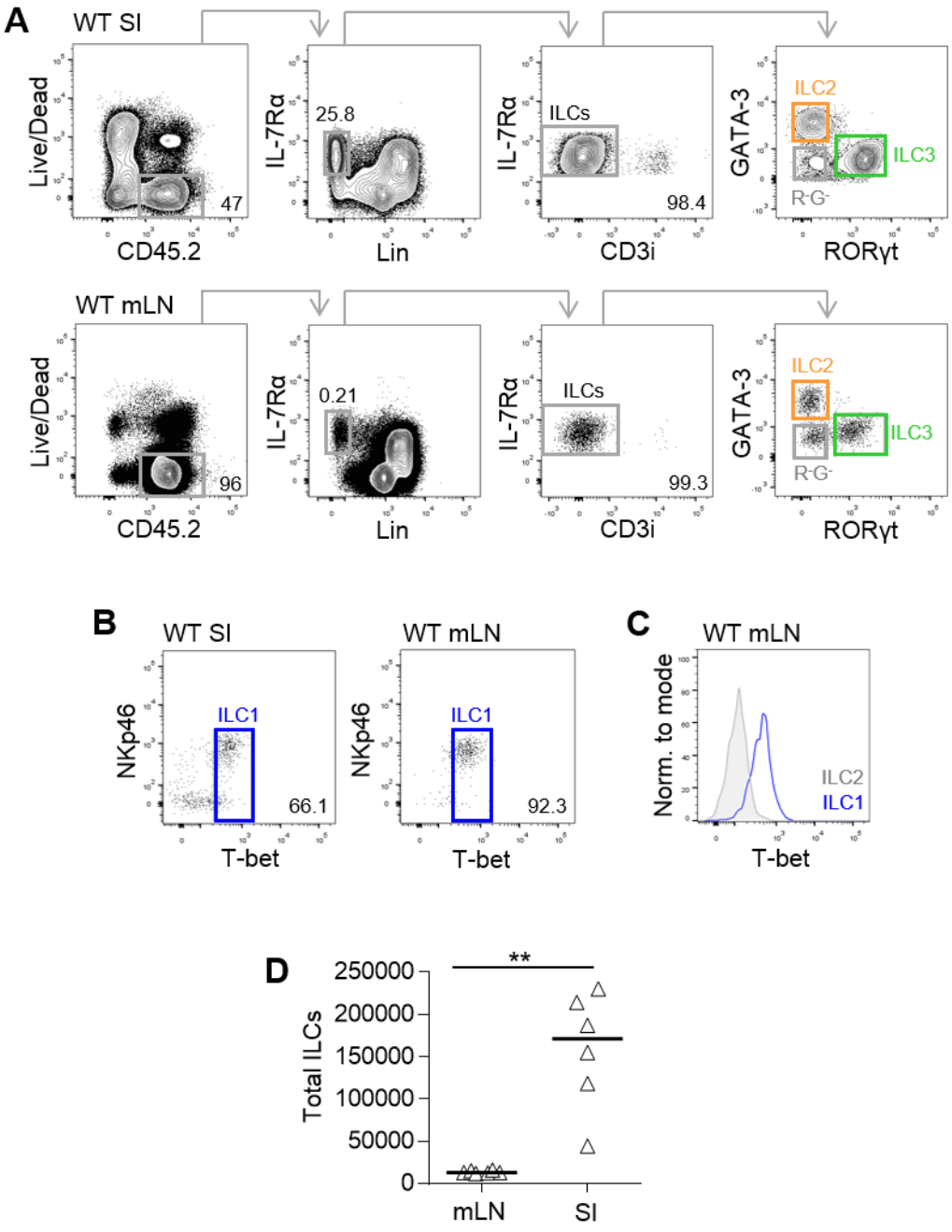
A
WT SI
Live/Dead
47
CD45.2
IL-7Rα
25.8
Lin
IL-7Rα
ILCs
98.4
CD3i
GATA-3
ILC2
ILC3
R-G-
RORγt
WT mLN
Live/Dead
96
CD45.2
IL-7Rα
0.21
Lin
IL-7Rα
ILCs
99.3
CD3i
GATA-3
ILC2
ILC3
R-G-
RORγt
B
WT SI
NKp46
ILC1
66.1
T-bet
WT mLN
NKp46
ILC1
92.3
T-bet
C
WT mLN
Norm. to mode
ILC2
ILC1
T-bet
D
Total ILCs
250000
200000
150000
100000
50000
0
**
mLN
SI

Fig. 3.1

conjunction with the T cell receptor and therefore completely absent on ILCs—and CD5, populations of T cells and ILCs could be kept sufficiently distinct to distinguish between using flow cytometry (Figure 3.1a). As an additional precaution antibodies against CD3 were also used intracellularly to detect CD3 expression within cells (CD3-epsilon intracellular, CD3i), thereby preventing contamination of the Lin^- IL-$7R\alpha^+$ ILC gate with any T cells which expressed low levels of surface CD3; although such cells were generally found to constitute only a minor population (Figure 3.1a). Cells which expressed CD11c, B220 and CD11b were also excluded in keeping with a gating strategy defined previously within our group, and therefore excluding cells of known lineages which could possibly fall within this IL-$7R\alpha^+$ cell gate.

In both the SI and mLN of WT mice three distinct populations of ILCs could be identified by their expression of key transcription factors. Following fixation and permeabilisation, isolated cells were incubated with antibodies against intracellular expression of GATA-3, RORγt and T-bet (Figure 3.1a-c). Those cells which expressed high levels of GATA-3 but not RORγt could be identified as the GATA-3 expressing group 2 ILCs (ILC2), whilst those which expressed RORγt could be broadly identified as group 3 ILCs (ILC3). In the mLN those ILCs which did not express either GATA-3 or RORγt were largely T-bet^+, and this was especially apparent when compared to T-bet^- GATA-3^+ ILC2 (Figure 3.1b,c), and these cells were identified as group 1 ILCs (ILC1). The use of transcription factor expression, coupled with key surface markers, to identify these cells proved an effective method of detection; with surface markers alone not always definitive and cytokine expression likely subject to change upon activation or tissue.

Analysis of the phenotype of these ILC subsets revealed that ILCs in the mLN in many ways resembled those which had been reported at other sites (Walker et al., 2013). NKp46, a natural cytotoxicity receptor (NCR), has been documented on 'helper-like' ILC1 but not ILC2, and accordingly is expressed by the majority of ILC1 in mLN whilst ILC2 are NKp46$^-$ (Figure 3.2a). NKp46 expression has also been reported on a subset of ILC3 which lack expression of CCR6 (Klose et al., 2013) and although this population could be identified within the mLN (Figure 3.2a), it constituted only a minor proportion of total RORγt$^+$ ILCs. Instead, the majority were NKp46$^-$ and, in keeping with previous publications (Klose et al., 2013), expressed CCR6. Throughout this investigation those ILC3 which express NKp46 will be referred to NCR$^+$ ILC3, whilst those which do not will be identified as LTi-like ILC3. The expression of CCR6 could be detected on those ILCs which expressed RORγt only (Figure 3.2a), thus identifying this chemokine receptor as a useful surrogate marker for the identification of ILC3 when intracellular staining is not possible. The expression of CD4 by ILCs was restricted primarily to group 3 ILCs, with LTi-like ILC3 found to be heterogeneous for this molecule and no expression detected on those ILC3 which lacked CCR6. (Figure 3.2a). Major-histocompatibility complex II (MHCII) expression by both ILC2 and ILC3 has been reported (Neill et al., 2010, Hepworth et al., 2013), generating interest in the potential of these cells to act as antigen-presenting cells (APCs). Within the mLN very little MHCII expression could be detected by ILC1s and ILC2s, but it was found to be expressed by a proportion of ILC3, once again primarily limited to those which expressed CCR6 (Figure 3.2a).

Given the phenotype data outlined above, it is highly likely that this investigation is focusing on the ILC populations which have been reported before. Analysis of cells which expressed IL-7Rα and GATA-3 or RORγt, at levels comparable with ILC2 and ILC3,

Figure 3.2 ILC subsets phenotypically resemble those previously reported.

Cells isolated from mLNs of naïve WT mice as specified in methods. Samples were analysed by flow cytometry. Live/Dead viability dye and anti-CD45 antibody only used where specified.

a) FACS plots showing the expression of known phenotypic cell surface markers on subsets of ILC from WT mLN, gated as in Figure 3.1a (including viability dye and CD45). ILC1 are RORγt$^-$ GATA-3$^-$ T-bet$^+$, ILC2 are RORγt$^-$ GATA-3$^+$, ILC3 are RORγt$^+$. Data is representative of at least 6 WT mice.

b) Pie chart showing the percentage of lymphocytes (gated on FSC/SSC) from WT mLN which are viable and CD45(.2)$^+$ (white). Data pooled from 6 WT mice from 2 independent experiments.

c) FACS plots showing gating of lineage markers on IL-7Rα$^+$ RORγt$^+$ (top) or IL-7Rα$^+$ GATA-3$^+$ (bottom) cells in mLN, at transcription factor expression levels ordinarily used to define subsets of ILCs. Cells pre-gated on FSC and SSC. Viability dye and CD45 expression not analysed as very little cell death detected in LN samples as shown in (b). Data representative of 3 WT mice from 1 independent experiment.

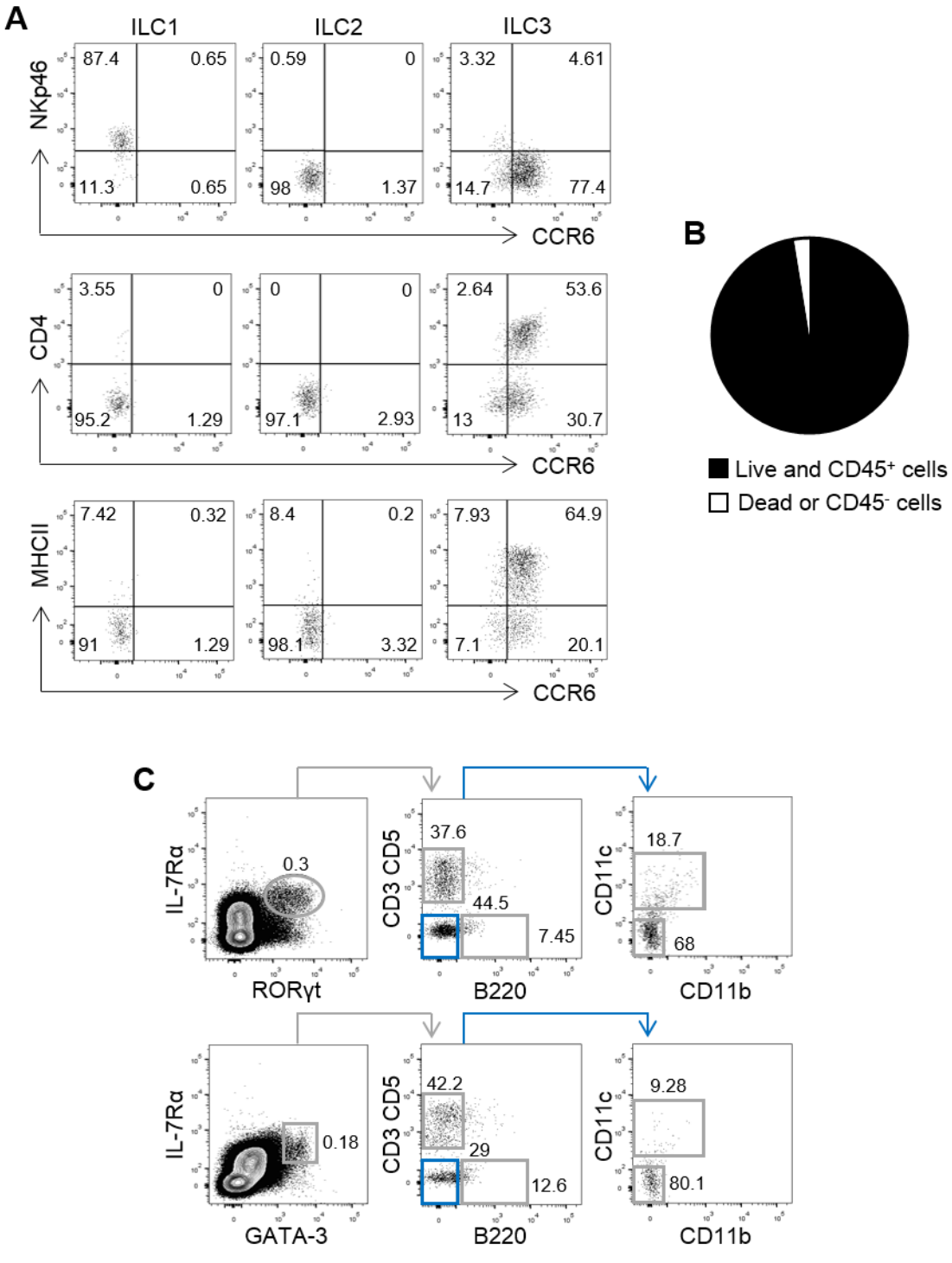
A
ILC1
ILC2
ILC3
NKp46
CD4
MHCII
CCR6
87.4
0.65
11.3
0.65
0.59
0
98
1.37
3.32
4.61
14.7
77.4
3.55
0
95.2
1.29
0
0
97.1
2.93
2.64
53.6
13
30.7
7.42
0.32
91
1.29
8.4
0.2
98.1
3.32
7.93
64.9
7.1
20.1
B
Live and CD45+ cells
Dead or CD45- cells
C
IL-7Rα
RORγt
0.3
CD3 CD5
B220
37.6
44.5
7.45
CD11c
CD11b
18.7
68
GATA-3
0.18
42.2
29
12.6
9.28
80.1

Fig. 3.2

revealed that those lineage marker-expressing cells with an ILC-like phenotype were primarily T cells (Figure 3.2c); therefore our inclusion of antibodies to CD3i wherever possible is a valid further precaution. Additionally, analysis of mLN cells incubated with a viability dye and antibodies against CD45 revealed that >95% of cells isolated from the mLN were live hematopoietic cells (Figure 3.2b). Our ability to extract cells from LNs with minimal cell death therefore meant that these markers were not included in the majority of experiments within this investigation, with the exception being when mLN tissue was compared to the SI.

3.2.2 ILC3 are enriched in mucosal tissue-draining LNs

Lymph nodes can be found at a number of different sites around the body, where they drain lymph from local tissue. Given that the immunological challenges faced by tissues at different sites can differ vastly, it is likely that the composition of cells in local LNs reflects this. To investigate whether differences were evident in the ILC subsets present, populations of these cells in a range of skin-draining peripheral LNs and mucosal tissue-draining LNs were compared. The LNs analysed included the skin-draining popliteal LN (popLN), inguinal LN (iLN) and brachial LN (bLN), and the mucosal tissue-associated mesenteric LN (mLN) and mediastinal LN (medLN).

All three groups of ILCs could be detected in all LNs analysed, using the gating strategy outlined in Figure 3.3a, unless otherwise stated. Although still the predominant population in skin-draining iLN and bLN, ILC3 were found to be particularly numerous in the mucosal tissue-draining mLN; most evident when the frequency of each subset was analysed per 10^6 lymphocytes (Figure 3.3b). The frequency of ILC3 per 10^6 lymphocytes in mLN tissue was found to be significantly higher than the frequency of either ILC1 or

Figure 3.3 ILC3 are enriched in LNs which drain mucosal sites

Cells isolated from LNs of naïve WT mice as specified in methods. Samples were analysed by flow cytometry and absolute numbers calculated.

All bars shown on graphs represent the median value. Data is representative of (a) or pooled (b-c) from 3 independent experiments. Statistical test used is Mann-Whitney non-parametric, two-tailed test. **P*<0.05, ***P*<0.01, ****P*<0.001 and *****P*<0.0001.

a) FACS plots showing gating on subsets of Lin^- IL-7Rα^+ ILCs in WT bLN (top) and mLN (bottom). Pre-gated on lymphocytes by FSC/SSC. ILC1 are RORγt^- GATA-3^- T-bet^+ ILCs. Lin is CD3/CD5/B220/CD11c.

b) Graph (left) showing the total number of ILC1, ILC2 and ILC3 in individual LNs. Total cells in mLN are divided by 5, unless otherwise stated, to account for multiple LNs draining mesentery. Graph (right) showing the frequency of each ILC subset per 10^6 lymphocytes (gated on FSC/SSC). (n=8,8,10).

c) Graph showing the percentage of total Lin^- IL-7Rα^+ ILCs which are RORγt^+ ILC3 (left) or GATA-3^+ ILC2 (right) in a range of LNs. For popLN and medLN analysis CD11b was not excluded and LNs from multiple WT mice were pooled to retrieve enough cells for analysis. popLN; popliteal LN, iLN; inguinal LN, bLN; brachial LN, mLN; mesenteric LN, medLN; mediastinal LN. (n=3,8,8,10,3).

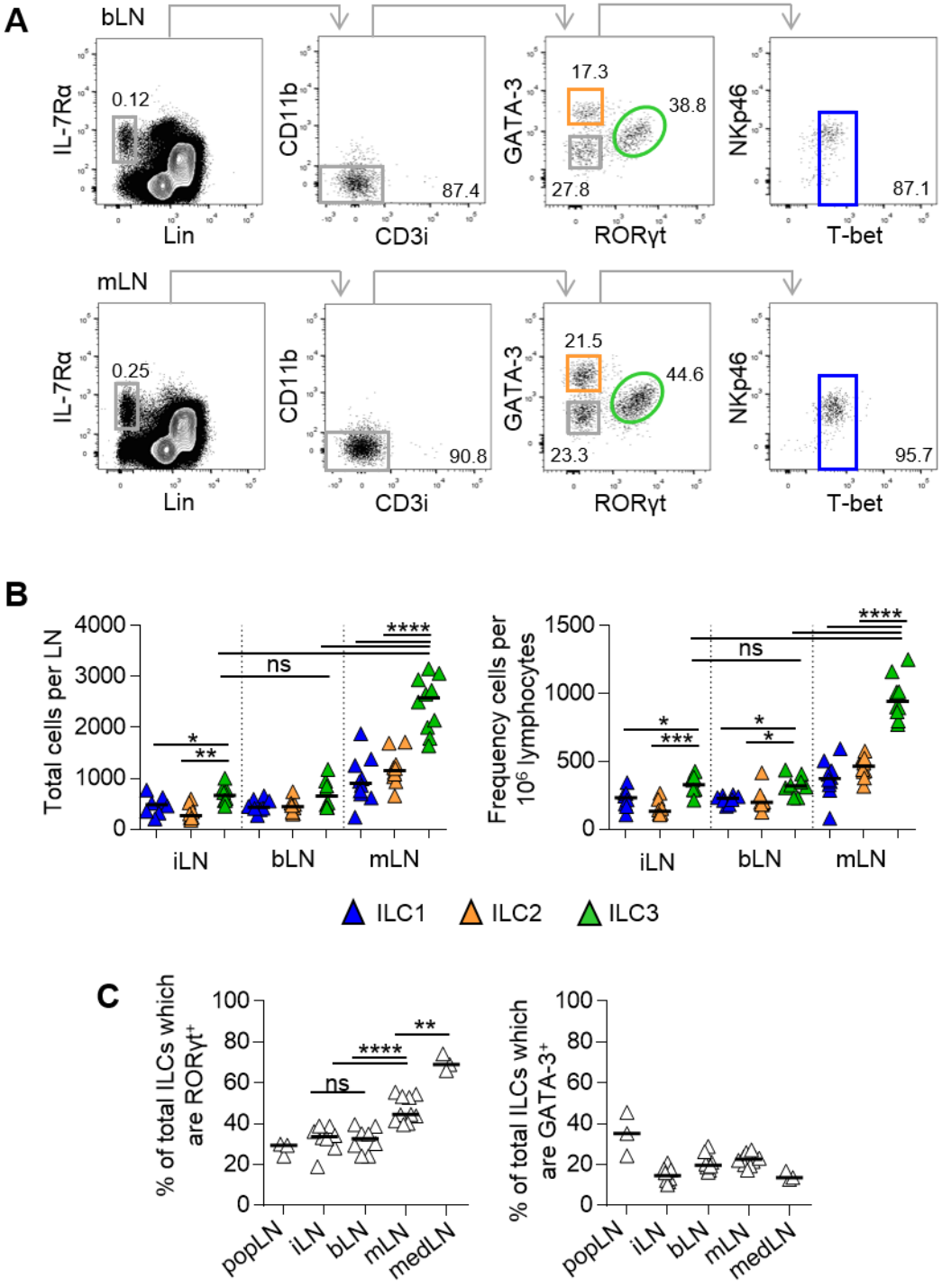
A
bLN
IL-7Rα
0.12
Lin
CD11b
87.4
CD3i
GATA-3
17.3
38.8
27.8
RORγt
NKp46
87.1
T-bet
mLN
IL-7Rα
0.25
Lin
CD11b
90.8
CD3i
GATA-3
21.5
44.6
23.3
RORγt
NKp46
95.7
T-bet
B
Total cells per LN
4000
3000
2000
1000
0
iLN
bLN
mLN
Frequency cells per 10⁶ lymphocytes
1500
1000
500
0
iLN
bLN
mLN
ILC1
ILC2
ILC3
C
% of total ILCs which are RORγt⁺
100
80
60
40
20
0
popLN
iLN
bLN
mLN
medLN
% of total ILCs which are GATA-3⁺
100
80
60
40
20
0
popLN
iLN
bLN
mLN
medLN

Fig. 3.3

ILC2. Although this observation was not exclusive to the mLN, for the frequency of ILC3 in iLN and bLNs was also statistically significantly higher than other ILC subsets, the frequency of ILC3 in the mLN was much higher than that found in either of these skin-draining LNs, and this was statistically significant (Figure 3.3b). Importantly, no significant difference was detected in the number or frequency of ILC3 when iLN and bLN were compared (Figure 3.3b), suggesting that, in this respect, these skin-draining LNs were similar.

In agreement with this, the percentage of total Lin^- IL-$7R\alpha^+$ ILCs which expressed RORγt was statistically significantly higher in the mLN than in either the iLN or bLN (Figure 3.3c). However, when the proportion of total ILCs which were $ROR\gamma t^+$ in iLN, bLN and mLN was compared to the popliteal LN (popLN) and medastinal LN (medLN) there appeared to be a bias towards ILC3 within those LNs known to drain mucosal surfaces. The popLN—a small, peripheral tissue-draining LN which drains the hind paw-pad—had the lowest percentage of ILC3, marginally lower than that found in skin-draining iLN and bLN. By contrast, the medLN—small LNs which drain the mucosal surfaces of the lung and upper respiratory tracts—was found to have the highest percentage of ILC3 of any LN analysed (Figure 3.3c), statistically significantly higher than even the mLN. The percentage of ILC2 did not, however, differ to any notable extent in the same LNs, although was found to be higher in the popLN (Figure 3.3c).

In the spleen, T-bet^+ ILC1 were found to be as numerous as ILC3, whilst ILC2 only made up a small percentage of the total population of ILCs (Figure 3.4b). Interestingly a proportion of $ROR\gamma t^-$ $GATA\text{-}3^-$ ILCs were found to not express high levels of T-bet but still express NKp46, a population not observed in LNs (Figure 3.4a). Although the number of

Figure 3.4 All subsets of ILC can be detected in the spleen

Cells isolated from spleen of naïve WT mice as specified in methods. Samples were analysed by flow cytometry and absolute numbers calculated.

All bars shown on graphs represent the median value. Statistical test used is Mann-Whitney non-parametric, two-tailed test. **P*<0.05, ***P*<0.01, ****P*<0.001 and *****P*<0.0001.

a) FACS plots showing gating on subsets of Lin$^-$ IL-7Rα$^+$ ILCs in WT spleen. Pre-gated on lymphocytes by FSC/SSC. ILC1 are RORγt$^-$ GATA-3$^-$ T-bet$^+$ ILCs. Lin is CD3/CD5/B220/CD11c. Data is representative of 2 independent experiments.

b) Graph (left) showing the total number of ILC1, ILC2 and ILC3 in whole spleen. Graph (right) showing each ILC subset as a percentage of the total Lin$^-$ IL-7Rα$^+$ ILCs. Data is pooled from 2 independent experiments. (n=6,6,6).

c) Graph showing the frequency of total Lin$^-$ IL-7Rα$^+$ ILCs per 10^6 lymphocytes in iLN, bLN, mLN and spleen. Data pooled from 3 (iLN, bLN and mLN) or 2 (spleen) independent experiments.

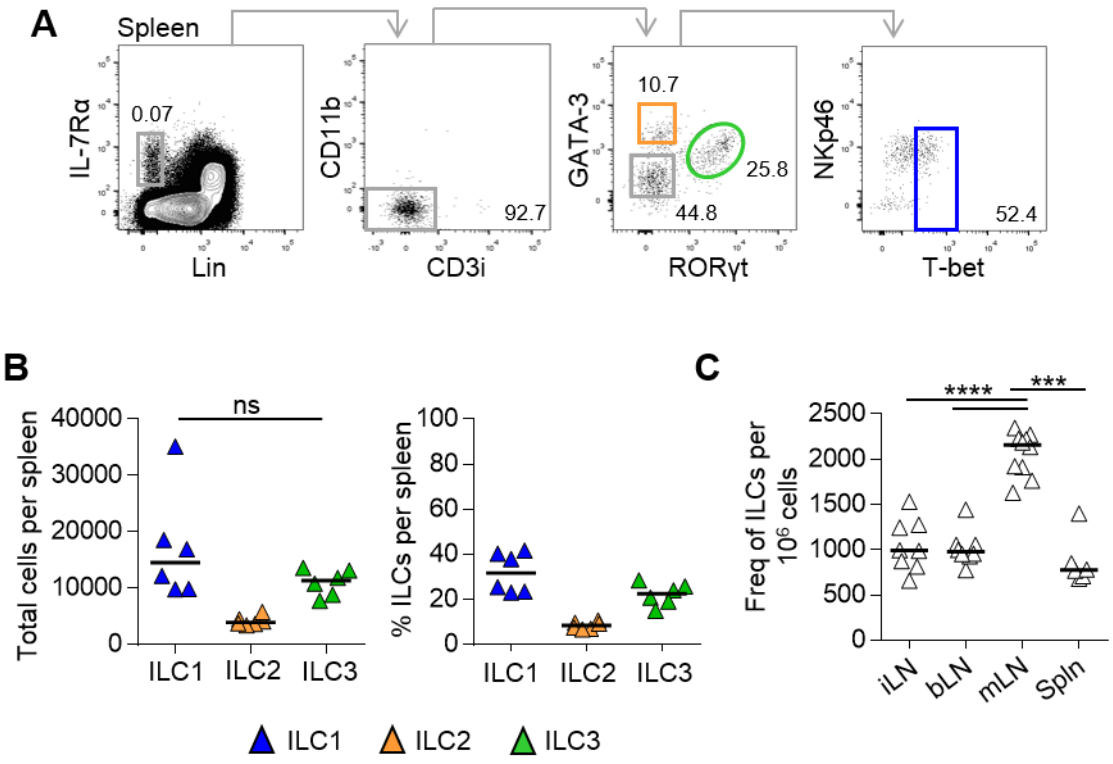
A
Spleen
IL-7Rα
0.07
Lin
CD11b
92.7
CD3i
GATA-3
10.7
25.8
44.8
RORγt
NKp46
52.4
T-bet
B
Total cells per spleen
40000
30000
20000
10000
0
ns
ILC1
ILC2
ILC3
% ILCs per spleen
100
80
60
40
20
0
ILC1
ILC2
ILC3
ILC1
ILC2
ILC3
C
Freq of ILCs per 10^6 cells
2500
2000
1500
1000
500
0
****
***
iLN
bLN
mLN
Spln

Fig. 3.4

each ILC subset was higher within the spleen, due to its size and cellularity, the frequency of ILCs was determined to be similar to or lower than that found in LNs. Analysis of the frequency of total Lin$^-$ IL-7Rα$^+$ ILCs per 10^6 lymphocytes within the iLN, bLN, mLN and spleen revealed that ILCs as a population of cells made up a statistically significantly higher proportion of total lymphocytes in the mLN than any other tissue analysed (Figure 3.4c).

3.2.3 Ex-RORγt$^+$ ILC3 are a minor ILC population in lymph nodes

Defining group 1 ILCs has been complicated not only by the debate surrounding whether or not conventional NK cells should be included within the ILC family, but also because of reports that populations of ILC3 can downregulate expression of the transcription factor RORγt, upregulate expression of T-bet and as a result resemble ILC1; becoming so-called 'ex-RORγt$^+$' ILCs (Klose et al., 2013, Vonarbourg et al., 2010). The use of RORγt cre x ROSA26 eYFP fate mapping mice—in which even transient expression of the transcription factor RORγt causes cells to permanently express a yellow fluorescent protein (YFP), thus enabling the fate of these cells to be mapped—allowed us to investigate to what extent these ex-RORγt$^+$ cells could be detected within the ILC1 population found in LNs.

Within the Lin$^-$ IL-7Rα$^+$ ILC population shown in Figure 3.5a the majority of cells which expressed RORγt at the time of *ex vivo* analysis were also YFP$^+$, thus confirming the successful expression of the YFP reporter protein. It was also possible to detect a population of cells which were YFP$^+$ but RORγt$^-$, confirming that there were indeed some ILCs which had once expressed, but since downregulated, RORγt expression. To investigate whether any of these RORγt$^-$ YFP$^+$ cells could resemble ILC1s, T-bet$^+$ cells were analysed for their expression of RORγt and YFP (Figure 3.5a). Cells which were T-bet$^+$ and

Figure 3.5 'Ex-RORγt$^+$' ILC3 are a minor population in LNs

Cells isolated from LNs of Rorc(γt) cre x Rosa26 eYFP mice as specified in methods. Samples were analysed by flow cytometry.

All bars shown on graphs represent the median value. Data representative of (a) or pooled from (b-d) 2 independent repeats, popLN and medLN pooled from multiple mice. Statistical test used is Mann-Whitney non-parametric, two-tailed test. *P<0.05, **P<0.01, ***P<0.001 and ****P<0.0001.

a) FACS plots showing gating for 'ex-RORγt$^+$ ILCs' in mLN tissue. Lin is CD3/CD5/B220/CD11c.

b) Graph showing the total number of Tbet$^+$ RORγt$^-$ YFP$^+$ 'ex-RORγt$^+$' ILCs, highlighted in blue in (a), per LN. (n=2,77,2).

c) Graph showing the percentage of total Lin$^-$ IL-7Rα$^+$ ILCs which were Tbet$^+$ RORγt$^-$ YFP$^+$. (n=2,77,2).

d) Percentage of total Tbet$^+$ RORγt$^-$ ILCs (ILC1) which are YFP$^+$ 'ex-RORγt$^+$' ILCs. (n=2,7,7,2).

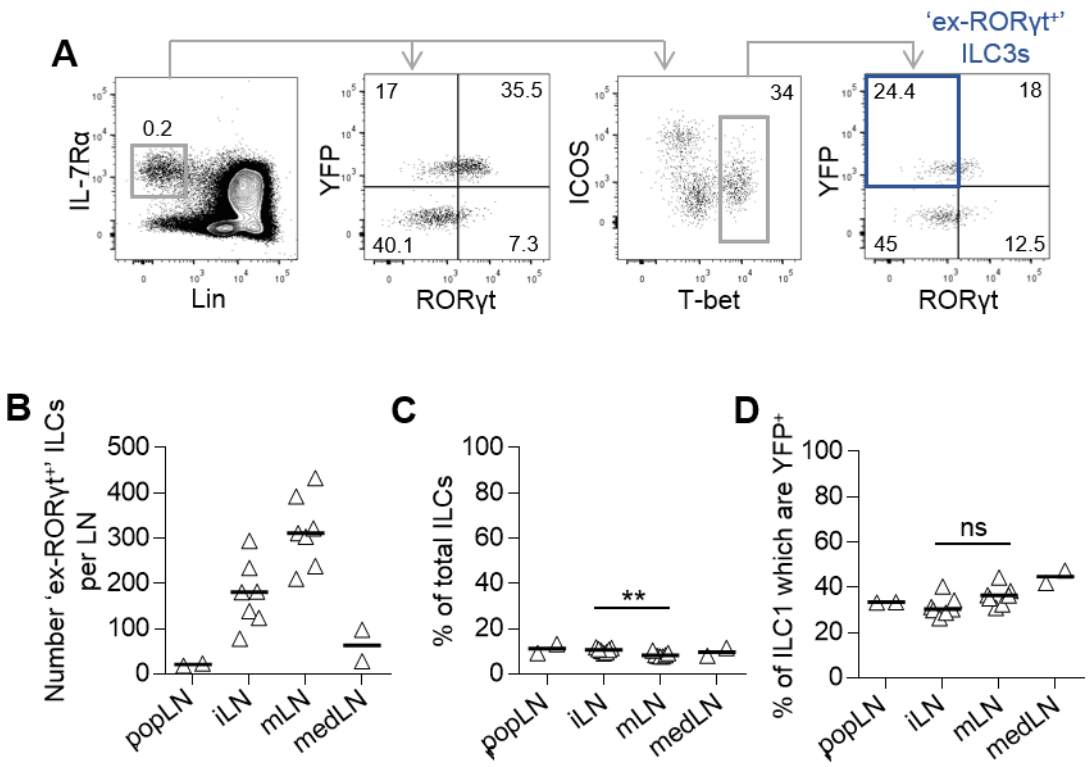
A
'ex-RORγt+' ILC3s
IL-7Rα
0.2
Lin
YFP
17
35.5
40.1
7.3
RORγt
ICOS
34
T-bet
YFP
24.4
18
45
12.5
RORγt
B
Number 'ex-RORγt+' ILCs per LN
500
400
300
200
100
0
popLN
iLN
mLN
medLN
C
% of total ILCs
100
80
60
40
20
0
**
popLN
iLN
mLN
medLN
D
% of ILC1 which are YFP+
100
80
60
40
20
0
ns
popLN
iLN
mLN
medLN

Fig. 3.5

YFP$^+$ but RORγt$^-$ could be identified in all LNs analysed (Figure 3.5b) and despite constituting only a minor percentage of total Lin$^-$ IL-7Rα$^+$ ILCs (Figure 3.5c), were found to comprise between 30-45% of total ILC1 (Figure 3.5d). This suggests that a proportion of ILC1s detected in LNs were in fact a population of 'ex-RORγt$^+$' ILC3, yet it is worth noting that plasticity within all subsets of ILCs is increasingly being reported (Bernink et al., 2015). It is therefore also possible that transient expression of RORγt by ILC1 within LNs is a phenomenon separate from the documented ability of ILC3 to alter their transcriptional profile to resemble ILC1, and highlights the difficulties associated with definitively defining these populations.

3.2.4 Phenotype of ILCs in different lymph nodes

Earlier in this chapter ILC3 within the mLN were shown to be primarily CCR6$^+$, with very few NKp46$^+$ ILC3 detected. This was also true of the skin-draining iLN and bLN (Figure 3.6a,b), with more than 80% of ILC3 in iLN, bLN and mLN expressing the chemokine receptor CCR6 (Figure 3.6b, median values). The proportion of ILC3 which expressed NKp46 was low in all LNs analysed, although a marginally lower percentage were detected within the mLN than iLN or bLN, and this difference was found to be statistically significant (Figure 3.6b). CD4 expression differed more convincingly, with a lower percentage of ILC3 within the mLN found to express CD4 than in the peripheral iLN and bLNs, and this was a statistically significant difference (Figure 3.6b). In contrast MHCII was expressed by a significantly higher percentage of ILC3 in the mLN than either the iLN or bLN (Figure 3.6b), perhaps indicative of a difference in the importance of ILC3-expressed MHCII at different sites.

Figure 3.6 Characterising the phenotype of ILC3 in LNs

Cells isolated from LNs of naïve WT mice as specified in methods. Samples were analysed by flow cytometry.

All bars shown on graphs represent the median value. Data is representative of (a) or pooled (b) from 2 (MHCII) or 3 independent experiments. Statistical test used is Mann-Whitney non-parametric, two-tailed test. **P*<0.05, ***P*<0.01, ****P*<0.001 and *****P*<0.0001.

a) FACS plots showing expression of phenotype markers on RORγt$^+$ ILC3s in iLN (top) and mLN (bottom).

b) Graphs showing the percentage of total Lin$^-$ IL-7Rα$^+$ RORγt$^+$ ILC3 which express CCR6, CD4, MHCII and NKp46 in iLN, bLN and mLN. (n=8,8,10 except MHCII where n=5,5,7).

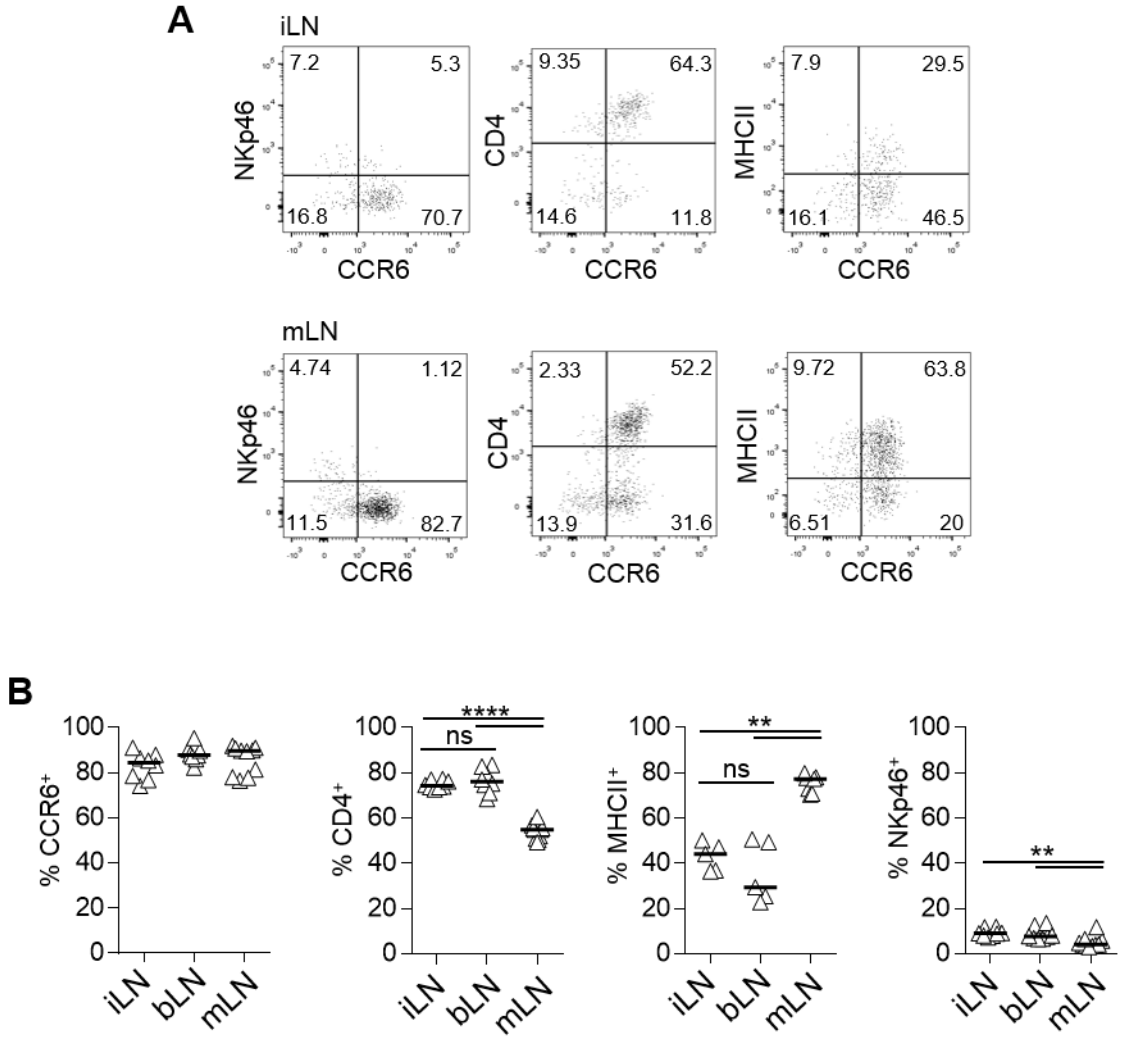
A
iLN
7.2
5.3
16.8
70.7
NKp46
CCR6
9.35
64.3
14.6
11.8
CD4
CCR6
7.9
29.5
16.1
46.5
MHCII
CCR6
mLN
4.74
1.12
11.5
82.7
NKp46
CCR6
2.33
52.2
13.9
31.6
CD4
CCR6
9.72
63.8
6.51
20
MHCII
CCR6
B
% CCR6+
% CD4+
ns
****
% MHCII+
ns
**
% NKp46+
**
iLN
bLN
mLN

Fig. 3.6

3.2.5 LN ILC populations differ in T cell-deficient mice

Previous investigations into the functions of ILC3 populations have often been carried out in mice which lacked T cells, using anti-CD90 antibodies to deplete ILC3 *in vivo* (Sonnenberg et al., 2012). This was in part due to the challenges associated with specifically depleting these cells *in vivo*, given that similar molecules are expressed by both ILCs and T cells. Analysis of ILC populations in the LNs of T cell-deficient $RAG^{-/-}$ and $ZAP\text{-}70^{-/-}$ mice was therefore important to enable comparison of our observations in WT mice with those of previous functional studies.

Expression of recombination-activating gene (RAG) proteins is important for the activity of a recombinase enzyme, which participates in the formation of a somatically rearranged T cell and B cell receptors. Successful rearrangement of these receptors is vital for the survival of T and B lymphocytes, and as a result all B and T lymphocytes are absent in RAG-deficient mice (Mombaerts et al., 1992). ZAP-70 is a protein tyrosine kinase, signalling through which is important during both T cell activation and thymic development. As a result, mice deficient in ZAP-70 lack $\alpha\beta TCR^{+}$ $CD4^{+}$ and $CD8^{+}$ mature T cells, but B cells are still present (Negishi et al., 1995). Therefore, although the architecture of LNs in $RAG^{-/-}$ mice is impaired as a result of the absence of lymphocytes, LNs from $ZAP\text{-}70^{-/-}$ mice still have detectable B cell follicles. Analysis of ILC populations within the mLNs of $RAG^{-/-}$ and $ZAP\text{-}70^{-/-}$ mice revealed striking differences to what had previously been observed in WT mice. Whilst ILC3 were the predominant ILC population in WT mLNs, GATA-3^{+} ILC2 made up the majority of total ILCs in both $RAG^{-/-}$ and $ZAP\text{-}70^{-/-}$ mice and ILC3 were comparably rare (Figure 3.7a-c). This observation was, however,

Figure 3.7 Composition of LN ILC populations differs in T cell-deficient mice

Cells isolated from LNs of naïve WT, $Rag^{-/-}$ and $ZAP70^{-/-}$ mice as specified in methods. Samples were analysed by flow cytometry.

All bars shown on graphs represent the median value. Data is representative of (a) or pooled (b-c) from at least 3 independent experiments. Statistical test used is Mann-Whitney non-parametric, two-tailed test. *P<0.05, **P<0.01, ***P<0.001 and ****P<0.0001.

a) FACS plots showing gating on subsets of Lin^- IL-7Rα^+ ILCs in WT (top), $Rag^{-/-}$ (middle) and $ZAP\text{-}70^{-/-}$ (bottom) mLNs. Lin is CD3/CD5/B220/CD11c. Arrows demonstrating gating strategy on WT FACS plots (top) apply to both $RAG^{-/-}$ and $ZAP\text{-}70^{-/-}$ also.

b) Graphs showing the total number of GATA-3^+ ILC2 (left) and RORγt^+ ILC3 (right) per individual mLN from WT, $Rag^{-/-}$ and $Zap70^{-/-}$ mice. Leftmost Y axis scale applies to both graphs.

c) Graphs showing the percentage of total Lin^- IL-7Rα^+ ILCs which are GATA-3^+ ILC2 (left) or RORγt^+ ILC3 (right) in mLN. Leftmost Y axis scale applies to both graphs.

d) Graphs showing the total number of ILC1, ILC2 and ILC3 per $Rag^{-/-}$ iLN (top) and the percentage of total ILCs which are ILC1, ILC2 or ILC3 in the same tissue (bottom).

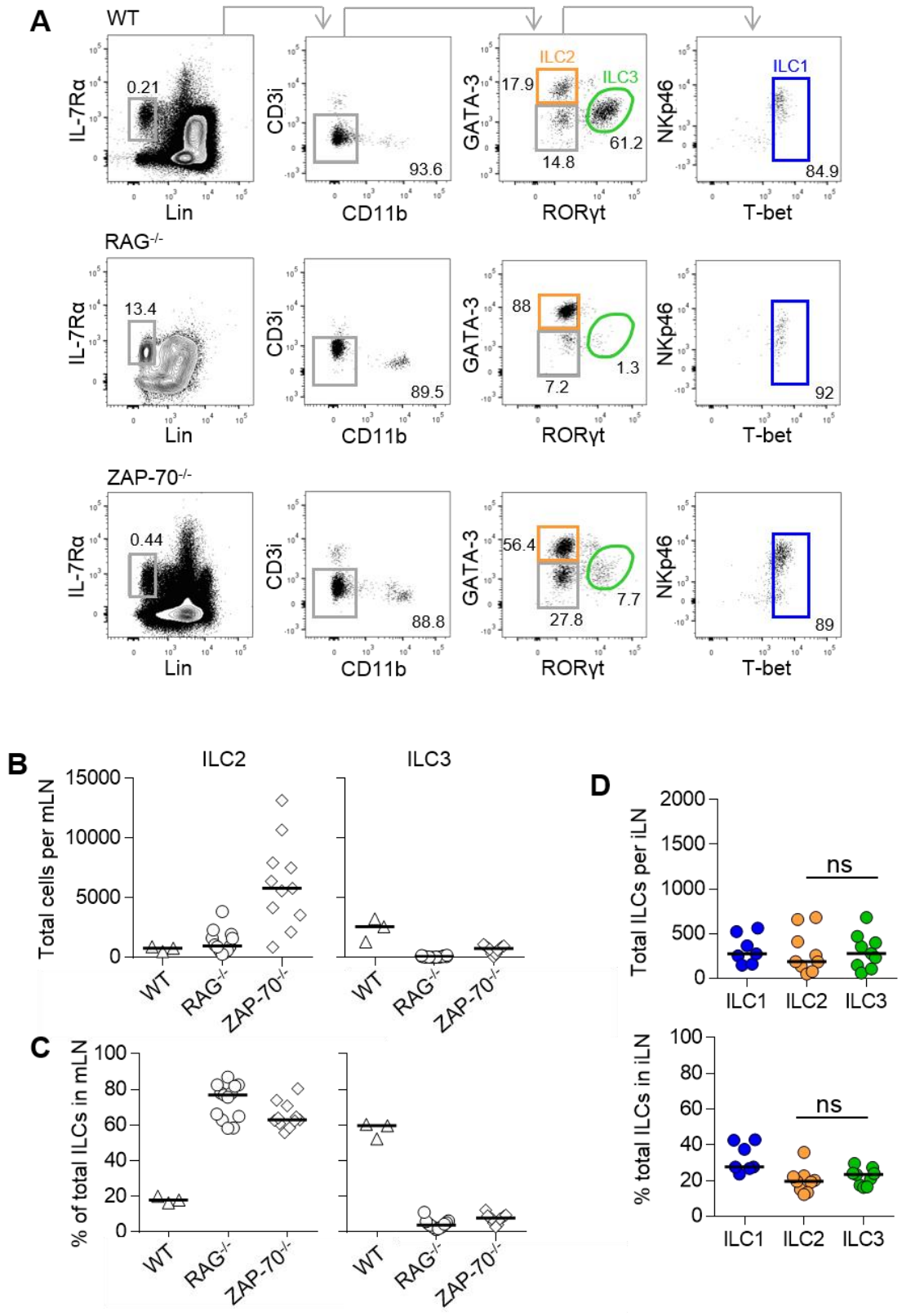
A
WT
IL-7Rα
0.21
Lin
CD3i
93.6
CD11b
GATA-3
ILC2
17.9
ILC3
61.2
14.8
RORγt
NKp46
ILC1
84.9
T-bet
RAG-/-
13.4
89.5
88
1.3
7.2
92
ZAP-70-/-
0.44
88.8
56.4
7.7
27.8
89
B
ILC2
ILC3
Total cells per mLN
15000
10000
5000
0
WT
RAG-/-
ZAP-70-/-
C
% of total ILCs in mLN
100
80
60
40
20
0
D
Total ILCs per iLN
2000
1500
1000
500
ns
ILC1
ILC2
ILC3
% total ILCs in iLN

Fig. 3.7

specific to the mLN, with the similar percentages of all ILCs detected in RAG$^{-/-}$ iLNs (Figure 3.7d) more comparable to what has previously been observed in WT mice.

3.3 LOCATION OF ILCS IN LYMPH NODES

3.3.1 Locating ILC2 and ILC3 in lymph node tissue sections

Whilst flow cytometry as an experimental technique is useful for enumerating and phenotyping ILCs, identifying ILCs in LNs using immunofluorescence microscopy provides an insight into their location and, as a result, the cell types with which they might interact; information lost when tissue is disrupted for flow cytometric analysis. Immunofluorescence microscopy therefore provides important clues as to the functions of cells of interest and valuable additional information to that which has been discussed above.

By refining previously established methods it was possible to identify and locate not only RORγt^{+} ILCs, as has been previously published (Withers et al., 2012), but also GATA-3^{+} ILCs within lymph node tissue. RORγt^{+} IL-7Rα^{+} cells which lacked expression of the T cell-marker CD3 could be identified within lymph node tissue (Figure 3.8a). Crucially anti-RORγt antibody staining coincided with nuclear DAPI staining, confirming that this was genuine intracellular transcription factor staining. In contrast, fluorescently labelled antibodies to both CD3 and IL-7Rα could be seen to bind to the non-nuclear portion of the cells (Figure 3.8a). Although CD3^{+} T cells also express IL-7Rα—with co-staining of these surface antibodies causing these cells to appear purple—those RORγt^{+} cells with notably high levels of this receptor were for the most part CD3^{-} and therefore not T cells (Figure 3.8a). This was consistent with earlier flow cytometry data, which showed that ILCs express particularly high levels of this receptor.

Figure 3.8 ILC3 and ILC2 can be located in LNs

Representative immunofluorescence microscopy images of WT mLN tissue sections. Images in (b) are serial sections of the same interfollicular area in a WT mLN. Smaller images are from regions of interest (ROI) marked by white dashed rectangles in corresponding images, and manually zoomed post-capture.

Sections all counterstained with DAPI.

a) Tilescanned image (left) showing interfollicular area of WT mLN stained for expression of RORγt, CD3 and IL-7Rα. Scale bar represents 100μm. Smaller images (right) are of RORγt^{+} CD3^{-} IL-7Rα^{+} cells from ROI manually zoomed post-capture. Scale bar represents 10μm.

b) Tilescanned image (left) showing interfollicular area of WT mLN stained for expression of RORγt, CD3 and IL-7Rα. Scale bar represents 100μm. Smaller images below are from marked ROI and scale bar represents 10μm. Tilescanned image (centre) showing interfollicular area of WT mLN stained for expression of GATA-3, CD3 and KLRG-1. Scale bar represents 100μm. Smaller images below are from marked ROI and scale bar represents 10μm. Tilescanned image (right) showing interfollicular area of WT mLN stained for expression of GATA-3, CD3 and ICOS. Scale bar represents 100μm. Smaller images below are from marked ROI and scale bar represents 10μm.

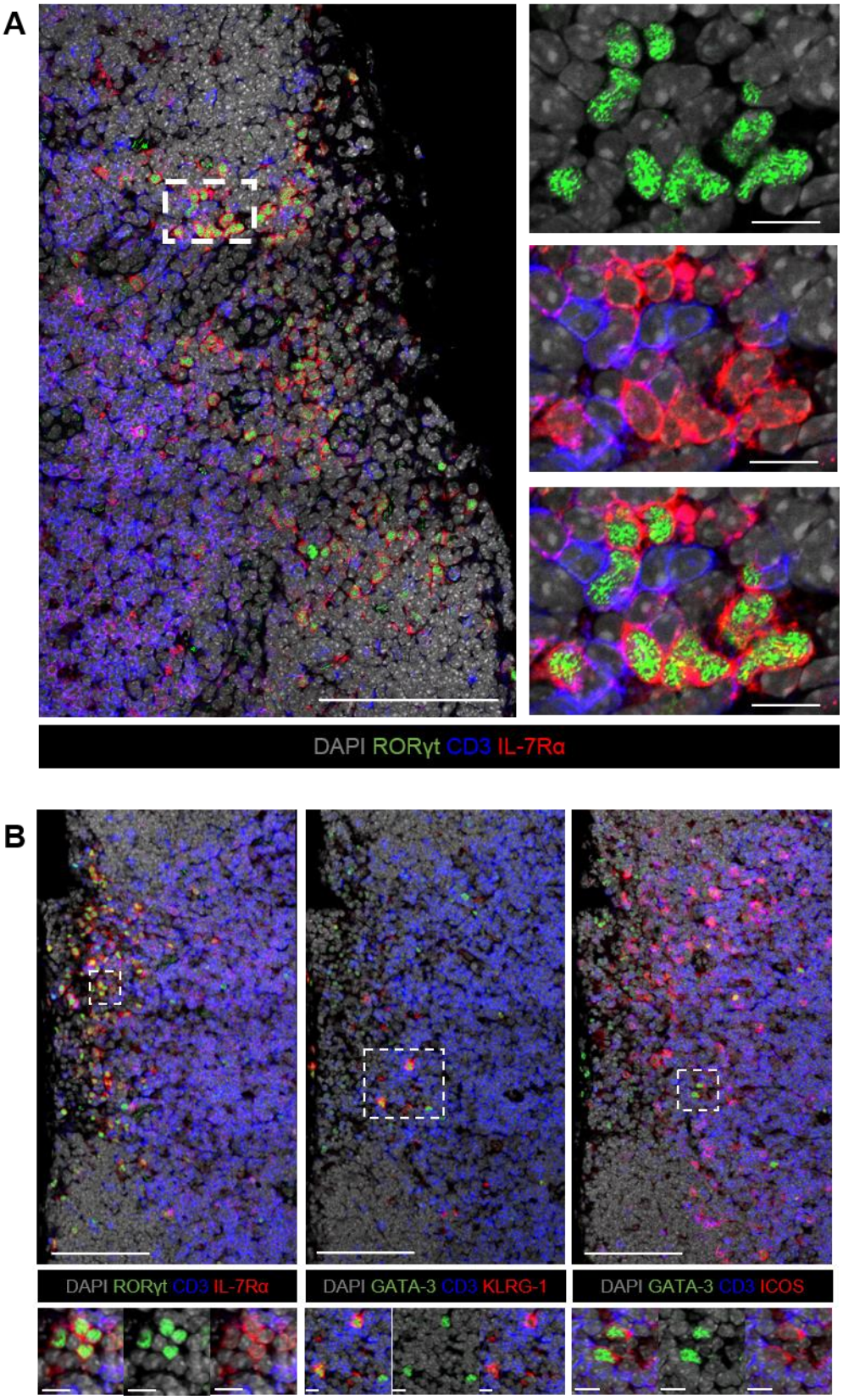
A
DAPI RORγt CD3 IL-7Rα
B
DAPI RORγt CD3 IL-7Rα
DAPI GATA-3 CD3 KLRG-1
DAPI GATA-3 CD3 ICOS

Fig. 3.8

Using this improved method of staining these RORγt^{+} CD3^{-} IL-7Rα^{+} ILCs were found to cluster in the interfollicular areas of LNs—those regions between B cell follicles and close to the subcapsular sinus—and at the B-T interface (Figure 3.8a) as previously reported (Withers et al., 2012); with B cell follicles here identified by their location and absence of CD3^{+} T cells. Strikingly, within these areas CD3^{-} cells which expressed the transcription factor GATA-3 and resembled ILC2 could also be detected (Figure 3.8b). Those CD3^{-} cells which expressed high levels of GATA-3 also expressed KLRG-1 (Figure 3.8b, centre) and ICOS (Figure 3.8b, right), two cell surface markers which have been reported to be expressed by ILC2 (Hoyler et al., 2012, Neill et al., 2010). Once again, close-up images of these cells revealed that the GATA-3 staining co-localised with the nucleus of the cells and that the surface expression of KLRG-1 and ICOS did not coincide with CD3 expression, thus confirming that these are very likely ILC2 and not GATA-3^{+} T cells.

3.3.2 ILC3 cluster in interfollicular areas of LNs

Whilst innate lymphoid cells are a rare cell type in WT lymph nodes, immunofluorescence microscopy staining has shown group 3 ILCs to cluster within highly specific areas in all LNs analysed, therefore increasing the potential for even a small population of cells to exert effects on others.

Large numbers of RORγt^{+} CD3^{-} IL-7Rα^{+} ILC3s could be found to cluster in the interfollicular areas of lymph nodes and at the B-T interface of mLNs (Figure 3.9a). These clusters could be observed within many, although not all, interfollicular areas. Large numbers of RORγt-expressing cells could also be detected in similar areas of other lymph nodes analysed in this study; the peripheral tissue-draining iLN (Figure 3.9b) and popLN

Figure 3.9 ILC3 can be detected in interfollicular regions of all LNs analysed

Representative immunofluorescence microscopy images of WT LN tissue sections. All images are tilescanned.

Sections all counterstained with DAPI.

a) Image showing interfollicular areas of WT mLN stained for expression of RORγt, CD3 and IL-7Rα. Scale bar represents 100μm.

b) Image showing interfollicular areas of WT iLN stained for expression of RORγt, CD3 and IL-7Rα. Scale bar represents 100μm.

c) Image showing popLN (top) and medLN (bottom) stained for expression of RORγt, CD3 and IL-7Rα, scale bar is 100μm. Images on right are zoomed in versions of numbered ROIs (highlighted by dashed white rectangle)of each LN, scale bar is 20μm.

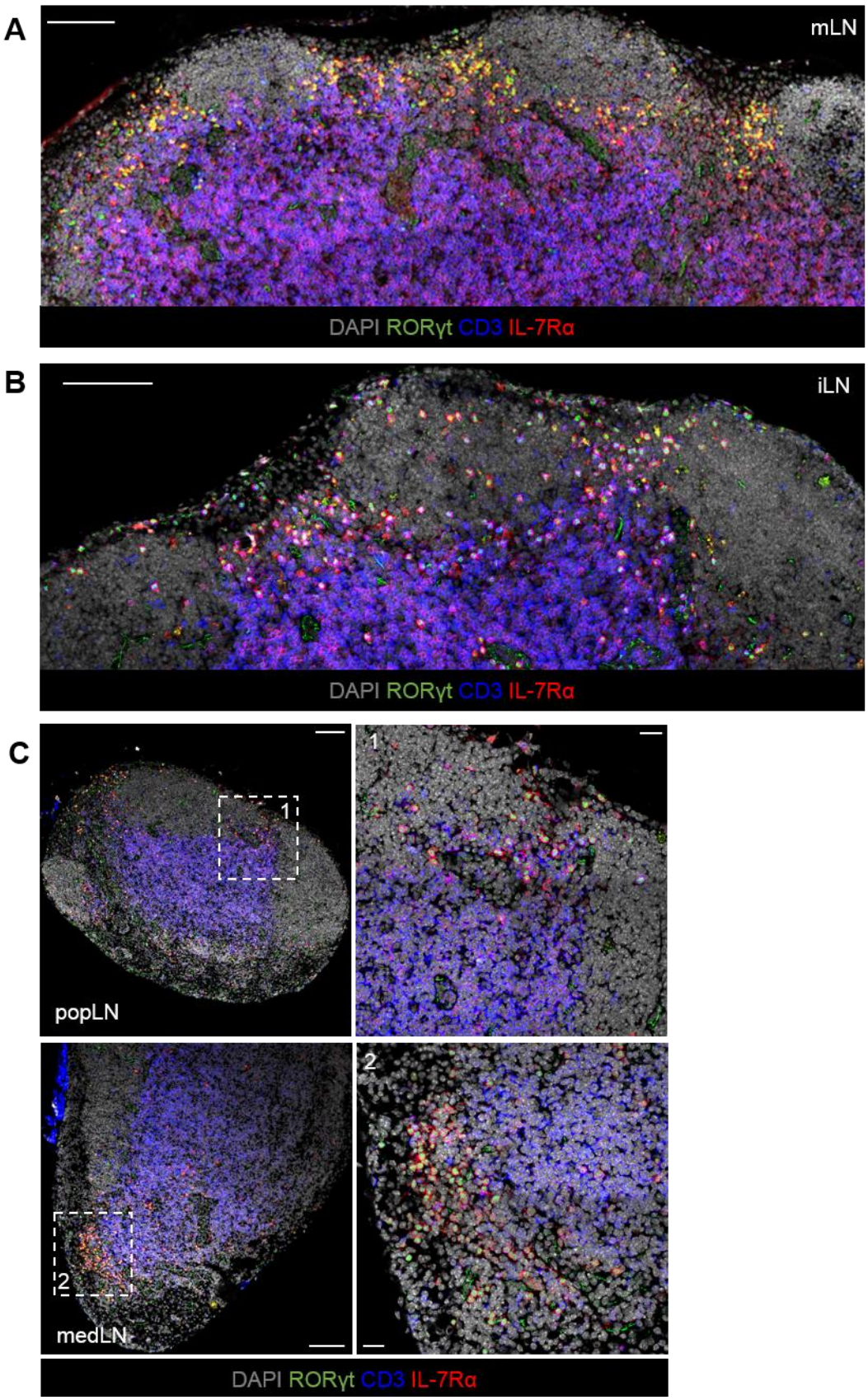
A
mLN
DAPI RORγt CD3 IL-7Rα
B
iLN
DAPI RORγt CD3 IL-7Rα
C
1
popLN
1
2
2
medLN
DAPI RORγt CD3 IL-7Rα

Fig. 3.9

(Figure 3.9c), and the mucosal tissue-draining medLN (Figure 3.9c), suggesting that the location of these cells does not change notably between lymph nodes at different sites. Upon further inspection, however, it became clear that although RORγt^{+} CD3^{-} IL-7Rα^{+} ILC3s could be detected in these regions in peripheral LNs, many of the RORγt-expressing cells present in fact expressed CD3 and were therefore RORγt^{+} T cells. Quantification of the proportion of RORγt-expressing, IL-7Rα^{hi} cells in the interfollicular areas of these LNs which lacked expression of CD3 revealed that there was indeed a significant difference. Tissues were analysed as shown in Figure 3.10a, with interfollicular areas here defined as the area between the B cell follicles and extending to the central points of each follicle, therefore including those cells which can be found to reside at the B-T interface. Proportions were calculated from the total RORγt^{+} IL-7Rα^{hi} cells within each defined area. This analysis revealed that those RORγt-expressing cells observed in the peripheral draining popliteal and inguinal LNs were indeed predominantly T cells (Figure 3.10b), although ILC3 were still present, and that this phenotype did not differ significantly between these two lymph nodes. In contrast, these areas in mLNs contained many RORγt^{+} ILC3 (Figure 3.10b) and relatively few RORγt-expressing T cells, a phenotype which was statistically significantly different to both peripheral LNs analysed. Notably, the medLN also had a large proportion of ILC3 within these areas, and although this phenotype was less defined than that seen in the mLN it was indicative of ILC3-enriched microenvironments existing in mucosal-draining LNs which were not found in those which drained the skin (Figures 3.10b).

3.3.3 ILC3 expression of chemokine receptors

The signals which attract ILC3s to this distinct location are not known, although one explanation has been the balance of chemokine receptors on their surface (Lane et al.,

2009). ILC3s have been reported to express mRNA for the chemokine receptors CXCR5, which binds the chemokine CXCL13, and CCR7 (Kim et al., 2008), which binds to CCL19 and CCL21. Within the organised microarchitecture of LNs CXCL13 facilitates the segregation of B cells, which express CXCR5, into B cell follicles (Ansel et al., 2000), whilst signalling through CCR7 attract T cells to the paracortical, T cell-dominated zone (Worbs et al., 2007). Up or down-regulation of either molecule results in the movement of cells to the B-T interface, a phenomenon which enables B and T lymphocytes to interact following activation (Ansel et al., 1999). To investigate further the proposal that it is the expression of these receptors which dictates ILC3 location, cell-surface expression of CXCR5 and CCR7 was analysed under different conditions.

Cells were cultured overnight, to allow for the testing of different conditions on chemokine receptor expression, before being analysed by flow cytometry. High levels of CXCR5 were detected on the surface of both Lin^+ IL-7Rα^- 'B cells' and Lin^- IL-7Rα^+ RORγt^+ ILCs (Figure 3.11a). Approximately half of ILC3 were found to express this receptor and no significant difference between ILC3s from mLNs and those from a pool of peripheral LNs (pLNs) could be detected (Figure 3.11c). Notably CXCR5 expression was primarily detected on ILCs which expressed RORγt, suggesting that neither ILC1 nor ILC2 express this marker to any great extent under these conditions (Figure 3.11b). CCR7, in contrast, was detected on Lin^+ $CD3i^+$ IL-7Rα^+ T cells but not on any ILC subset (Figure 3.11a-c). It could be possible that expression of mRNA for this molecule in ILC3s (Kim et al., 2008) does not result in functional cell surface expression under these circumstances, or alternatively that, although detectable on our positive T cell control population, the level of this marker on ILC subsets is below our level of detection by flow cytometry and a more sensitive method should be used. These results indicated that, in terms of CXCR5

Figure 3.10 RORγt$^+$ T cells co-localise with ILC3 in peripheral LNs

Representative immunofluorescence microscopy images of WT LN tissue sections. All scale bars are 100μm.

Sections all counterstained with DAPI, data representative of (a) or pooled from 1-3 interfollicular areas from 3 WT mice. Statistical test used is Mann-Whitney non-parametric, two-tailed test. *P<0.05, **P<0.01, ***P<0.001 and ****P<0.0001.

a) Images from analysis of interfollicular areas in stated LNs (detailed in bottom left hand corner). Interfollicular areas were defined as areas between follicles and to the mid-point of B-T interface. RORγt$^+$ IL-7Rα^{hi} cells are circled, those which express CD3 in white, and those which are CD3$^-$ in yellow.

b) Graph showing percentage of RORγt$^+$ IL-7Rα^{hi} cells within these regions which are CD3$^-$ ILC3s.

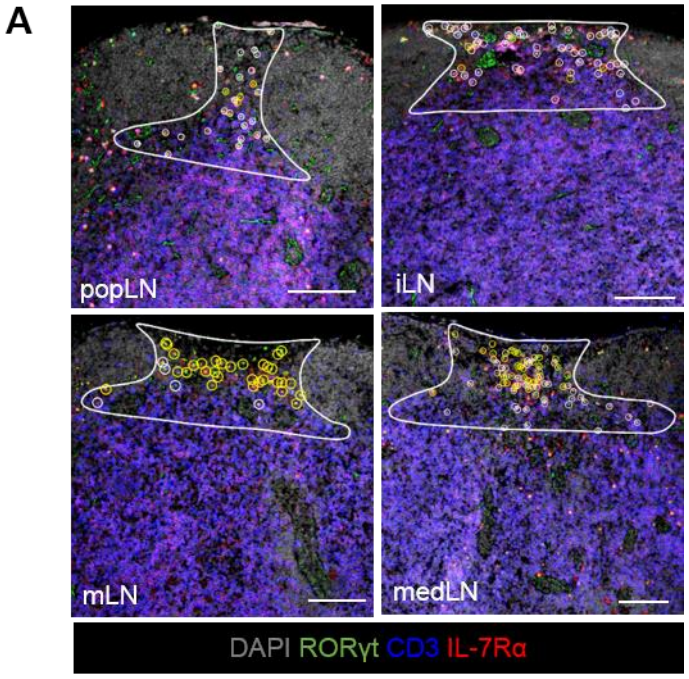
A
popLN
iLN
mLN
medLN
DAPI RORγt CD3 IL-7Rα
B
% of RORγt^hi IL-7Rα^hi cells
100
80
60
40
20
0
**
ns
popLN
iLN
mLN
medLN

Fig. 3.10

expression, ILC3 in pLNs and mLNs analysed did not differ significantly. Interestingly, CXCR5 expression did seem to correlate with high expression of RORγt, with a RORγt^{lo} population appearing CXCR5^{-} (Figure 3.11b). Whether or not these cells locate differently within tissues as a result is yet to be seen, and further work would be needed to ensure that this population exists within directly *ex vivo*, un-cultured tissue.

We also investigated whether any change in chemokine receptor expression, and therefore potentially location, could be induced by the introduction of TLR-ligand Pam3CSK4—a lipoprotein which resembles the acylated amino terminus of bacterial lipopolysaccharide (LPS) and has been shown to bind to TLR1 and TLR2 (Jin et al., 2007) —into the cell culture medium. Although this system did not differentiate between whether ILC3 were responding to TLR-ligands directly or indirectly (as the culture was set up using non-sorted lymph node cell suspension), a statistically significant reduction in the percentage of ILC3 which expressed CXCR5 was observed when compared to culture only controls. This correlated with a lower median fluorescence intensity (MFI) of staining on those ILC3s which were CXCR5^{+}, indicative of downregulation of CXCR5 expression on the surface of even those cells which remained positive. In both mLN (Figure 3.12a,c) and pLNs (Figure 3.12e) there was a significant reduction in the percentage of ILC3 which expressed CXCR5 compared to culture only controls. Additionally there was also a clear reduction in the intensity of CXCR5 staining on those ILC3s which were CXCR5^{+} following treatment with TLR ligands, indicative of downregulation of CXCR5 from the surface of even those cells which remained positive (Figure 3.12a,b). When the MFI of CXCR5 expression by CXCR5^{+} ILC3 and CXCR5^{+} 'B cells' was analysed under each condition there was significantly less CXCR5 detected on the surface of CXCR5^{+} ILC3s treated with TLR ligands in both mLN and pLN, whilst the MFI of

Figure 3.11 Expression of chemokine receptors by ILCs

Cells isolated from LNs of naïve WT mice as specified in methods. Peripheral LNs (pLNs) are a pool of axillary LN, brachial LN and inguinal LNs. All cells cultured overnight at 37°C in culture media prior to analysis by flow cytometry.

All bars shown on graphs represent the median value. Data is representative of (a,b) or pooled (c,d) from 3 independent experiments. Statistical test used is Mann-Whitney non-parametric, two-tailed test. **P*<0.05, ***P*<0.01, ****P*<0.001 and *****P*<0.0001.

a) FACS plots showing CCR7 expression by Lin^+ IL-$7R\alpha^+$ $CD3i^+$ T cells, CXCR5 expression by Lin^+ IL-$7R\alpha^-$ $CD3i^-$ 'B cells' (top) and both CXCR5 and CCR7 expression by Lin^- IL-$7R\alpha^+$ $ROR\gamma t^+$ ILCs (bottom, pre-gated on Lin^- IL-$7R\alpha^+$ cells highlighted in red) isolated from WT mLN. Lin is CD3/CD5/B220/CD11c.

b) CXCR5 and CCR7 staining on all Lin^- IL-$7R\alpha^+$ cells from WT mLN.

c) Graphs showing the percentage of $ROR\gamma t^+$ ILC3 which express CXCR5 (left) or CCR7 (right) in pLNs and mLN of WT mice.

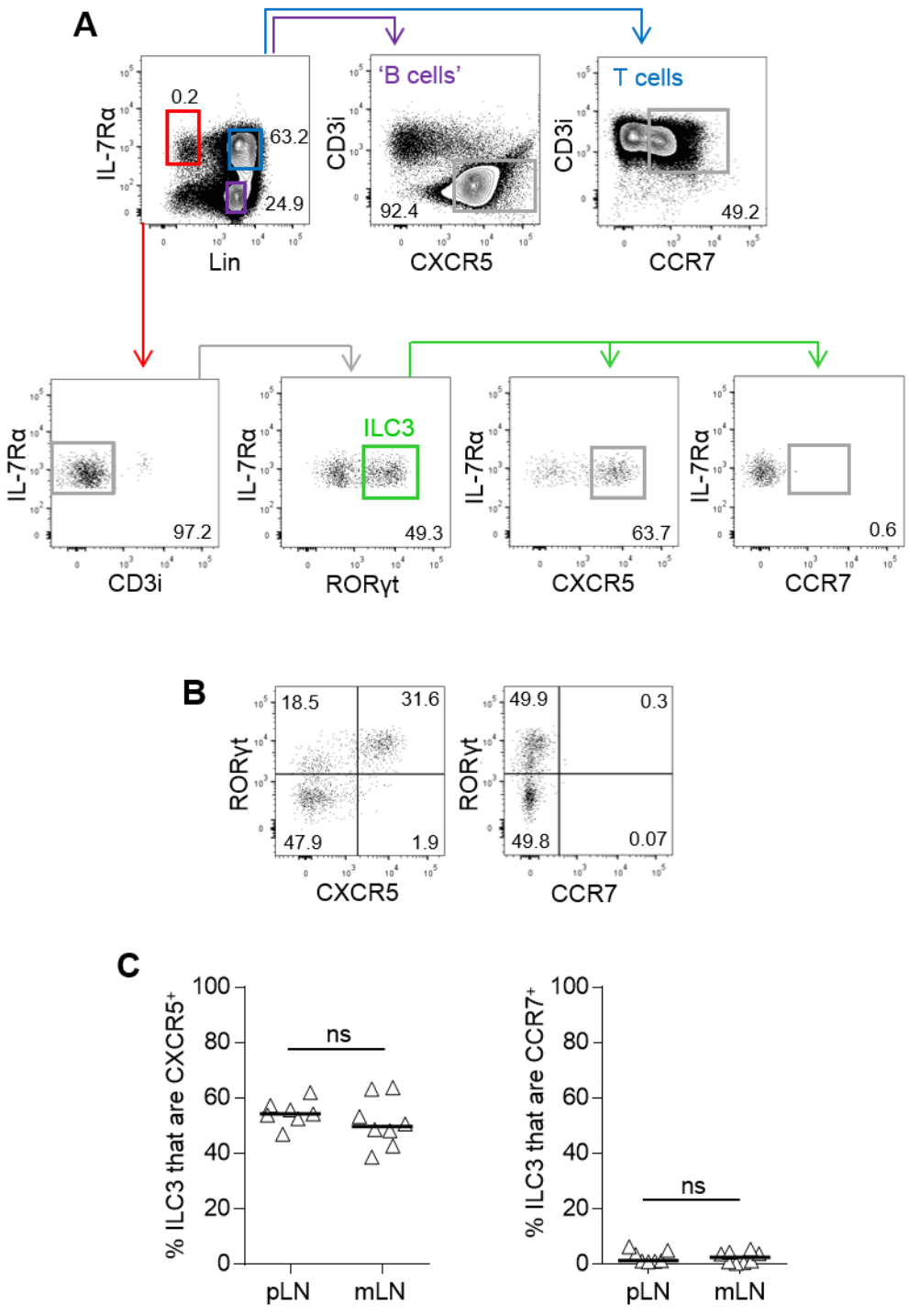
A
IL-7Rα
Lin
0.2
63.2
24.9
'B cells'
CD3i
CXCR5
92.4
T cells
CD3i
CCR7
49.2
IL-7Rα
CD3i
97.2
IL-7Rα
RORγt
ILC3
49.3
IL-7Rα
CXCR5
63.7
IL-7Rα
CCR7
0.6
B
RORγt
CXCR5
18.5
31.6
47.9
1.9
RORγt
CCR7
49.9
0.3
49.8
0.07
C
% ILC3 that are CXCR5+
100
80
60
40
20
0
ns
pLN
mLN
% ILC3 that are CCR7+
100
80
60
40
20
0
ns
pLN
mLN

Fig. 3.11

CXCR5 expression on CXCR5$^+$ B cells by comparison significantly increased in treated samples (Figure 3.12b,d,f). It is not at this point clear whether or not this is indicative of ILC migration away from the B cell follicles in response to the presence of ligands which stimulate TLRs, and therefore a phenotype that might be seen *in vivo* upon immunological challenge.

LTi cells have been shown to be highly dependent upon the cytokine IL-7 for support in adult tissue (Schmutz et al., 2009) and fittingly express high levels of the IL-7 receptor, IL-7Rα. Lymphatic epithelial cells (LECs) within the interfollicular regions of LNs have been shown to produce IL-7 (Onder et al., 2012), therefore we hypothesised that the clustering of ILC3 in these regions reflected a requirement for vital survival signals. To examine the relationship between IL-7 signalling and the expression of CXCR5 on the surface of ILC3 we added IL-7 to the culture medium and compared to culture-only controls. Binding of IL-7 and signalling through IL-7Rα results in the downregulation of IL-7Rα in mature T cells (Park et al., 2004), and this has been proposed to prevent excess consumption of this cytokine. In the presence of IL-7 not only did T cells downregulate expression of IL-7Rα, but 'helper-like' ILCs also (Figure 3.13a). In cultures with added IL-7 very few cells were found to express IL-7Rα in comparison to the culture only controls, evidence that IL-7 signalling had indeed taken place, and the gating strategy was adapted accordingly (Figure 3.13a). By nature of this method there was contamination of a small population of IL-7Rα$^-$ RORγt$^+$ cells within the ILC3 gate, however both culture only and treated samples were directly comparable. Interestingly, when both culture only and IL-7 treated mLN samples were compared there was no statistically significant difference in the number of ILC3, indicating that within this time increased levels of IL-7 did not impact survival (Figure 3.12b), and that the loss of a distinct IL-7Rα$^+$ Lin$^-$ population of cells in this

Figure 3.12 ILC3 downregulate CXCR5 in presence of TLR ligands

Cells isolated from LNs of naïve WT mice as specified in methods. Peripheral LNs are pool of axillary LN, brachial LN and inguinal LNs. All cells cultured overnight at 37°C in culture media +/- Pam3CSK4 TLR1/2 agonist (TLRL) prior to analysis by flow cytometry.

All bars shown on graphs represent the median value. Data is representative of (a,b) or pooled (c-f) from 3 independent experiments. Statistical test used is Mann-Whitney non-parametric, two-tailed test. **P*<0.05, ***P*<0.01, ****P*<0.001 and *****P*<0.0001.

MFI; median fluorescence intensity, TLRL; TLR ligand.

a) FACS plots showing expression of CXCR5 by RORγt$^+$ ILC3 from WT mLN following overnight culture with (bottom) or without (top) TLRL. Gated as shown in Figure 3.11a.

b) Histograms showing the level of CXCR5 expression on Lin$^+$ IL-7Rα$^-$ 'B cells' (left) and Lin$^-$ IL-7Rα$^+$ RORγt$^+$ ILC3 (right) from WT mLN, as gated in Figure 3.1a. Blue line represents cells which have been cultured overnight with TLRL, grey filled histogram shows cells from culture media only controls. Y axis is normalised to mode.

c) Percentage of RORγt$^+$ ILC3 in mLN samples +/- TLRL which are CXCR5$^+$.

d) MFI of CXCR5 staining on CXCR5$^+$ ILC3 (left) and CXCR5$^+$ 'B cells' (right) from mLN samples +/- TLRL. Y axis on leftmost graph applies to both.

e) Percentage of RORγt$^+$ ILC3 in pLN samples +/- TLRL which are CXCR5$^+$.

f) MFI of CXCR5 staining on CXCR5$^+$ ILC3 (left) and CXCR5$^+$ 'B cells' (right) from mLN samples +/- TLRL. Y axis on leftmost graph applies to both.

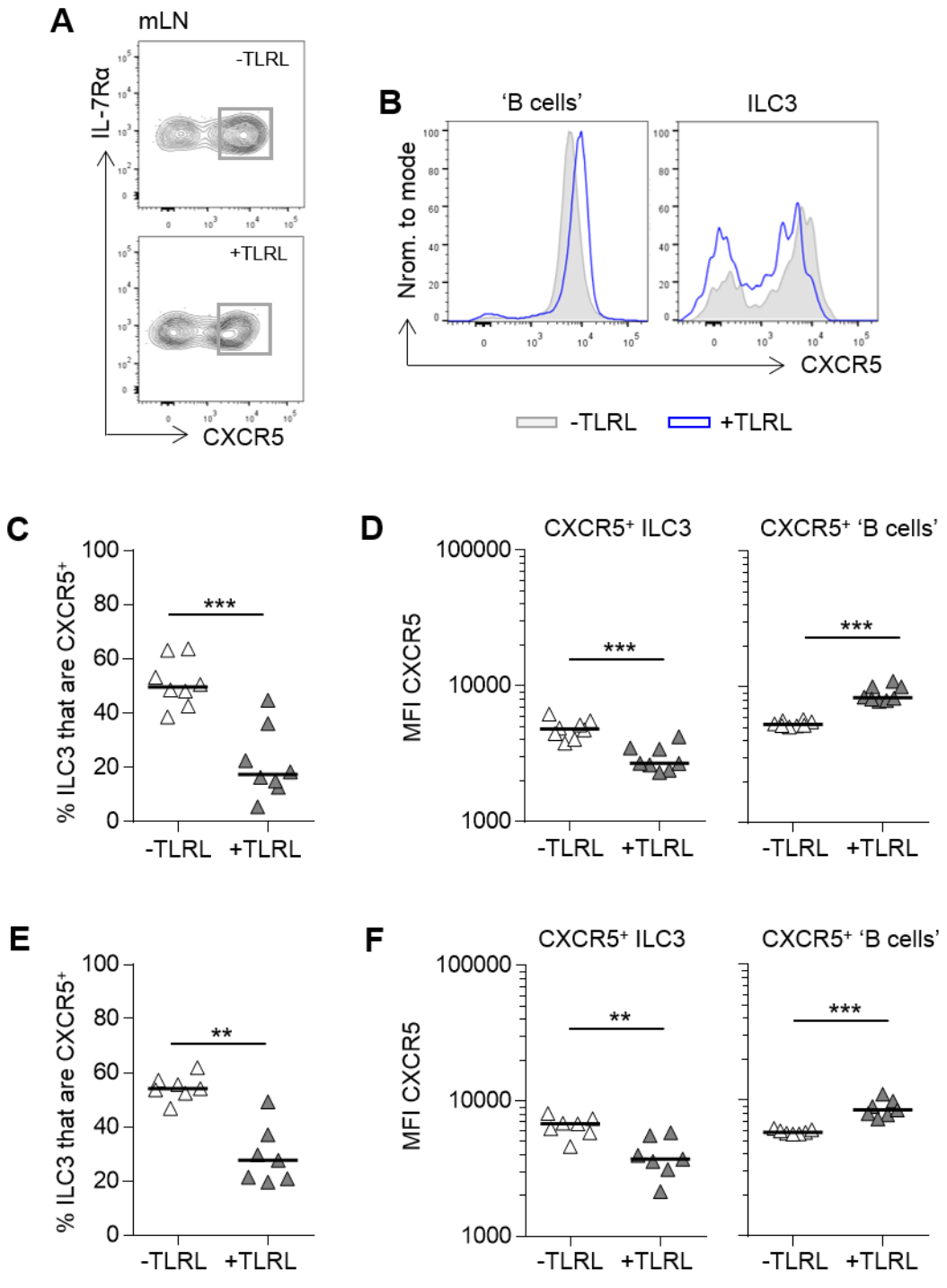
A
mLN
-TLRL
+TLRL
IL-7Rα
CXCR5
B
'B cells'
ILC3
Nrom. to mode
CXCR5
-TLRL
+TLRL
C
% ILC3 that are CXCR5+
***
-TLRL
+TLRL
D
CXCR5+ ILC3
CXCR5+ 'B cells'
MFI CXCR5
100000
10000
1000
***
***
-TLRL
+TLRL
E
% ILC3 that are CXCR5+
**
-TLRL
+TLRL
F
CXCR5+ ILC3
CXCR5+ 'B cells'
MFI CXCR5
100000
10000
1000
**
***
-TLRL
+TLRL

Fig. 3.12

Figure 3.13 ILC3 downregulate CXCR5 moderately in presence of IL-7

Cells isolated from LNs of naïve WT mice as specified in methods. Peripheral LNs are pool of axillary LN, brachial LN and inguinal LNs. All cells cultured overnight at 37°C in culture media +/- IL-7 prior to analysis by flow cytometry.

All bars shown on graphs represent the median value. Data is representative of (a,b) or pooled (c,d) from 3 independent experiments. Statistical test used is Mann-Whitney non-parametric, two-tailed test. **P*<0.05, ***P*<0.01, ****P*<0.001 and *****P*<0.0001.

a) FACS plots showing gating strategy for RORγt$^+$ ILCs from WT mLN following overnight culture with (bottom) or without (top) IL-7. Lin is CD3/CD5/B220/CD11c.

b) Graph showing the total number of ILC3 per sample following overnight culture of the same number of cells +/- IL-7. Cells from WT mLN.

c) Graph showing the percentage of RORγt$^+$ ILC3 which are CXCR5$^+$ in mLN (left) and pLN (right) samples following overnight culture +/- IL-7.

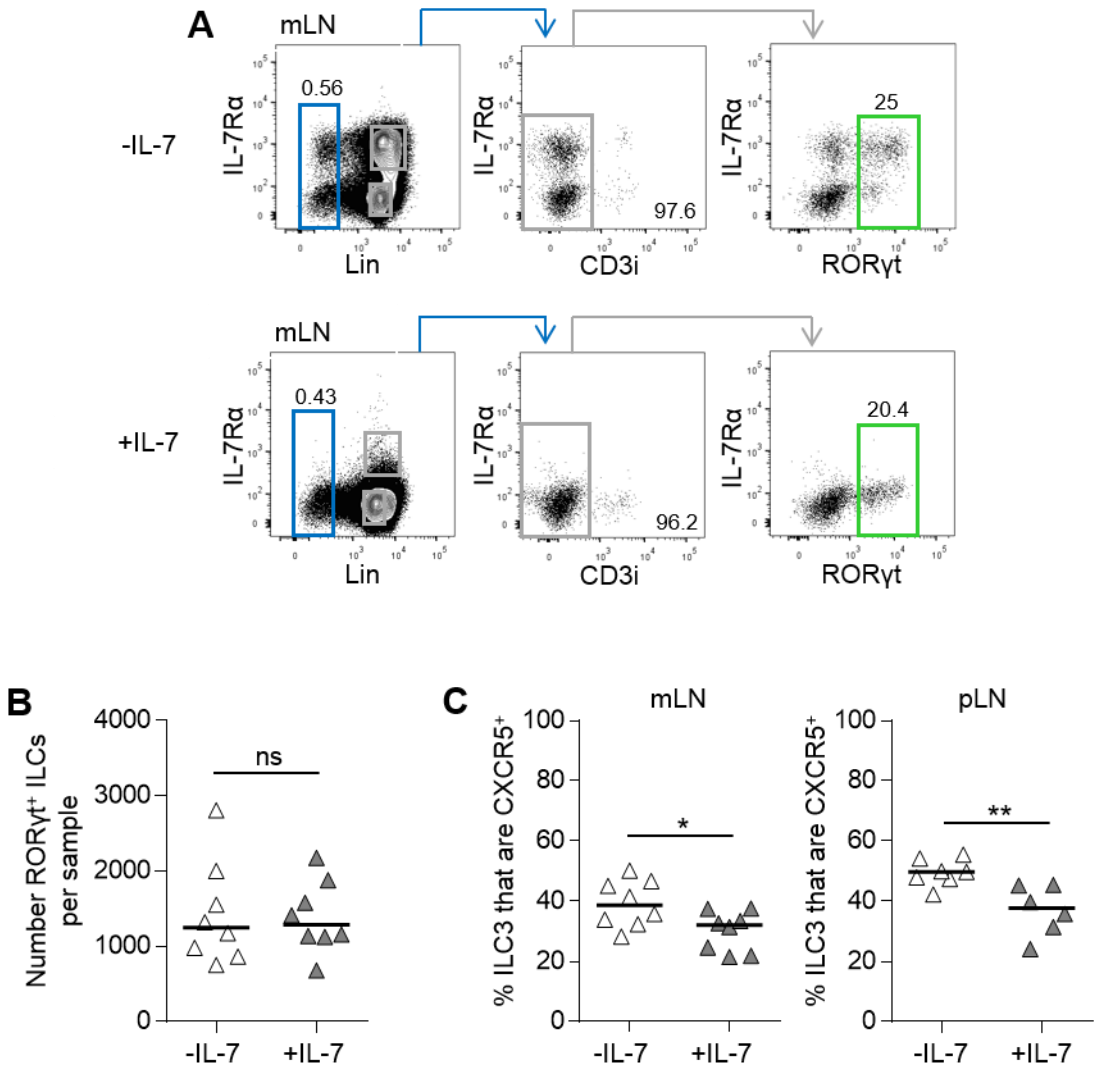
A
mLN
-IL-7
+IL-7
IL-7Rα
Lin
CD3i
RORγt
0.56
97.6
25
0.43
96.2
20.4
B
Number RORγt+ ILCs per sample
4000
3000
2000
1000
0
ns
-IL-7
+IL-7
C
mLN
pLN
% ILC3 that are CXCR5+
100
80
60
40
20
0
*
**
-IL-7
+IL-7

Fig. 3.13

experiment was not the result of ILC3 cell death. There was however a decrease in the percentage of ILC3 which expressed CXCR5 in both mLN and pLN cultures where IL-7 was present but, although statistically significant, the decrease was only moderate (Figure 3.12c).

3.3.4 RORγt$^+$ cell types in peripheral versus mucosal LNs

Whilst investigating the interfollicular areas of peripheral tissue-draining LNs it was noted that populations of RORγt-expressing T cells could be found within these regions, which were not detectable within the mucosal tissue-draining mLN. To further explore this observation an analysis of all RORγt$^+$ IL-7Rα$^+$ cells within iLN, bLN and mLN was carried out. RORγt-expressing cells appeared to constitute a higher proportion of total cells in the iLN and bLN than in the mLN (Figure 3.14a), and large populations of RORγt$^+$ T cells which were present in the iLN were notably absent in the mLN (Figure 3.14a,b). In keeping with both flow cytometry and immunofluorescence microscopy data, CD3$^-$ cells which resembled ILC3 made up a higher proportion of total RORγt-expressing cells in the mLN than in the iLN or bLN (Figure 3.14b,c), indicative of an increased importance for these cells at this site. RORγt-expressing cell populations in iLN and bLN tissue were found to be largely similar. The dominant RORγt-expressing populations in these LNs were a population of RORγt$^+$ γδ T cells and a population of γδTCR$^-$ T cells which expressed very high levels of IL-7Rα (Figure 3.14c). The identity of this cell type was not established in this investigation, however both of these RORγt-expressing IL-7Rα^{hi} T cells and γδ T cells were found to be largely absent in the mLN (Figure 3.14a-c). It therefore seems likely, although not definitively shown, that these two populations account for the differences detected in the interfollicular areas of peripheral LNs. A more detailed flow cytometric analysis into the phenotype of these cell types was later reported (Mackley et al., 2015).

Figure 3.14 Predominant RORγt-expressing cell types differ in peripheral and mucosal tissue-draining LNs

Cells isolated from LNs of naïve WT mice as specified in methods. Samples were analysed by flow cytometry.

All bars shown on graphs represent the median value. Data is representative of (a) or pooled (b,c) from 2 (mLN) or 3 (iLN, bLN) independent experiments. Statistical test used is Mann-Whitney non-parametric, two-tailed test. *P<0.05, **P<0.01, ***P<0.001 and ****P<0.0001.

a) FACS plots showing gating on populations of RORγt$^+$ IL-7Rα$^+$ cells (pre-gated on FSC and SSC).

b) Graphs comparing percentage of total RORγt$^+$ IL-7Rα$^+$ cells which are named cell types in iLN (n=12) and mLN (n=8).

c) Graphs showing the percentage of total RORγt$^+$ IL-7Rα$^+$ cells which are stated cell populations in iLN, bLN and mLN. (n=12,11,8). Y axis on leftmost graph applies to all.

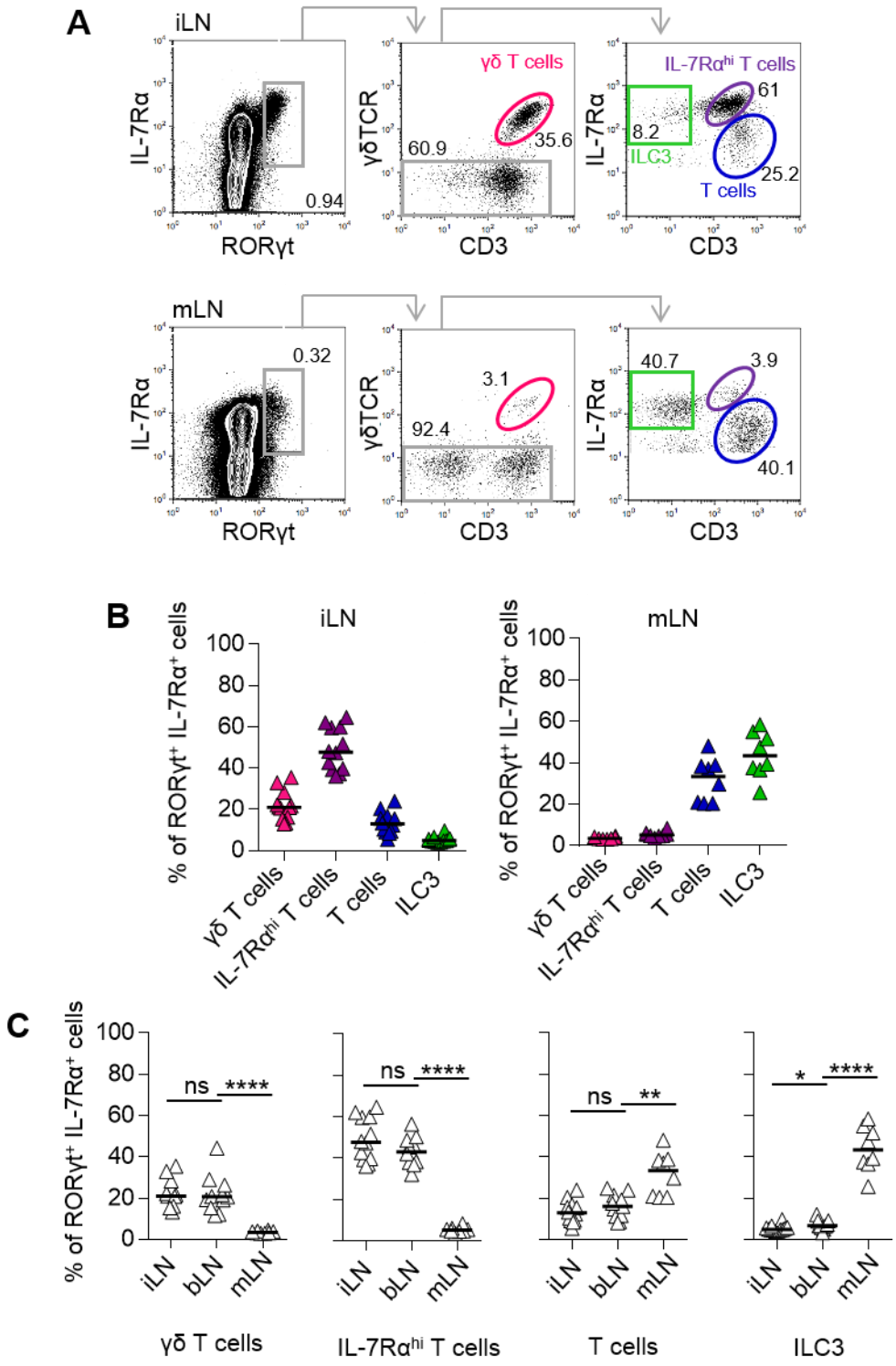
A
iLN
IL-7Rα
RORγt
0.94
γδTCR
CD3
γδ T cells
60.9
35.6
IL-7Rα
CD3
IL-7Rα^hi T cells
61
8.2
ILC3
25.2
T cells
mLN
0.32
3.1
92.4
40.7
3.9
40.1
B
iLN
mLN
% of RORγt+ IL-7Rα+ cells
γδ T cells
IL-7Rα^hi T cells
T cells
ILC3
C
ns
****
**
*
iLN
bLN
mLN
γδ T cells
IL-7Rα^hi T cells
T cells
ILC3

Fig. 3.14

3.3.5 Interfollicular regions are unaffected by the loss of RORγt^{+} cells

The specific deletion of ILCs is made challenging by their similarities to other cell types, including T cells. The most elegant methods of deletion require sophisticated mouse models, however it is possible to gain an indication of the result of removing ILCs by using bone marrow chimera mice and antibody-mediated depletion. To analyse the importance of RORγt-expressing cells within the interfollicular microenvironment of LNs, we generated chimeric mice by lethally irradiating RORγt$^{+/-}$ hosts and subsequently reconstituting with either WT or RORγt$^{-/-}$ bone marrow. Enhanced depletion of ILC3s, which are known to be resistant to irradiation (Dudakov et al., 2012), was achieved by the subsequent treatment with anti-CD90 or control antibody, with CD90 expressed by all ILC subsets (Walker et al., 2013). Although not ILC3-specific, as this method results in the absence of all RORγt-expressing cell types and non-specific targeting of CD90^{+} cell populations, it did allow us to study the lack of ILC3 in a mouse where LNs are still present and the opportunity to explore the effect of the loss of RORγt-expressing cell types from the interfollicular areas where they cluster.

Gating on cells which were Lin^{-} IL-7Rα^{+} revealed that three populations of ILC could be detected within iLNs of RORγt$^{+/-}$:WT chimeras based on expression of GATA-3 and RORγt, and therefore the reconstitution of our irradiated hosts had been successful (Figure 3.15a). By comparison in RORγt$^{+/-}$:RORγt$^{-/-}$ chimeras no population of RORγt^{+} ILCs could be detected, showing not only that these mice had been reconstituted with RORγt$^{-/-}$ bone marrow, but also that the irradiation and anti-CD90 depletion of existing ILC3s within host lymph nodes had been effective (Figure 3.15a,b). Despite the efficiency of this

Figure 3.15 Interfollicular regions of LNs appear unchanged in absence of RORγt-expressing cells

Chimeras were generated by lethally irradiating RORγt$^{+/-}$ mice before hosts reconstituting with WT or RORγt$^{-/-}$ bone marrow cells. WT:RORγt$^{-/-}$ mice were further treated with anti-CD90.2 antibody. iLNs were analysed by flow cytometry and mLNs by immunofluorescence microscopy.

All bars shown on graphs represent the median value. Data from 1 independent experiment, and images (d,e) representative of mLNs from 3 in RORγt$^{+/-}$:WT and 6 RORγt$^{+/-}$:RORγt$^{-/-}$ mice.

a) FACS plots showing gating strategy for ILC populations in iLNs of RORγt$^{+/-}$:WT or RORγt$^{+/-}$:RORγt$^{-/-}$ chimeras. Lin is CD3/B220/CD11b/CD11c.

b) Graph showing the number of each RORγt^{+} ILCs per iLN in RORγt$^{+/-}$:WT (WT) and RORγt$^{+/-}$:RORγt$^{-/-}$ (KO) chimeras. (n=2,6).

c) Image showing area of RORγt$^{+/-}$:WT and RORγt$^{+/-}$:RORγt$^{-/-}$ mLN tissue stained for expression of RORγt, CD3 and IL-7Rα. Scale bar represents 100μm.

d) Image showing similar areas of mLN in RORγt$^{+/-}$:WT and RORγt$^{+/-}$:RORγt$^{-/-}$ chimeras, stained for expression of IgM, MadCAM-1 and CD3. Scale bar represents 100μm.

e) Image showing similar areas of mLN in RORγt$^{+/-}$:WT and RORγt$^{+/-}$:RORγt$^{-/-}$ chimeras, stained for expression of F4/80 and CD169. Scale bar represents 100μm.

f) Image showing similar areas of mLN in RORγt$^{+/-}$:WT and RORγt$^{+/-}$:RORγt$^{-/-}$ chimeras, stained for expression of RANKL and IgM. Scale bar represents 100μm.

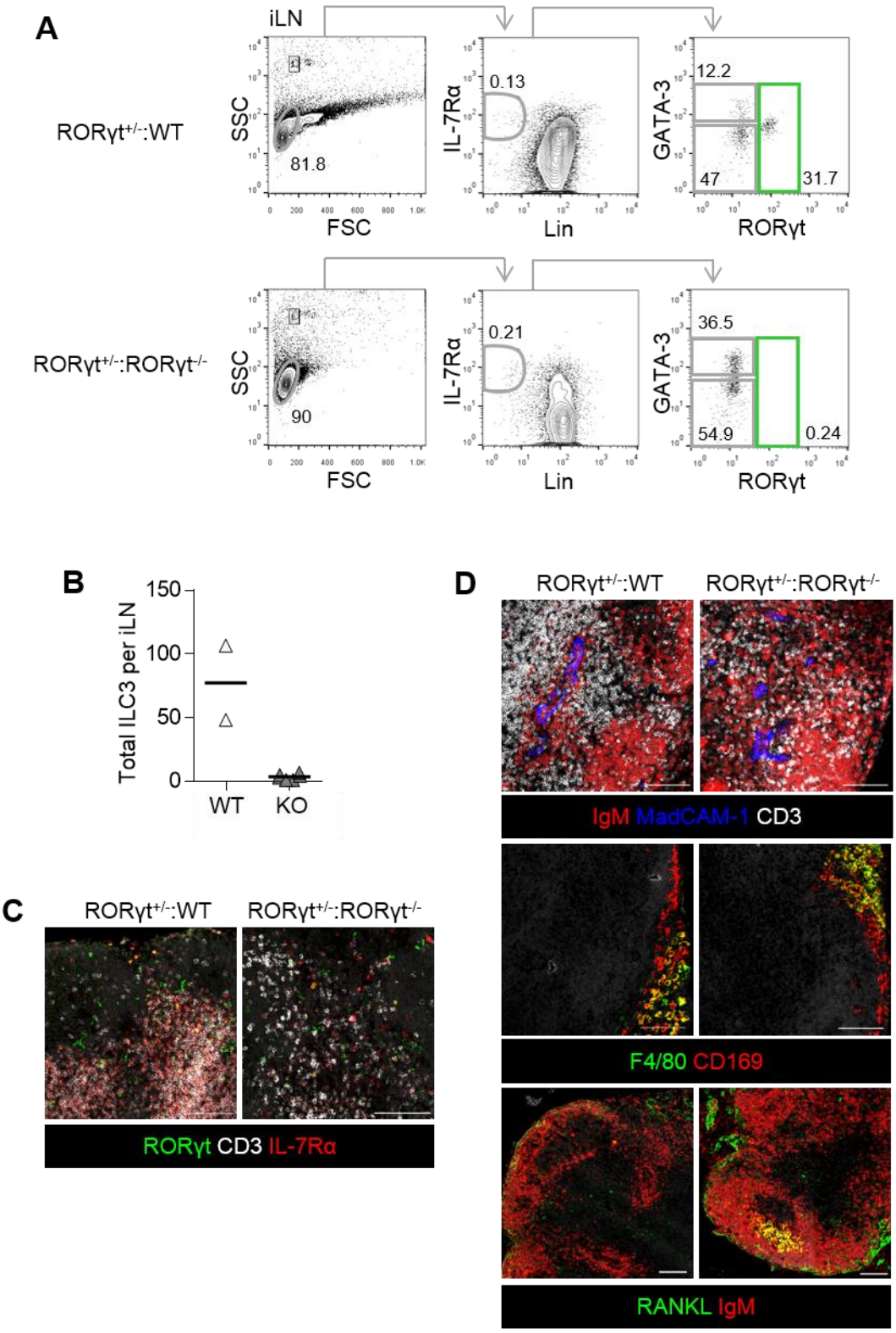
A
iLN
RORγt+/-:WT
RORγt+/-:RORγt-/-
SSC
FSC
81.8
90
IL-7Rα
Lin
0.13
0.21
GATA-3
RORγt
12.2
47
31.7
36.5
54.9
0.24
B
Total ILC3 per iLN
150
100
50
0
WT
KO
C
RORγt+/-:WT
RORγt+/-:RORγt-/-
RORγt CD3 IL-7Rα
D
RORγt+/-:WT
RORγt+/-:RORγt-/-
IgM MadCAM-1 CD3
F4/80 CD169
RANKL IgM

Fig. 3.15

depletion a small number of RORγt^{+} ILCs could still be detected in mLN tissue by immunofluorescence microscopy, an observation which we were later able to explain by different rates of efficiency in removal of these cells by irradiation in mLN and peripheral LNs, however their number was much reduced when compared to controls (Figure 3.15c).

The overall structure of the mLN remained similar, suggesting that the loss of RORγt-expressing cells does not result in notable morphological changes, however there were notably fewer CD3^{+} cells within RORγt$^{+/-}$:RORγt$^{-/-}$ lymph nodes. The reason for this is unknown, but could be as a result of the use of anti-CD90 antibodies which can also target T cells. Although chimeras were not analysed for a number of weeks following antibody treatment, it cannot be discounted that this could account for any effects that we observe. The presence HEVs, as based on expression of MadCAM-1, did not appear to be perturbed and detection of IgM showed the location of B cell follicles (Figure 3.15d). Macrophages have been reported to line the subcapsular sinus of LNs (Junt et al., 2007), and could be detected in this study by their expression of F4/80 and CD169, but did not appear to be affected by the loss of RORγt-expressing cells within these regions. Additionally, within the subcapsular region resides a population of marginal reticular cells (MRCs) which have been reported to RANKL, otherwise known as TRANCE (Katakai et al., 2008), with no detectable loss of this stromal layer in the absence of RORγt-expressing cells (Figure 3.15d).

3.4 SUMMARY

In depth characterisation of ILC subsets in a range of LNs has revealed differences between those LNs which drain mucosal tissues and those which drain peripheral tissues, such as the skin. I have found that ILCs which express RORγt are more numerous in mLN

tissue than in either the bLN or iLN, and form a higher proportion of total ILCs in both the medLN and mLN—LNs which drain the mucosal surfaces of the respiratory tract and gut respectively—than in those LNs which drain the peripheral tissues. Analysis of total RORγt-expressing cells within a selection of these LNs has revealed that, whilst ILC3 make up the highest proportion of RORγt^{+} IL-7Rα^{+} cell types in the mLN, RORγt^{+} T cell populations dominate in the iLN and bLN. This finding fits with our observation of RORγt^{+} T cells clustering in the interfollicular areas of iLNs, regions which, in the mLN, were primarily occupied by ILC3. These observations taken together appeared indicative of an increased requirement for ILC3 within those LNs which drain mucosal tissues. A higher percentage of ILC3 expressed MHCII in the mLN compared to either the iLN or bLN, perhaps indicative of an increased requirement for ILC3-expressed MHCII in this LN which drains the gut.

Interestingly, the ILC composition of mLNs from T cell-deficient mice differed considerably from those of WT mice. Markedly fewer ILC3 were detected in mLNs from RAG$^{-/-}$ mice, which lack both mature T and B lymphocytes, despite there being similar numbers of each ILC subset in iLNs. A similar phenotype was apparent in ZAP-70$^{-/-}$ mice, where mature T cells are absent but B cells and LN B cell follicles are still present, suggesting that this phenotype was not due to the lack of organised lymphoid architecture and subsequent effects on ILC3. Strikingly, ILC2 were now the predominant ILC population in these LNs, present at much higher numbers than seen in WT controls. This seemed unlikely to be a broad effect on ILC development in this mice, since iLNs of RAG$^{-/-}$ mice did not show the same trend. The reason for fewer ILC3 in T cell-deficient mLNs is unknown, however whether or not the large numbers of ILC2 detected instead is as a result of their absence would be interesting to explore further.

All three groups of ILC could be detected in all WT LNs analysed, and strikingly ILC2 could be detected within the interfollicular areas of the mLN alongside ILC3. The location of ILC1 has not yet been elucidated, in part due to our focus on group 2 and group 3 ILC subsets, but also because of difficulties in staining for T-bet expression. Why these cells sit in these areas is not yet known, and we explored whether this was due to a balance of chemokine receptors on the cell surface. CXCR5 could be detected on the surface of ILC3, but not ILC2, and CCR7 was not detectable by the methods used, despite CCR7 mRNA in LTi cells having previously been reported (Kim et al., 2008). We determined that various factors could affect CXCR5 expression by ILC3 *in vitro*. Inclusion of a TLR1/2 agonist resulted in a lower percentage of ILC3 expressing CXCR5, and apparent downregulation of CXCR5 levels on those which remained CXCR5^{+}. What was not clear from this study was whether this effect was as a result of direct signalling to ILC3, as human LTi-like ILCs have been reported to express TLR2 (Crellin et al., 2010), or indirect effects on other cell types. It would be interesting to see whether this held true *in vivo*; whether loss of CXCR5 resulted in different location of ILC3, and whether this would take place in the context of TLR stimulation during an immune response. Also explored was the possibility that receiving signals by IL-7 would have an effect on expression of CXCR5. One hypothesis for their distinctive location within these regions was their requirement for IL-7 signalling, as has previously been shown for adult LTi cells (Schmutz et al., 2009). In a manner similar to T cells, we showed that IL-7 signalling resulted in the downregulation of IL-7Rα from the surface of ILCs. Although moderate changes in the level of CXCR5 expression were detected upon addition of IL-7 to cultures, what this reflects *in vivo* is not clear and requires further investigation. Given that CXCR5 was not detected on the surface of ILC2 yet they can be found to reside within the same areas as ILC3, it would appear unlikely

that expression of this chemokine receptor was the primary mechanism of their location to this region, and other factors should be considered. LTi cells have previously been shown to interact with stromal cells; to provide signals required for the formation of LNs (Mebius, 2003), and interact with fibroblastic reticular cells (FRCs) to help repair damaged secondary lymphoid tissue following viral infection (Scandella et al., 2008). Depletion of RORγt-expressing cells in chimeric mice did not have a noticeable effect on structural elements within the interfollicular regions of mLN within the timeframe of our experiments, although this was not analysed in the context of infection.

Those experiments which looked at the number and phenotype of ILC populations in WT LNs at steady state were carried out in externally sourced WT mice, so as to minimise animal facility-specific differences and enable this experiment to be repeated by researchers at different institutions. One interesting observation has been that the differences in numbers of ILC3 between skin-draining and mesenteric LNs were less in WT mice which had been bred and maintained in our animal facility, perhaps suggesting that ILC3 numbers are influenced by microbial flora which is likely to be distinct between facilities. Certainly, it can be argued that the mLN represents a more 'activated' type of LN, given its location draining the gut, therefore an increased number of ILC3 might be the result of an ongoing immune response. On a similar note, the peripheral popLN, a LN which is arguably less often required to respond to an immunological challenge than the mLN given its location draining the hind paw, was found to have the lowest proportion of ILC3 of all analysed. Equally, and not mutually exclusively, the observation of ILC3 in the mLN could be as a result of it draining the ILC3-enriched gut tissue and both of these possibilities will be explored in upcoming chapters.

CHAPTER 4. CHARACTERISING ILCS IN DRAINING LYMPH NODES

4.1 INTRODUCTION

In light of the presence of all three groups of ILC within all lymph nodes analysed, and the potentially influential location of ILC2 and ILC3, we next investigated whether any changes in these cells could be observed in a draining lymph node (dLN) following immunisation. Owing to its function draining antigen from the microorganism-enriched gut, the mLN is likely to be continuously exposed to antigen and therefore more activated than those LNs found at other sites. It is therefore possible that the ILC composition of the mLN in fact reflects that of an 'activated' LN, and could perhaps be induced in a skin-draining LN following immunisation.

Following immunisation, antigen-presenting dendritic cells (DCs) carrying antigen can drain to the local lymph node via the lymph and lymphatic vessels. DCs presenting this antigen in the context of MHCII will then interact with naïve $CD4^+$ T cells within this structure and activate an adaptive immune response. ILCs, like dendritic cells, have been shown to express MHCII and to process and present peptide (Neill et al., 2010, Hepworth et al., 2013); with this discovery changing the way in which the potential roles of ILCs are viewed. Certainly within lymph nodes a proportion of ILC3s express this molecule, as demonstrated in Chapter 3.

Although there are still relatively few studies on the function of ILC-expressed MHCII, those that exist indicate that expression of MHCII by ILCs can affect an immune response in vastly different ways. ILC3 in the gut have been shown to contribute to the prevention of inappropriate $CD4^+$ T cell responses to commensal bacteria through a MHCII-mediated

mechanism (Hepworth et al., 2013). Mice in which MHCII had been specifically deleted from ILC3 ($MHCII^{\Delta ILC3}$) but not other antigen-presenting cell types developed intestinal inflammation, indicating that antigen-presentation by ILC3 in the gut is important for the ability of the immune system to tolerate the presence of commensal microbiota. The authors found that $MHCII^{+}$ ILC3 isolated from murine mesenteric LN did not express the co-stimulatory molecules CD80 and CD86 (Hepworth et al., 2013). Antigen presentation to T cells without further stimulation from co-stimulatory molecules has been shown to limit their responses (Schwartz, 2003), and fittingly ILC3s have been shown to induce the apoptosis of responding T cells in a MHCII-dependent manner (Hepworth et al., 2015). Interestingly, MHCII expression was restricted to those ILC3 that lacked NKp46 expression (Hepworth et al., 2013), which were found in Chapter 3 of this investigation to be the predominant population in lymph nodes.

Whilst ILC3 in the gut and gut-associated lymphoid tissues lack expression of co-stimulatory molecules (Hepworth et al., 2013), some ILC3 isolated from the spleen have been shown to be able to modestly upregulate expression of CD80 and CD86. This was true of murine *ex vivo* splenic $CD4^{+}$ NCR^{-} ILC3 stimulated with IL-1β, but not those NCR^{-} ILC3 isolated from the small intestine lamina propria (von Burg et al., 2014). The authors also found that the proliferation of a specific population of $CD4^{+}$ T cells two days following exposure to OVA-based antigens was impaired in the spleens of mice where MHCII was deleted from ILC3 (von Burg et al., 2014), indicating that antigen presentation by splenic ILC3, by contrast, promotes $CD4^{+}$ T cell responses within this tissue. Mice in which LTi cells are deficient have also previously been shown to have normal splenic primary $CD4^{+}$ T cell responses although long-term maintenance of memory populations was perturbed (Withers et al., 2012), so it is clear that there is more to be explored. It seems likely that

differences in the phenotype, and consequently function, of ILC3s at different sites reflects the different immunological challenges faced.

Although CD80 and CD86 expression by group 3 ILCs needs further investigation, co-stimulatory molecule expression has also been reported by ILC2. ILC2 expressing MHCII and the co-stimulatory molecules CD80 and CD86 were found to be capable of inducing T cell proliferation *in vitro* (Oliphant et al., 2014). MHCII-mediated ILC2 interaction with T cells was found to be important for the production of IL-13 by ILC2, and for the efficient expulsion of intestinal helminth *N. Brasiliensis* (Oliphant et al., 2014). Interestingly ILC2 expression of MHCII appears to be site-dependent; with expression documented on ILC2 in the lymph nodes, spleen and Peyer's patches, but less so on ILC2 from the lung, peritoneal and bronchoalveolar lavages (Oliphant et al., 2014). This area of ILC biology is under-explored, with much still to be discovered about the role of ILCs as antigen-presenting cells. Given that lymph nodes are recognised as important sites for the generation of adaptive $CD4^+$ T cell responses we chose to investigate the antigen-presenting potential of ILCs within these tissues.

To investigate this we focussed on a draining lymph node immune response to immunisation in the skin. Analysis of an endogenous $CD4^+$ T cell response within peripheral LNs of mice where ILC3 lack MHCII expression has shown a significantly increased number of these cells responding to immunisation compared to controls, consistent with ILC3-expressed MHCII being important in these tissues (Mackley et al., 2015). We utilised a robust draining lymph node model which targeted the skin-draining popliteal or brachial and axillary lymph nodes, using a population of responding $CD4^+$ T cells to track the magnitude of the immune response. Studies of DC ($CD11c^+$ $MHCII^{hi}$ cells)

trafficking in response to skin painting with a chemical stimulant have shown that DCs arrive within the draining peripheral LN within one day, with their numbers decreasing within the draining LN over time (Tomura et al., 2014). We chose to investigate both the number and phenotype of ILCs in a draining LN at both early and late timepoints in a primary immune response, so as to better understand the potential roles of these cells in influencing an adaptive immune response.

This chapter will firstly describe the number of each ILC subset within draining peripheral LNs at early and late timepoints following immunisation, with any accumulation of ILCs potentially indicative of a function in the immune response. It will also explore the expression of antigen-presenting machinery by these cells at different timepoints, comparing their levels of expression to those seen on DCs. Finally it will investigate whether or not changes in ILC number within a draining lymph node are due to proliferation of these cells or another mechanism, such as trafficking.

4.2 DRAINING LYMPH NODE MODELS

4.2.1 TCR transgenic CD4$^+$ T cell system

In order to study the response of ILC populations to immunisation, it was important to be able to track the progress and magnitude of an immune response within lymph nodes. To do this we made use of two existing TCR transgenic CD4$^+$ T cell populations, SM1 (McSorley et al., 2002) or OTII cells (Barnden et al., 1998). Either SM1 or OTII cells were adoptively transferred into our experimental mice the day prior to immunisation, which allowed us to trace responding cells of a known antigen-specificity by either allotype markers or the expression of their specific TCR. Immunising with their known cognate antigen—FliC peptide, a subunit protein of flagellin, for SM1 cells and ovalbumin (OVA)

for OTII cells—allowed us to identify an activated $CD4^+$ T cell population and verify that the immunisation had been successful. Two TCR transgenic systems were adopted as a result of difficulties in maintaining our colony of $RAG^{-/-}$ SM1 mice.

We identified SM1 T cells by their expression of CD3, CD4 and either CD45.1 or CD45.2; the expression of which was used to distinguish donor $CD4^+$ T cells from allotype-marked hosts (Figure 4.1a). CD44 expression was used to determine those cells which had seen their cognate antigen following immunisation and had become activated (Figure 4.1a,b). Similarly, responding OTII cells could be recognised by their expression of CD3, CD4 and CD44 and the use of an antibody against Vβ5.1/2 TCR^+ T cells, which allowed us to identify those $CD4^+$ T cells which respond to OVA, the majority of which were our adoptively transferred OTII cells (Figure 4,1b), when allotype discrimination was not possible. In all cases TCR transgenic T cells were isolated from secondary lymphoid tissue of the donor mouse, analysed to calculate the exact number of SM1 or OTII cells to be transferred, and injected intravenously into hosts the day prior to immunisation to allow for circulation of the cells to tissues.

4.2.2 Targeting immune responses to skin-draining lymph nodes

Introducing the cognate antigen for the TCR transgenic population being analysed subcutaneously into the footpad of host mice induced an immune response in the local draining lymph node. Immunising in the hind footpad of mice resulted in an immune response in the draining popliteal lymph node (popLN), located behind the knee. Strains of *L. monocytogenes* (Lm) expressing specific peptides have been used previously within our laboratory to induce a robust immune response (Marriott et al., 2014), and in this study *L. monocytogenes* expressing FliC peptide (Lm-FliC) was used to stimulate SM1 T

Figure 4.1 Comparison of TCR transgenic T cell gating strategies

Draining LNs from WT mice 4 days p.i. Mice received 10^4 SM1 or 10^5 OTII transgenic $CD4^+$ T cells intravenously (i.v) a day before immunisation. Cells were isolated from LNs as specified in methods. Samples were analysed by flow cytometry and representative FACS plots shown.

a) FACS plots showing the gating strategy for $CD44^{hi}$ SM1 T cells in draining popLN 4 days p.i. in the hind paw pad with Lm-FliC. Pre-gated on FSC and SSC.

b) FACS plots showing the gating strategy for $CD44^{hi}$ OTII T cells in draining brachial and axillary LNs 4 days p.i in the front paw pads with alum-ppt NP-OVA. Pre-gated on FSC and SSC.

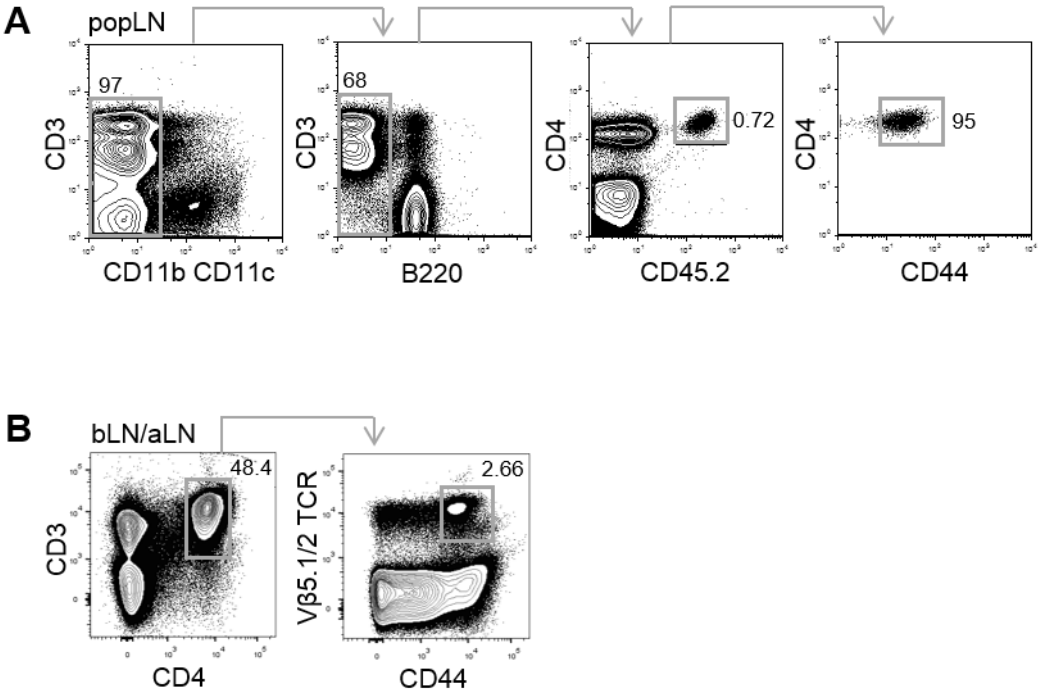
A
popLN
97
CD3
CD11b CD11c
68
CD3
B220
CD4
0.72
CD45.2
CD4
95
CD44
B
bLN/aLN
48.4
CD3
CD4
2.66
Vβ5.1/2 TCR
CD44

Fig. 4.1

cells. At the first timepoint analysed, 4 days following immunisation with Lm-FliC, a population of $CD44^{hi}$ $CD45.2^{+}$ SM1 T cells could be detected in the draining popLN, which was not present in the contralateral non-draining popLN (ndLN; Figure 4.2a). These cells were negative for CD11b, CD11c and B220, but the CD3 gate was generous to account for relatively low CD3 expression on SM1 T cells in this system (Figure 4.1a). Nonetheless the number of non-SM1 T cells which will have been included because of this is negligible, as demonstrated by the low numbers seen in ndLNs. SM1 $CD4^{+}$ T cells could still be detected in the draining popliteal LN up to 12 days post-immunisation (p.i), with numbers peaking between day 4 and day 8 (Figure 4.2b). This response looked to be largely specific to the draining popliteal lymph node at early timepoints, with no significant increase in SM1 T cell number 4 days p.i in the draining iLN when compared to the contralateral iLN (Figure 4.2c), whilst a highly statistically significant increase was observed in the draining popLN (Figure 4.2b).

This draining LN model was also effective when applied to the front paw-pad, with the immune response then detectable within the draining brachial (bLN) and axillary lymph nodes (aLN) located beneath the arm. Paw-pad immunisation with aluminium hydroxide-precipitated (alum-ppt) NP-OVA resulted in the expansion of $CD44^{hi}$ OTII cells in the draining lymph node when compared to mice which had been immunised instead with PBS (Figure 4.2d,e). This was as opposed to analysing the contralateral LN, as in the popLN study detailed above, and a refinement which serves as a better control and avoids any potential discrepancies caused by the re-circulation of cells to the contralateral lymph node by later timepoints. The higher number of OTII cells detected in this system is most likely due to the increased numbers initially transferred—10^5 naïve OTII cells in

Figure 4.2 Tracking CD4$^+$ T cell responses in dLNs

(a-c) All WT mice received 10^4 SM1 TCR transgenic CD4$^+$ T cells i.v a day before immunisation with Lm-FliC in one hind paw pad. Draining popLNs (dLN) were compared to non-draining contralateral popLN controls (ndLN).

(d,e) All WT mice received 10^5 OTII TCR transgenic CD4$^+$ T cells intravenously a day before immunisation with PBS or alum ppt NP-OVA in both front paw pads. Brachial and axillary LNs were pooled and analysed.

Samples were analysed by flow cytometry and absolute numbers per lymph node calculated. All bars shown on graphs represent the median value. Statistical test used is Mann-Whitney non-parametric, two-tailed test. *P<0.05, **P<0.01, ***P<0.001 and ****P<0.0001.

a) FACS plots showing gating on populations of adoptively transferred SM1 T cells 4, 6, 8 and 12 days (D4, D6, D8 and D12 respectively) p.i. ndLN control is also shown (top). Gating strategy is as shown in Figure 4.1a.

b) Graph showing the total number of CD44^{hi} SM1 T cells per popLN at stated timepoints p.i. ndLNs are pooled contralateral controls from across all timepoints. Data pooled from 1 (D12), 2 (D6) or 3 (D4,8) independent experiments. (n=30,11,8,12,4).

c) Graph showing the total number of CD44^{hi} SM1 T cells per iLN at stated timepoints p.i. ndLNs are pooled contralateral controls from across all timepoints. Data pooled from 1 independent experiment. (n=16,4,4,4,4).

d) FACS plots showing gating on populations of CD44^{hi} OTII T cells pooled from bLNs and aLNs. D1; day 1. Cells pre-gated on CD3$^+$ CD4$^+$ T cells as shown in Figure 4.1b.

e) Graph showing the total number of CD44^{hi} OTII cells per LN at stated timepoints p.i. PBS controls are pooled from across all timepoints. Data pooled from 2 (D4,8) or 3 (D1) independent experiments. (n=19,10,6,6).

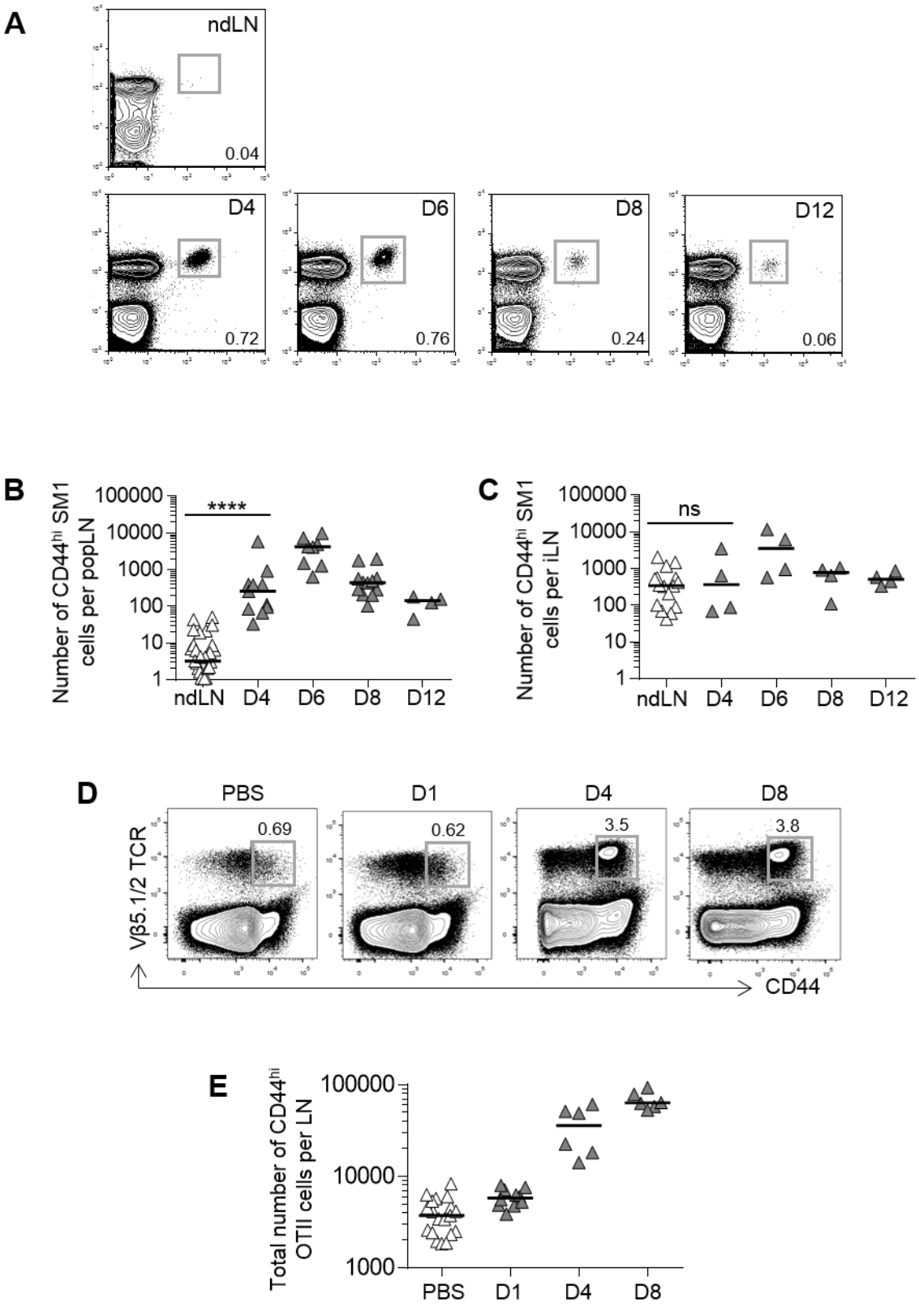
A
ndLN
0.04
D4
0.72
D6
0.76
D8
0.24
D12
0.06
B
Number of CD44hi SM1 cells per popLN
****
ndLN
D4
D6
D8
D12
C
Number of CD44hi SM1 cells per iLN
ns
D
PBS
D1
D4
D8
0.69
0.62
3.5
3.8
Vβ5.1/2 TCR
CD44
E
Total number of CD44hi OTII cells per LN
PBS
D1
D4
D8

Fig. 4.2

comparison to 10^4 naïve SM1 T cells, which made these cells easier to detect and characterise within small LNs—and differences in the adjuvant used.

4.3 CHARACTERISATION OF ILC NUMBER AND PHENOTYPE IN DRAINING LNS

4.3.1 ILCs increase in number in a dLN

Given the lack of experimental data describing ILC responses in draining LNs we sought to investigate this further. During the popLN immunisation timecourse outlined in Figure 4.2 we enumerated the number of LTi-like cells present, at this time identifying them using only cell-surface markers. Prior to the discovery of CCR6 as an effective surface marker for RORγt-expressing ILCs, a subset of LTi-like cells could be identified in LNs by their lack of lineage markers (CD3/CD11b/CD11c/B220)—taking care to exclude any CD45.2 $CD3^{lo}$ SM1 T cells that could fall within this population—expression of IL-7Rα and expression of CD4 (Figure 4.3a). At the time of this study the existence of other populations of ILC was not widely known. Nonetheless, as neither ILC1 nor ILC2 express CD4 this analysis is specific for $CD4^+$ group 3 ILCs. Within the population of cells which were negative for common lineage defining markers, cells which expressed both IL-7Rα and CD4 could be identified (Figure 4.3a,b). Although still rare in popLNs at steady state, the number of these cells was increased in draining popLNs 4-8 days following immunisation with Lm-FliC, but appeared to begin to return to steady state levels between day 8 and 12 (Figure 4.3b,c).

The observation that these cell types increased in number during an immune response led us to optimise this model further, analysing ILC subsets in draining LNs beneath the arm rather than in the leg by immunising in the front paw pad. This was in part due to the ease of isolating cells from brachial and axillary LNs, rather than the small popLN, but also

Figure 4.3 CD4$^+$ LTi-like ILC3 accumulate in draining popLNs

All WT mice received 10^4 SM1 TCR transgenic CD4$^+$ T cells i.v a day before immunisation with Lm-FliC in one hind paw pad. Draining popLNs (dLN) were compared to non-draining contralateral popLN controls (ndLN). Samples were analysed by flow cytometry and absolute numbers per lymph node calculated.

All bars shown on graphs represent the median value. Data representative of (a) or pooled from 1 (D12), 2 (D6) or 3 (D4,8) independent experiments. Statistical test used is Mann-Whitney non-parametric, two-tailed test. *P<0.05, **P<0.01, ***P<0.001 and ****P<0.0001.

a) Gating strategy showing populations of CD4$^+$ LTi-like ILC3 in contralateral non-draining popLN (top) and draining popLN 4 days p.i (bottom).

b) FACS plots showing CD4$^+$ LTi-like ILC3 across stated timepoints, pre-gated as shown in (a).

c) Graph showing the total number of CD4$^+$ LTi-like ILC3 per popLN at stated timepoints p.i. ndLNs are pooled contralateral controls from across all timepoints. (n=30,11,8,12,4).

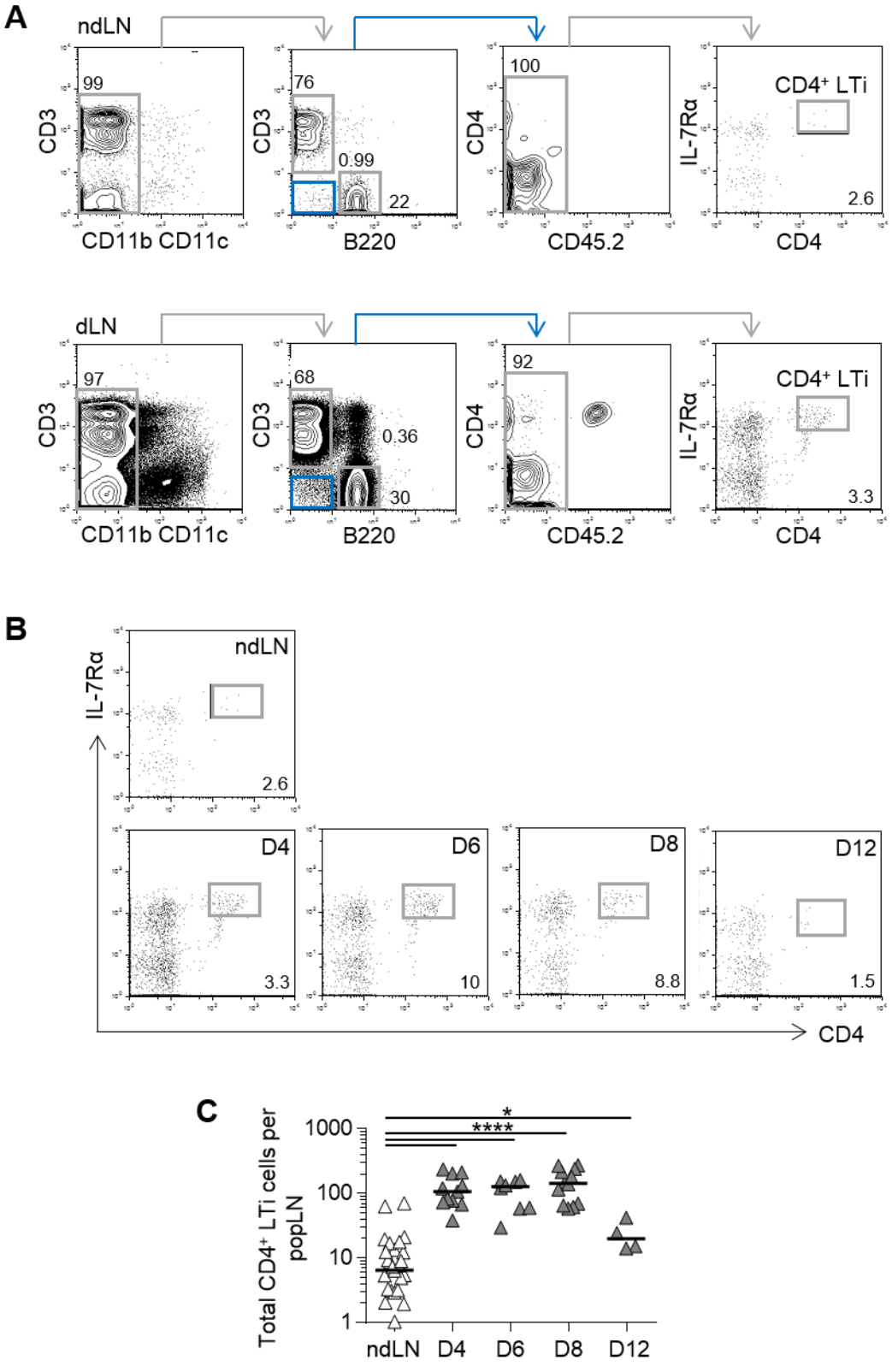
A
ndLN
99
CD3
CD11b CD11c
76
0.99
22
B220
100
CD4
CD45.2
CD4⁺ LTi
IL-7Rα
2.6
CD4
dLN
97
68
0.36
30
92
3.3
B
IL-7Rα
2.6
D4
3.3
D6
10
D8
8.8
D12
1.5
CD4
C
Total CD4⁺ LTi cells per popLN
1000
100
10
1
*
****
ndLN
D4
D6
D8
D12

Fig. 4.3

because ILC characterisation studies outlined in Chapter 3 have shown the popLN to have relatively few ILC3. The adjuvant used at the time of immunisation was also adapted. Pilot data shown in Figure 4.4, using a more sophisticated method of gating ILCs (Figure 4.4a), revealed that alum-ppt FliC peptide induced a larger expansion of both SM1 T cell and ILC populations in dLNs than FliC peptide expressed by *L. monocytogenes* (Figure 4.4b-d). Numbers of total Lin^- IL-$7R\alpha^+$ ILCs were statistically significantly increased in those mice which had been immunised with alum-ppt FliC when compared to those immunised with Lm-FliC 8 days p.i (Figure 4.4b). This corresponded to a statistically significant increase in numbers of ILC1 and ILC3 (Figure 4.4c). Immunisation with alum-ppt FliC also resulted in a greater expansion of SM1 T cells than Lm-FliC (Figure 4.4d) and as a result alum was used as an adjuvant in the experiments detailed below.

4.3.2 An optimised draining lymph node model

Having observed an increase in ILC number following immunisation we sought to characterise ILCs in draining LNs further by phenotyping each subset at early and late timepoints during an immune response; in particular to investigate their potential to act as APCs. To achieve this our optimised draining lymph node model was used. WT mice were immunised in the front paw pads, and the immune response analysed in the draining brachial and axillary LNs. OTII $CD4^+$ T cells were used in this particular study as a result of difficulties in maintaining the $RAG^{-/-}$ SM1 mouse colony, however both TCR transgenic systems have been found to be effective as a readout of the magnitude of the immune response. Mice were therefore immunised with NP-OVA to target the adoptively transferred OTII cells, and this protein was alum-precipitated to induce a robust immune response.

Figure 4.4 Comparison of the magnitude of response to different adjuvants

All WT mice received 105 SM1 TCR transgenic CD4+ T cells i.v a day before immunisation with Lm-FliC in one front paw pad and alum-ppt FliC in the other. Draining bLNs were compared to mice in which both paw pads were immunised with PBS, 8 days p.i. Samples were analysed by flow cytometry and absolute numbers per LN calculated.

All bars shown on graphs represent the median value. Data representative of 1 independent pilot experiment. Statistical test used is Mann-Whitney non-parametric, two-tailed test. *P<0.05, **P<0.01, ***P<0.001 and ****P<0.0001.

a) Gating strategy showing populations of ILCs in PBS control LN. Lin is CD3/CD5/B220/CD11c.

b) Graph showing the total number of Lin^- IL-$7R\alpha^+$ ILCs per LN 8 days following immunisation with PBS, Lm-FliC (Lm) or alum-ppt FliC (Alum). (n=3,4,4).

c) Graphs showing the number of ILC1, ILC2 and ILC3 per LN 8 days p.i with PBD (white triangles), Lm-FliC (grey triangles) or alum-ppt FliC (black triangles). ILC1 are defined as $ROR\gamma t^-$ $GATA\text{-}3^-$ ILCs. (n=3,4,4).

d) Total number of $CD44^{hi}$ SM1 T cells per LN 8 days following immunisation with PBS, Lm-FliC (Lm) or alum-ppt FliC (Alum). (n=3,4,4).

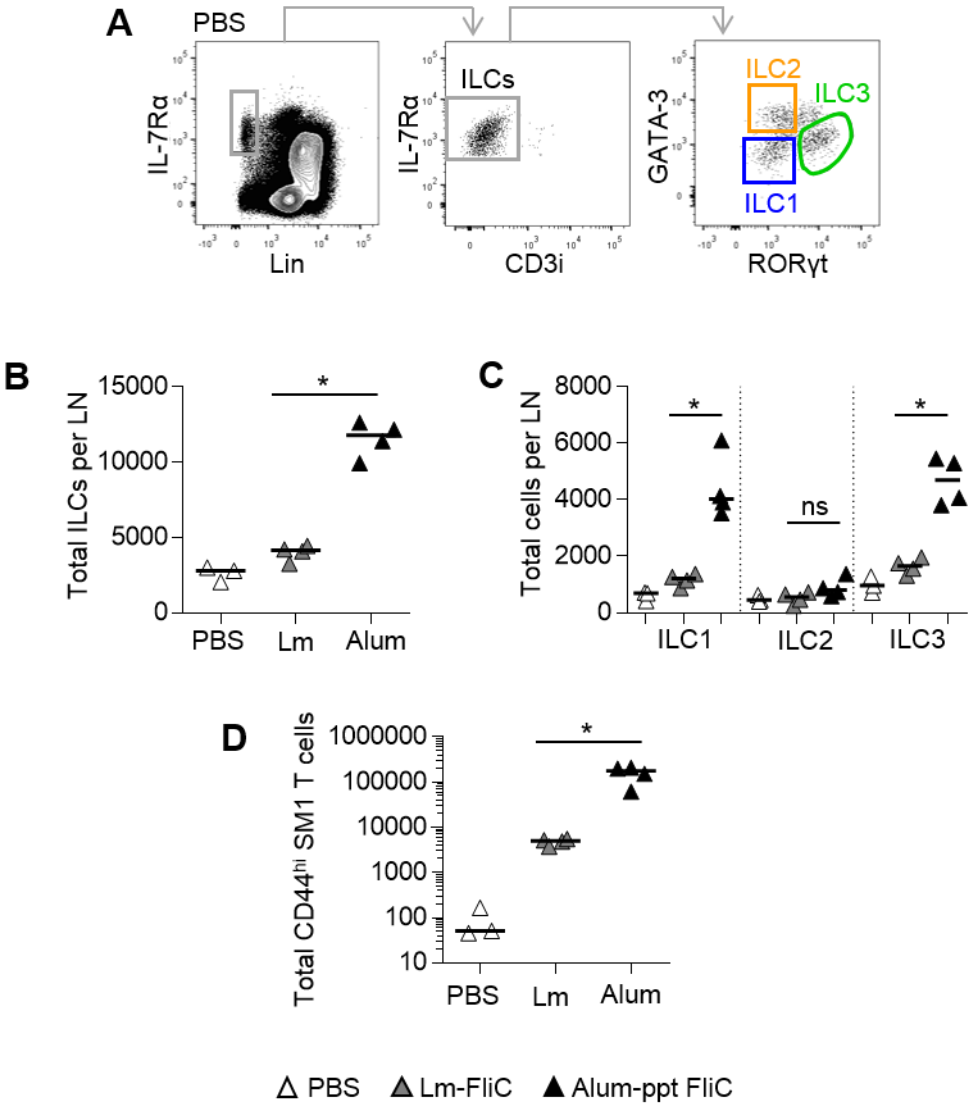
A
PBS
IL-7Rα
Lin
ILCs
IL-7Rα
CD3i
GATA-3
RORγt
ILC2
ILC3
ILC1
B
Total ILCs per LN
15000
10000
5000
0
PBS
Lm
Alum
*
C
Total cells per LN
8000
6000
4000
2000
0
ILC1
ILC2
ILC3
*
ns
*
D
Total CD44hi SM1 T cells
1000000
100000
10000
1000
100
10
PBS
Lm
Alum
*
PBS
Lm-FliC
Alum-ppt FliC

Fig. 4.4

4.3.3 ILCs as antigen-presenting cells

All three groups of ILC could be detected in a pool of brachial and axillary LNs from mice taken one day (approximately 20-22hrs) following immunisation with either PBS or alum-ppt NP-OVA. Three groups of ILCs could be identified from a population of lineage (CD3/CD5/B220/CD11b/CD11c) negative IL-7Rα$^+$ cells, based on their expression of GATA-3 (ILC2), RORγt (ILC3) or absence of both transcription factors (ILC1; Figure 4.5a). Cells identified as ILC3 were then further split into those which were NKp46$^-$ (LTi-like ILC3) and those which were NKp46$^+$ MHCII$^-$ (NCR$^+$ ILC3). One day p.i the total number of Lin$^-$ IL-7Rα$^+$ ILCs per LN were found to be increased in comparison to control LNs (Figure 4.5b), with statistically significant increases detected specifically in the number of ILC2 and LTi-like ILC3 populations (Figure 4.5c). To understand whether this increase in number was indicative of ILCs playing a role early in immune responses we next sought to characterise the phenotype of these cells at this timepoint.

As it has been reported that some ILC2 and ILC3 express MHCII and are capable of presenting antigen to CD4$^+$ T cells (Oliphant et al., 2014, Hepworth et al., 2013, von Burg et al., 2014) we thought it relevant to investigate whether, in the context of a peripheral LN immune response, ILCs resembled professional APCs in their expression of MHCII and the co-stimulatory molecules CD80 and CD86. In order to make this comparison populations of DCs detected during our response were phenotyped. Two distinct populations of MHCII$^+$ CD11c$^+$ CD3$^-$ B220$^-$ DCs could be detected in draining LNs of both PBS and alum-ppt NP-OVA treated mice 1 day p.i (Figure 4.6a), and these DC populations could be distinguished by their differential levels of MHCII. Those DCs which expressed

Figure 4.5 Numbers of dLN ILC2 and LTi-like ILC3 moderately increase early in an immune response

All WT mice received 10^5 OTII TCR transgenic $CD4^+$ T cells intravenously a day before immunisation with PBS or alum-ppt NP-OVA in both front paw pads. Cells were isolated and pooled from bLN and aLNs 1 day p.i as detailed in methods. Samples were analysed by flow cytometry and absolute numbers per lymph node calculated. Lin^- IL-$7R\alpha^+$ $ROR\gamma t^+$ ILC3s were further split into those which express NKp46 at a level comparable to ILC1 (NCR^+ $MHCII^-$ ILC3) and those which do not (LTi-like ILC3), whilst ILC1 are defined as Lin^- IL-$7R\alpha^+$ $ROR\gamma t^-$ GATA-3^- cells.

All bars shown on graphs represent the median value. Data representative of (a) or pooled from (b,c) 3 independent experiments. Statistical test used is Mann-Whitney non-parametric, two-tailed test. **P*<0.05, ***P*<0.01, ****P*<0.001 and *****P*<0.0001.

a) FACS plots showing gating on populations of ILCs in pooled bLN and aLNs 1 day p.i with alum-ppt NP-OVA (D1). Lin is CD3/CD5/B220/CD11b/CD11c.

b) Graph showing the total number of Lin^- IL-$7R\alpha^+$ ILCs per LN in PBS control mice (white triangles) or 1 day p.i with alum-ppt NP-OVA (grey triangles). (n=9,10).

c) Graph showing the number of ILC1, ILC2, LTi-like ILC3 or NCR^+ ILC3 per LN in PBS controls or 1 day p.i with alum-ppt NP-OVA (D1). (n=9,10).

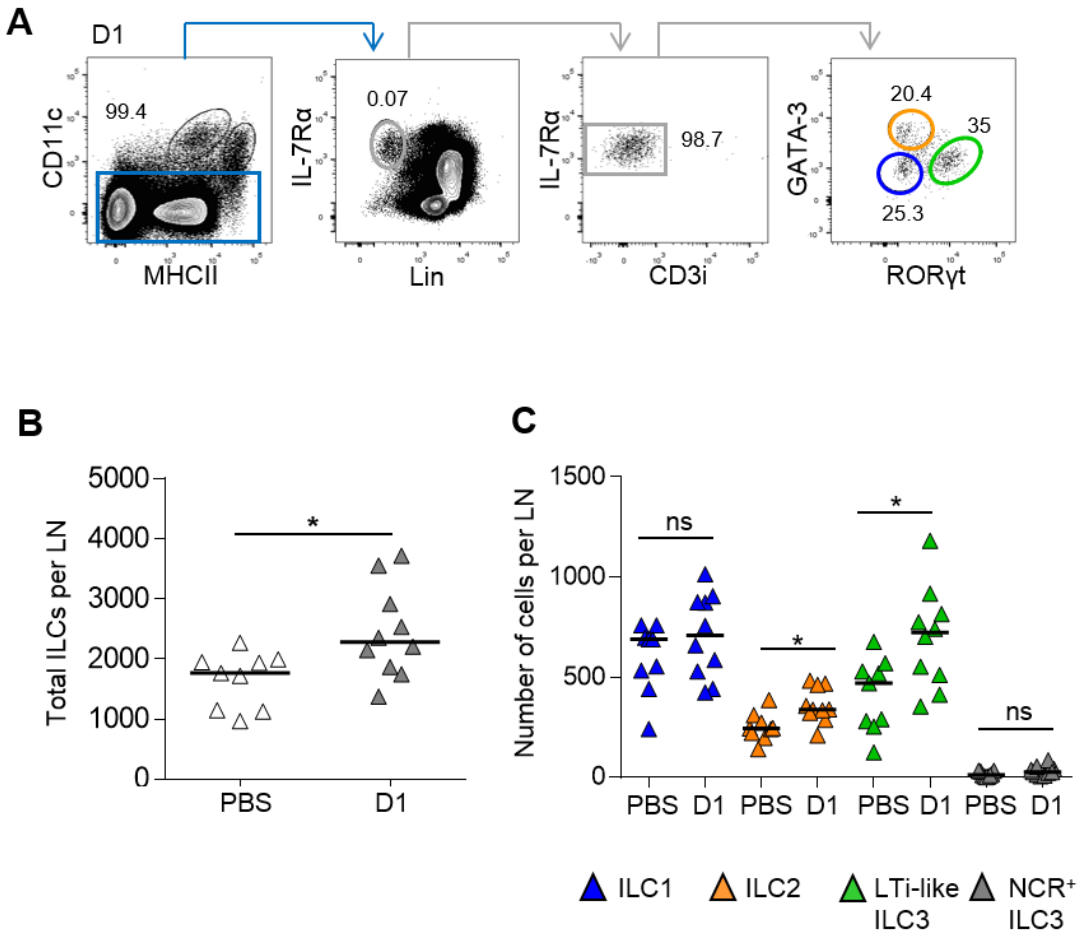
A
D1
CD11c
99.4
MHCII
IL-7Rα
0.07
Lin
IL-7Rα
98.7
CD3i
GATA-3
20.4
35
25.3
RORγt
B
Total ILCs per LN
5000
4000
3000
2000
1000
0
*
PBS
D1
C
Number of cells per LN
1500
1000
500
0
ns
*
*
ns
PBS D1 PBS D1 PBS D1 PBS D1
ILC1
ILC2
LTi-like ILC3
NCR+ ILC3

Fig. 4.5

Figure 4.6 Characterising DCs early in an immune response

All WT mice received 10^5 OTII TCR transgenic $CD4^+$ T cells intravenously a day before immunisation with PBS or alum-ppt NP-OVA in both front paw pads. Cells were isolated and pooled from bLN and aLNs 1 day p.i as detailed in methods. Samples were analysed by flow cytometry and absolute numbers per lymph node calculated. $CD11c^+$ cells were split into those which expressed intermediate levels of MHCII ($MHCII^+$) and those whose levels were high ($MHCII^{hi}$). iLN, bLN and aLNs from non-immunised $CD80^{-/-}CD86^{-/-}$ mice were used to control for expression of CD80 and CD86.

All bars shown on graphs represent the median value. Data representative of (a,c,e) or pooled from (b,d,f-h) 3 independent experiments. Statistical test used is Mann-Whitney non-parametric, two-tailed test. *P<0.05, **P<0.01, ***P<0.001 and ****P<0.0001.

a) FACS plots showing gating on $CD11c^+$ $MHCII^+$ DCs in bLN and aLN 1 day p.i with alum-ppt NP-OVA.

b) Graph showing the total number of $MHCII^+$ and $MHCII^{hi}$ DCs per LN 1 day following immunisation with PBS or alum-ppt NP-OVA (D1).

c) FACS plot showing expression of phenotypic markers CD11b and CD103 on $CD11c^+$ $MHCII^{hi}$ DCs as gated in (a).

d) Graph showing the percentage of $MHCII^{hi}$ DCs which express CD103 or CD11b 1 day p.i with PBS or alum-ppt NP-OVA (D1).

e) FACS plots showing the expression of CD80 and CD86 on WT $MHCII^{hi}$ DCs (left) from bLN and aLN 1 day p.i with alum-ppt NP-OVA, compared to $MHCII^{hi}$ DCs from naïve $CD80^{-/-}CD86^{-/-}$ mice (right), as gated in (a).

f) Graphs showing percentage of $MHCII^{hi}$ DCs which are $CD80^+$ and/or $CD86^+$ (co-$stim^+$) in bLN and aLN 1 day p.i with PBS or alum-ppt NP-OVA (D1) and compared to $CD80^{-/-}CD86^{-/-}$ controls.

g) Graph showing percentage of $MHCII^{hi}$ DCs which are $CD86^+$ in bLN and aLN 1 day p.i with PBS or alum-ppt NP-OVA (D1) and compared to $CD80^{-/-}CD86^{-/-}$ controls.

h) Graph showing the percentage of $MHCII^{hi}$ DCs which are $CD80^+$ and $CD86^+$ in bLN and aLNs 1 day p.i with PBS or alum-ppt NP-OVA (D1) and compared to $CD80^{-/-}CD86^{-/-}$ controls.

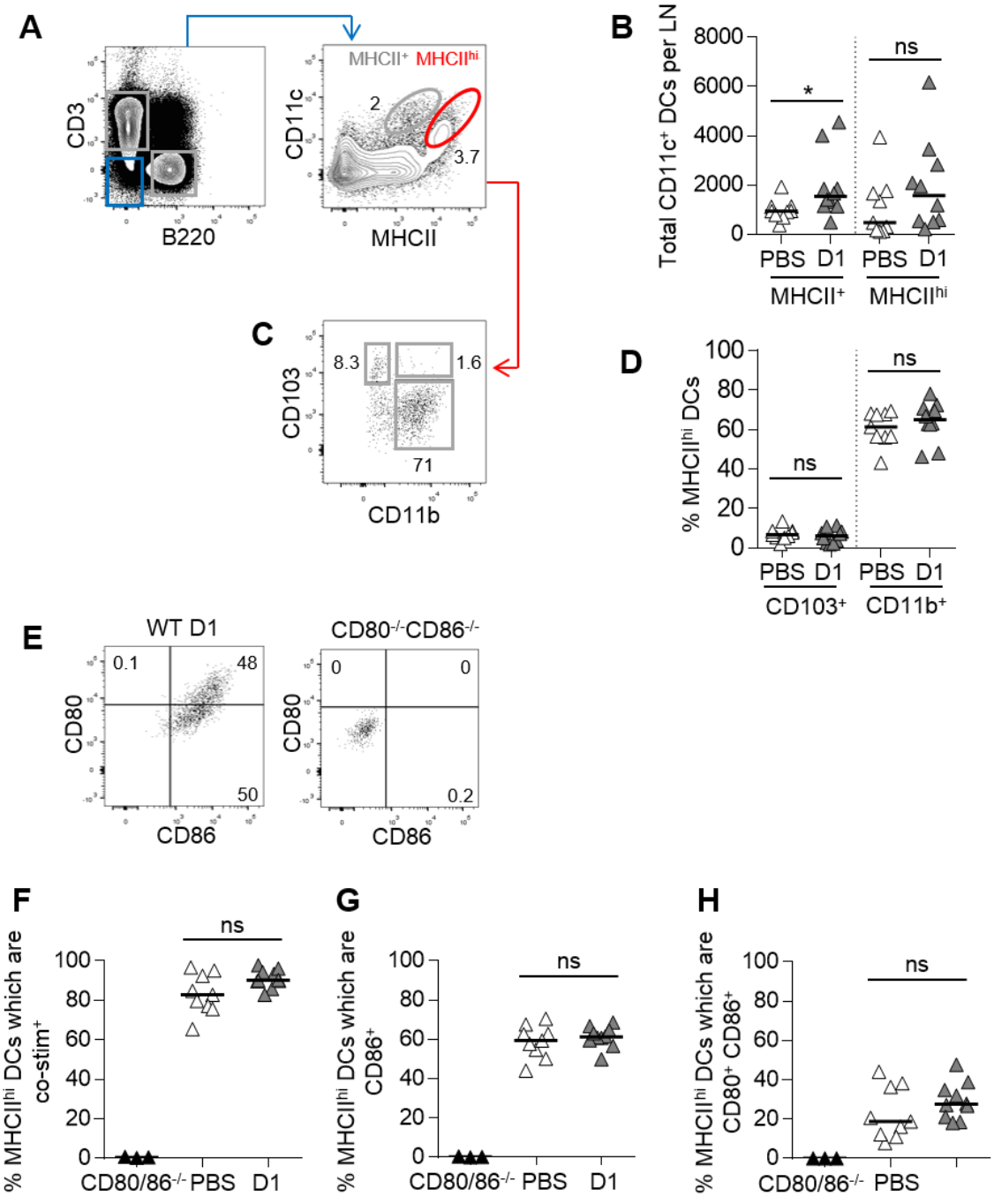
A
CD3
B220
MHCII+ MHCIIhi
CD11c
2
3.7
MHCII
B
Total CD11c+ DCs per LN
8000
6000
4000
2000
0
*
ns
PBS D1 PBS D1
MHCII+ MHCIIhi
C
CD103
8.3
1.6
71
CD11b
D
% MHCIIhi DCs
100
80
60
40
20
0
ns
ns
PBS D1 PBS D1
CD103+ CD11b+
E
WT D1
CD80-/-CD86-/-
CD80
0.1
48
50
0
0
0.2
CD86
F
% MHCIIhi DCs which are co-stim+
ns
CD80/86-/- PBS D1
G
% MHCIIhi DCs which are CD86+
ns
CD80/86-/- PBS D1
H
% MHCIIhi DCs which are CD80+ CD86+
ns
CD80/86-/- PBS

Fig. 4.6

high levels of MHCII may include skin-derived DCs, whilst those which have intermediate expression of MHCII and higher expression of CD11c have previously been described as LN-resident DCs (Tomura et al., 2014). Analysis of the number of each DC population per LN revealed that although the median number of both populations increased following immunisation, only the increase in MHCII^{+} DCs was statistically significant at this timepoint (Figure 4.6b). The phenotype of the MHCII^{hi} DC population in dLNs was also found not to change significantly between PBS and alum-ppt NP-OVA treated mice, with the cells found to be primarily CD11b^{+}, and only a small population expressing CD103 (Figure 4.6c,d). Interestingly, although ILCs are generally considered a rare population in LNs, DC populations are also relatively rare within LNs at this timepoint, therefore it is feasible that ILCs could play a role in antigen-presentation provided they possess the molecules required. Analysis of DC populations also provided a positive control for expression of the co-stimulatory molecules CD80 and CD86, whilst comparison to LNs from CD80$^{-/-}$CD86$^{-/-}$ mice served as an effective negative control (Figure 4.6e). Analysis revealed that >80% of MHCII^{hi} DCs expressed CD80 and/or CD86 (co-stim^{+}) in dLNs from both PBS control and alum-ppt NP-OVA treated mice (Figure 4.6f), but although a higher percentage of MHCII^{hi} DCs expressed both molecules simultaneously in those mice immunised with alum-ppt NP-OVA both this, and their expression of CD86 alone, was not statistically significantly increased (Figure 4.6 f-h).

MHCII expression was analysed on populations of ILC1, ILC2 and LTi-like ILC3, with NCR^{+} ILC3 here partly defined by their absence of MHCII and therefore excluded. Expression of MHCII to some extent could be seen by all ILC subsets, however most notably on ILC2 and LTi-like ILC3 (Figure 4.7a-c). For each ILC subset, the percentage of cells that expressed MHCII did not differ significantly between PBS controls and alum-ppt NP-OVA dLNs

Figure 4.7 A proportion of ILC2 and LTi-like ILC3 express MHCII in draining LNs

All WT mice received 10^5 OTII TCR transgenic $CD4^+$ T cells intravenously a day before immunisation with PBS or alum-ppt NP-OVA in both front paw pads. Cells were isolated and pooled from bLN and aLNs 1 day p.i as detailed in methods. Samples were analysed by flow cytometry and absolute numbers per lymph node calculated. ILC1 are defined as $ROR\gamma t^-$ $GATA\text{-}3^-$ ILCs.

All bars shown on graphs represent the median value. Data representative of (a) or pooled from (b,c) 3 independent experiments. Statistical test used is Mann-Whitney non-parametric, two-tailed test. **P*<0.05, ***P*<0.01, ****P*<0.001 and *****P*<0.0001.

a) FACS plots showing expression of MHCII on ILC2 (left, $GATA\text{-}3^+$) and LTi-like ILC3 (right, $ROR\gamma t^+$ $NKp46^-$) in bLN and aLNs 1 day p.i with PBS (top) or alum-ppt NP-OVA (bottom). Cells shown are pre-gated on Lin^- $IL\text{-}7R\alpha^+$ ILCs.

b) Graph showing the total number of ILC1, ILC2 and LTi-like ILC3 which express MHCII per LN. (n=9,10).

c) Graph showing percentage of each ILC population which express MHCII. (n=9,10).

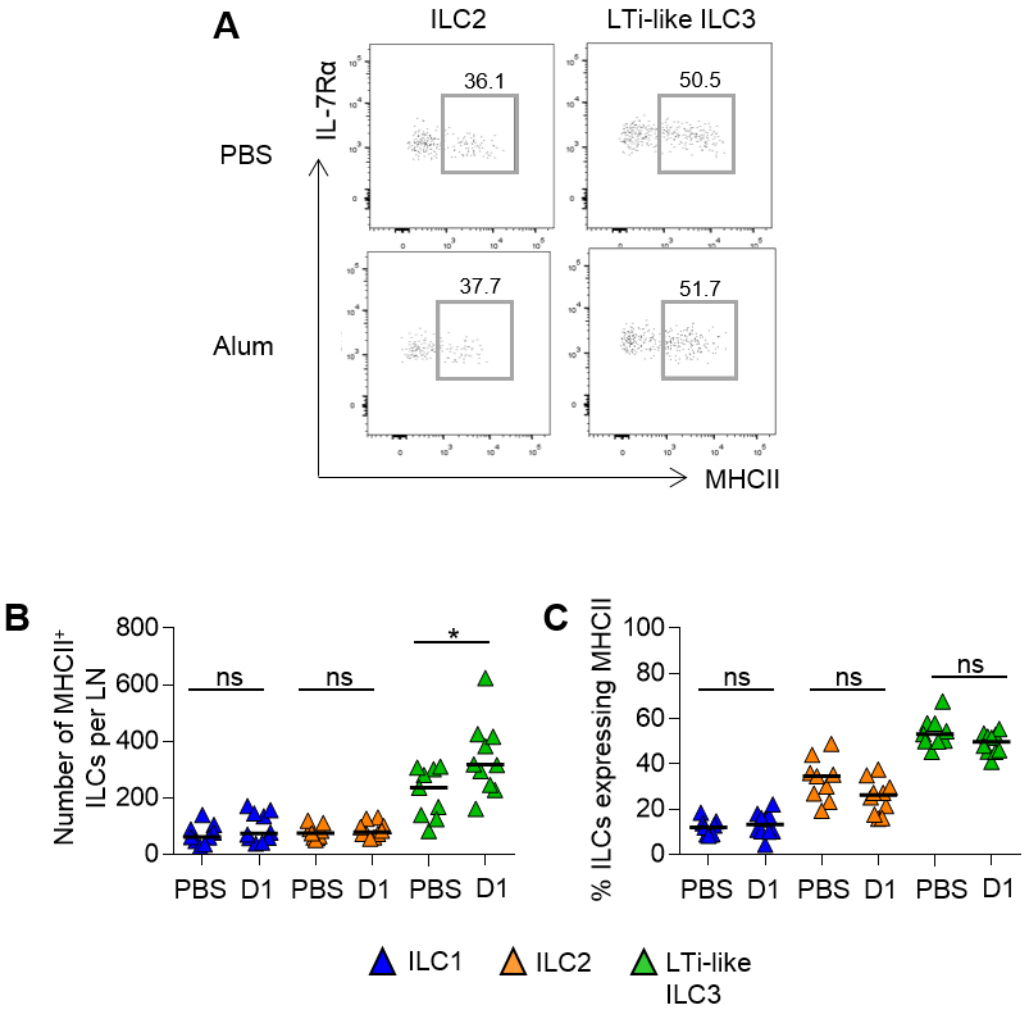
A
ILC2
LTi-like ILC3
PBS
Alum
IL-7Rα
MHCII
36.1
50.5
37.7
51.7
B
Number of MHCII+ ILCs per LN
800
600
400
200
0
ns
ns
*
PBS D1 PBS D1 PBS D1
C
% ILCs expressing MHCII
100
80
60
40
20
0
ns
ns
ns
PBS D1 PBS D1 PBS D1
ILC1
ILC2
LTi-like ILC3

Fig. 4.7

(Figure 4.7c), however the number of LTi-like ILC3 which expressed the molecule was moderately increased in dLNs, and this was statistically significant (Figure 4.7b). Analysis of co-stimulatory molecule expression by MHCII$^+$ ILCs revealed some expression of CD80 and CD86 by both ILC2 and LTi-like ILC3 (Figure 4.8a). Approximately 50% of MHCII$^+$ ILC2 (Figure 4.8b) and 30-35% of MHCII$^+$ LTi-like ILC3 (Figure 4.8c) expressed CD80 and/or CD86 (described as co-stim$^+$) in a pool of bLN and aLN, and this did not differ significantly between dLNs from PBS control and alum-ppt NP-OVA immunised mice. When expression of each molecule was investigated in more detail, MHCII$^+$ ILC2 were found to express primarily CD86 (Figure 4.8d), whilst LTi-like ILC3 showed no apparent bias (Figure 4.8e).

Although from Figure 4.8(a-e) it might be possible to conclude that a proportion of MHCII$^+$ ILC2 and LTi-like ILC3 look comparable to professional antigen-presenting cells in their expression of MHCII and co-stimulatory molecules, DCs express much higher levels of these molecules than LTi-like ILC3. Comparison of levels of both CD80 and CD86, in terms of intensity of fluorescence detected, on MHCII$^+$ LTi-like ILC3 and MHCII^{hi} DCs revealed a much bigger difference between staining levels on DCs when compared to those in CD80$^{-/-}$CD86$^{-/-}$ controls than on LTi-like ILC3 (Figure 4.8f). Therefore, although there are CD80 and/or CD86 expressing MHCII$^+$ ILCs within these LNs, their scarcity and low level of expression of key co-stimulatory molecules suggests that their role as APCs naïve CD4$^+$ T cell proliferation would be minor in comparison to DCs.

4.3.4 Phenotyping ILCs at later timepoints in an immune reponse

Given our previous observation, in Figures 4.3 and 4.4, of ILC number increasing at later timepoints during an immune response we also sought to analyse their number and

Figure 4.8 Characterising co-stimulatory molecule expression by ILCs early in an immune response

All WT mice received 10^5 OTII TCR transgenic $CD4^+$ T cells intravenously a day before immunisation with PBS or alum-ppt NP-OVA in both front paw pads. Cells were isolated and pooled from bLN and aLNs 1 day p.i, as detailed in methods. Samples were analysed by flow cytometry and absolute numbers per lymph node calculated. Non-immunised $CD80^{-/-}$ $CD86^{-/-}$ mice were used to control for expression of CD80 and CD86.

All bars shown on graphs represent the median value. Data representative of (a) or pooled from (b-e) 3 independent experiments. Statistical test used is Mann-Whitney non-parametric, two-tailed test. **P*<0.05, ***P*<0.01, ****P*<0.001 and *****P*<0.0001.

a) FACS plots showing expression of CD80 and CD86 by $MHCII^+$ ILC2 (top) and $MHCII^+$ LTi-like ILC3 (bottom) in LNs 1 day p.i with PBS or alum-ppt NP-OVA (D1) and compared to naïve $CD80^{-/-}CD86^{-/-}$ mice.

b) Graph showing the percentage of $MHCII^+$ ILC2 which express CD80 and/or CD86 (co-$stim^+$) in naïve $CD80^{-/-}CD86^{-/-}$ (black triangles) or 1 day p.i with PBS (white triangles) or alum-ppt NP-OVA (D1, grey triangles).

c) Graph showing the percentage of $MHCII^+$ LTi-like ILC3 which express CD80 and/or CD86 (co-$stim^+$) in naïve $CD80^{-/-}CD86^{-/-}$ or 1 day p.i with PBS or alum-ppt NP-OVA (D1).

d) Graph showing the percentage of $MHCII^+$ ILC2 which express CD80, CD80 or both molecules 1 day p.i with PBS or alum-ppt NP-OVA (D1).

e) Graph showing the percentage of $MHCII^+$ LTi-like ILC3 which express CD80, CD80 or both molecules 1 day p.i with PBS or Alum ppt NP-OVA (D1).

f) Histograms showing expression of CD80 and CD86 on $MHCII^{hi}$ $CD11c^+$ DCs (left) and $MHCII^+$ LTi-like ILC3 (right) 1 day p.i with PBS or alum-ppt NP-OVA. Naïve $CD80^{-/-}CD86^{-/-}$ control shown alongside (filled histogram). Y axis is normalised to mode.

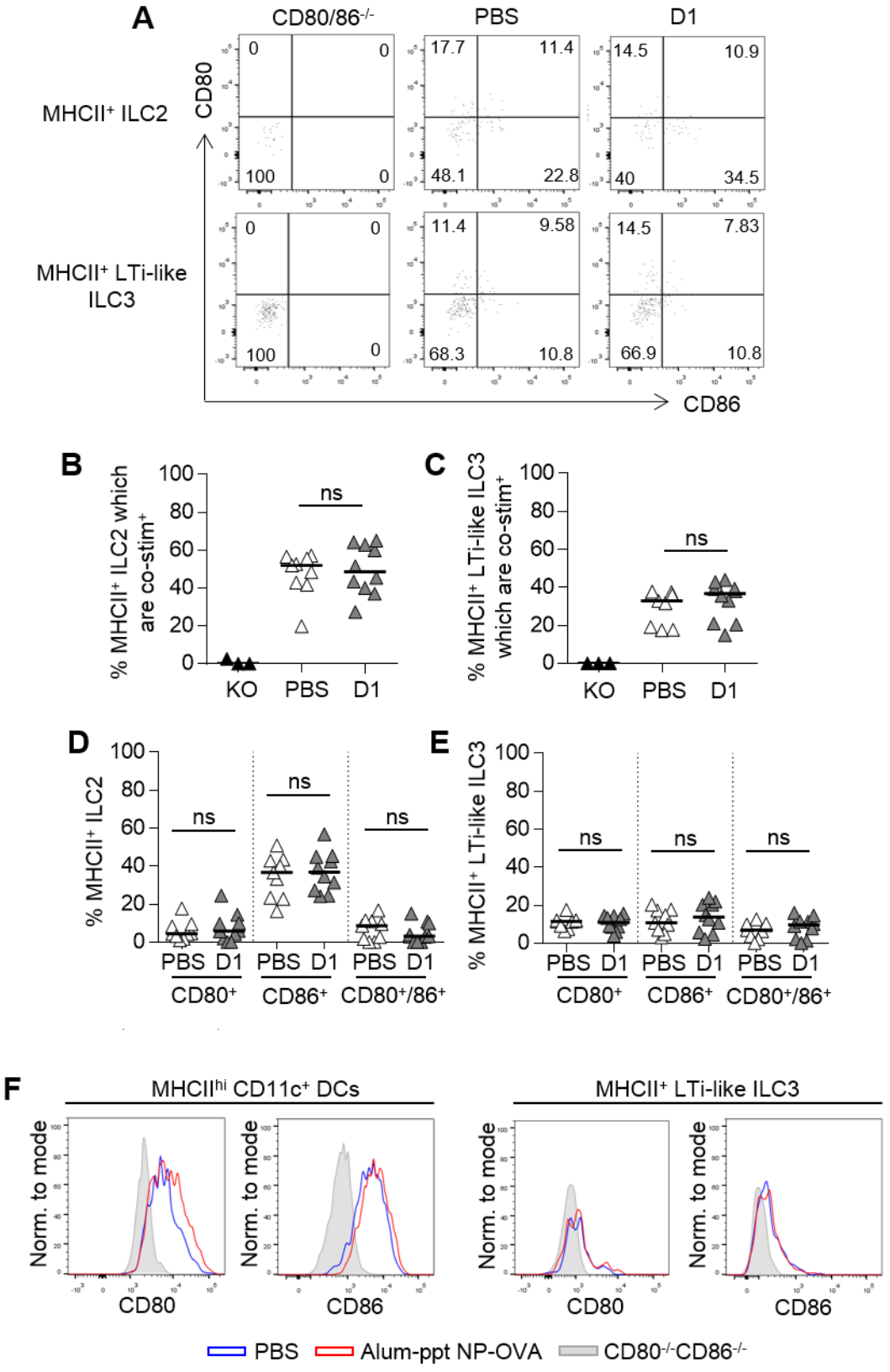
A
CD80/86-/-
PBS
D1
MHCII+ ILC2
MHCII+ LTi-like ILC3
CD80
CD86
0
100
17.7
48.1
22.8
14.5
40
34.5
10.9
11.4
9.58
68.3
10.8
7.83
66.9
B
% MHCII+ ILC2 which are co-stim+
C
% MHCII+ LTi-like ILC3 which are co-stim+
KO
PBS
D1
ns
D
% MHCII+ ILC2
E
% MHCII+ LTi-like ILC3
CD80+
CD86+
CD80+/86+
F
MHCIIhi CD11c+ DCs
MHCII+ LTi-like ILC3
Norm. to mode
PBS
Alum-ppt NP-OVA
CD80-/-CD86-/-

Fig. 4.8

phenotype, in a manner similar to that discussed above, both 4 and 8 days p.i. Each subset was once again identified as lineage (CD3/CD5/B220/CD11b/CD11c) negative cells which expressed high levels of IL-7Rα, and then further distinguished by expression of transcription factors and other surface markers (Figure 4.9a). Surprisingly, although total number of ILCs did increase at day 4 (D4) p.i with alum-ppt NP-OVA, this was not determined to be statistically significant from PBS controls in this study, whilst the increase in total ILCs by day 8 (D8) was found to be highly statistically significant (Figure 4.9b). This draining LN model has consistently revealed a biological trend towards increases in the number of ILCs in a dLN, however in this particular study only the increase in NCR^+ ILC3 was found to be statistically significant 4 days p.i. (Figure 4.9c); nonetheless the trend remained the same, with moderate increases in the median number of ILC2 and LTi-like ILC3. By day 8, however, all subsets had statistically significantly increased in comparison to PBS controls (Figure 4.9c), with LTi-like ILC3 marginally the most abundant ILC per LN at this timepoint.

Four days p.i there was no significant difference in the number of each ILC subset which expressed MHCII in dLNs from PBS controls and alum-ppt NP-OVA immunised mice, and similarly to at D1 timepoints no difference in the overall percentages were observed (Figure 4.10a,b). Although 8 days following immunisation there was a significant increase in the number of LTi-like ILC3 which were $MHCII^+$ in dLNs compared to PBS controls (Figure 4.10c) this appeared to correspond to an overall decrease in the total percentage of LTi-like ILC3 which expressed this molecule (Figure 4.10d). As with early in an immune response a proportion of $MHCII^+$ ILC2s expressed CD80 and/or CD86 (co-$stim^+$) at both D4 and D8 timepoints, and although there was an increase in the median percentage of co-stimulatory positive cells, this was not statistically significant at either timepoint

Figure 4.9 Numbers of dLN ILCs increase more substantially at later timepoints in an immune response

All WT mice received 10^5 OTII TCR transgenic $CD4^+$ T cells intravenously a day before immunisation with PBS or alum-ppt NP-OVA in both front paw pads. Cells were isolated and pooled from bLN and aLNs 1 day p.i, as detailed in methods. Samples were analysed by flow cytometry and absolute numbers per lymph node calculated. Lin^- IL-7Rα^+ RORγt^+ ILC3 subset further split into those which express NKp46 at a level comparable to ILC1 (NCR^+ $MHCII^-$ ILC3) and those which do not (LTi-like ILC3), whilst ILC1 are defined as Lin^- IL-7Rα^+ RORγt^- GATA-3^- cells.

All bars shown on graphs represent the median value. Data representative of (a) or pooled from (b,c) 2 independent experiments. Statistical test used is Mann-Whitney non-parametric, two-tailed test. **P*<0.05, ***P*<0.01, ****P*<0.001 and *****P*<0.0001.

a) FACS plots showing gating on populations of ILCs in bLN and aLNs 4 (centre) or 8 days (bottom) days p.i. with alum-ppt NP-OVA and compared to PBS control (top). Cells are pre-gated on $CD11c^-$ cells and Lin is CD3/CD5/B220.

b) Graph showing the total number of Lin^- IL-7Rα^+ ILCs per LN in PBS control mice (white triangles) or 4 and 8 days p.i with alum-ppt NP-OVA (D4, D8; grey triangles). PBS controls are pooled from both D4 and D8 timepoints. (n=10,6,6).

c) Graph showing the number of ILC1, ILC2, LTi-like ILC3 or NCR^+ ILC3 per LN in PBS (P) controls, 4 days or 8 days p.i with alum-ppt NP-OVA (D4, D8). PBS controls are pooled from both D4 and D8 timepoints (n=10,6,6).

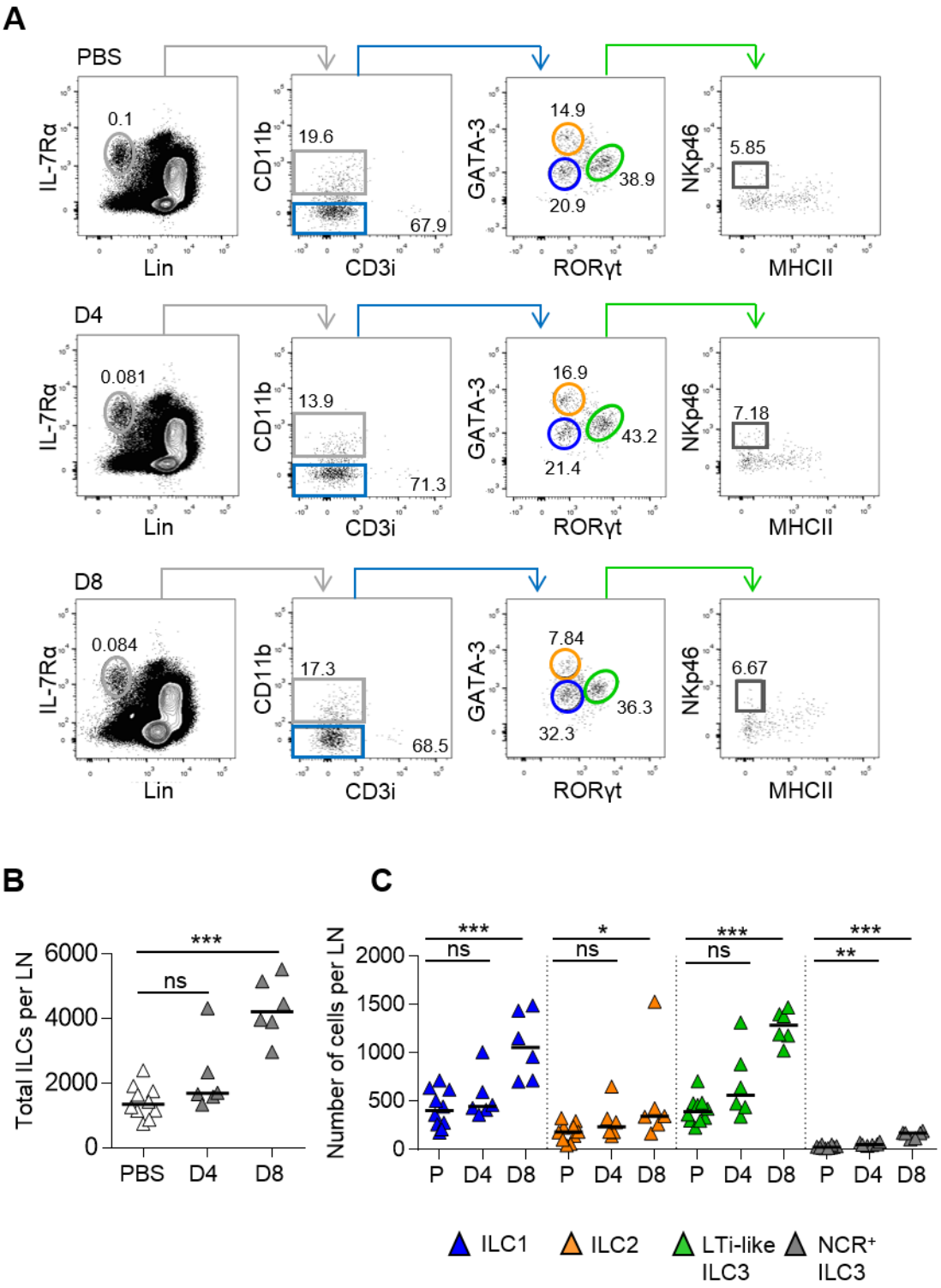
A
PBS
D4
D8
IL-7Rα
Lin
CD11b
CD3i
GATA-3
RORγt
NKp46
MHCII
0.1
19.6
67.9
14.9
38.9
20.9
5.85
0.081
13.9
71.3
16.9
43.2
21.4
7.18
0.084
17.3
68.5
7.84
36.3
32.3
6.67
B
Total ILCs per LN
6000
4000
2000
0
***
ns
PBS
D4
D8
C
Number of cells per LN
2000
1500
1000
500
0
***
ns
*
ns
***
ns
***
**
P
D4
D8
ILC1
ILC2
LTi-like ILC3
NCR+ ILC3

Fig. 4.9

Figure 4.10 A proportion of ILC2 and LTi-like ILC3 express MHCII in draining LNs at later timepoints in an immune response

All WT mice received 10^5 OTII TCR transgenic $CD4^+$ T cells intravenously a day before immunisation with PBS or alum-ppt NP-OVA in both front paw pads. Cells were isolated and pooled from bLN and aLNs 1 day p.i, as detailed in methods. Samples were analysed by flow cytometry and absolute numbers per lymph node calculated. ILC1 are defined as $ROR\gamma t^-$ $GATA\text{-}3^-$ ILCs.

All bars shown on graphs represent the median value. Data pooled from 2 independent experiments. Statistical test used is Mann-Whitney non-parametric, two-tailed test. **P*<0.05, ***P*<0.01, ****P*<0.001 and *****P*<0.0001.

a) Graph showing the total number of ILC1, ILC2 and LTi-like ILC3 which express MHCII per LN 4 days p.i with PBS or alum-ppt NP-OVA (D4). (n=5,6).

b) Graph showing the percentage of ILC1, ILC2 and LTi-like ILC3 which express MHCII 4 days p.i with PBS or alum-ppt NP-OVA (D4). (n=5,6).

c) Graph showing the total number of ILC1, ILC2 and LTi-like ILC3 which express MHCII per LN 8 days p.i with PBS or alum-ppt NP-OVA (D8). (n=5,6).

d) Graph showing the percentage of ILC1, ILC2 and LTi-like ILC3 which express MHCII 8 days p.i with PBS or alum-ppt NP-OVA (D8). (n=5,6).

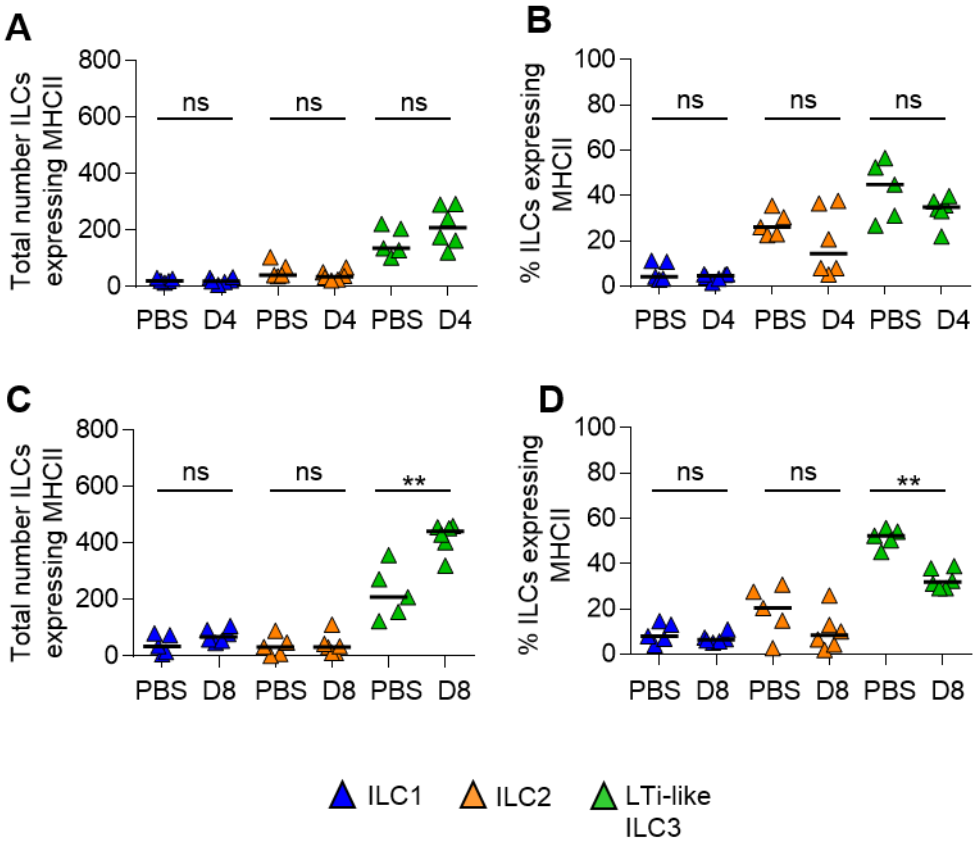
A
Total number ILCs expressing MHCII
800
600
400
200
0
ns
ns
ns
PBS D4 PBS D4 PBS D4
B
% ILCs expressing MHCII
100
80
60
40
20
0
ns
ns
ns
PBS D4 PBS D4 PBS D4
C
Total number ILCs expressing MHCII
800
600
400
200
0
ns
ns
**
PBS D8 PBS D8 PBS D8
D
% ILCs expressing MHCII
100
80
60
40
20
0
ns
ns
**
PBS D8 PBS D8 PBS D8
ILC1
ILC2
LTi-like ILC3

Fig. 4.10

(Figure 4.11a), nor was there any significant increase in the percentage of MHCII$^+$ LTi-like ILC3 which expressed either molecule (Figure 4.11b). As seen previously at day 1 p.i there was no obvious bias of MHCII$^+$ LTi-like ILC3 towards expression of CD80, CD86 or both molecules (Figure 4.11d), however in contrast to the phenotype seen at day 1 MHCII$^+$ ILC2 at day 4 and day 8 timepoints did not appear to express very much CD86, expressing instead CD80 (Figure 4.11c). As this was also true of PBS controls, this difference was unlikely to be due to the immunisation, perhaps instead indicating subtle differences between ILCs in male mice (D1 timepoint) versus female (D4 and D8) or other factors unknown. It is important however to take into account that if the number of MHCII$^+$ co-stim$^+$ ILC2 or LTi-like ILC3 are analysed as a percentage of the total ILC2 or LTi-like ILC3 in a LN at either timepoint, as opposed to just those which are MHCII$^+$, this is only a very small percentage of total ILCs (Figure 4.11e,f).

4.3.5 Ability of ILCs to proliferate following immunisation

These data so far have shown a modest increase in ILC number at early timepoints in an immune response, followed by a more substantial accumulation by day 8 p.i. To determine the mechanism of this increase expression of the proliferation marker Ki67 was analysed to determine whether evidence of increased ILC proliferation could account for the increase seen. A proportion of ILC1 and ILC2 could be seen to express Ki67—a marker of cell cycling and proliferation—at steady state (Figure 4.12a,b), in contrast to LTi-like ILC3 which uniformly lacked Ki67 expression. NCR$^+$ ILC3 Ki67 expression was more varied than in other subsets, probably reflecting some expression of Ki67 by these cells but also that the number of this ILC3 subset is so low in lymph nodes that, perhaps for this reason, this analysis is more variable. Although there were some significant changes in the percentage of Ki67$^+$ ILC when each subset was analysed across the timecourse—with the

Figure 4.11 Characterisation of co-stimulatory molecule expression by ILC2 and LTi-like ILC3

All WT mice received 10^5 OTII TCR transgenic $CD4^+$ T cells intravenously a day before immunisation with PBS or alum-ppt NP-OVA in both front paw pads. Cells were isolated and pooled from bLN and aLNs 1 day p.i, as detailed in methods. Samples were analysed by flow cytometry and absolute numbers per lymph node calculated. Non-immunised $CD80^{-/-}$ $CD86^{-/-}$ mice were used to control for expression of CD80 and CD86.

All bars shown on graphs represent the median value. Data pooled from 2 independent experiments. Statistical test used is Mann-Whitney non-parametric, two-tailed test. *P<0.05, **P<0.01, ***P<0.001 and ****P<0.0001.

a) Graph showing the percentage of $MHCII^+$ ILC2 which express CD80 and/or CD86 (co-$stim^+$) in naïve $CD80^{-/-}CD86^{-/-}$ (black triangles) or 4 (left) or 8 (right) days p.i with PBS (white triangles) or alum-ppt NP-OVA (D4, D8; grey triangles).

b) Graph showing the percentage of $MHCII^+$ LTi-like ILC3 which express CD80 and/or CD86 (co-$stim^+$) in naïve $CD80^{-/-}CD86^{-/-}$ or 4 (left) or 8 (right) days p.i with PBS or alum-ppt NP-OVA (D4, D8).

c) Graph showing the percentage of $MHCII^+$ ILC2 which express CD80, CD80 or both molecules 4 (left) or 8 (right) days p.i with PBS or alum-ppt NP-OVA (D4, D8).

d) Graph showing the percentage of $MHCII^+$ LTi-like ILC3 which express CD80, CD80 or both molecules 4 (left) or 8 (right) days p.i with PBS or alum-ppt NP-OVA (D4, D8).

e) Graph showing the percentage of total ILC2 which express CD80 and/or CD86 (co-$stim^+$) in naïve $CD80^{-/-}CD86^{-/-}$ or 4 (left) or 8 (right) days p.i with PBS or alum-ppt NP-OVA (D4, D8).

f) Graph showing the percentage of total LTi-like ILC3 which express CD80 and/or CD86 (co-$stim^+$) in naïve $CD80^{-/-}CD86^{-/-}$ or 4 (left) or 8 (right) days p.i with PBS or alum-ppt NP-OVA (D4, D8).

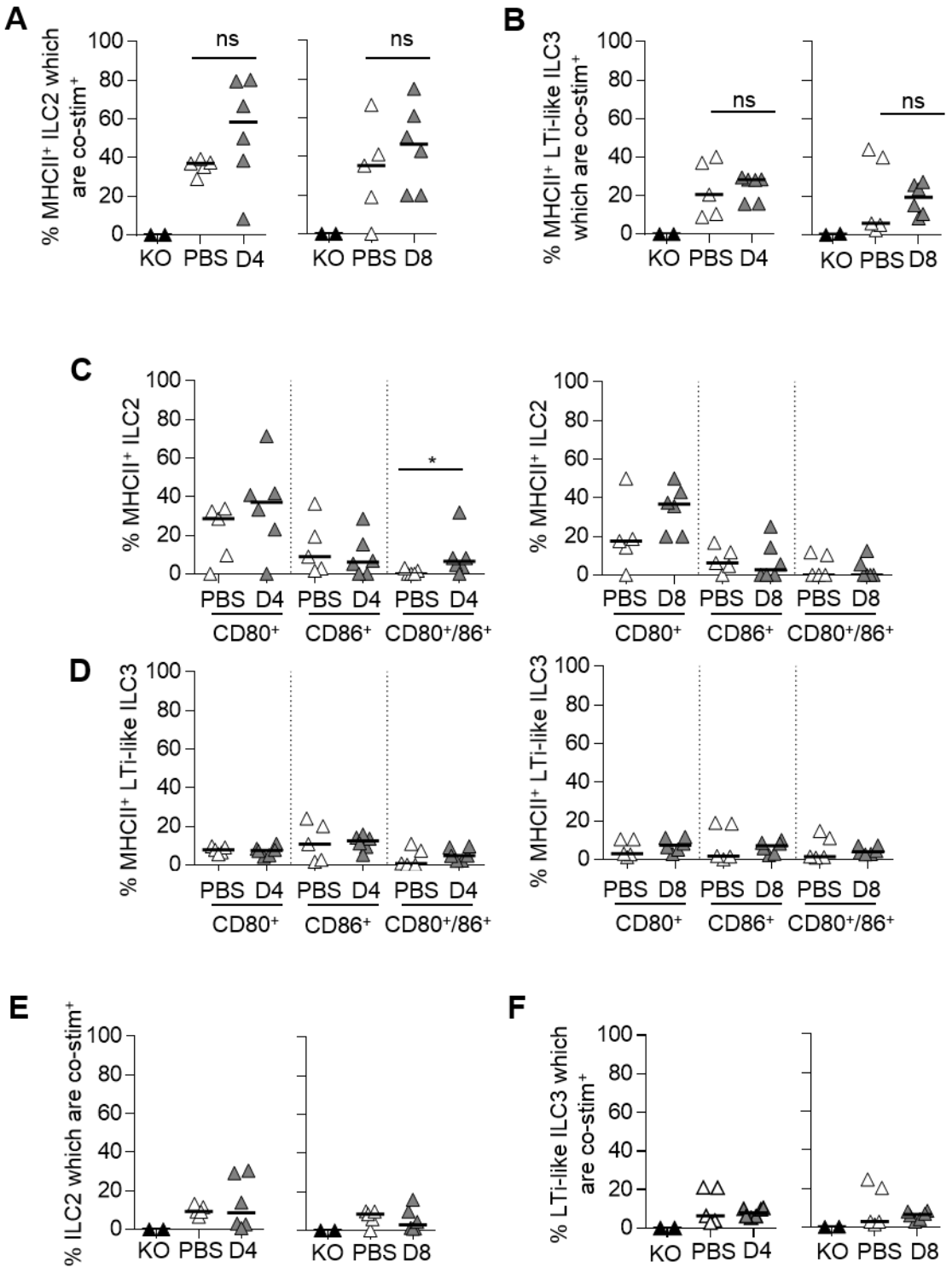
A
% MHCII+ ILC2 which are co-stim+
ns
ns
KO PBS D4
KO PBS D8
B
% MHCII+ LTi-like ILC3 which are co-stim+
ns
ns
KO PBS D4
KO PBS D8
C
% MHCII+ ILC2
*
PBS D4
CD80+
CD86+
CD80+/86+
PBS D8
D
% MHCII+ LTi-like ILC3
E
% ILC2 which are co-stim+
F
% LTi-like ILC3 which are co-stim+

Fig. 4.11

Figure 4.12 ILCs do not proliferate substantially in draining LNs

All WT mice received 10^5 OTII TCR transgenic $CD4^+$ T cells intravenously a day before immunisation with PBS or alum-ppt NP-OVA in both front paw pads. Cells were isolated and pooled from bLN and aLNs 1 day p.i, as detailed in methods. Samples were analysed by flow cytometry and absolute numbers per lymph node calculated. Lin^- IL-$7R\alpha^+$ $ROR\gamma t^+$ ILC3 subset further split into those which express NKp46 at a level comparable to ILC1 (NCR^+ $MHCII^-$ ILC3) and those which do not (LTi-like ILC3), whilst ILC1 are defined as Lin^- IL-$7R\alpha^+$ $ROR\gamma t^-$ $GATA\text{-}3^-$ cells.

All bars shown on graphs represent the median value. Data representative of (a,c) or pooled from (b,d) 2 (D4, D8) or 3 (D1) independent experiments. Statistical test used is Mann-Whitney non-parametric, two-tailed test. *P<0.05, **P<0.01, ***P<0.001 and ****P<0.0001.

a) FACS plots showing Ki67 expression by ILC subsets in PBS controls and 1 day p.i with alum-ppt NP-OVA (D1).

b) Graphs showing the percentage of each subset of ILC which were $Ki67^+$ 1, 4 and 8 days p.i with either PBS (P) or alum-ppt NP-OVA (D1, D4, D8). Y axis scale on the leftmost graph applies to all. (n=9,10,5,6,5,6).

c) FACS plots showing Ki67 expression by $MHCII^-$ (blue) and $MHCII^+$ (red) ILC2 in PBS control mice.

d) Graph showing the percentage of $MHCII^-$ and $MHCII^+$ ILC2 which express Ki67 in bLN and aLNs of PBS control mice pooled from across all timepoints. (n=9,9).

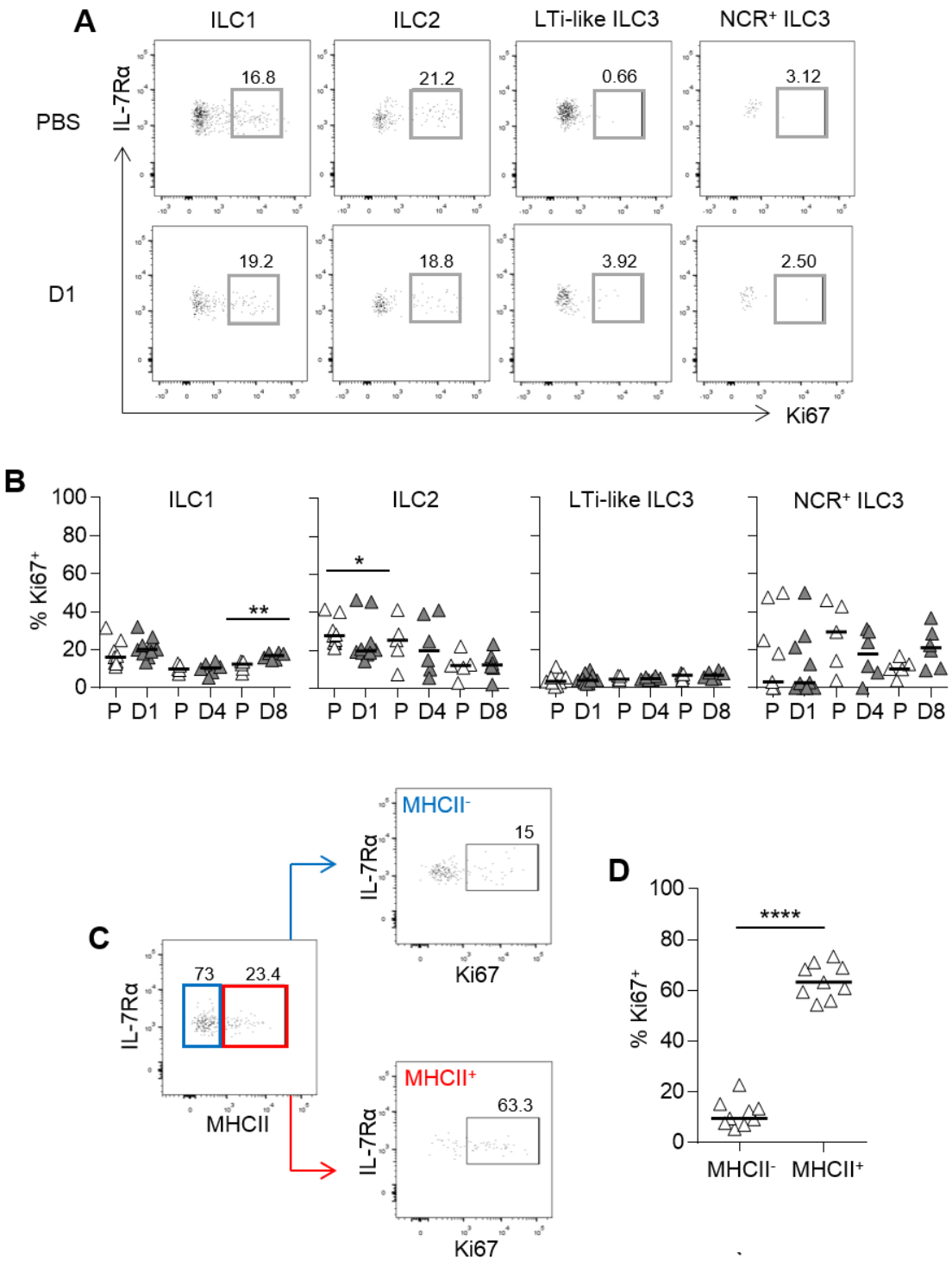
A
ILC1
ILC2
LTi-like ILC3
NCR⁺ ILC3
PBS
D1
IL-7Rα
Ki67
16.8
21.2
0.66
3.12
19.2
18.8
3.92
2.50
B
ILC1
ILC2
LTi-like ILC3
NCR⁺ ILC3
% Ki67⁺
P D1 P D4 P D8
C
MHCII⁻
MHCII⁺
IL-7Rα
MHCII
Ki67
73
23.4
15
63.3
D
% Ki67⁺
MHCII⁻
MHCII⁺
****

Fig. 4.12

percentage Ki67$^+$ ILC1 increased at day 8 p.i with alum-ppt NP-OVA (Figure 4.12b) and the percentage of Ki67$^+$ significantly decreased at day 1 p.i when compared to PBS controls (Figure 4.12b)—Ki67 expression by ILCs in draining lymph nodes appears largely comparable to those analysed at steady state, certainly not increased to an extent which would explain the increase in ILC number.

Strikingly further analysis of MHCII$^-$ and MHCII$^+$ ILC2 populations in PBS control brachial and axillary lymph nodes revealed that those ILC2 which expressed MHCII also expressed significantly more Ki67 (Figure 4.12c,d), perhaps implying fundamental differences between these two ILC2 populations.

4.3.6 ILCs do not accumulate in dLNs of CD80$^{-/-}$CD86$^{-/-}$ mice.

To further investigate the potential pathways regulating ILC accumulation in the draining LN, we used CD80$^{-/-}$CD86$^{-/-}$ mice to provide some further insight into the mechanisms involved in ILC increase in LNs. CD80$^{-/-}$CD86$^{-/-}$ mice were used to study the effects of immunisation on ILCs in a system where the ability of T cells to respond was impaired. In these mice all cell types lack the expression of the co-stimulatory molecules CD80 and CD86, one result being that antigen-presenting cells are unable to provide co-stimulatory signals to T cells through interaction with CD28 (Green et al., 1994). In the absence of this signal T cells are unable to become activated and proliferate even in the presence of their cognate antigen, and therefore both T cell responses and T cell-dependent processes are affected. These mice proved useful in analysing the effect of a T cell response on the response of ILCs to immunisation. Analysis of the ILC composition of brachial and axillary LNs taken from PBS control mice revealed that the number of ILC1, ILC2, LTi-like ILC3 and NCR$^+$ ILC3 did not differ significantly between WT and CD80$^{-/-}$CD86$^{-/-}$ mice (Figure

4.13a,b). The absence of CD80 and CD86 did not therefore have any effect on the number of ILCs present in LNs at steady state.

To verify the abrogation of T cell activation within these mice, OTII TCR transgenic $CD4^+$ T cells were transferred intravenously into WT and $CD80^{-/-}CD86^{-/-}$ mice, which were immunised the following day with either PBS or alum-ppt NP-OVA. Analysis of total OTII cell number per LN 4 days p.i revealed that whilst there had been an increase in OTII cell number in the lymph nodes of alum-ppt NP-OVA immunised WT mice compared with PBS controls, there had been no such increase in $CD80^{-/-}CD86^{-/-}$ mice (Figure 4.13c,d). This was consistent with an impairment in T cell activation and proliferation resulting from the inability of APCs to provide 'signal 2', and supported by the fact that OTII cells within immunised $CD80^{-/-}CD86^{-/-}$ mice had lower levels of Ki67 than those in immunised WT mice (Figure 4.13d).

Analysis of ILC1, ILC2, LTi-like ILC3 and NCR^+ ILC3 populations in WT mice revealed that all had increased in number when compared to PBS controls (Figure 4.13e), consistent with earlier biological trends. By comparison, in $CD80^{-/-}CD86^{-/-}$ mice, despite the numbers of ILCs at resting state not being significantly different to those in WT mice, there had been no significant increase in number following immunisation (Figure 4.13e); and when numbers of ILC1, LTi-like ILC3 and NCR^+ ILC3 in alum-ppt NP-Ova immunised WT and $CD80^{-/-}CD86^{-/-}$ LNs were compared they were found to differ statistically significantly at day 4.

4.4 SUMMARY

Characterisation of the response of ILC populations to immunisation has revealed that ILCs accumulate in a draining peripheral LN during an immune response but, despite

Figure 4.13 ILCs do not accumulate in dLNs of mice which lack CD80 and CD86

WT mice compared to $CD80^{-/-}CD86^{-/-}$ mice. All mice received 10^5 OTII transgenic $CD4^+$ T cells intravenously a day before immunisation with either PBS (control) or alum-ppt NP-OVA in both front paw pads. All mice were taken at 4 days p.i and a cell suspension made from brachial and axillary LNs as specified in methods. Samples were analysed by flow cytometry and absolute numbers per lymph node calculated. Lin^- IL-$7R\alpha^+$ $ROR\gamma t^+$ ILC3 subset further split into those which express NKp46 at a level comparable to ILC1 (NCR^+ ILC3) and those which do not (LTi-like ILC3), whilst ILC1 are defined as Lin^- IL-$7R\alpha^+$ $ROR\gamma t^-$ GATA-3^- cells.

All bars shown on graphs represent the median value. Data representative of (a,c) or pooled from (b,d,e) 3 independent experiments. Statistical test used is Mann-Whitney non-parametric, two-tailed test. *P<0.05, **P<0.01, ***P<0.001 and ****P<0.0001.

a) FACS plots showing gating ILC populations in WT and $CD80^{-/-}CD86^{-/-}$ LNs 4 days p.i with PBS or alum-ppt NP-OVA. Cells were pre-gated on Lin^- (CD3/CD5/B220/CD11b/CD11c, $CD3i^-$) IL-$7R\alpha^+$ ILCs.

b) Graph showing the total number of each ILC subset per LN in WT (white) and $CD80^{-/-}CD86^{-/-}$ (grey) PBS control mice. (n=6,8).

c) FACS plots showing gating on $CD44^{hi}$ OTII cells in WT (top) and $CD80^{-/-}CD86^{-/-}$ (bottom) mice 4 days p.i with PBS or alum-ppt NP-OVA (D4). Cells are pre-gated on $CD3^+$ $CD4^+$ T cells and Vβ5.1/2 TCR is used for OTII cell detection.

d) Graph (top) showing the total number of $CD44^{hi}$ OTII cells per LN in WT (white) and $CD80^{-/-}CD86^{-/-}$ (grey) mice 4 days p.i with PBS or alum-ppt NP-OVA (D4) and the percentage of $CD44^{hi}$ OTII cells which are $Ki67^+$ (bottom). (n=6,8,8,9).

e) Graphs showing the total number of each subset of ILC per LN in WT (white) and $CD80^{-/-}CD86^{-/-}$ (grey) mice 4 days p.i with PBS or alum-ppt NP-OVA (D4). Leftmost Y axis scale applies to all graphs.

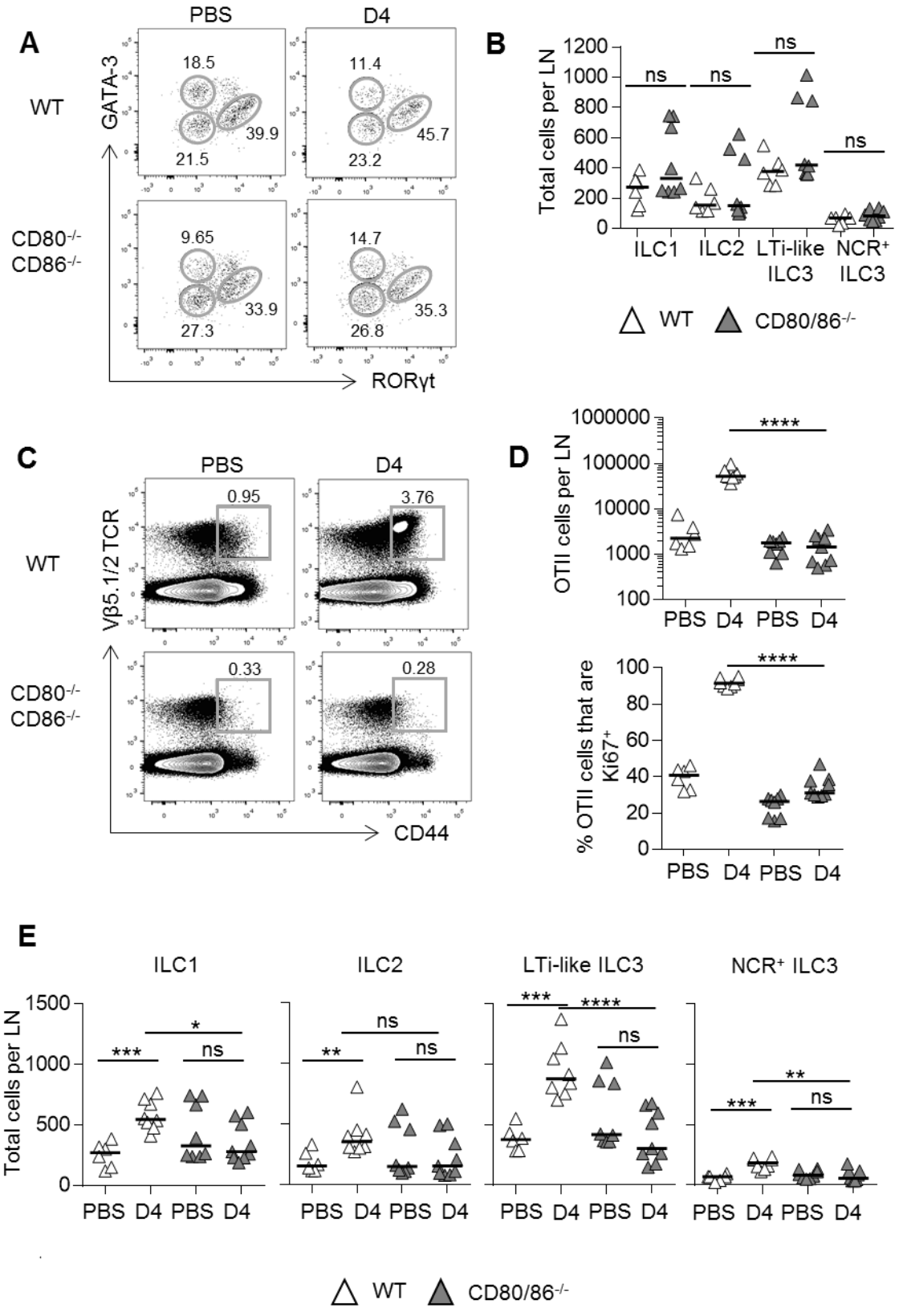
A
PBS
D4
WT
CD80-/-
CD86-/-
GATA-3
RORγt
18.5
39.9
21.5
11.4
45.7
23.2
9.65
33.9
27.3
14.7
35.3
26.8
B
Total cells per LN
ILC1
ILC2
LTi-like ILC3
NCR+ ILC3
ns
WT
CD80/86-/-
C
Vβ5.1/2 TCR
CD44
0.95
3.76
0.33
0.28
D
OTII cells per LN
% OTII cells that are Ki67+
****
E
ILC1
ILC2
LTi-like ILC3
NCR+ ILC3
Total cells per LN
*
**
***

Fig. 4.13

some expression of MHCII and co-stimulatory molecules, seem unlikely to function like DCs as inducers of primary $CD4^+$ T cell responses.

Using an optimised draining LN model we were able to analyse changes in ILC number and phenotype across a timecourse, focusing first on early timepoints in an immune response. DCs have been shown to accumulate within a draining peripheral LN by 1 day post immunological stimulation of the skin (Tomura et al., 2014) and in this investigation we show an increase in the total number of ILCs at this timepoint, as well as specific increases in populations of ILC2 and LTi-like ILC3.

MHCII expression has previously been detected on ILC3 (Hepworth et al., 2013) and ILC2 (Oliphant et al., 2014) isolated from the mLN. We show here that a proportion of ILC2 and LTi-like ILC3 within pooled brachial and axillary LNs express MHCII, although there was no convincing evidence that these cells upregulated expression of this molecule following immunisation. A proportion of $MHCII^+$ ILC2 and LTi-like ILC3 were also found to express low levels of CD80 and/or CD86, thus theoretically making them capable of presenting antigen to naïve $CD4^+$ T cells and providing the signals required for activation at early timepoints following immunisation. The rarity of these cells, coupled with comparably lower levels of expression of co-stimulatory molecules than DC makes it seem unlikely that ILCs contribute to this process in any meaningful way.

All populations of ILCs had increased more substantially by day 8 of the immune response. Although LTi-like ILC3 had accumulated significantly by this timepoint, it is not clear that the ILC compartment began to resemble that observed in mucosal draining LNs. ILC2 have previously been reported to accumulate in draining medLNs following intranasal administration of type 2 immunity-inducing cytokines (Wolterink et al., 2012), however

in this study ILC2 increase was mild in comparison to the increase of other ILC subsets. This was in spite of the use of alum as an adjuvant in the latter part of this study for its capacity to induce a stronger immune response to antigen in our draining LN model, and this adjuvant is widely known to induce robust type 2 immune responses (Lindblad, 2004). It would therefore be of interest to investigate the ability of different immunisation methods to induce ILC accumulation within these LNs, in addition to a better understanding of the mechanism by which these cells accumulate in the first place.

Analysis of Ki67 expression by ILC subsets across this timecourse revealed little difference in proliferation between ILCs in PBS control LNs and those from mice immunised with alum-ppt NP-OVA. ILC2 were generally more proliferative than either ILC1 or LTi-like ILC3, but this did not appear to be related to the ongoing immune response. Proliferation of this subset has previously been documented in response to IL-2 in spleens of $RAG^{-/-}$ mice (Roediger et al., 2013) and ILC2s have been shown to respond to the production of this cytokine by T cells (Oliphant et al., 2014), however this does not seem to be the case in the immune response documented here despite the presence of activated T cells in alum-ppt NP-OVA treated mice. Interestingly a higher proportion of $MHCII^{+}$ ILC2 express Ki67 than their $MHCII^{-}$ counterparts in PBS controls, although it is not clear why this should be the case at steady state and may be indicative of differences between these two subsets of ILC2.

An absence of an ongoing T cell response did however appear to affect accumulation of ILCs within draining LNs. No accumulation of any ILC subset could be detected in $CD80^{-/-}$ $CD86^{-/-}$ mice. Although low levels of CD80 and CD86 can be detected on the surface of ILCs within these LNs it seems highly unlikely that it is the absence of these molecules on ILCs

themselves which causes this phenotype. One possible explanation is the lack of a T cell-dependent immune response within $CD80^{-/-}CD86^{-/-}$ draining LNs. In these mice APCs are unable to provide the necessary co-stimulatory signals following antigen presentation, and as a result T cells do not become activated. It is possible that signals resulting from T cell expansion and activation subsequently facilitate the accumulation of ILCs. Whether or not this is a direct effect of T cell activation, or due to impairments of other elements of the immune response in these mice is yet to be seen.

Overall, there is no evidence that ILCs change their phenotype to become potent professional antigen-presenting cells or increase in number substantially in the skin-draining LN immune responses investigated in this study. Although it can be argued that the number and phenotype of DC populations within this study similarly did not change notably early in an immune response, these cells are fundamentally better at this function than populations of ILCs. All subsets of ILCs had accumulated most noticeably at later timepoints in the immune response, but it is not clear that this increase in ILC numbers is indicative of a role in skin-draining immune responses or just as a result of LN enlargement and shutdown. To address this, sophisticated genetic mouse models of ILC depletion will need to be used, and although these exist for the deletion of populations of ILC2 (Oliphant et al., 2014) and the specific deletion of MHCII on ILC3 (Hepworth et al., 2013, von Burg et al., 2014), they are not as yet widely available.

CHAPTER 5. DETERMINING THE MECHANISM OF ILC ENTRY INTO LNS

5.1 INTRODUCTION

My analysis of changes in ILC populations in peripheral LNs responding to immunisation revealed that ILCs increase in number in a draining LN in a manner independent of cell proliferation. Rather, this may instead reflect an ability of these cells to migrate and enter lymph nodes from distant tissues. Trafficking of certain immune cells from the peripheral and mucosal tissues to the local draining LNs has been well-established, as are many of the mechanisms which underlie this process.

Entry of cells into secondary lymphoid tissue such as spleen and lymph nodes can be through the blood or in the case of lymph nodes also via the afferent lymph. Naïve lymphocytes migrate through many different lymph nodes, entering from the blood at high endothelial venules (HEVs) and leaving through the efferent lymph, which eventually filters back into the blood via the thoracic duct (von Andrian and Mempel, 2003, Gowans and Knight, 1964). By comparison, immune cells which patrol the peripheral tissues gain entry to the lymph nodes through the lymph, entering lymphatic vessels in the tissues which then transport them to the local lymph node through the afferent lymphatics. Both of these mechanisms of entry rely on the expression of distinct chemokine receptors and molecules which facilitate cell entry through the HEVs or lymphatics.

The chemokine receptor CCR7 has previously been described in this investigation for its role in dictating cell movement within the organised structure of the lymph nodes; however it also plays a vital role in enabling cells to migrate to, and enter these structures in the first place. The ligands for CCR7—CCL19 and CCL21—are expressed within the

lymph nodes and attract cells expressing CCR7 from the blood or tissues. Well-known cell types which express CCR7 are naïve T cells and dendritic cells (DCs) (Forster et al., 2008).

Naïve T cells enter the lymph nodes through HEVs in a CCR7-dependent manner. Lymph nodes from mice which lack expression of CCR7 are depleted of T cells (Forster et al., 1999). $CCR7^{-/-}$ T cells are impaired in their ability to enter LNs yet are present in the spleen, demonstrating the different homing requirements of these secondary lymphoid tissues (Forster et al., 1999). T cells which have been recruited into tissues are also capable of entering LNs through the afferent lymphatics, in a process which is similarly dependent on CCR7 (Debes et al., 2005, Bromley et al., 2005). DCs upregulate CCR7 upon activation (Sallusto et al., 1998), expression of which facilitates their migration to the local draining LN. Given that DCs reside in peripheral tissues, their entry into LNs is thought to be primarily through the afferent lymphatics. Whilst the number of DCs in peripheral organs of $CCR7^{-/-}$ mice is similar to WT, $CCR7^{-/-}$ DCs are impaired in their ability to home to lymphoid tissues in response to challenge (Forster et al., 1999).

Expression of CCR7 mRNA has previously been reported by adult LTi cells, although no role had been ascribed to its expression. CCR7 mRNA was detected in both adult and embryonic splenic LTi cells from T cell-deficient mice (Kim et al., 2008) and more recently expression of CCR7 was detected on the surface of $NKp46^{-}$ ILC3 in the small intestine by flow cytometry (Klose et al., 2013). Given that CCR7 expression has been shown to be integral to the trafficking of cells into these structures we hypothesised that expression of this molecule by ILCs could enable them to enter LNs and provide evidence of their ability to migrate from non-lymphoid tissues.

In this chapter I will investigate whether or not ILC entry into LNs is consistent with trafficking from peripheral and mucosal tissues. Focusing on group 3 ILCs, I explore the role of CCR7 on ILCs in a range of different lymph nodes at steady state and in skin-draining LNs following immunisation. Finally I will investigate whether or not the presence of group 3 ILCs in lymph nodes is important for a primary $CD4^+$ T cell immune response.

5.2 ROLE OF CCR7 SIGNALLING

5.2.1 ILC requirement for CCR7 for entry into LNs differs between tissues

To determine whether or not the presence of ILC subsets within lymph nodes was dependent upon CCR7 we compared the number of ILC1, ILC2, LTi-like ILC3 and NCR^+ ILC3 in the spleen, mLN and iLNs of WT and $CCR7^{-/-}$ mice. Lymph nodes in $CCR7^{-/-}$ mice have previously been described as having fewer of naïve T cells (Forster et al., 1999), due to impaired entry of T cells into these structures in the absence of CCR7 signalling. In keeping with this, we observed substantially lower numbers of $CD4^+$ T cells within mLNs from $CCR7^{-/-}$ mice, and which differed statistically significantly from WT controls (Figure 5.1a).

Within all secondary lymphoid tissue analysed from $CCR7^{-/-}$ mice it was possible to detect the three main groups of ILC, based on their expression on GATA-3, RORγt or T-bet (Figure 5.1b-e). Analysis of $CCR7^{-/-}$ spleens revealed no significant difference in the total number of ILC1, ILC2 or LTi-like ILC3 in the absence of CCR7 when compared to WT controls. The number of NCR^+ ILC3 was however lower in $CCR7^{-/-}$ spleen when compared to WT and, although a mild phenotype, this was found to be statistically significant (Figure 5.1c). This finding was consistent with published data showing that entry of certain cells

into this secondary lymphoid tissue is less dependent upon CCR7 than entry into lymph nodes; with CCR7$^{-/-}$ T cells having previously been shown to be present in the spleen despite being fewer in LNs (Forster et al., 1999). Importantly, this result indicated that any differences observed in the ILC composition of CCR7$^{-/-}$ mouse LNs should not be attributed solely to the impaired ability of any subset to develop in the absence of CCR7.

Within the mLN of CCR7$^{-/-}$ mice there were found to be lower numbers of LTi-like ILC3 than detected in WT controls, and this difference was statistically significant (Figure 5.1d). This phenotype was specific to LTi-like ILC3 since numbers of ILC1, ILC2 and NCR^{+} ILC3 were not affected within this tissue. By contrast statistically significantly lower numbers of all ILC subsets were detected in CCR7$^{-/-}$ iLNs when compared to WT iLN controls, although the greatest difference was still found in the LTi-like ILC3 population (Figure 5.1e). This observation was particularly relevant in light of earlier data suggesting inherent differences between the ILC composition of mucosal-tissue draining and peripheral tissue-draining LNs. These data suggested that whilst within the mLN LTi-like ILC3 alone require CCR7 signalling to be functional in order to achieve the numbers observed in WT controls, in the iLN this applied to all subsets; raising interesting questions about the differing requirements for ILCs to enter lymph nodes at different sites.

5.2.2 CCR6^{+} ILC3 express functional CCR7

Although these data indicated a reliance of certain ILCs on CCR7 signalling, the use of CCR7$^{-/-}$ mice does not allow for differentiation between cell-intrinsic or cell-extrinsic requirement for this receptor. Despite reports of CCR7 mRNA expression by LTi cells (Kim et al., 2008) we have previously struggled to detect its presence on the surface of ILCs

Figure 5.1 Characterisation of ILCs in CCR7$^{-/-}$ mice

Tissues from naïve WT mice compared to CCR7$^{-/-}$ mice. Cells were isolated from iLN, mLN and spleen as specified in methods. Samples were analysed by flow cytometry and absolute numbers per LN calculated. Numbers shown represent the number of cells per individual LN or whole spleen. Lin^{-} IL-7Rα^{+} RORγt^{+} ILC3 subset further split into those which express NKp46 at a level comparable to ILC1 (NCR^{+} ILC3) and those which do not (LTi-like ILC3), whilst ILC1 are defined as Lin^{-} IL-7Rα^{+} RORγt^{-} GATA-3^{-} Tbet^{+} cells.

All bars shown on graphs represent the median value. Data representative of (b) or pooled from (a,c-e) 3 independent experiments. Statistical test used is Mann-Whitney non-parametric, two-tailed test. **P*<0.05, ***P*<0.01, ****P*<0.001 and *****P*<0.0001.

a) Graph showing the total number of CD3i^{+} CD4^{+} T cells in individual mLN from WT or CCR7$^{-/-}$ mice. (n=7,9).

b) FACS plots showing gating on ILC populations in mLN from WT and CCR7$^{-/-}$ mice. Cells pre-gated on FSC/SSC. GATA-3^{-} RORγt^{-} cells further gated on T-bet. Lin is CD3/CD5/B220/CD11b/CD11c.

c) Total number of ILC1, ILC2, NCR^{+} ILC3 (NKp46^{+}) and LTi-like ILC3 (NKp46^{-}) per spleen of WT (white triangles) and CCR7$^{-/-}$ (grey triangles) mice. (n=7,9).

d) Total number of ILC1, ILC2, NCR^{+} ILC3 (NKp46^{+}) and LTi-like ILC3 (NKp46^{-}) per individual mLN of WT (white triangles) and CCR7$^{-/-}$ (grey triangles) mice. (n=7,9).

e) Total number of ILC1, ILC2, NCR^{+} ILC3 (NKp46^{+}) and LTi-like ILC3 (NKp46^{-}) per iLN of WT (white triangles) and CCR7$^{-/-}$ (grey triangles) mice. (n=7,5).

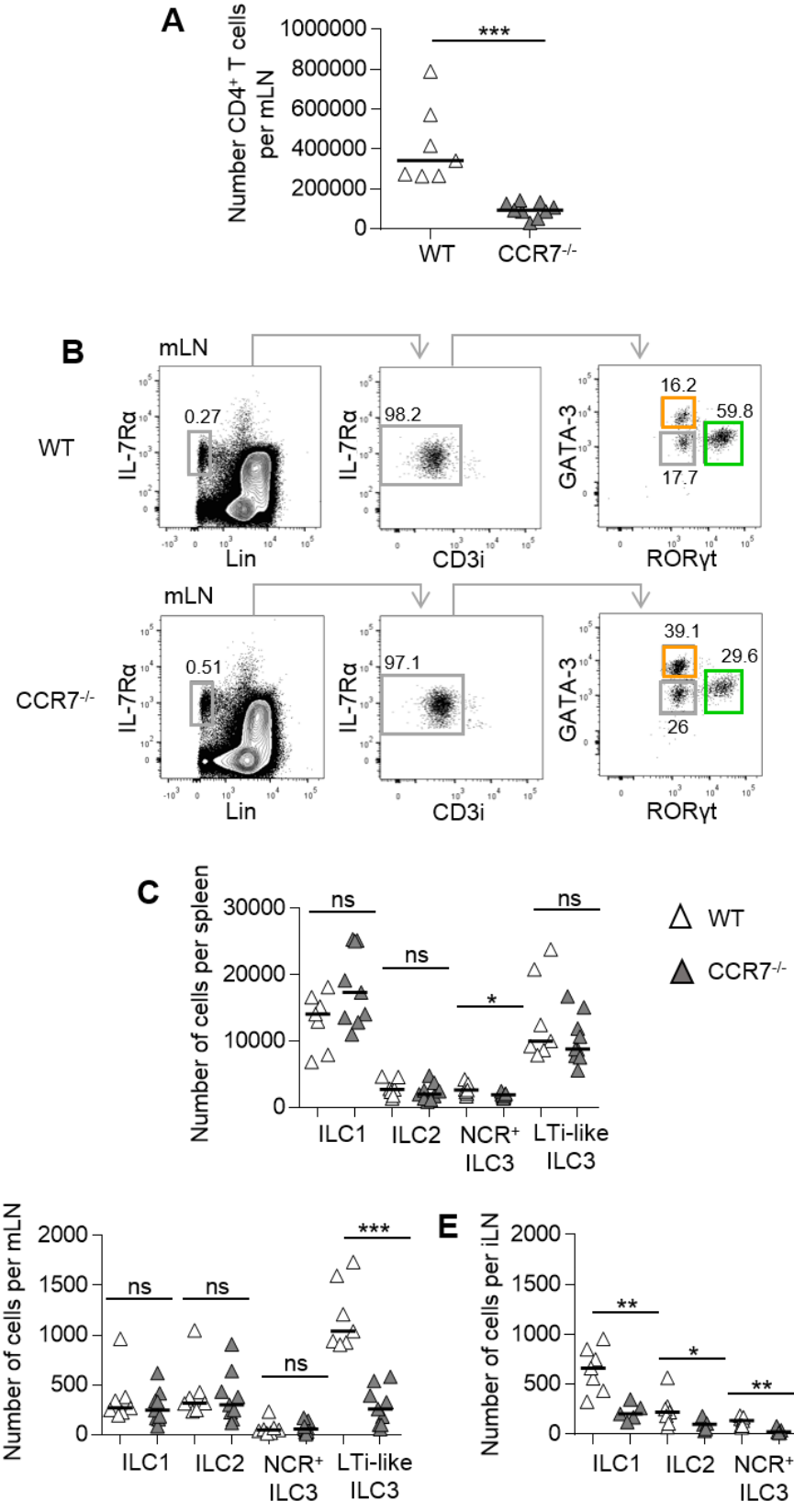
A
Number CD4+ T cells per mLN
1000000
800000
600000
400000
200000
0
***
WT
CCR7-/-
B
mLN
WT
IL-7Rα
0.27
Lin
98.2
CD3i
GATA-3
16.2
59.8
17.7
RORγt
mLN
CCR7-/-
0.51
97.1
39.1
29.6
26
C
Number of cells per spleen
30000
20000
10000
0
ns
ns
*
ns
ILC1
ILC2
NCR+ ILC3
LTi-like ILC3
WT
CCR7-/-
D
Number of cells per mLN
2000
1500
1000
500
0
ns
ns
ns
***
ILC1
ILC2
NCR+ ILC3
LTi-like ILC3
E
Number of cells per iLN
2000
1500
1000
500
0
**
*
**
**
ILC1
ILC2
NCR+ ILC3
LTi-like ILC3

Fig. 5.1

with conventional staining methods, such as fluorescently-tagged antibodies against CCR7 and analysis by flow cytometry (Figure 3.11). An alternative method of labelling CCR7-expressing cells was therefore attempted. A chemokine capture assay was utilised (Ford et al., 2013), where fluorescently labelled CCL19, a chemokine shown to bind specifically to CCR7, was incubated with cells from mLN and chemokine uptake by CCR7-expressing cells later assessed using flow cytometry. Gating on $CD4^+$ T cells, our positive control, showed that the majority were positive for the CCL19-bound fluorochrome (Figure 5.2a,b), thus indicating that these cells had bound and most likely endocytosed CCL19 and providing validation of the method. Crucially very little fluorescence was detected within $CD4^+$ T cells which lacked CCR7, therefore detection of the fluorescently-tagged chemokine was specifically as a result of it binding to CCR7 (Figure 5.2b). Given that the biotinylated CCL19 was incubated with fluorescently-tagged streptavidin (SA-647) prior to this assay, a further control where SA-647 was present without chemokine was also assessed. Despite serving as a better indicator of functional cell surface CCR7 expression, no convincing level of fluorescently-tagged CCL19 could be detected within the population of $CCR6^+$ ILC3 in this pilot study (Figure 5.2b), here using surface markers to detect ILC populations.

Although possible to conclude from this that expression of CCR7 mRNA within these cells does not result in functional expression on the cell surface, it may also be that these methods, whilst effective in detecting CCR7 on $CD4^+$ T cells, are not sensitive enough to detect it at the level expressed by ILC3. This led us to utilise a different approach. Using a transwell migration assay system we were able to isolate those cells which were capable of migrating towards CCL21, a ligand of CCR7 which binds specifically to this receptor.

Figure 5.2 CCR7 not detected on ILC3 using chemokine capture assay

Chemokine capture assay using cells from naive WT and CCR7$^{-/-}$ mice. WT Cells were isolated and pooled from a range of LNs, including mLN, iLN, aLN and bLN as specified in methods, then divided into four samples when stained. Cells were incubated with CCL19-647 or SA-647 alone. ILCs were identified using only surface markers and cells were not fixed. Samples were analysed by flow cytometry. Cells from CCR7$^{-/-}$ mice were used as a control.

Pilot data which is representative of 2 WT mice under these experimental conditions.

a) FACS plots showing gating on CD4^{+} T cells (top, pre-gated on FSC/SSC) or Lin^{-} IL-7Rα^{+} ILCs (bottom, pre-gated on FSC/SSC) from WT LNs. Lin is CD5/B220/CD11b/CD11c.

b) FACS plots showing detection of CCL19-647 on WT CD4^{+} T cells (top) or CCR6^{+} ILCs (bottom), alongside SA-647 only and CCR7$^{-/-}$ mouse controls.

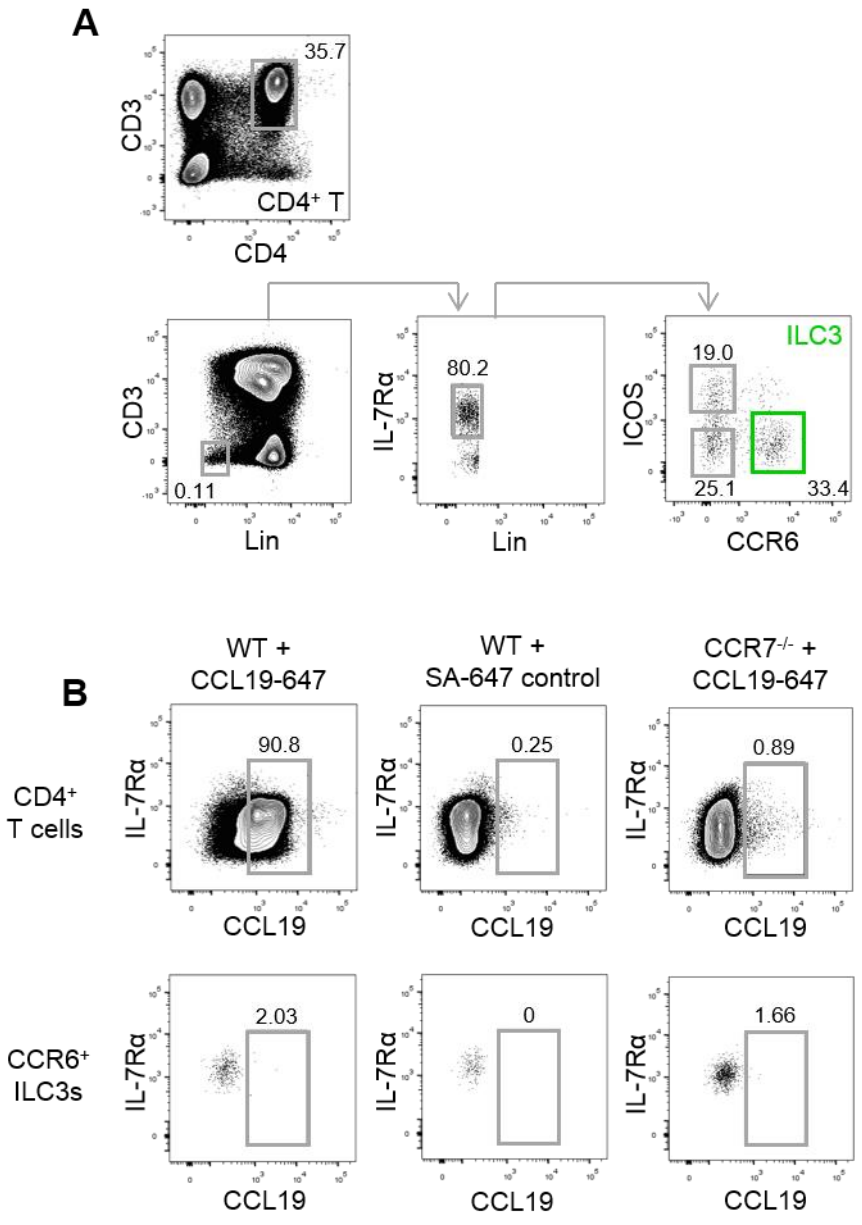
A
35.7
CD3
CD4⁺ T
CD4
CD3
0.11
Lin
80.2
IL-7Rα
Lin
ILC3
19.0
ICOS
25.1
33.4
CCR6
B
WT +
CCL19-647
WT +
SA-647 control
CCR7-/- +
CCL19-647
CD4⁺
T cells
90.8
0.25
0.89
IL-7Rα
CCL19
CCR6⁺
ILC3s
2.03
0
1.66
IL-7Rα
CCL19

Fig. 5.2

This assay therefore could reveal those cells which express even low levels of CCR7, whilst additionally providing evidence that expression of CCR7 is functional.

Within our system an 'input' well containing cells isolated from WT mLN was immersed in a solution of RPMI 2% FBS and 20nM CCL21, separated by a membrane which prevented the passive transfer of cells from the input well to that containing the chemokine solution yet allowed those cells which expressed CCR7 to actively migrate through in the direction of the chemoattractive gradient. The ability of both CCL19 and CCL21 to induce cell migration using this assay was assessed in a pilot study and found to be comparable, therefore CCL21 alone was chosen for use in final experiments, and a concentration of 20nM CCL21 was found to be sufficient to induce cell migration. The use of a whole LN suspension allowed the capacity of multiple cell types to migrate toward CCL21 to be assessed. Using the gating strategy outlined in Figure 5.3(a), $CD4^+$ T cells, B cells, DCs, ILC2 and ILC3 could be identified, and it should here be noted that in this study ILCs expressing low levels of CD11b—lower than that detected on IL-7Rα^- counterparts—were included, as it is not clear that these cells cannot acquire low levels of this molecule from interactions with other cell types (Gray et al., 2012).

The proportion of each specified cell type which had migrated from the input well, and could as a result be detected within the well containing chemokine ('output'), could then be calculated as a percentage of the total number of each cell type retrieved from both input and output wells, as detailed in the methods. RPMI 2% FBS only 'no chemokine' controls were used to assess non-chemokine specific migration of cells across the transwell membrane, whilst additionally comparing the ability of $CCR7^{-/-}$ cells to migrate towards a CCL21 gradient ensured that any migration seen in this assay was specifically

Figure 5.3 A proportion of ILC3 migrate in response to a ligand of CCR7

Chemokine transmigration assay using cells from naive WT and $CCR7^{-/-}$ mice. 2 x 10^6 WT or $CCR7^{-/-}$ cells isolated from mLN were used in each well, as specified in methods and CCL21 used at a concentration of 20nM. ILCs were identified using only surface markers and cells were not fixed. Samples were analysed by flow cytometry.

Data is representative of (a) or pooled (b) from 2 independent experiments. Bars show median value. Statistical test used is Mann-Whitney non-parametric, two-tailed test. *P<0.05, **P<0.01, ***P<0.001 and ****P<0.0001.

a) FACS plots showing gating on $CD3^+$ $CD4^+$ T cells, $CD3^-$ $B220^-$ $CD11c^+$ 'DCs' and $CD3^-$ $B220^-$ $CD11c^-$ $CD5^-$ $CD11b^{lo}$, IL-$7R\alpha^+$ ILCs retrieved from input (top) and output (bottom) wells (pre-gated on FSC/SSC). ILCs are further split into $CCR6^-$ $ICOS^+$ ILC2 and $CCR6^+$ ILC3.

b) Graphs showing the percentage of stated cell types from WT mLN (white triangles) or $CCR7^{-/-}$ mLN (grey triangles) which have migrated during this assay, calculated from the total cells retrieved from both wells, as specified in methods. Each sample was analysed in triplicate (WT) or duplicate ($CCR7^{-/-}$) and graphs display average values. WT + no chemokine controls (black triangles) and $CCR7^{-/-}$ + 20nM CCL21 controls (grey triangles) are shown alongside. Cell types are defined as shown in (a). (n=4,2,4).

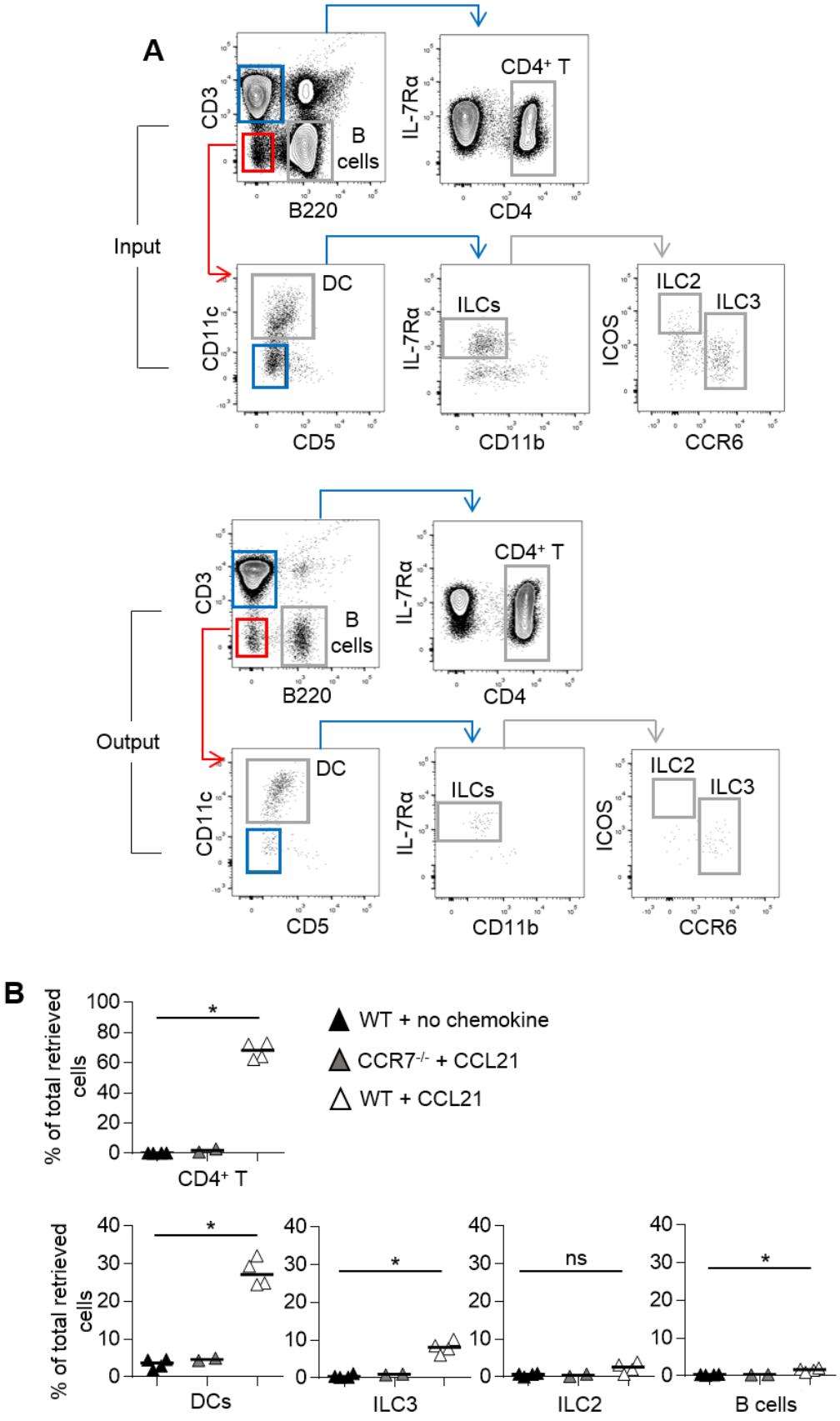
A
Input
Output
CD3
B220
B cells
CD4⁺ T
IL-7Rα
CD4
DC
CD11c
CD5
ILCs
CD11b
ILC2
ILC3
ICOS
CCR6
B
% of total retrieved cells
WT + no chemokine
CCR7-/- + CCL21
WT + CCL21
CD4⁺ T
DCs
ILC3
ILC2
B cells
*
ns

Fig. 5.3

due to CCL21 binding to CCR7. Each experimental sample was analysed in either duplicate ($CCR7^{-/-}$) or triplicate (WT no chemokine control, WT + 20nM CCL21), and average values are shown in Figure 5.3(b).

Following incubation $CD4^+$ T cells were detected within the output well, with approximately 70% of $CD4^+$ T cells having migrated to the well containing CCL21 within this time (Figure 5.3a,b). Given that we have previously detected evidence of CCR7 expression on the surface of $CD4^+$ T cells (Figure 5.2b) this was expected and confirmed the validity of the approach. Importantly, very few $CD4^+$ T cells, or indeed any other cell types analysed, were retrieved from the output well in the no-chemokine controls or in samples where all cells lacked expression of CCR7 (Figure 5.3b), thereby confirming that the migration seen was as a result of CCL21 binding to CCR7. By comparison <2% of B cells had migrated in this time, supporting the concept that although B cells are capable of expressing CCR7 (Reif et al., 2002) they are less dependent upon this molecule than T cells (Figure 5.3a,b). A proportion of the $CD3^-$ $B220^-$ $CD11c^+$ putative dendritic cell and Lin^- IL-$7R\alpha^+$ $CCR6^+$ ILC3 population had also migrated into the output well in response to CCL21. Approximately 30% of putative dendritic cells could be found within the output well following incubation, along with approximately 8% of ILC3. Although the percentage of migrating ILC3 was low in comparison to $CD4^+$ T cells and putative DCs, the proportion was statistically significant when compared to the no-chemokine control (Figure 5.3a,b) and no migration was detected by ILC3 lacking CCR7, therefore demonstrating that a proportion of ILC3 were capable of migrating toward CCL21 in a CCR7-dependent manner. The proportion of Lin^- IL-$7R\alpha^{hi}$ $CCR6^-$ $ICOS^+$ ILC2 within the output well, however, was not found to be statistically significantly higher than that seen in the no

chemokine control (Figure 5.3b), in keeping with prior observations of no ILC2 dependency for CCR7 within the mLN (Figure 5.1d).

5.2.3 CCR7-dependency of LTi-like ILC3 is in part cell intrinsic

These data indicate that CCR7 is functionally expressed on at least a proportion of CCR6^{+} ILC3 within the mLN. To determine whether the lower numbers of LTi-like ILC3 isolated from CCR7$^{-/-}$ lymph nodes resulted from the loss of direct signalling through CCR7 on the surface of LTi-like ILC3 themselves or cell extrinsic effects resulting from the loss of CCR7 signalling on other cell types, a mixed bone marrow chimera (BMC) approach was used. These chimeric mice, generated to have equal amounts of WT and CCR7$^{-/-}$ bone marrow, enabled a direct comparison of the ability of both CCR7$^{+/+}$ and CCR7$^{-/-}$ cells to re-populate secondary lymphoid tissue following the depletion of host cells using irradiation. This approach therefore provided an environment where CCR7 signalling was on some cells functional and any defect in the ability of CCR7$^{-/-}$ LTi-like ILC3 to enter lymphoid tissue regardless would indicate their requirement for direct cell-intrinsic CCR7 signalling. To generate WT:CCR7$^{-/-}$ mixed BMCs equal amounts of WT (CD45.1^{+}) and CCR7$^{-/-}$ (CD45.2^{+}) bone marrow was introduced into WT host mice, which had been lethally irradiated. For comparison, WT:WT control mice were generated using equal amounts of WT (CD45.1^{+}) and WT (CD45.2^{+}) bone marrow. Six to eight weeks following irradiation mice were culled and analysed, which allowed sufficient time for lymphoid cells to re-populate the secondary lymphoid tissue. The ability of both CCR7$^{+/+}$ and CCR7$^{-/-}$ cells to enter spleen and lymph nodes was then analysed, with their expression of either CD45.1 or CD45.2 used to determine their origin (Figure 5.4a,b).

Figure 5.4 Experiments in mixed bone marrow chimeras (BMCs) suggest that LTi-like ILC3 CCR7-dependency is in part cell-intrinsic

Chimeras were generated by lethally irradiating WT ($CD45.1^+$) mice and reconstituting with a 1:1 ratio of either WT $CD45.1^+$ and WT $CD45.2^+$ bone marrow (WT:WT) or WT $CD45.1^+$ and $CCR7^{-/-}$ $CD45.2^+$ bone marrow (WT:KO). iLN, mLN and spleen were taken for analysis and cells isolated as specified in methods. Samples were analysed by flow cytometry and absolute numbers per lymph node calculated.

All bars shown on graphs represent the median value. Dotted line shows 50%. Data representative of (a-b) or pooled from (c) 2 (spleen) or 3 (iLN and mLN) independent experiments. Statistical test used is Mann-Whitney non-parametric, two-tailed test. **P*<0.05, ***P*<0.01, ****P*<0.001 and *****P*<0.0001.

a) FACS plots showing gating strategy for $CD4^+$ T cells and LTi-like ILC3. Lin is CD3/CD5/B220/CD11b/CD11c.

b) FACS plots showing CD45.1 and CD45.2 expression by $CD4^+$ T cells (left) and LTi-like ILC3 (right) in WT:WT and WT:KO mLNs.

c) Graphs showing the percentage of $CD4^+$ T cells (top) or LTi-like ILC3 (bottom) from iLN, mLN and spleen which are $CD45.1^+$ (white triangles) or $CD45.2^+$ (grey triangles).

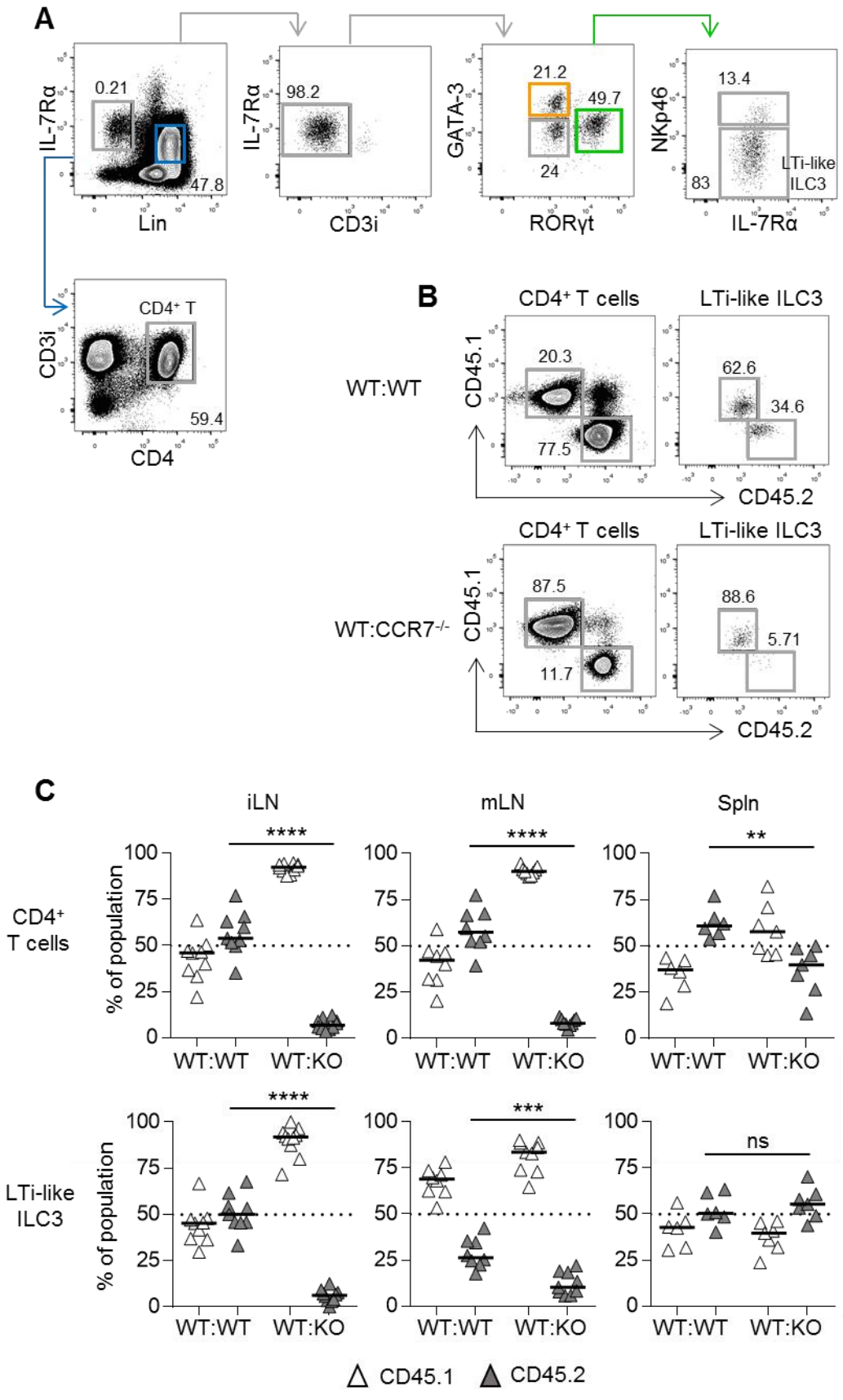
A
IL-7Rα
0.21
47.8
Lin
IL-7Rα
98.2
CD3i
GATA-3
21.2
49.7
24
RORγt
NKp46
13.4
83
LTi-like ILC3
IL-7Rα
CD3i
CD4+ T
59.4
CD4
B
CD4+ T cells
LTi-like ILC3
WT:WT
CD45.1
20.3
77.5
62.6
34.6
CD45.2
CD4+ T cells
LTi-like ILC3
WT:CCR7-/-
CD45.1
87.5
11.7
88.6
5.71
CD45.2
C
iLN
mLN
Spln
CD4+ T cells
% of population
****
****
**
100
75
50
25
0
WT:WT
WT:KO
LTi-like ILC3
% of population
****
***
ns
CD45.1
CD45.2

Fig. 5.4

Analysis of WT:WT chimeric inguinal and mesenteric LN tissue revealed that approximately 50% of the total $CD4^+$ T cell population had originated from each donor, the anticipated result given that both sets of WT cells should be identical in their ability to enter lymph nodes (Figure 5.4c). By contrast, the majority of $CD4^+$ T cells isolated from WT:$CCR7^{-/-}$ lymph nodes had originated from the WT ($CD45.1^+$) donor, thereby indicating that $CCR7^{-/-}$ $CD4^+$ T cells were unable to enter these tissues in the absence of cell-intrinsic CCR7 signalling (Figure 5.4b,c); consistent with the ability of CCR7-sufficient $CD4^+$ T cells to migrate towards ligands of CCR7 (Figure 5.3b). Certainly, if compared to $CD45.2^+$ $CD4^+$ T cells from WT:WT chimeras, $CD45.2^+$ $CCR7^{-/-}$ $CD4^+$ T cells made up a statistically significantly lower percentage of the total population than would be expected were there no effect of CCR7 deficiency on this cell type (Figure 5.4c). Similar analysis of this population in the spleen revealed that whilst there was still a statistically significantly lower percentage of $CCR7^{-/-}$ $CD4^+$ T cells than their equivalent in WT:WT mice, the phenotype was less exaggerated, consistent with the idea that T cell entry into this tissue is less dependent upon CCR7 (Forster et al., 1999) (Figure 5.4c) and demonstrating that thymic emigration of T cells was not completely abrogated in these mice in the absence of CCR7 (Ueno et al., 2004). Naïve T cell entry to LNs has been found to be primarily through HEVs (Forster et al., 2008), therefore it seems likely that these results primarily reflect entry of naïve $CD4^+$ T cells from the blood rather than the lymph and it is worth noting here that the approach outlined above cannot definitively distinguish between the two.

Like $CD4^+$ T cells, $CD45.2^+$ $CCR7^{-/-}$ LTi-like ILC3 within WT:$CCR7^{-/-}$ inguinal and mesenteric LNs made up a statistically significantly lower percentage of the total LTi-like ILC3 population than their $CD45.2^+$ WT counterparts in WT:WT controls (Figure 5.4b,c), whilst in the spleen there was no significant difference. Within iLNs analysed it was

apparent that the inability of CCR7$^{-/-}$ LTi-like ILC3 to re-populate the tissue in numbers comparable to WT LTi-like ILC3 was not ameliorated by the presence of CCR7-sufficient cells, thereby indicating that LTi-like ILC3 require cell-intrinsic CCR7 signalling for entry into iLNs (Figure 5.4c). In mLNs, however, this is less clear. The difference between the percentage of cells that had originated from CD45.2^{+} donors in WT:WT and WT:CCR7$^{-/-}$ mice, although statistically significant, was less pronounced than in the iLN, and appeared to be partially masked by a skewing of the population towards that of CD45.1^{+} origin, not observed when looking at other cell types or in other tissues.

Given that, in general, the contribution of CD45.1^{+} and CD45.2^{+} donor bone marrow had been consistently evenly proportioned during these experiments it seemed unlikely that this 'skewing' arose from problems with the bone marrow injected. It was, however, possible that this could be due to the persistence of CD45.1^{+} host LTi-like ILC3 despite irradiation. LTi cells have previously been reported to display some resistance to irradiation techniques (Dudakov et al., 2012), and previously we have had to employ additional methods, such as antibody-mediated depletion, to eliminate RORγt^{+} ILCs from murine hosts entirely. To investigate this phenomenon mixed BMCs, similar to those outlined above, were generated in CD45.1^{+}CD45.2^{+} WT host mice, thereby allowing the identification of not only donor CD45.1^{+} and CD45.2^{+} cell populations, but also those CD45.1^{+}CD45.2^{+} cells which have persisted from the host. Analysis of these new chimeras revealed that a number of LTi-like ILC3 within the mLN, but not the iLN or spleen, were indeed resistant to lethal doses of irradiation. Comparison of the origin of RORγt^{+} ILC3 from iLN, mLN and spleen in these new WT:WT chimeras showed that whilst in the iLN and spleen CD45.1^{+}CD45.2^{+} persisting ILC3 made up less than 20% of total RORγt^{+} ILC3, in the mLN they constituted approximately 50% (Figure 5.5a-c). This apparent resistance

to irradiation was found to be specific to these mLN-resident LTi-like ILC3, with only low percentages of CD45.1$^+$CD45.2$^+$ host CD4$^+$ T cells, ILC2 or NCR$^+$ ILC3 detected in any tissues analysed (Figure 5.5a,c).

This provided an explanation as to why, in the mixed BMC approach shown in Figure 5.4, a skewing of the bone marrow towards that of the host was detectable only in populations of LTi-like ILC3, and only in the mLN. To avoid this complication, the experiment outlined in Figure 5.4 was repeated using CD45.1$^+$ CD45.2$^+$ WT hosts, with any CD45.1$^+$CD45.2$^+$ host cells detected subtracted from the overall cell type population before percentages were calculated, thereby removing any bias from this persisting host population. Bone marrow from these new chimeras, isolated at the time of harvesting and tissue analysis, was also analysed to ensure that WT:WT and WT:CCR7$^{-/-}$ chimeras were comparable. This analysis revealed that CD45.2$^+$ bone marrow constituted 40-45% of the total bone marrow (here not excluding host cells, which were a minor population), with no significant difference between WT:WT and WT:CCR7$^{-/-}$ chimeras (Figure 5.6a,b).

Gating of allotype-marked populations in WT:WT and WT:CCR7$^{-/-}$ chimeras was as shown in Figure 5.6(c). Analysis of CD4$^+$ T cells revealed a similar result to that seen previously, with CCR7$^{-/-}$ CD4$^+$ T cells statistically significantly impaired in their ability to enter all secondary lymphoid tissue, but most notably the inguinal and mesenteric LNs. LTi-like ILC3 were once again found to be dependent upon cell-intrinsic CCR7 signalling for entry into iLN, with significantly fewer CD45.2$^+$ (CCR7$^{-/-}$) LTi-like ILC3 detected than in WT:WT chimeras (Figure 5.7a). In the mLN, the bias towards CD45.1 had now been resolved with

Figure 5.5 LTi-like ILC3 in the mLN of chimeric mice display resistance to irradiation

Chimeras were generated by lethally irradiating WT ($CD45.1^+CD45.2^+$) mice and reconstituting with a 1:1 ratio of WT $CD45.1^+$ and WT $CD45.2^+$ bone marrow (WT:WT). Cells isolated from iLN, mLN and spleen (spln) as specified in methods. Samples were analysed by flow cytometry.

All bars shown on graphs represent the median value. Data representative of (a-b) or pooled from (c) 2 independent experiments. Statistical test used is Mann-Whitney non-parametric, two-tailed test. **P*<0.05, ***P*<0.01, ****P*<0.001 and *****P*<0.0001.

a) FACS plots showing the gating strategy for $CD4^+$ T cells, ILC2, LTi-like ILC3 and NCR^+ ILC3 from WT:WT mLN. Both gating strategies for ILCs (top) and $CD4^+$ T cells (bottom) are pre-gated on FSC/SSC. Lin is CD3/CD5/B220/CD11b/CD11c.

b) FACS plots showing CD45.1 and CD45.2 staining on all $ROR\gamma t^+$ ILC3 in iLN, mLN and spleen from WT:WT chimeras. $CD45.1^+$ WT donor, $CD45.2^+$ WT donor and $CD45.1^+CD45.2^+$ WT host populations are shown.

c) Graphs showing the percentage of each specified cell population which are $CD45.1^+CD45.2^+$ WT host cells in iLN, mLN and spleen. (n=7,6,7).

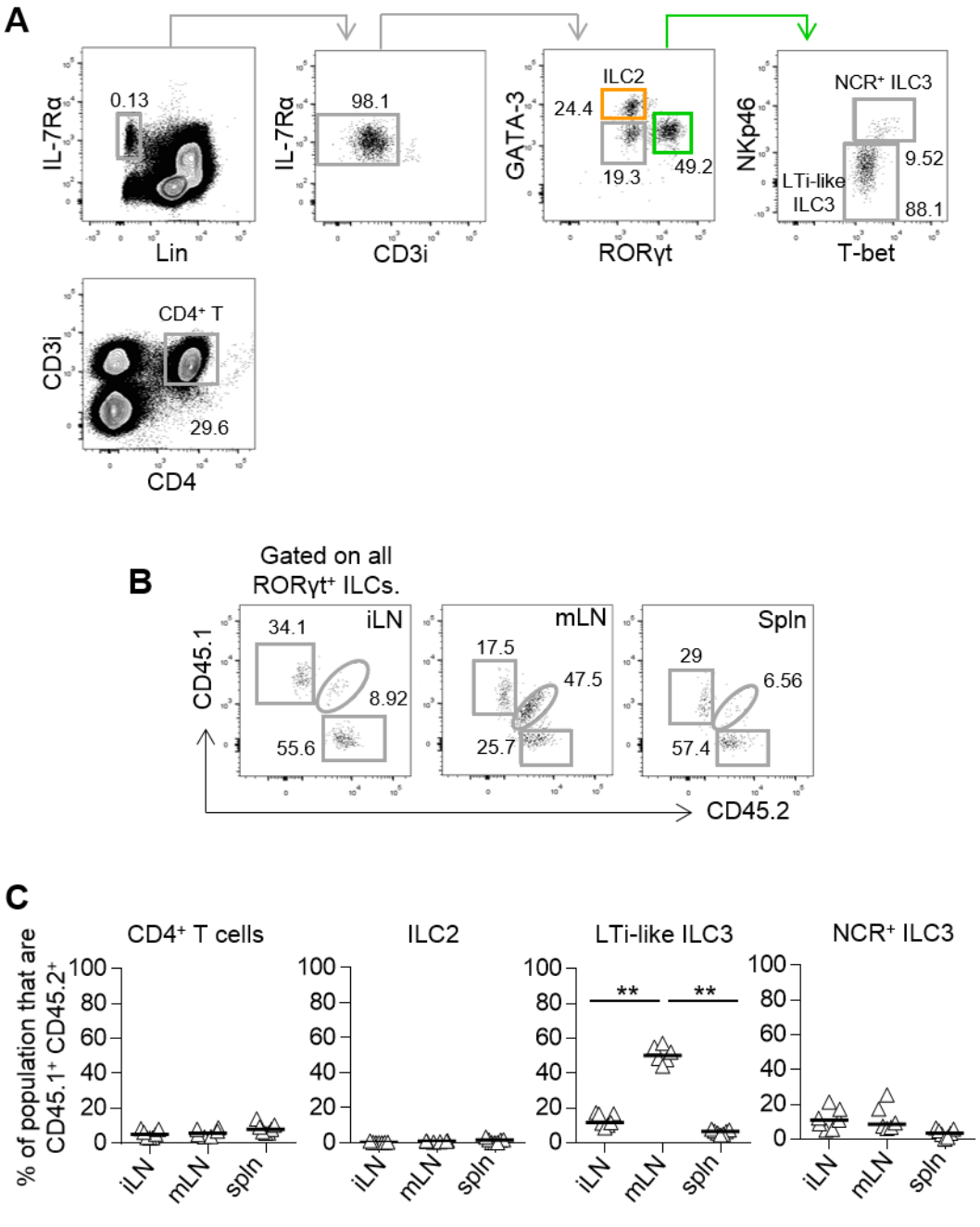
A
IL-7Rα
0.13
Lin
IL-7Rα
98.1
CD3i
GATA-3
ILC2
24.4
19.3
49.2
RORγt
NKp46
NCR⁺ ILC3
LTi-like ILC3
9.52
88.1
T-bet
CD3i
CD4⁺ T
29.6
CD4
B
Gated on all RORγt⁺ ILCs.
CD45.1
iLN
34.1
8.92
55.6
mLN
17.5
47.5
25.7
Spln
29
6.56
57.4
CD45.2
C
% of population that are CD45.1⁺ CD45.2⁺
CD4⁺ T cells
ILC2
LTi-like ILC3
NCR⁺ ILC3
100
80
60
40
20
0
**
**
iLN
mLN
spln

Fig. 5.5

Figure 5.6 A refined mixed BMC model can be used to exclude persisting host cells

Chimeras were generated by lethally irradiating WT ($CD45.1^+CD45.2^+$) mice and reconstituting with a 1:1 ratio of either WT $CD45.1^+$ and WT $CD45.2^+$ bone marrow (WT:WT) or WT $CD45.1^+$ and $CCR7^{-/-}$ $CD45.2^+$ bone marrow (WT:KO). Cells were isolated from mLN and bone marrow as specified in methods. Samples were analysed by flow cytometry.

Data representative of (a,c) or pooled from (b) 2 independent experiments. Statistical test used is Mann-Whitney non-parametric, two-tailed test. *P<0.05, **P<0.01, ***P<0.001 and ****P<0.0001.

a) FACS plots showing CD45.1 and CD45.2 staining on bone marrow cells from WT:WT and WT:KO chimeras, pre-gated on FSC/SSC.

b) Percentage of cells (gated on FSC/SSC) from bone marrow of WT:WT and WT:KO chimeras which are $CD45.2^+$ $CD45.1^-$. Dotted line shows 50%, bars represent median values. (n=7,7).

c) FACS plots showing CD45.1 and CD45.2 staining on $CD4^+$ T cells, ILC2, LTi-like ILC3 and NCR^+ ILC3, as gated in Figure 5.5a, from WT:WT and WT:KO mLNs. $CD45.1^+$ WT donor, $CD45.2^+$ WT donor and $CD45.1^+CD45.2^+$ WT host populations are shown.

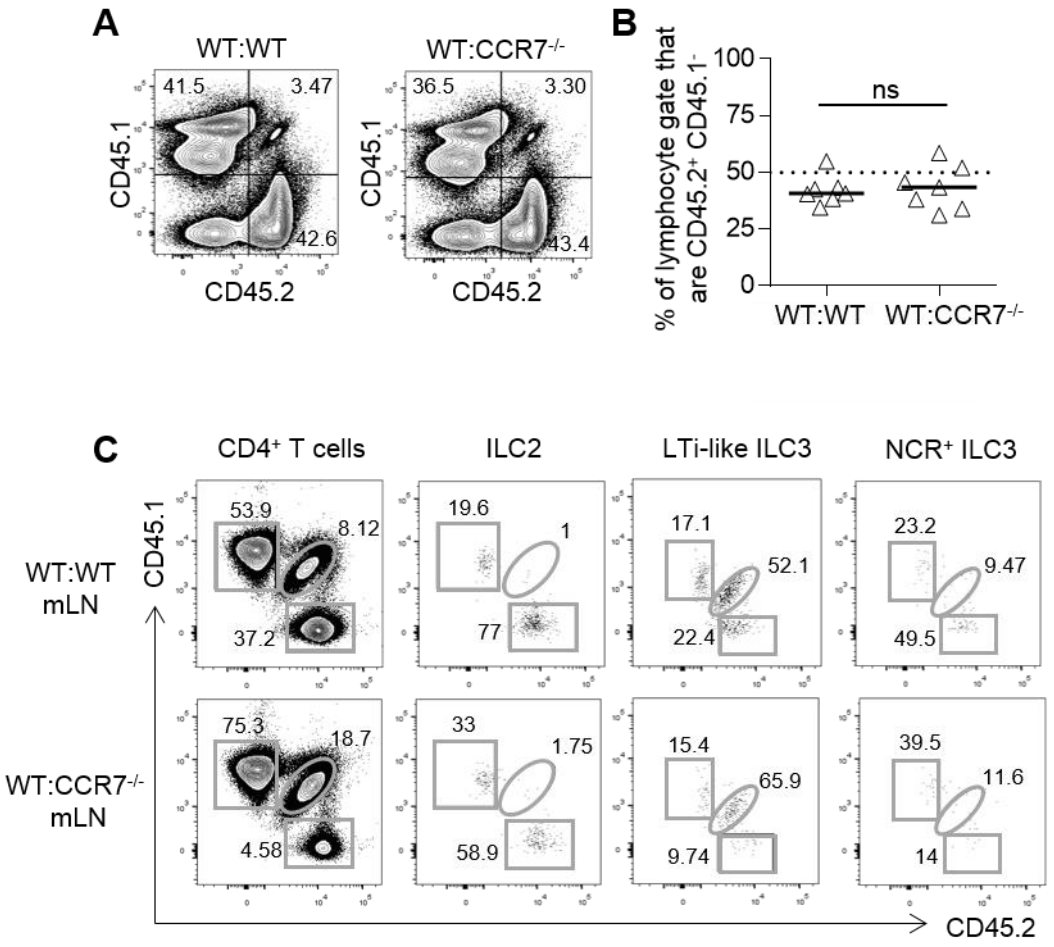
A
WT:WT
WT:CCR7-/-
41.5
3.47
42.6
36.5
3.30
43.4
CD45.1
CD45.2
B
% of lymphocyte gate that are CD45.2+ CD45.1-
100
75
50
25
0
ns
WT:WT
WT:CCR7-/-
C
CD4+ T cells
ILC2
LTi-like ILC3
NCR+ ILC3
WT:WT mLN
WT:CCR7-/- mLN
CD45.1
CD45.2
53.9
8.12
37.2
19.6
1
77
17.1
52.1
22.4
23.2
9.47
49.5
75.3
18.7
4.58
33
1.75
58.9
15.4
65.9
9.74
39.5
11.6
14

Fig. 5.6

Figure 5.7 Experiments in refined mixed BMCs are consistent with LTi-like ILC3 CCR7-dependency being in part cell-intrinsic

Chimeras were generated by lethally irradiating WT ($CD45.1^+CD45.2^+$) mice and reconstituting with a 1:1 ratio of either WT $CD45.1^+$ and WT $CD45.2^+$ bone marrow (WT:WT) or WT $CD45.1^+$ and $CCR7^{-/-}$ $CD45.2^+$ bone marrow (WT:KO). Cells were isolated from iLN, mLN and spleen (spln) as specified in methods. Samples were analysed by flow cytometry.

All bars shown on graphs represent the median value. Data pooled from 2 independent experiments. Dotted line shows 50%. Statistical test used is Mann-Whitney non-parametric, two-tailed test. *P<0.05, **P<0.01, ***P<0.001 and ****P<0.0001.

a) Percentage of $CD4^+$ T cells, LTi-like ILC3, NCR^+ ILC3 and ILC2 from iLN, mLN and spleen of WT:WT and WT:KO chimeras which are $CD45.1^+$ (white triangles) or $CD45.2^+$ (grey triangles). $CD45.1^+CD45.2^+$ host cell populations were excluded from analysis prior to calculating percentages as detailed in the methods.

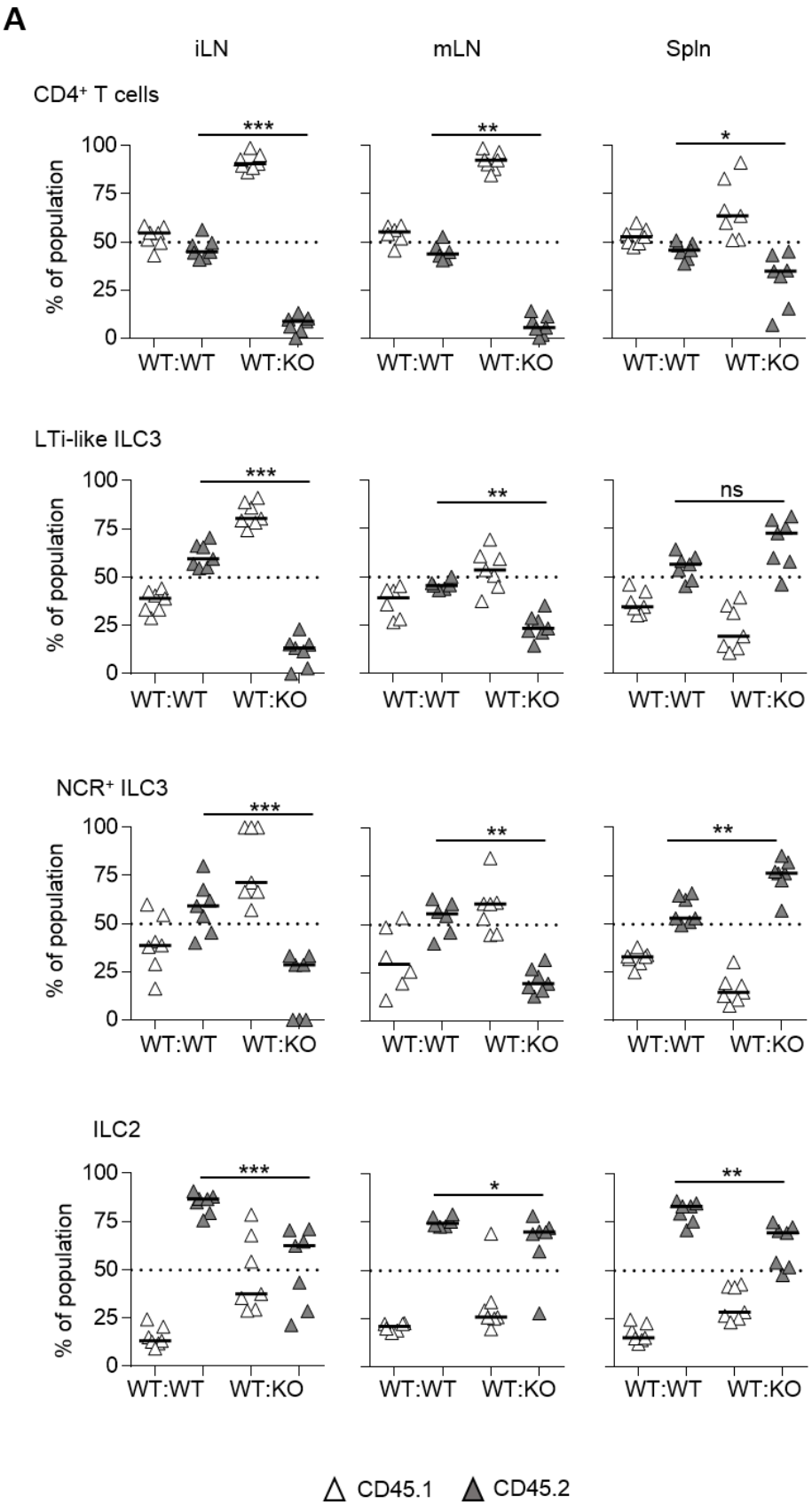
A
iLN
mLN
Spln
CD4+ T cells
LTi-like ILC3
NCR+ ILC3
ILC2
% of population
100
75
50
25
0
WT:WT
WT:KO
***
**
*
ns
CD45.1
CD45.2

Fig. 5.7

the exclusion of persisting host cells, revealing that, although significant, the difference between the ability of CD45.2^{+} WT LTi-like ILC3 and CD45.2^{+} CCR7$^{-/-}$ LTi-like ILC3 was indeed less exaggerated in this tissue if compared to iLN (Figure 5.7a). This may therefore indicate a partial reliance on cell-intrinsic CCR7 signalling for LTi-like ILC3 to re-populate the mLN, but also some effect of CCR7-dependent cell-extrinsic factors.

The ability of CD45.2^{+} CCR7$^{-/-}$ NCR^{+} ILC3 to enter inguinal and mesenteric LNs of mixed BMCs was impaired compared to their CD45.2^{+} WT counterparts (Figure 5.7a), although the phenotype was most pronounced in the iLN. Lower numbers of NCR^{+} ILC3 had previously been detected in the iLN and spleen of CCR7$^{-/-}$ mice when compared to WT controls, but not in the mLN (Figure 5.1c,d). CCR7$^{-/-}$ NCR^{+} ILC3 in fact made up a significantly higher proportion of NCR^{+} ILC3 within the spleen of WT:CCR7$^{-/-}$ mixed BMCs than CD45.2^{+} WT NCR^{+} ILC3 from WT:WT controls (Figure 5.7a), although the reason for this is difficult to elucidate from this data alone. The ILC2 populations within these LNs were biased towards CD45.2^{+} donors in both WT:WT and WT:CCR7$^{-/-}$ mice (Figure 5.7a) and although the reason for this was unknown it was consistently seen across all mixed BMC experiments. Comparison of CD45.2^{+} ILC2 from WT:WT and WT:CCR7$^{-/-}$ mice revealed that, although statistically significant, CCR7$^{-/-}$ ILC2 were only mildly impaired in their ability to re-populate host mLN and spleen in mixed BMCs, but more so in the iLN (Figure 5.7a), tissue in which data in straight CCR7$^{-/-}$ mice had previously indicated that ILC2 depend upon CCR7 (Figure 5.1e). Nonetheless it is not clear that either NCR^{+} ILC3 or ILC2 are completely dependent upon cell-intrinsic CCR7 signalling and cannot be excluded that CCR7-dependent cell-extrinsic effects play a part.

5.2.4 Numbers of LTi-like ILC3 are normal in the small intestine of CCR7$^{-/-}$ mice.

With the knowledge that LTi-like ILC3 entry into secondary lymphoid tissue is impaired in the absence of CCR7 signalling, we hypothesised that these cells might accumulate in non-lymphoid tissues of CCR7$^{-/-}$ mice. To investigate this, the number of LTi-like ILC3 within the small intestine lamina propria (SILP) of WT and CCR7$^{-/-}$ mice was analysed. Within the SILP of both WT and CCR7$^{-/-}$ mice a large population of lineage^{-} (CD3 CD5 B220 CD11b CD11c, CD3i^{-}) IL-7Rα^{+} ILCs could be detected. From this population all three groups of ILC could be detected based on their expression of GATA-3 (ILC2), RORγt (ILC3) (Figure 5.8a,b) or T-bet (ILC1). In both WT and CCR7$^{-/-}$ SILP RORγt^{+} ILC3s constitute the majority of ILCs, with ILC1 a relatively minor population within this tissue (Figure 5.8b). Using CCR6 in addition to RORγt as a marker of LTi-like ILC3, and thus allowing direct comparison between the predominant ILC3 population found in the mLN and similar cells in the gut, the total number of LTi-like ILC3 per individual mLN or whole SILP was analysed. As previously observed the number of LTi-like ILC3 in the mLN of CCR7$^{-/-}$ mice is lower than that seen in WT (Figure 5.8c), however there was no statistically significant difference in the number isolated from WT and CCR7$^{-/-}$ SILP (Figure 5.8c). There does not, therefore, appear to be a significant accumulation of CCR7$^{-/-}$ LTi-like ILC3 in this tissue despite their impaired ability to enter the draining lymph node. Given the large number of these cells within the SI (Figure 5.8d), it seems possible that it is below the sensitivity of the assay to detect such slight fluctuations as these. When other ILC populations in the SILP of WT and CCR7$^{-/-}$ mice were analysed alongside ILC3 (here comparing all RORγt^{+} ILCs), it emerged that there was no statistically significant difference in the number of any population in this tissue in the absence of CCR7 (Figure 5.8e), although such differences have previously been reported (Kim et al., 2015).

Figure 5.8 Similar numbers of ILCs detected in the SI of WT and CCR7$^{-/-}$ mice

Cells were isolated from naïve WT and CCR7$^{-/-}$ small intestine lamina propria (SI) as specified in methods. mLNs were taken alongside and cells isolated as normal. Both SI and mLN samples were analysed using Live/Dead viability dye and anti-CD45 antibody in addition to normal markers. Samples were analysed by flow cytometry and absolute numbers calculated.

All bars shown on graphs represent the median value. Data representative of (a-b) or pooled from (c-d) 2 independent experiments. Statistical test used is Mann-Whitney non-parametric, two-tailed test. *P<0.05, **P<0.01, ***P<0.001 and ****P<0.0001.

a) FACS plots showing gating on viability dye negative (live), CD45^{+} cells in WT SI.

b) FACS plots showing gating on subsets of ILCs in WT and CCR7$^{-/-}$ SI. Lin^{-} IL-7Rα^{+} CD3i^{+} cells are excluded but gating not shown. Lin is CD3/CD5/B220/CD11b/CD11c.

c) Graphs showing the total number of LTi-like ILC3 (CCR6^{+} NKp46^{-}) per individual mLN (left) or in whole SI (right) in WT (white triangles) and CCR7$^{-/-}$ (grey triangles) mice. (n=6,6).

d) Graph showing the total number of RORγt^{+} ILC3s in WT mLN (whole tissue) or WT SI (whole tissue). (n=6,6).

e) Graph showing the total number of ILC1, ILC2 and all RORγt^{+} ILC3 in WT (white triangles) and CCR7$^{-/-}$ (grey triangles) SI. ILC1 are defined as Lin^{-} IL-7Rα^{+} RORγt^{-} GATA-3^{-} Tbet^{+}. (n=6,6).

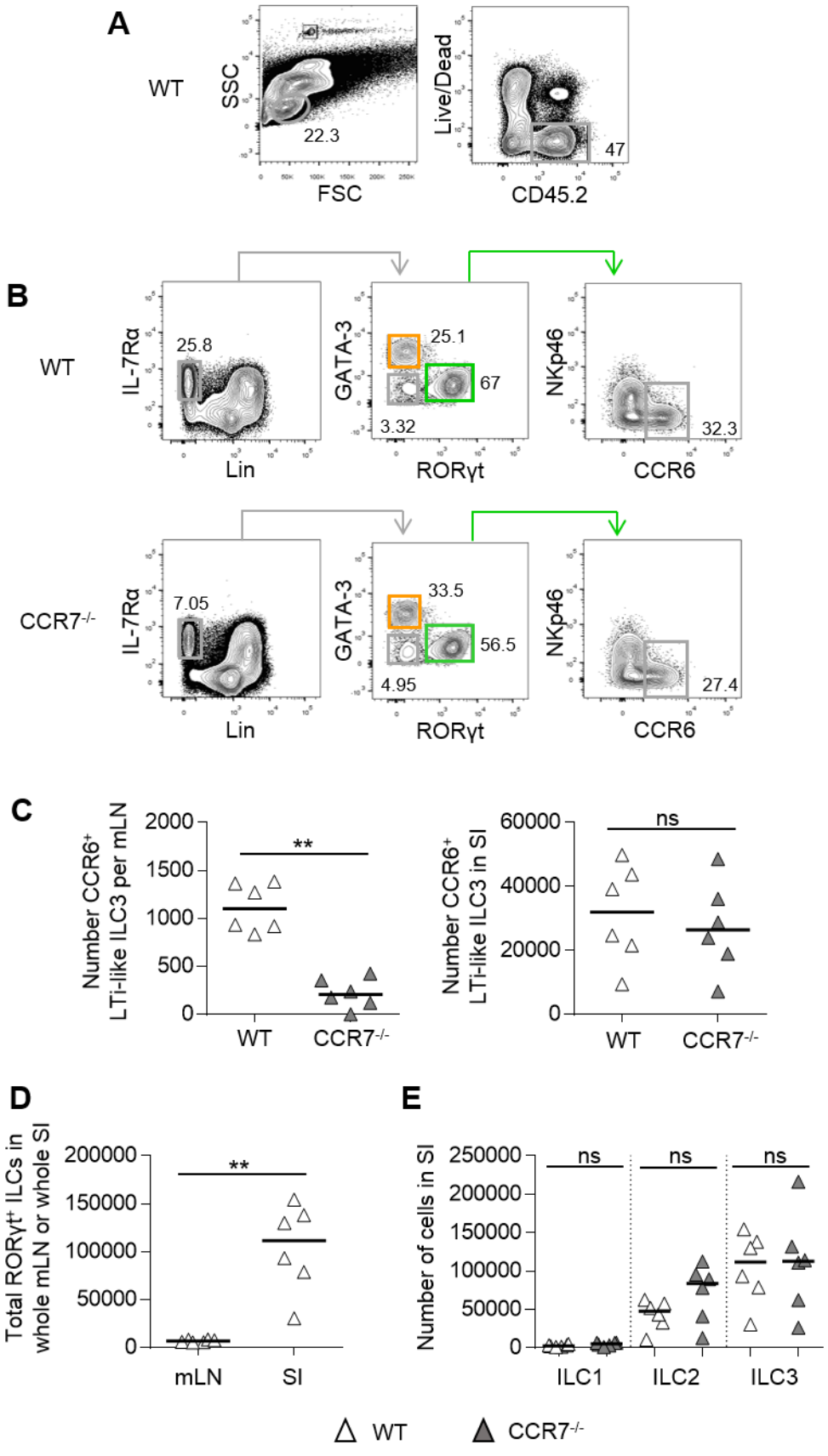
A
WT
SSC
22.3
FSC
Live/Dead
47
CD45.2
B
WT
IL-7Rα
25.8
Lin
GATA-3
25.1
67
3.32
RORγt
NKp46
32.3
CCR6
CCR7-/-
IL-7Rα
7.05
Lin
GATA-3
33.5
56.5
4.95
RORγt
NKp46
27.4
CCR6
C
Number CCR6+ LTi-like ILC3 per mLN
2000
1500
1000
500
0
**
WT
CCR7-/-
Number CCR6+ LTi-like ILC3 in SI
60000
40000
20000
0
ns
WT
CCR7-/-
D
Total RORγt+ ILCs in whole mLN or whole SI
200000
150000
100000
50000
0
**
mLN
SI
E
Number of cells in SI
250000
200000
150000
100000
50000
0
ns
ns
ns
ILC1
ILC2
ILC3
WT
CCR7-/-

Fig. 5.8

5.3 INVESTIGATING THE MECHANISM OF ILC ACCUMULATION IN DRAINING LNS

5.3.1 ILCs do not accumulate in draining LNs in the absence of CCR7

CCR7 signalling has previously been described as necessary for timely immune responses to immunological challenge (Forster et al., 1999), in part because of its requirement by antigen-presenting cells to home from the site of infection to the local draining LN. ILCs have been well-characterised in the skin however it is not definitively known whether these cells can traffic from this site to secondary lymphoid tissue. We have previously shown that certain ILCs within skin-draining LNs express low levels of markers generally associated with APCs, accumulate within draining lymph nodes following immunisation in a manner which does not involve proliferation and that, like APCs, ILCs depend upon CCR7 signalling for entry into peripheral tissue-draining lymph nodes. We therefore hypothesised that the increased number of ILCs detected within draining brachial and axillary LNs could be due to ILCs trafficking from the site of immunisation in a CCR7-dependent manner.

To investigate whether the increase in numbers of ILCs seen in draining LNs is dependent upon CCR7, WT and $CCR7^{-/-}$ mice were immunised in both front paw-pads with either alum-precipitated (alum-ppt) antigen or PBS, and cells analysed within the draining brachial and axillary LNs 4 days p.i. The adoptive transfer of TCR transgenic $CD4^+$ T cells prior to immunisation, allowed us to track the magnitude and progress of the immune response within the draining LN. Although all T cells transferred were from TCR transgenic strains of mice, adoptively transferred $CD4^+$ T cells used in the initial experiment were SM1, activated using alum-ppt FliC peptide, and those in the

experimental repeat were OTII, activated using alum-ppt NP-Ova. This was due to problems arising in the maintenance of the RAG$^{-/-}$ SM1 colony and each individual repeat is specified in Figure 5.9(c). As this had no apparent impact on the numbers of ILCs between experimental repeats, here the results are combined (Figure 5.9e). In WT draining LNs 4 days p.i the number of CD44^{hi} TCR transgenic CD4^{+} T cells can be seen to increase compared to PBS controls, consistent with the activation and expansion of these cells (Figure 5.9a,c). In alum-ppt antigen immunised LNs from CCR7$^{-/-}$ mice at this timepoint, however, there was no statistically significant increase in TCR transgenic T cell number in comparison to PBS controls, and significantly fewer TCR transgenic CD4^{+} T cells than seen in WT alum-ppt antigen dLNs (Figure 5.9a,c). Given that the adoptively transferred TCR transgenic T cells are CCR7-sufficient it is unlikely that this difference is due to the inability of donor T cells to enter the lymph nodes of CCR7$^{-/-}$ mice, rather is more likely to reflect the inability of CCR7$^{-/-}$ APCs to traffic into the draining LN and activate the TCR transgenic T cells following immunisation.

Analysis of the numbers of each ILC subset in PBS controls revealed that, as seen previously in peripheral tissue-draining iLN tissue (Figure 5.1e), there are significantly lower numbers of all subsets of ILCs in brachial and axillary LNs of CCR7$^{-/-}$ mice than WT (Figure 5.9d). Four days following immunisation the numbers of all ILC subsets could be seen to increase in comparison to PBS controls, statistically significantly so with the exception of ILC2 (Figure 5.9b,e). By contrast no significant difference in the number of any ILC subset could be detected in CCR7$^{-/-}$ dLNs (Figure 5.9b,e), which could be taken to indicate that the increase observed in WT draining LNs was a CCR7-dependent phenomenon. Certainly, in comparison to WT dLNs 4 days p.i with alum-ppt antigen there were significantly fewer of all ILC subsets in CCR7$^{-/-}$ dLNs (Figure 5.9e).

Figure 5.9 ILCs do not accumulate in draining LNs of CCR7$^{-/-}$ mice

Comparison of WT and CCR7$^{-/-}$ mice. Mice in one experimental repeat received 10^5 OTII TCR transgenic CD4$^+$ T cells intravenously a day before immunisation with either PBS or alum-ppt NP-OVA in both front paw pads, whilst mice in an independent repeat received 10^5 SM1 TCR transgenic CD4$^+$ T cells and either PBS or alum-ppt FliC peptide in both front paw pads. Tissues were taken 4 days p.i (D4) and a cell suspension made from brachial and axillary LNs as specified in methods. Samples were analysed by flow cytometry and absolute numbers per lymph node calculate. Lin$^-$ IL-7Rα$^+$ RORγt$^+$ ILC3 subset further split into those which express NKp46 at a level comparable to ILC1 (NCR$^+$ ILC3) and those which do not (LTi-like ILC3), whilst ILC1 are defined as Lin$^-$ IL-7Rα$^+$ RORγt$^-$ GATA-3$^-$ T-bet$^+$ cells.

All bars shown on graphs represent the median value. Data representative of (a,b) or pooled from (c-e) 2 independent experiments. Statistical test used is Mann-Whitney non-parametric, two-tailed test. **P*<0.05, ***P*<0.01, ****P*<0.001 and *****P*<0.0001.

a) FACS plots showing gating on CD44^{hi} OTII T cells from WT or CCR7$^{-/-}$ brachial and axillary LNs, 4 days p.i with alum-ppt NP-OVA. Cells are pre-gated on CD3i$^+$ CD4$^+$ T cells and CD45.1 is used for OTII or SM1 cell detection.

b) FACS plots showing gating on ILC populations in WT and CCR7$^{-/-}$ control and immunised mice a 4 days p.i. Cells were pre-gated on Lin$^-$ (CD3/CD5/B220/CD11b/CD11c, CD3i$^-$) IL-7Rα$^+$ ILCs.

c) Graph showing the total number of CD44^{hi} OTII T cells (circles) and SM1 T cells (triangles) per LN in WT (white) and CCR7$^{-/-}$ (grey) mice 4 days post immunisation with PBS or alum-ppt antigen (D4). (n=5,7,5,6).

d) Graph showing the total number of each ILC subset per LN in WT (white triangles) and CCR7$^{-/-}$ (grey triangles) PBS control mice. (n=5,5).

e) Graphs showing the total number of each stated ILC population per LN in WT (white triangles) or CCR7$^{-/-}$ (grey triangles) mice 4 days p.i with PBS of alum-ppt antigen (D4). Y axis on the left-most graph applies to all. (n=5,7,5,6).

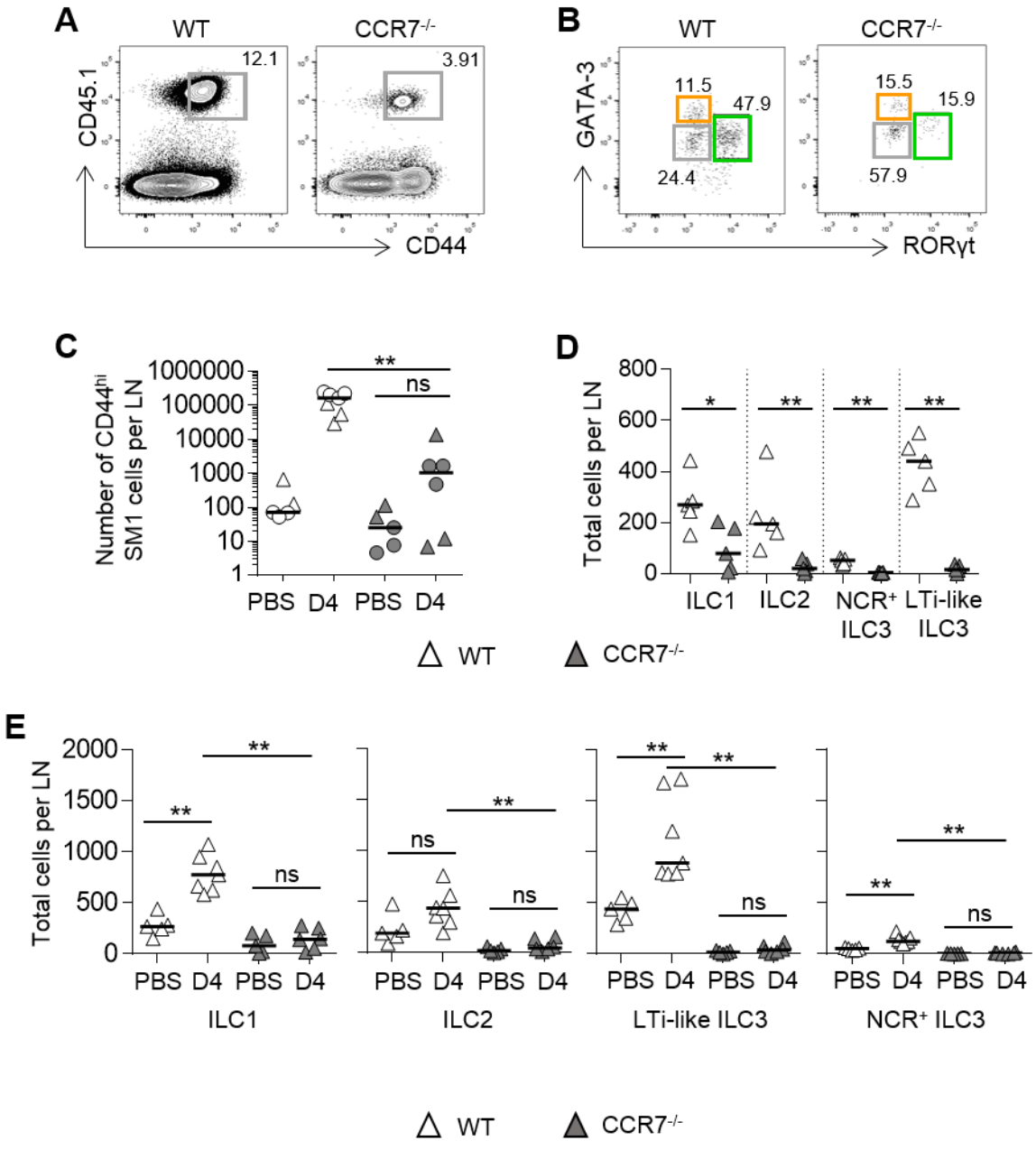
A
WT
CCR7-/-
12.1
3.91
CD45.1
CD44
B
WT
CCR7-/-
11.5
47.9
24.4
15.5
15.9
57.9
GATA-3
RORγt
C
Number of CD44hi SM1 cells per LN
1000000
100000
10000
1000
100
10
1
**
ns
PBS D4 PBS D4
WT
CCR7-/-
D
Total cells per LN
800
600
400
200
0
*
**
**
**
ILC1
ILC2
NCR+ ILC3
LTi-like ILC3
E
Total cells per LN
2000
1500
1000
500
0
**
**
ns
ns
**
ns
**
**
ns
**
ns
PBS D4 PBS D4
ILC1
ILC2
LTi-like ILC3
NCR+ ILC3
WT
CCR7-/-

Fig. 5.9

In WT:CCR7$^{-/-}$ mixed BMCs, the ability of LTi-like ILC3 to re-populate inguinal lymph nodes was found to be dependent on cell-intrinsic CCR7 signalling, and given the similarities between iLN and brachial and axillary LNs already documented it could be speculated that this is also true under this circumstance. Although this experiment in straight CCR7$^{-/-}$ mice does not rule out a role for CCR7-dependent cell-extrinsic factors, such as APC exclusion and the absence of a strong T cell response, it does reveal a dependency on CCR7 for ILC accumulation in draining LNs following immunisation.

5.4 ILC3 DEFICIENCY DOES NOT AFFECT NUMBERS IN PRIMARY CD4$^+$ T CELL RESPONSE

5.4.1 Chimeric mouse models

Bone marrow chimeras have been described previously in Chapter 3 as a method to remove RORγt-expressing cells in a mouse in which all secondary lymphoid tissue is present; with one caveat of straight RORγt$^{-/-}$ mice being impaired LN development (Sun et al., 2000). Irradiating WT mice and then reconstituting the haematopoietic compartment with RORγt$^{-/-}$ bone marrow has been a useful tool to analyse the potential functions of ILC3, given the limited availability of models to genetically delete ILC3 from WT hosts. To investigate whether or not primary CD4$^+$ T cell responses within LNs depended upon the presence of RORγt-expressing cells, and perhaps more specifically group 3 ILCs, the response of antigen-specific CD4$^+$ T cell populations was analysed within chimeric WT and RORγt-deficient mice.

WT:WT and WT:RORγt$^{-/-}$ chimeric mice received an adoptive transfer of 10^5 SM1 CD4$^+$ T cells and mLNs were analysed 7 days post-intraperitoneal (i.p) immunisation with alum-

ppt FliC peptide. Analysis of chimeras for the presence of each ILC subset revealed that although RORγt^{+} ILC3 were markedly reduced in the mLNs of WT:RORγt$^{-/-}$ mice when compared to WT:WT controls, they were not completely depleted (Figure 5.10a,b). The discovery that LTi-like ILC3 within the mLN are particularly resistant to irradiation (Figure 5.5) highlights a caveat with this method, and anti-CD90.2 antibodies were used during the generation of these chimeric mice in an attempt to remove any persisting ILC3s. Interestingly WT:RORγt$^{-/-}$ mice had increased numbers of ILC1 and IL2 when compared to WT:WT controls, and this was found to be statistically significant (Figure 5.10b). Analysis of the number of CD44^{hi} SM1 T cells within these mice 7 days p.i revealed no significant difference between this primary CD4^{+} T cell response in WT:WT and WT:RORγt$^{-/-}$ chimeras (Figure 5.10c).

This result was indicative of no notable role for ILC3 in the analysed immune response, however we further refined our chimeric mouse model to address the caveat of persisting ILC3 within WT:RORγt$^{-/-}$ mice. The discovery that CCR7$^{-/-}$ LNs have significantly fewer ILC3 than those from WT mice suggested that these would make better hosts, removing the need for anti-CD90.2 antibody depletion which could have effects on cells other than ILC3. In keeping with the draining LN models detailed in Chapter 4, we now analysed a local draining LN response within the skin-draining bLN and aLNs. Given that we found LTi-like ILC3 to be susceptible to irradiation within the peripheral tissue-draining iLN (Figure 5.5), irradiation-induced depletion is likely to be more efficient within these LNs.

5.4.2 Numbers of antigen-specific CD4^{+} T cells unaffected by ILC3 absence

On discovering that CCR7$^{-/-}$ mice have notably fewer ILC3 than WT mice in all LNs analysed it was decided that these would be a more suitable choice of bone marrow

Figure 5.10 Similar numbers of responding CD4$^+$ T cells detected following immunisation in ILC3-deficient chimeric mice

Chimeras were generated by lethally irradiating WT mice before reconstituting with WT or RORγt$^{-/-}$ bone marrow cells. Mice were further treated with two doses of anti-CD90.2 antibody (WT:RORγt$^{-/-}$) or anti-rat IgG control (WT:WT) intraperitoneally (i.p) and then left for 6-12 weeks. Prior to analysis all mice received 10^5 SM1 T cells and were immunised the following day with 100μg alum-ppt FliC i.p. Chimeras were taken at D7 post-immunisation and a cell suspension made from mLNs as specified in methods. Samples were analysed by flow cytometry and absolute numbers per individual mLN calculated.

All bars shown on graphs represent the median value. Data representative of (a) or pooled from (b-c) 2 independent experiments. Statistical test used is Mann-Whitney non-parametric, two-tailed test. *P<0.05, **P<0.01, ***P<0.001 and ****P<0.0001.

a) FACS plots showing gating strategy for ILC populations in WT:WT (WT) or WT:RORγt$^{-/-}$ (KO) chimeras 7 days p.i with alum-ppt FliC. Cells were pre-gated on host CD45.1$^-$ cells. Lin is CD3/CD5/B220/CD11b/CD11c.

b) Graphs showing the number of each ILC subset per WT or KO chimeric mLN 7 days p.i with alum-ppt FliC. ILC1 are RORγt$^-$ GATA-3$^-$ T-bet$^+$ (n=7,7).

c) Graphs showing the number of CD44^{hi} SM1 T cells (CD3$^+$ CD4$^+$ CD45.1$^+$ CD44^{hi}) per mLN 7 days p.i with alum-ppt FliC.

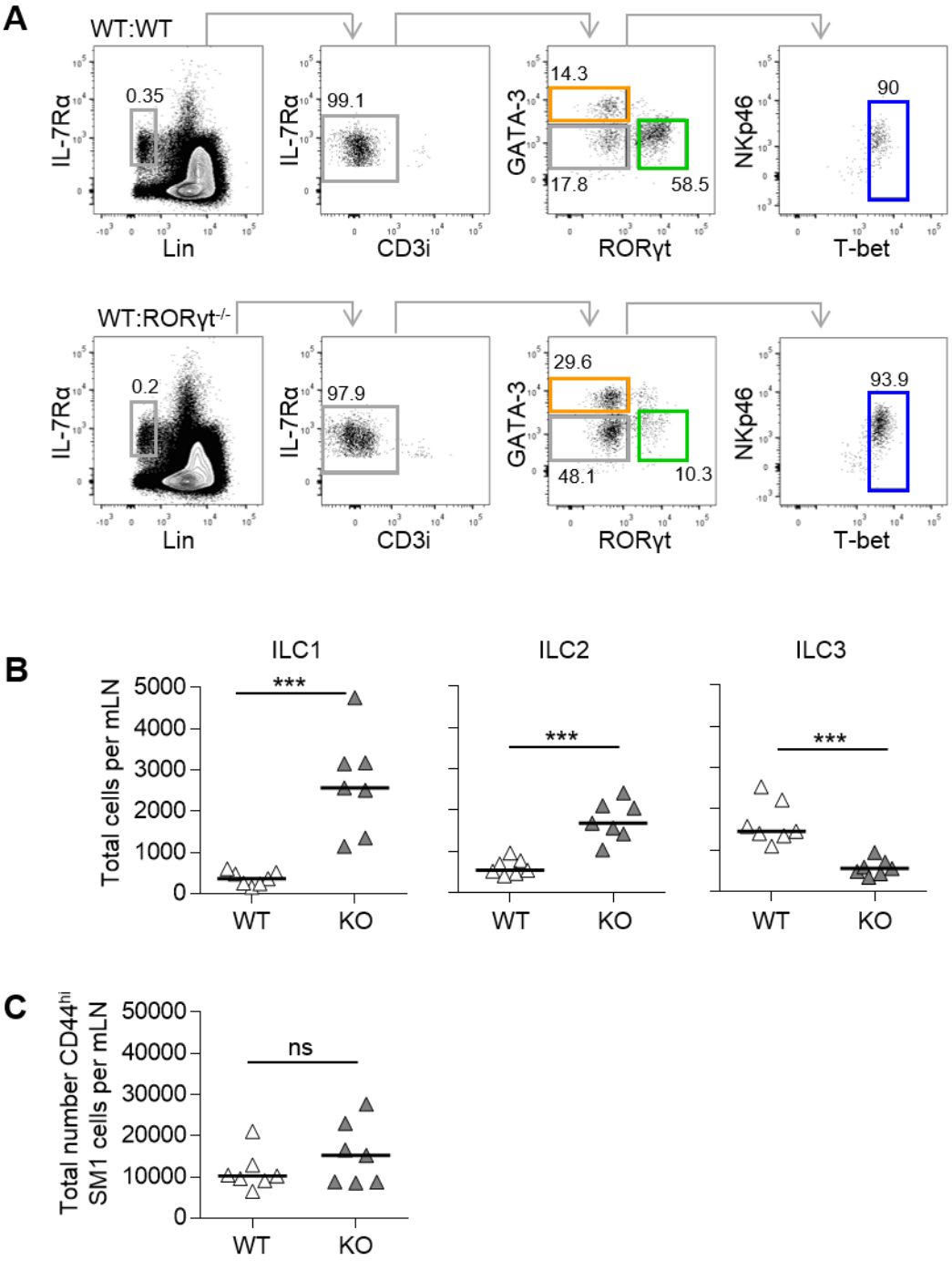
A
WT:WT
0.35
IL-7Rα
Lin
99.1
IL-7Rα
CD3i
14.3
17.8
58.5
GATA-3
RORγt
90
NKp46
T-bet
WT:RORγt-/-
0.2
IL-7Rα
Lin
97.9
IL-7Rα
CD3i
29.6
48.1
10.3
GATA-3
RORγt
93.9
NKp46
T-bet
B
ILC1
ILC2
ILC3
Total cells per mLN
5000
4000
3000
2000
1000
0
***
***
***
WT
KO
WT
KO
WT
KO
C
Total number CD44hi SM1 cells per mLN
50000
40000
30000
20000
10000
0
ns
WT
KO

Fig. 5.10

chimera host. With fewer ILC3 to begin with irradiation of these mice might be sufficient to deplete these cells alone, removing the requirement for, non-ILC specific, anti-CD90 antibodies. CCR7$^{-/-}$ host mice were lethally irradiated and reconstituted with WT or RORγt$^{-/-}$ bone marrow, whilst replacing the bone marrow compartment with CCR7-sufficient cells should negate any effect of the CCR7-deficient host. All chimeras received 10^5 OTII CD4$^+$ T cells and were immunised in the front paw pads with alum-precipitated NP-OVA. Mice were taken 6 days p.i and cells from the brachial and axillary LNs analysed.

Analysis of ILC populations in CCR7$^{-/-}$:WT (WT) and CCR7$^{-/-}$:RORγt$^{-/-}$ (RORγt$^{-/-}$) chimeras revealed that whilst all three groups of ILCs were present within WT chimeras, very few RORγt$^+$ ILC3 could been detected in RORγt$^{-/-}$ brachial and axillary LNs (Figure 5.11a), although there was no statistically significant difference in the total number of Lin$^-$ IL-7Rα$^+$ ILCs (Figure 5.11b). Enumeration of each group of ILCs per LN revealed that there were statistically significantly fewer ILC3 within RORγt$^{-/-}$ LNs than WT (Figure 5.11c), and although some ILC3 were still present within RORγt$^{-/-}$ tissue, the median number of ILC3 per LN was 91.8% decreased compared to that in WT control LNs (Figure 5.11c; calculated from median values). This depletion was therefore more efficient than that previously seen in WT:RORγt$^{-/-}$ chimeras, where the median number of ILC3 per LN was only 62.4% decreased compared to WT control mice (Figure 5.10b; calculated from median values), despite the absence of anti-CD90 treatment. Notably, the loss of ILC3 in RORγt$^{-/-}$ chimeras was accompanied by an increase in numbers both ILC1 and ILC2 when compared to WT controls (Figure 5.11a,c), and this increase was statistically significant in the case of ILC2; consistent with the increase seen in these populations in Figure

Figure 5.11 Using CCR7$^{-/-}$ mice as chimeric mouse hosts results in improved ILC3 depletion

Chimeras were generated by irradiating CCR7$^{-/-}$ (CD45.2^{+}) mice before reconstituting hosts with WT or RORγt$^{-/-}$ bone marrow cells. Mice later received 10^5 OTII transgenic CD4^{+} T cells i.v and were immunised in both front paw pads with alum-ppt NP-OVA or PBS the following day. Chimeras were taken 6 days p.i and a cell suspension made from brachial and axillary LNs, as specified in methods. Samples were analysed by flow cytometry and absolute numbers per lymph node calculated.

All bars shown on graphs represent the median value. Data representative of (a) or pooled from (b-c) 2 independent experiments. Statistical test used is Mann-Whitney non-parametric, two-tailed test. *P<0.05, **P<0.01, ***P<0.001 and ****P<0.0001.

a) FACS plots showing the gating strategy for ILC populations in CCR7$^{-/-}$:WT (WT) or CCR7$^{-/-}$:RORγt$^{-/-}$ (KO) chimeras 6 days p.i with alum-ppt NP-OVA. Lin is CD3/CD5/B220/CD11b/CD11c.

b) Graph showing the number of total Lin^{-} IL-7Rα^{+} ILCs in WT and KO chimeras 6 days p.i with alum-ppt NP-OVA (n=8,11).

c) Graphs showing the number of each ILC subset in WT and KO chimeras 6 days p.i with alum-ppt NP-OVA. ILC1 are RORγt^{-} GATA-3^{-} T-bet^{+} (n=8,11). Y axis scale on leftmost graph applies to all.

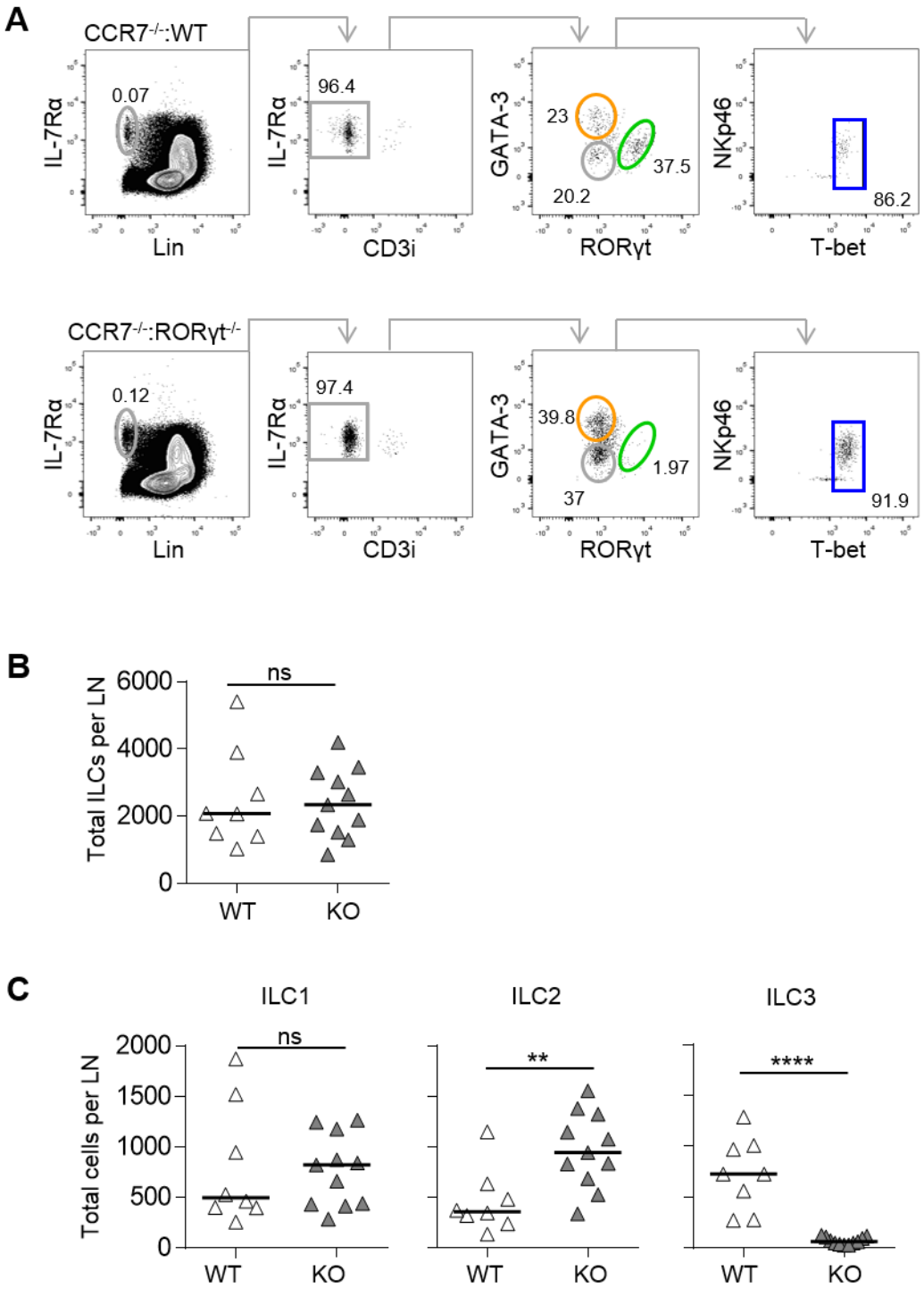
A
CCR7-/-:WT
0.07
IL-7Rα
Lin
96.4
IL-7Rα
CD3i
23
20.2
37.5
GATA-3
RORγt
NKp46
86.2
T-bet
CCR7-/-:RORγt-/-
0.12
IL-7Rα
Lin
97.4
IL-7Rα
CD3i
39.8
37
1.97
GATA-3
RORγt
NKp46
91.9
T-bet
B
Total ILCs per LN
6000
4000
2000
0
ns
WT
KO
C
ILC1
ILC2
ILC3
Total cells per LN
2000
1500
1000
500
0
ns
**
****
WT
KO
WT
KO
WT
KO

Fig. 5.11

5.10(b). Whether this was as a result of the absence of the transcription factor RORγt in general or the specific absence of ILC3 is not clear.

In order to properly interpret any effect seen in the OTII $CD4^+$ T cell response, it was necessary to assess the general phenotype of LN-resident cells within these chimeric mice. The total number of $CD45.1^-$ 'host' T and B lymphocytes was enumerated and $CD4^+$ T cells, here excluding adoptively transferred $CD45.1^+$ OTII cells, were analysed for either an activated ($CD44^{hi}$ $CD62L^{lo}$) or Treg ($FoxP3^+$ $CD25^+$) phenotype (Figure 5.12a). There was found to be statistically significantly fewer total T cells within $ROR\gamma t^{-/-}$ chimeras compared to WT, although no statistically significant difference in the number of B cells (Figure 5.12b), and this was still the case when restricted to those host T cells expressing CD4 (Figure 5.12c). Analysis of CD44 and CD62L expression indicated that a higher percentage of $CD4^+$ T cells within $ROR\gamma t^{-/-}$ chimeras had a $CD44^{hi}$ $CD62L^{lo}$ 'activated' phenotype than in WT chimeras (Figure 5.12c). $FoxP3^+$ $CD25^+$ Tregs also constituted a higher percentage of total 'host' $CD4^+$ T cells within $ROR\gamma t^{-/-}$ mice, although this corresponded with a statistically significantly lower number of total Tregs than seen in WT chimeras (Figure 5.12d).

Analysis of the OTII $CD4^+$ T cells response, using CD45.1 and VβTCR5.1/5.2 as markers of OTII cells (Figure 5.13a), revealed that although the median number of $CD44^{hi}$ OTII cells detected in $ROR\gamma t^{-/-}$ chimeras was lower than that observed in WT chimeras, the difference was not significant (Figure 5.13b). When phenotypic markers were analysed it was found that the percentage of total $CD4^+$ OTII cells which had a $FoxP3^+$ $CD25^+$ Treg phenotype was negligible (Figure 5.13a), whilst the percentage of total OTII $CD4^+$ T cells which were $CD44^{hi}$ $CD62L^{lo}$ did not differ significantly from those in WT chimeras (Figure

Figure 5.12 Total T cells are fewer in RORγt-deficient BMCs

Chimeras were generated by irradiating CCR7$^{-/-}$ (CD45.2^{+}) mice before reconstituting hosts with WT or RORγt$^{-/-}$ bone marrow cells. Mice later received 10^5 OTII transgenic CD4^{+} T cells i.v and were immunised in both front paw pads with alum-ppt NP-OVA or PBS the following day. Chimeras were taken 6 days p.i and a cell suspension made from brachial and axillary LNs, as specified in methods. Samples were analysed by flow cytometry and absolute numbers per lymph node calculated.

All bars shown on graphs represent the median value. Data representative of (a) or pooled from (b-d) 2 independent experiments. Statistical test used is Mann-Whitney non-parametric, two-tailed test. *P<0.05, **P<0.01, ***P<0.001 and ****P<0.0001.

a) FACS plots showing analysis of the phenotype of CD4^{+} T cells in CCR7$^{-/-}$:WT (WT) or CCR7$^{-/-}$:RORγt$^{-/-}$ (KO) chimeras. Cells are pre-gated on CD45.1^{-} host cells to exclude adoptively transferred OTII cells from this analysis.

b) Graphs showing the total number of T (CD3^{+} B220^{-}) and B (B220^{+} CD3^{-}) lymphocytes per LN in WT and KO chimeras.

c) Graphs showing the total number of CD4^{+} T cells per LN in WT and KO chimeras (left), and the percentage of CD4^{+} T cells which have a CD44^{hi} CD62^{lo} phenotype (right).

d) Graphs showing the total number of CD4^{+} T cells per LN with a Treg phenotype (left, FoxP3^{+} CD25^{+}), and the percentage of CD4^{+} T cells which are Tregs (right).

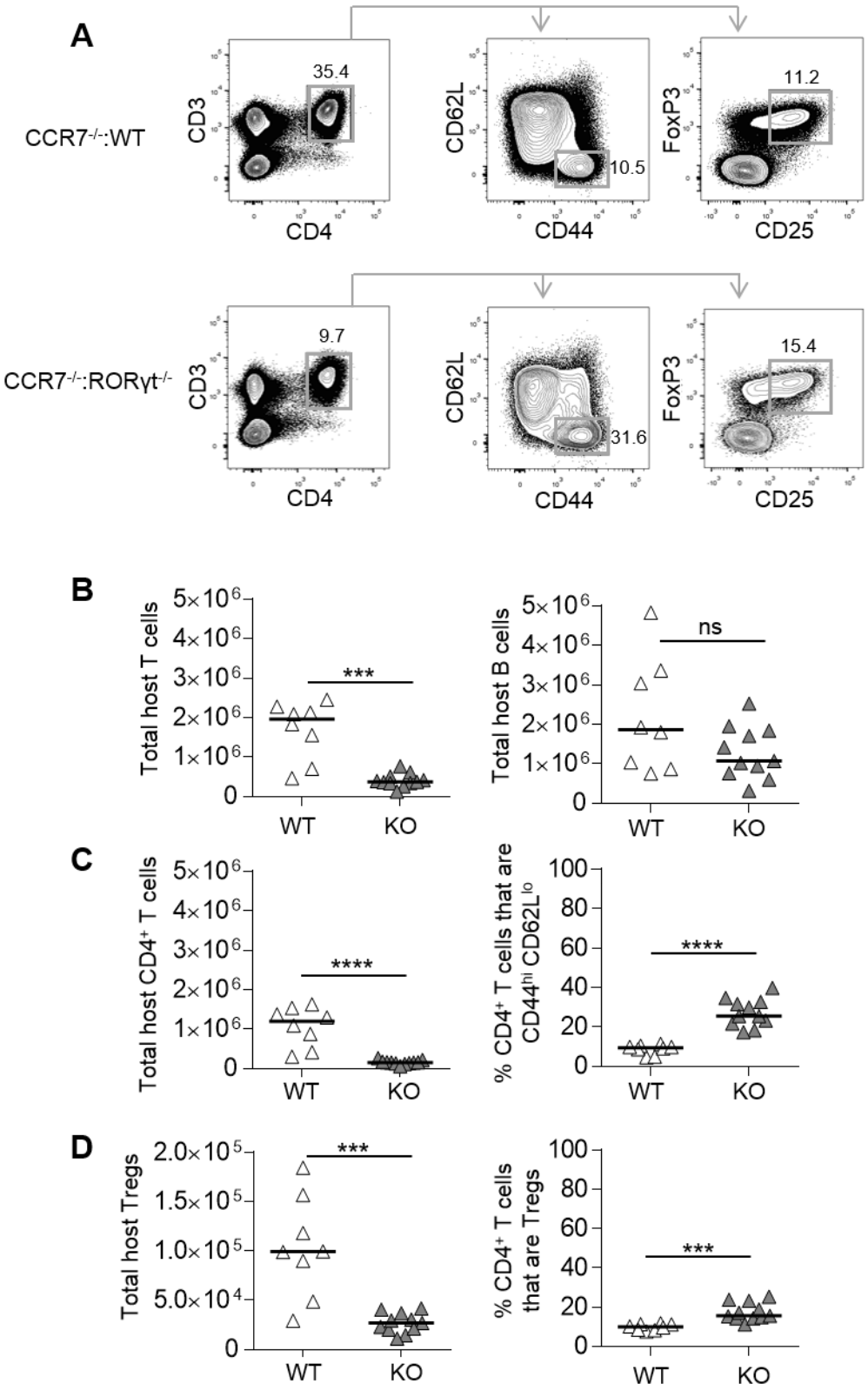
A
CCR7-/-:WT
CD3
CD4
35.4
CD62L
CD44
10.5
FoxP3
CD25
11.2
CCR7-/-:RORγt-/-
9.7
31.6
15.4
B
Total host T cells
5×10^6
4×10^6
3×10^6
2×10^6
1×10^6
0
***
WT
KO
Total host B cells
ns
C
Total host CD4+ T cells
****
% CD4+ T cells that are CD44hi CD62Llo
100
80
60
40
20
D
Total host Tregs
2.0×10^5
1.5×10^5
1.0×10^5
5.0×10^4
% CD4+ T cells that are Tregs

Fig. 5.12

Figure 5.13 Numbers of responding OTII CD4$^+$ T cells do not differ significantly in ILC3-deficient BMCs

Chimeras were generated by irradiating CCR7$^{-/-}$ (CD45.2$^+$) mice before reconstituting hosts with WT or RORγt$^{-/-}$ bone marrow cells. Mice later received 10^5 OTII transgenic CD4$^+$ T cells i.v and were immunised in both front paw pads with alum-ppt NP-OVA or PBS the following day. Chimeras were taken 6 days p.i and a cell suspension made from brachial and axillary LNs, as specified in methods. Samples were analysed by flow cytometry and absolute numbers per lymph node calculated.

All bars shown on graphs represent the median value. Data representative of (a) or pooled from (b-c) 2 independent experiments. Statistical test used is Mann-Whitney non-parametric, two-tailed test. **P*<0.05, ***P*<0.01, ****P*<0.001 and *****P*<0.0001.

a) FACS plots showing the analysis of the phenotype of CD4$^+$ OTII T cells in CCR7$^{-/-}$:WT (WT) or CCR7$^{-/-}$:RORγt$^{-/-}$ (KO) chimeras. Cells are pre-gated on CD45.1$^+$ cells to identify cells which originate from the OTII TCR transgenic donor.

b) Graph showing the total number of CD44^{hi} OTII cells per LN in WT and KO chimeras

c) Graph showing the percentage of total OTII T cells (CD45.1$^+$ CD3$^+$ CD4$^+$ Vβ5.1/5.2 TCR$^+$) in WT and KO chimeras which have an activated CD44^{hi} CD62L^{lo} phenotype as shown in (a).

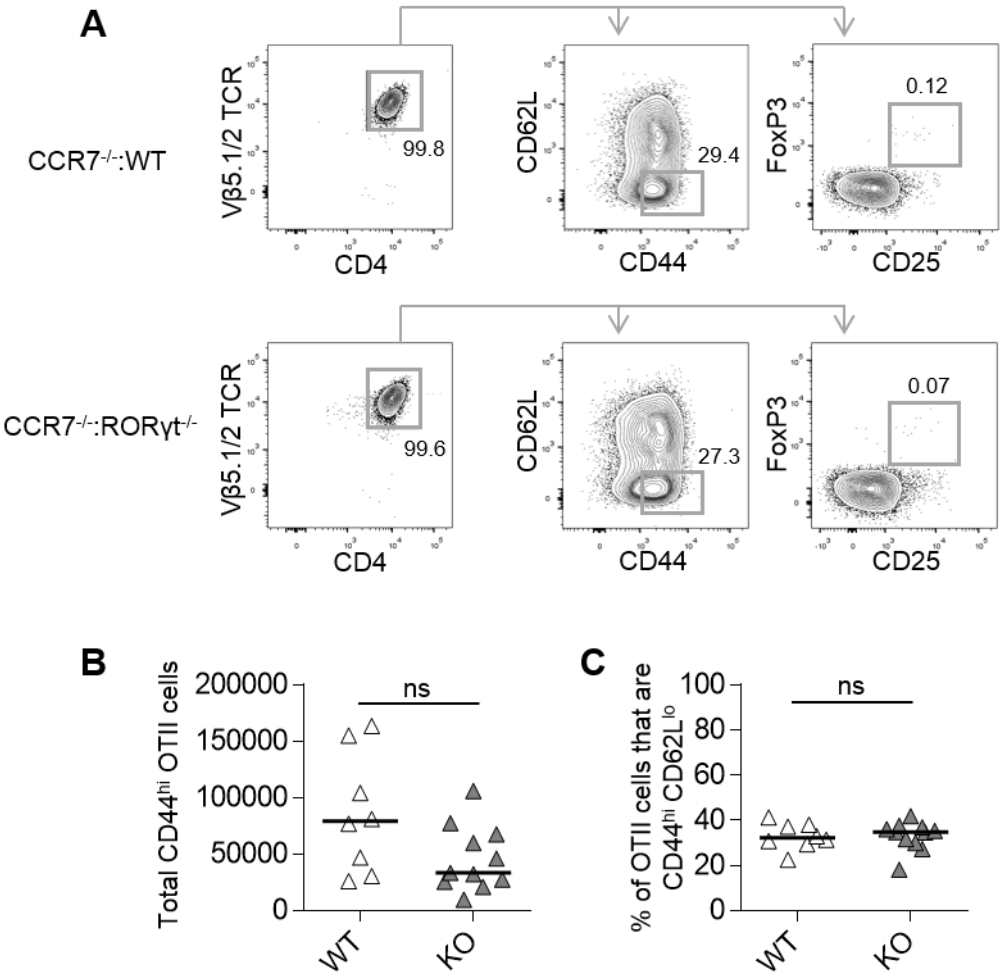
A
CCR7-/-:WT
Vβ5.1/2 TCR
99.8
CD4
CD62L
29.4
CD44
FoxP3
0.12
CD25
CCR7-/-:RORγt-/-
Vβ5.1/2 TCR
99.6
CD4
CD62L
27.3
CD44
FoxP3
0.07
CD25
B
Total CD44hi OTII cells
200000
150000
100000
50000
0
ns
WT
KO
C
% of OTII cells that are CD44hi CD62Llo
100
80
60
40
20
0
ns
WT
KO

Fig. 5.13

5.13a,c). These models therefore did not reveal a role for RORγt-expressing cells, including ILC3, in the primary $CD4^+$ T cell response analysed, however there were many caveats associated with this method of depleting cells and these are discussed below.

5.5 SUMMARY

The observation that LTi cells expressed CCR7 mRNA (Kim et al., 2008) indicated that these cells might be capable of migrating from the peripheral or mucosal tissues to LNs. In this investigation I have shown that numbers of certain ILC subsets are lower in LNs of $CCR7^{-/-}$ mice, consistent with impaired entry of ILCs into these tissues in the absence of this chemokine receptor. This appeared to be site-dependent, with numbers of all ILC subsets found to be lower in $CCR7^{-/-}$ mouse peripheral LNs analysed at steady state, but only LTi-like ILC3 in the mLN. Whether or not this reflects different requirements for entry into the mLN or other LNs, or differences in the ILCs at these sites is unclear, and it is not possible to tell from this investigation whether CCR7-dependent ILC entry into LNs is through the afferent lymphatics or circulation.

Our data in mixed bone marrow chimeras suggests that the phenotype observed in $CCR7^{-/-}$ mice is at least in part due to the abrogation of cell-intrinsic CCR7 signalling. Within this investigation a proportion of LTi-like ILC3 were found to migrate towards a ligand of CCR7, albeit to a lesser extent than $CD4^+$ T cells, indicating functional expression of this chemokine receptor by ILC3. Although we struggled to detect CCR7 expression on the surface of ILCs—despite a range of methods being used and successful detection on $CD4^+$ T cells—CCR7 mRNA has been shown to be expressed by LTi cells (Kim et al., 2008) and the protein detected on the surface of $NKp46^-$ $ROR\gamma t^+$ ILCs from the SI (Klose et al., 2013). A recent study using $CCR7^{-/-}$ mice reported similar results; observing a

CCR7-dependency for ILC3 in the mLN, whilst ILC2 within this tissue were unaffected, although in this study they were able to detect high levels of CCR7 expression by ILC3 (Kim et al., 2015). Unlike the data presented in this investigation, however, a dependency on CCR7 was also described for ILC1 within the mLN and differences in ILC populations detected within CCR7$^{-/-}$ SI when compared to WT mice (Kim et al., 2015).

Further differences between ILC populations in mesenteric and peripheral tissue-draining LNs were highlighted by our discovery that LTi-like ILC3 within the mLN, but not spleen or iLN, are comparably resistant to irradiation. Whether or not this suggests that LTi-like ILC3 populations at different sites are in fact fundamentally different remains to be seen, but could also be as a result of differences in behaviour caused by ILC interactions with LN stromal cells at these sites. For example, stromal cells within the mLN have been shown to produce more retinoic acid, which plays an important in the induction of gut-homing programs on T cells, than those in peripheral LNs (Hammerschmidt et al., 2008). Even when transplanted into the mesentery it was found that peripheral LNs were unable to perform this role, highlighting the fundamental differences between different LNs themselves (Hammerschmidt et al., 2008). There are therefore a number of factors which could contribute to the differences in ILC populations which we see, and which could be explored further through transplant experiments as outlined above, or by sorting and phenotyping ILC populations from different sites.

The lack of ILC accumulation in draining LNs of CCR7$^{-/-}$ mice could be seen as an indication that the accumulation of ILCs in WT LNs undergoing an immune response is due to CCR7-dependent trafficking of ILCs from other sites. In this investigation we showed that the presence of all ILC subsets within peripheral LNs at steady state was dependent upon

CCR7. Certainly our results from Chapter 4 suggest that accumulation is by a mechanism other than proliferation of cells within the LN itself. Our observation in CCR7$^{-/-}$ draining LNs does however closely mirror results seen in CD80$^{-/-}$CD86$^{-/-}$ mice in Chapter 4, where the T cell response was similarly abrogated; in CD80$^{-/-}$CD86$^{-/-}$ mice as a result of lack of co-stimulation, and within CCR7$^{-/-}$ mice likely due to impaired DC trafficking. The role of CCR7 cell-intrinsic signalling in this process could be investigated by analysing accumulation of CCR7$^{-/-}$ ILC subsets in mice where a normal immune response is restored, but whether other factors, such as signals from cells undergoing an immune response or processes such as lymph node shutdown contribute to ILC accumulation within draining LNs is yet to be seen.

Finally, RORγt-deficient bone marrow chimeras were used to get an insight into whether RORγt-expressing cells are required for normal expansion of responding CD4^{+} T cells during a LN primary immune response. Given the many similarities of ILCs with other lineages of cells, in transcription factor expression and surface markers, it has proved challenging to selectively remove these cells without affecting other cell populations. Genetic deletion of group 3 ILCs presents the additional challenge that a deficiency of LTi cells prevents the embryonic development of LNs (Sun et al., 2000). Bone marrow chimeras allow the deletion of these cells in hosts whose LNs have already formed. This model involves the deletion of host cells using irradiation, followed by the reconstitution of the haematopoietic compartment with bone marrow cells which lack the expression of RORγt, therefore the result is the depletion of all RORγt-expressing cell types, including ILC3. The radiation-resistance of LTi-like ILC3 has been shown in this investigation and a variety of methods, including the use of depleting antibodies and CCR7$^{-/-}$ mice as hosts, explored. The use of α-CD90 depleting antibodies in addition to irradiation of WT hosts

resulted in relatively poor depletion of RORγt^{+} ILCs, and it could not be ruled out that the depleting antibodies were having an effect on other CD90^{+} cells types, despite the fact that chimeras were left a number of weeks post-treatment and prior to use. Refinement of this method to use irradiated CCR7$^{-/-}$ hosts removed the need for additional antibody depletion, as very few ILC3 reside within the LNs in the first place, and resulted in the effective removal of more than 90% of ILC3 from brachial and axillary LNs.

In both chimeric models analysed within this chapter no significant difference was detected in the numbers of an antigen-specific population of CD4^{+} T cells at day 6 or 7. Analysis of activation markers also did not reveal a higher level of activation within this responding T cell population, which could have been indicative of a dysregulated response. There were however differences in the non-OTII populations of T cells analysed in CCR7$^{-/-}$:RORγt$^{-/-}$ chimeras compared to controls, although it is not possible to say from this experiment the exact reason why this was the case. These experiments using bone marrow chimeras therefore indicate no requirement for RORγt-expressing cells types, including ILC3, in the primary CD4^{+} T cell responses analysed, consistent with previous findings in the LTi-deficient spleen (Withers et al., 2012). These bone marrow chimeras were however associated with a number of caveats. Many chimeric mice had to be removed from these experiments and culled as a result of them reaching clinical end points, whilst those used within this investigation showed signs of being unwell; likely consistent with these mice having an impaired immune system in the absence of RORγt-expressing cells and as a result of the high doses of irradiation required to deplete host cells. More sophisticated genetic approaches to specifically delete subsets of ILCs are increasingly being reported. The use of these models in the future would avoid many of the caveats associated with these experiments and yield a more definitive answer.

CHAPTER 6. DISCUSSION

In this thesis I have robustly characterised populations of ILCs in LNs, defined the location of these cells, identified novel mechanisms by which ILCs enter these tissues and explored changes upon immunisation.

6.1 ILC3 ARE ENRICHED IN MUCOSAL TISSUE DRAINING LNS

The presence of subsets of ILCs in the mLN had been reported previously (Hepworth et al., 2013, Price et al., 2010), however less was known about their existence in peripheral LNs which drain the skin. This was likely in part due to the difficulties associated with isolating rare populations of cells from such small LNs. Our ability to isolate these cells from a range of different peripheral and mucosal tissue draining LNs allowed us to identify and characterise these cells, revealing that all ILC subsets were present in all LNs analysed. This investigation also revealed differences in the proportions of each ILC subset found in LNs which drain different sites. While all subsets of ILC are more numerous in the mesenteric LN (mLN) than either the skin-draining inguinal (iLN) or brachial LNs (bLN), ILC3 are particularly enriched. Similarly, the proportion of ILC3 in mediastinal LNs (medLN), which drain the respiratory tract, is notably higher than that detected in other LNs, particularly those which drain the skin. This suggests that group 3 ILCs are enriched in LNs which drain tissues with the highest antigen burden, likely indicative of an increased requirement for these cells in LNs which drain mucosal barrier sites. The specific enrichment of LTi-like ILC3 within the mLN was particularly interesting due to its location draining the ILC-enriched gut, upon which much of ILC research is focussed, and some of the possible reasons for this are discussed below.

6.1.1 ILC3 in tolerance to gut-derived antigens

ILC3 have been shown to be better represented within the small intestine than in the skin or lung (Spencer et al., 2014), and have been found to carry out many important functions within the gut. IL-22 produced by ILC3s has been shown to be important for the maintenance of barrier surface integrity and for the prevention of systemic spread of commensal bacteria (Sonnenberg et al., 2012). When properly excluded, intestinal commensal bacteria exist symbiotically with their host, providing help with digestion (Brestoff and Artis, 2013) and proving crucial in preventing colonisation of the epithelium by potentially pathogenic bacterial strains (Kamada et al., 2013). The ability of the host to tolerate the presence of microorganisms in numbers as large as those found within the gut is due to effective barrier surfaces, the careful maintenance of these surfaces by innate cells, and the ability of the immune system to tolerate their presence. In addition to their role in maintaining these barrier surfaces, ILC3 have been shown to promote this state of tolerance by directly influencing adaptive immune responses (Hepworth et al., 2013, Hepworth et al., 2015).

Induction of immunological tolerance to food and commensal bacterial antigens in the periphery is vital. Despite many levels of regulation during the development of lymphocyte populations, there are T and B cells which exist within the periphery that are specific for harmless or self-antigens (Walker and Abbas, 2002). Whilst processes, such as negative selection and deletion of developing $CD4^+$ T cells which respond to self-antigen presented in the context of MHCII, help to remove such cells prior to their emigration from the thymus (Hogquist et al., 2005), certain antigens, such as those from commensal bacteria or food, are not present at this point. As a consequence, $CD4^+$ T cells which can respond to harmless commensal microbial antigens can emerge into the

periphery where they could cause detrimental inflammatory immune responses in the gut. Although Treg cells have been shown to suppress such immune responses (Ai et al., 2014) ILC3 are also now known to play a role (Hepworth et al., 2013, Hepworth et al., 2015).

LTi cells have already been implicated in the process of negative selection of self-reactive naïve T cells in the thymus (Rossi et al., 2007), but recent reports suggest that their influence on immune tolerance extends to regulating those T cells which make it to the periphery in a process termed intestinal selection (Hepworth et al., 2015). MHCII^{+} ILC3 have been shown to reside within the gut and mLN tissue (Hepworth et al., 2013) and in this investigation we find that a higher proportion of mLN-resident ILC3 express this molecule than their peripheral LN counterparts. Although capable of acquiring, processing and presenting antigen these cells were reported to lack expression of the co-stimulatory molecules CD80 and CD86, rendering them unable to provide the co-stimulatory signals required to activate CD4^{+} T cells (Hepworth et al., 2013, Mueller et al., 1989). Consistent with our understanding of T cell activation, antigen presentation by ILC3 to CD4^{+} T cells would likely render these cells anergic and unable to respond to further stimulation (Schwartz, 2003). Antigen presentation by ILC3 *in vitro* did not result in CD4^{+} T cell proliferation (Hepworth et al., 2013). Indeed, in keeping with a regulatory role, mice in which MHCII was selectively deleted from ILC3 (MHCII$^{\Delta ILC3}$), but not other antigen-presenting cell types, were found to develop spontaneous intestinal inflammation resulting from dysregulated CD4^{+} T cell responses to commensal bacteria (Hepworth et al., 2013). The mechanism of ILC3 MHCII-mediated regulation of CD4^{+} T cell responses has been shown to involve inducing apoptosis in responding T cells, removing those cells

which react inappropriately to innocuous antigens in a manner which shares many similarities to negative selection in the thymus (Hepworth et al., 2015).

6.1.2 APC-induced tolerance takes place in the mLN

Although there is likely to be a contribution of gut-associated lymphoid tissues such as the Peyer's patches (PPs) and isolated lymphoid follicles (ILFs) to the induction of oral tolerance, the mLN has been shown to play an important role. For example, LTα$^{-/-}$ mice which lack both lymph nodes and PPs lack immune tolerance to oral antigens, yet the selective rescue of mLN development in these mice was sufficient to restore induction of oral tolerance, even in the absence of PPs (Spahn et al., 2002). A population of CD103^{+} gut-resident DCs have been shown to acquire innocuous antigens within the gut and migrate to the mLNs, where they present these peptides in the context of MHCII to naïve T cells to initiate tolerance (Pabst et al., 2007). The importance of antigen sampling specifically at this mucosal site is demonstrated by the fact that DCs are programmed to promote tolerance by the production of cytokines and retinoic acid (RA) by gut epithelial cells (Iliev et al., 2009). This can then be implemented by the DCs, by rendering those T cells which recognise the antigen anergic or by inducing them to become T regulatory cells which suppress the immune response (Pabst et al., 2007).

6.1.3 Trafficking of ILCs to the mLN

The location of ILC3-mediated regulation of intestinal CD4^{+} T cell responses has not yet been elucidated. We have published that CCR6^{+} ILC3 are capable of trafficking from the small intestine to the mLN, and this publication is included at the end of this thesis (Mackley et al., 2015). Given that migration of DCs to the mLN has been shown to be important in DC-generated tolerance to mucosal antigens (Pabst et al., 2007) it seems

feasible that ILC3 within this LN may be similarly involved. Homing and entry of dendritic cells into lymph nodes depends upon their expression of the chemokine receptor CCR7 (Forster et al., 2008) and the induction of tolerance to oral antigens is impaired in CCR7$^{-/-}$ mice (Worbs et al., 2006). In this investigation we demonstrate that, like dendritic cells, the ability of ILC3 to enter the mLN is dependent upon signalling through the chemokine receptor CCR7. Numbers of LTi-like ILC3 in the mLN of CCR7$^{-/-}$ mice were significantly lower than in WT controls, whilst numbers in the spleen did not notably differ. Interestingly, within the mLN this applied to the LTi-like ILC3 population alone, with populations of ILC1, ILC2 and NCR^{-} ILC3 unaffected by the absence of CCR7. Although we could not detect CCR7 expression on the surface of ILC3 with our methods, a recent study has detected high levels of expression of this receptor on certain subsets of ILCs and in agreement with our investigation has found CCR7 to be important for ILC3, but not ILC2, entry into the mLN (Kim et al., 2015). In contrast to our findings, however, was the detection of an ILC1 dependency on CCR7 for entry into the mLN, in addition to differences in ILC populations within the SI of CCR7$^{-/-}$ mice (Kim et al., 2015) and further investigation would be required to address these differences.

Whilst our experiments in mixed bone marrow chimeras demonstrated that the entry of LTi-like ILC3 into the skin-draining iLN appeared to be highly dependent upon cell-intrinsic CCR7 signalling, the mechanism of CCR7-dependent entry into the mLN was less clear. Although cell-intrinsic CCR7 signalling appeared to be required in part, and CCR6^{+} ILC3 from the mLN were found to be capable of migrating towards CCL21 in a CCR7-dependent manner, it is not clear that entry of these cells to the mLN does not also require some CCR7-dependent cell-extrinsic factors. The lymph nodes of CCR7$^{-/-}$ mice have been shown to have fewer T cells (Forster et al., 1999), and consistent with this we

detected fewer $CD4^+$ T cells within the mLN of $CCR7^{-/-}$ mice than in WT mice. Interestingly our data in $RAG^{-/-}$ and $ZAP70^{-/-}$ mice revealed that relatively few ILC3 can be detected within the mLN of T cell deficient mice, despite being the predominant ILC population in the mLN of WT mice. Analysis of T cell deficient iLNs suggested that this observation was specific to the mLN, so perhaps the presence of T cells in LNs is, by some unknown mechanism, required for ILC3 entry to mLNs in addition to cell-intrinsic CCR7 signalling. The data presented in this investigation shows clear similarities between the migratory behaviour of ILC3 and DCs. Whilst it is possible to conclude that the increased number of ILC3 within the mLN is as a result of trafficking of cells from the ILC3-enriched intestinal tissue, it must also be noted that ILC3 make up an even larger proportion of the total ILC population in mediastinal LNs (medLN) despite very few ILC3 residing within the lung (Spencer et al., 2014). Although these cells could migrate to the medLN from a different site—the medLN also drains the intraperitoneal cavity (Kool et al., 2008) for example, although it is not known that this area is enriched in ILC3—this perhaps indicates that the increased number of ILC3 in mucosal-draining LNs is not as a result of constitutive trafficking, or that this is tissue-specific. Either way, it is indicative of an increased requirement for these cells within LNs which drain barrier sites.

It is not yet clear from this investigation whether CCR7-dependent entry of ILC3 into the mLN is a result of entry from the blood or lymph. As tissue-resident innate cells, entry of ILC3 through the lymph and lymphatic vessels would seem more likely, as has been established for DCs (Randolph et al., 2005). ILCs have been detected in human peripheral blood, although these are reported to be mostly ILC2 (Mjosberg et al., 2011), and it is possible that an ILC3 precursor population circulates in this way. A proportion of ILC3 in the mLN have been reported to express the gut-homing receptors CCR9 and α4β7,

indicative of an ability of these cells to home to the gut should they enter the circulation (Kim et al., 2015). In addition the chemokine receptor CCR6, expressed by the majority of ILC3 in the LN, has been shown to be important for the homing of another RORγt-expressing cell type, Th17 cells, to the small intestine (Esplugues et al., 2011), so it is possible that CCR6 may dictate the LN exit of these ILC3. Whether or not ILC3 transport antigen to the mLN has also not yet been established, despite their capacity to do so. Nonetheless the phenotype of group 3 ILCs within LNs certainly fits with this proposed function. Whilst a proportion of ILC3 within the gut express NKp46 (Vonarbourg et al., 2010) and are classed as NCR^+ ILC3, the vast majority of ILC3 in the lymph nodes that we analysed were $NKp46^-$ LTi-like ILC3, and this is indicative of a specific enrichment of this subset within the mLN. It has previously been reported that MHCII expression is found solely on those ILC3 which lack expression of NCRs (Hepworth et al., 2013) and as shown in our LN analysis a large proportion of LTi-like ILC3 within LNs do express MHCII, with the percentage highest in the mLN. Our study of $CCR7^{-/-}$ mLNs revealed that NCR^+ ILC3 did not depend upon signalling via CCR7 for LN entry, suggesting that it is primarily the LTi-like ILC3, and therefore the subset capable of expressing MHCII, which traffic in a manner similar to DCs. Whether or not migration of these cells is instigated by the acquisition of antigen or other signals still needs to be explored.

Although ILC3 have been shown to regulate $CD4^+$ T cell responses by inducing apoptosis in a MHCII-dependent manner (Hepworth et al., 2015) it is possible that ILC3 could also carry out this function by additional mechanisms. It is, for example, possible that these cells could regulate some $CD4^+$ T cell responses by inducing Tregs. ILC3 have previously been shown indirectly promote support of Tregs through their production of CSF2 and effects on other innate cells (Mortha et al., 2014), and within the mLN $ROR\gamma t^+$ LTi cells

have been shown to sit within close proximity to FoxP3^{+} Treg cells (F. McConnell, unpublished observations). Although Hepworth *et al* (2013) did not detect impaired Treg function which could account for the dysregulation of T cell responses seen in MHCII$^{\Delta ILC3}$ mice this was not analysed in an antigen-specific manner (Hepworth et al., 2013). Either way, from our findings and those of other groups it seems feasible that increased numbers of ILC3 reside in LNs which drain mucosal sites so as to limit immune responses to harmless antigen.

6.1.4 Is the mLN a more favourable environment for ILC3?

One striking observation made of mLN-resident ILC3 in this study is their resistance to irradiation. The radiation-resistance of LTi cells has previously been documented in the thymus (Dudakov et al., 2012), but in this study LTi-like ILC3 in the mLN, but not skin-draining iLN or spleen, were found to be resistant to irradiation. It is feasible that this is due to a lack of LTi-like ILC3 proliferation, and certainly data from our group points towards these cells having a low rate of turnover (D. Withers, unpublished observations). Revealingly this suggests that, despite their similar phenotype, LTi-like ILC3 may have different properties depending on their location. Whether or not this reflects differences in the ILC population themselves, or is the result of variations in signals received in different LNs should be explored further. Some mLN stromal cell populations have been reported to be fundamentally different to those found in peripheral LNs. Stromal cells within the mLN have been shown to produce more retinoic acid (RA), a metabolite which has been shown to contribute to the induction of a gut-homing phenotype on T cells; a role that peripheral LNs cannot emulate, even if transplanted into the mesentery (Hammerschmidt et al., 2008). Whether or not differences such as this accounts for the irradiation resistance of LTi-like ILC3 within the mLN, or their enrichment in this LN,

remains to be seen. RA, for example, has been shown to be important for the maintenance of ILC3s in the SI, with numbers of ILC3 diminished in mice where RA signalling is inhibited (Spencer et al., 2014). It is possible that increased levels of this molecule within the mLN in part contributes to ILC3 persistence at this site. Signalling by RA has also been shown to affect the proliferative capacity of ILC3 within the SI, although in this case resulting in a higher proportion of ILC3 proliferating (Spencer et al., 2014) and therefore does not support our hypothesis of a low rate of turnover providing resistance to irradiation. Nonetheless, it is not clear whether this is the case in the mLN. It would therefore be of interest to understand more of ILC cross-talk with LN stromal cells, as such interactions could affect the properties of ILCs and stromal cells alike. On a separate note, this persistence of LTi-like ILC3 even following irradiation may well be beneficial to the host following medical interventions such as chemotherapy, where the development of intestinal mucositis and loss of epithelial barrier integrity can be a problem (Pico et al., 1998).

6.2 LOCATION IN LNS PROVIDES OPPORTUNITIES FOR ILC SUBSETS TO INFLUENCE AN ADAPTIVE IMMUNE RESPONSE

6.2.1 ILC3 cluster in interfollicular areas and at the B-T interface

Determining the location of cells in LNs using immunofluorescence microscopy provides an invaluable insight into their potential functions. LTi cells have previously been shown to cluster in the interfollicular regions of murine mLNs (Withers et al., 2012) and we looked at this observation in more detail in this study. Within the mLN clusters of ILC3 could be detected within interfollicular areas and at the interface between B cell follicles and the T cell-dominated area. An possible explanation for their location at these sites has been that it is dictated by their expression of a balance of the chemokine receptors CXCR5,

which attracts cells to the B cell follicles, and CCR7, which attracts cells to the paracortical zone (Lane et al., 2009). We found that a proportion of *ex vivo* overnight cultured ILC3, but not ILC2, expressed CXCR5. CCR7 expression by group 3 ILCs, although not detected using our methods, has been previously reported at the mRNA level (Kim et al., 2008). The ability of some ILC3 to migrate towards a ligand of CCR7 was demonstrated within this study, although to a much lesser extent than $CD4^+$ T cells. It is still not clear whether or not these chemokine receptors dictated the location of these cells, however in the absence of CCR7 ILC3 do not reside within LN B cell follicles (D. Withers unpublished observations), and it is possible instead that the chemokine CCR6, expressed by LTi-like ILC3, plays a role.

It is within these ILC-enriched interfollicular regions and further into the parcortical zone that high endothelial venules (HEVs), the vessels which facilitate lymphocyte entry into LNs from the blood, can be found. Naïve $CD4^+$ T cells enter LNs through HEVs to sample antigens presented by APCs before leaving through the efferent lymph to re-circulate to other lymphoid tissues (von Andrian and Mempel, 2003). ILC3 clustering at this site could therefore have the opportunity to interact with these cells through MHCII, as discussed above, or by other mechanisms. This location also puts ILC3 in a position to interact with other lymphocytes, such as re-circulating, long-lived memory $CD4^+$ T cells. When an adaptive immune response is initiated a small population of responding lymphocytes will persist long after pathogen clearance to become memory cells. These long-lasting cells are capable of mounting a rapid but specialised adaptive immune response should the same threat be detected again (Sprent, 1997). Although the survival of memory $CD4^+$ T cells is thought to be independent of MHCII (Swain et al., 1999), and as a result antigen re-stimulation, there is evidence that signalling through MHCII does maintain the quality of

memory T cell responses (Kassiotis et al., 2002), possibly by serving as a mechanism to bring cells together for the provision of other signals. LTi cells have already been shown to be important in supporting $CD4^+$ memory T cells in mice (Withers et al., 2012), although the mechanism by which they do this is not known, and it would be interesting to explore whether memory $CD4^+$ T cell responses are impaired in $MHCII^{\Delta ILC3}$ mice.

This location also provides ILC3 with the opportunity to interact with APCs which enter LNs through the afferent lymph (Braun et al., 2011). It is possible that ILCs could influence cells of the innate immune system through the release of cytokines or by direct interaction, and that this in turn could influence the result of an adaptive immune response. Certainly, ILC2-derived cytokine has previously been shown to induce DC migration to draining LNs and indirectly promote the generation of a Th2 response (Halim et al., 2014). Whether cytokine-mediated effects can be exerted by ILCs residing within the LNs is unclear. This striking location therefore provides ILC3 with the opportunity to interact with a wide range of different cells, whether of the adaptive immune system or the innate.

6.2.2 ILC2 and ILC3 co-localise in mLN tissue

Within this study ILC2 were identified in LN tissue by their expression of GATA-3 and ILC2-associated surface markers. ILC2 could be found within the same regions as ILC3, although they were comparatively fewer in number within the mLN tissue and this analysis did not exclude the possibility that they also located elsewhere. The proximity of these two subsets in LNs perhaps provides an opportunity for cross-talk, although this has not been demonstrated in this investigation. It is also possible that ILC2 and ILC3 are in competition for signals within this interfollicular niche. Spencer et al (2014) have found

that vitamin A deficiency in mice results in impaired ILC3 responses, but increased numbers of ILC2 in the small intestine. This was found to be in part due to an increased responsiveness of ILC2 to IL-7 signals (Spencer et al., 2014). Although previously shown to be expressed mostly by reticular cells in the T cell zone (Link et al., 2007), IL-7 has also been found to be generated by lymphatic endothelial cells (LECs) which are enriched in the interfollicular regions of LNs (Onder et al., 2012), so it is possible that these two populations of ILCs are in competition for this cytokine. Certainly, during this investigation there have been several occasions when a reduction in the number of ILC3 within LNs has been associated with an increase in the number of ILC2. Very few ILC3 were detected specifically within the mLNs of RAG$^{-/-}$ and ZAP-70$^{-/-}$ mice, and this was accompanied by higher numbers of ILC2 than those seen in WT mice. The same was true of RORγt$^{-/-}$ chimeric mice, where mice lacked RORγt-expressing cells and as a result had no ILC3. Whilst in bone marrow chimeric mice this could be attributed to differences in the development of ILCs from bone marrow progenitor cells in the absence of RORγt, RAG$^{-/-}$ mice were found to have similar proportions of ILC2 and ILC3 in iLNs, suggesting that this was a mLN-specific effect and not related to development. The reason for a bias towards ILC2 in these mice is still unknown, however our data is consistent with there being a relationship between numbers of these two subsets. This would be interesting to investigate further, particularly if differences in ILC subsets within these areas could have an effect on the progression and shaping of an immune response.

6.2.3 Interfollicular microenvironment differs between peripheral and mucosal draining LNs

In this study, this interfollicular microenvironment was found to be notably different in skin-draining LNs. Despite the presence of many RORγt-expressing cells within the

interfollicular areas of skin-draining peripheral popliteal (popLN) and inguinal LNs (iLN) quantitative analysis revealed that, in contrast to the mLN, many of these cells expressed CD3 and were therefore T cells. In this study differences were detected in the RORγt$^+$ T cell types present in mLNs and pLNs, which may account for this observation, and a number of RORγt-expressing T cell populations have been reported in the skin. Alongside ILC3, RORγt$^+$ γδ T cells been shown to be important sources of IL-17 in a murine model of psoriasis (Pantelyushin et al., 2012), and populations of RORγt$^+$ invariant NKT (iNKT) cells have been shown to reside in the skin whilst a phenotypically similar iNKT cell population can be detected in peripheral LNs (Doisne et al., 2009). What is striking is the correlation between the expression of the transcription factor RORγt and location of cells to the interfollicular area. This can perhaps be explained by an increased requirement for IL-7 signalling, as RORγt-expressing cells within the interfollicular areas of LNs in this study mostly expressed high levels of IL-7Rα. IL-7 has been shown to be produced by LECs, which are enriched in interfollicular areas of LNs and this was proposed to provide essential homeostatic survival signals to nearby IL-7Rα$^+$ cells (Onder et al., 2012). Certainly LTi cell survival in adult tissue has been shown to be supported by signalling by this cytokine (Schmutz et al., 2009), and the importance of this signalling may provide an explanation as to why these cells cluster at this location. Another reason could be expression of the chemokine receptor CCR6. CCR6 expression by subsets of group 3 ILCs is well-established (Klose et al., 2013), and we have shown that ILC3 in LNs are predominantly CCR6$^+$. CCR6 expression has also been documented on populations of RORγt-expressing T cells, such as CD4$^+$ Th17 cells (Esplugues et al., 2011) and RORγt$^+$ iNKT cells (Doisne et al., 2009). Transcriptional profiling of lymph node LECs has shown that they express CCL20 (Malhotra et al., 2012), the chemokine which binds to CCR6,

therefore migration towards these sites could be instructed by this, although analysis of LNs from CCR6-deficient mice would give further indication.

6.3 ILC POPULATIONS IN A DRAINING LN

The position of these cells at the interfollicular regions and interface between B cell follicles and T cell zone (B-T interface) of lymph nodes also places them in a position to participate in an immune response. One hypothesis for our initial observation of numerous ILC3 within the mLN was that this reflected the phenotype of an 'activated' LN, given that the mLN is likely exposed to a larger amount of antigen than its skin-draining counterparts. Draining lymph node models therefore enabled us to analyse whether ILC populations of 'activated' peripheral LNs increased in number, and to characterise these cells to see whether, and by what manner, they could influence this immune response. Both group 2 and group 3 ILCs, like DCs, have been shown to express MHCII and be capable of presenting peptide to $CD4^+$ T cells (Oliphant et al., 2014, Hepworth et al., 2013, von Burg et al., 2014). The immunological result of this presentation is however likely to be highly dependent on their expression of the co-stimulatory molecules CD80 and CD86, although a potential role for others, such as OX40L and CD30L (Kim et al., 2005), which were not analysed in this study should not be excluded. Whilst ILC3 in the mLN have been shown to lack expression of CD80 and CD86, and $MHCII^+$ ILC3 in the gut suppress $CD4^+$ T cell responses to commensal bacteria (Hepworth et al., 2013), ILC3 derived from the spleen and cultured in IL-1β have been shown to be capable of expressing moderate levels of CD80 and CD86 and inducing the proliferation of $CD4^+$ T cells in an antigen-specific manner (von Burg et al., 2014). Similarly ILC2 expressing MHCII have been shown to be able to induce $CD4^+$ T cell proliferation *in vitro* (Oliphant et al., 2014). Little is known of the response of ILCs to immunological challenge in skin-draining LNs, and it has not been

established whether ILCs in these LNs express co-stimulatory molecules at steady state or following immunisation. In this investigation we sought to assess the ILC response to immunisation in the paw pad by looking at quantitative and phenotypical changes in ILC populations in the draining axillary and brachial LNs (aLN, bLN).

We found ILC3 to constitute a lower proportion of total ILCs within skin-draining inguinal and brachial LNs (bLN) than in the mLN or medLN. The discovery of ILCs in the skin is relatively recent and comparatively less has been published on their function in this tissue compared to the gut, likely in part a result of the difficulties associated with isolating cells from the skin. ILC2 have been reported in the skin of both mice and humans (Kim et al., 2013, Roediger et al., 2013) and these cells have been shown to be enriched in patients with a type 2 inflammatory skin disorder (Salimi et al., 2013). Whilst ILC3 have also been reported in the skin (Pantelyushin et al., 2012, Villanova et al., 2014) the general ILC bias in this tissue is thought to be skewed towards GATA-3^{+} ILC2 (Spencer et al., 2014). Interestingly in this investigation we do not see this ILC2 bias reflected in either the skin-draining LNs or the medLN—which drains the lung—at steady state, although large numbers of ILC2 have been reported to accumulate within the medLNs of mice following intranasal administration of IL-33 (Wolterink et al., 2012).

6.3.1 ILCs accumulate in a draining LN but are atypical APCs

Activated DCs have been shown to arrive within a peripheral draining LN (dLN) within one day of stimulation of the skin (Tomura et al., 2014) and in our study numbers of both ILC2 and LTi-like ILC3 were found to be moderately increased in dLNs at this timepoint when compared to controls. Although a proportion of both ILC2 and LTi-like ILC were found to express MHCII, this did not appear to be specific to the immune response, with

similar percentages observed in both dLNs and control. Although co-stimulatory molecules could be detected on the surface of some MHCII^{+} ILC2 and ILC3, the level of expression was notably lower than that detected on professional APCs. Even following accumulation, these ILCs were relatively few and the low levels of CD80 and CD86 on their surface makes it seem unlikely that these cells could efficiently contribute to the priming of naïve CD4^{+} T cells at this timepoint. This finding fits with the description of these cells as atypical APCs (Kambayashi and Laufer, 2014), as opposed to cells which could replace the function of DCs.

ILC number increased most notably at later timepoints analysed, perhaps indicating that these cells play a role following the initial establishment of the immune response. Deficiency of ILC3 has previously been shown to have no effect of primary CD4^{+} T cell responses in the spleen (Withers et al., 2012), although analysis of numbers of responding CD4^{+} T cells in pLNs of MHCII$^{\Delta ILC3}$ mice six days following immunisation has previously shown some evidence of dysregulation of T cell responses in the absence of MHCII-mediated ILC3 signalling (Mackley et al., 2015). Whether or not this increase in the number of ILC3 is simply a result of LN expansion or could be related to a role at these later timepoints, such as the provision of signals to T cells which will go on to become memory cells, was unclear but would be interesting to investigate further. Although there was an increase in the number of ILC3 in draining peripheral LNs, it was not clear that these now resembled the mLN. Although ILC3 can still be detected within the interfollicular areas of draining peripheral LNs (E. Mackley, unpublished observations) it was difficult to make any conclusions due to their scarcity in the enlarged LN. Repeated exposure of a peripheral LN to antigen would perhaps be a better test of this hypothesis, and an interesting line of investigation for the future.

Although we detected an increase in the number of ILCs in a draining LN the number of ILC2 detected in the dLNs across the entire timecourse was still low. Despite the adjuvant used, aluminium hydroxide, being known to promote a robust type 2 immune response (Lindblad, 2004) the increase in number of ILC2 observed in the dLN following immunisation with alum-ppt NP-OVA was moderate across all timepoints, yet ILC2 have previously been reported to accumulate in the medLNs during an immune response to intranasal administration of OVA (Wolterink et al., 2012). It is possible that the mild increase seen could be a result of ILC2 not participating in dLN immune responses from the skin, or perhaps that our method of immunising was not well targeted to this population.

6.3.2 Mechanism of ILC accumulation in draining LNs suggests trafficking

We sought to determine whether the increases in numbers of ILCs could be related to trafficking from the tissue, as has been shown in the gut (Mackley et al., 2015). No increased proliferation was detected in any population of ILC which could account for the increased numbers of ILCs seen, despite ILC2 having previously been shown to proliferate in response to T cell-produced IL-2 (Oliphant et al., 2014). This raised the possibility that ILCs may traffic into the dLNs from other sites. Unlike in the mLN where, in this study, only LTi-like ILC3 displayed a CCR7-dependency, all ILCs are lower in the skin-draining iLN of $CCR7^{-/-}$ mice and this was also found to be true in $CCR7^{-/-}$ axillary and brachial LNs at steady state. It is not clear that other populations of ILCs in this tissue express high levels of CCR7, nor has the expression of this molecule by ILCs been explored at many different sites. In keeping with a hypothesis of cell trafficking in a CCR7-dependent manner, no accumulation of ILCs was detected in the dLNs of $CCR7^{-/-}$ mice following immunisation, despite an increase in WT controls. Although mixed bone marrow chimera

experiments in this study have shown that the inability of CCR7$^{-/-}$ ILC3 to enter the resting iLN was at least in part a cell-intrinsic defect, and this likely also applies to the aLN and bLN, whether or not cell-intrinsic CCR7 signalling is required for ILC3 entry following immunisation still remains to be seen.

An immunisation experiment in CD80$^{-/-}$CD86$^{-/-}$ mice gave similar results, with ILCs failing to accumulate in the dLN in the absence of CD80 and CD86. Given the low expression of these molecules detected on the surface of ILCs in this tissue, it seems unlikely that this is a direct effect of loss of CD80 and CD86 expression on these cells. One factor that experiments in CCR7$^{-/-}$ and CD80$^{-/-}$CD86$^{-/-}$ mice had in common was a lack of a T cell response within the draining LN. In CCR7$^{-/-}$ mice very little expansion of an adoptively transferred antigen-specific population of CD4^{+} T cells was detected, despite these cells themselves being CCR7-sufficient and thus capable of entering the LN. This was most likely due to impaired CCR7$^{-/-}$ DC migration to the draining LN (Forster et al., 2008, Braun et al., 2011) and the subsequent lack of T cell priming. CD80$^{-/-}$CD86$^{-/-}$ mice were similarly unable to mount a CD4^{+} T cell response, in this case likely because of the lack of essential co-stimulatory signals following antigen-presentation. It is therefore possible that a T cell-derived signal is required to instruct ILC increase in LNs, and could explain why ILC increase was primarily at later timepoints in an immune response. ILC2 have previously been shown to respond to T cell-produced IL-2 and cross-talk with T cells has been demonstrated to be important for their function. (Oliphant et al., 2014, Mirchandani et al., 2014). IL-2 has also been shown to induce the proliferation of ILC2 in the spleen of RAG-1$^{-/-}$ mice (Roediger et al., 2013), however these findings do not explain the results of our study, where no increased ILC proliferation was detected even in the presence of an ongoing T cell response. The possibility that T cells play a role in the entry of ILC3 into the

mLN has been discussed previously, and it is possible that the abrogation of a T cell response in draining peripheral LNs is responsible for the phenotype seen. It is, however, not clear from these studies whether draining LNs in CCR7$^{-/-}$ and CD80$^{-/-}$CD86$^{-/-}$ mice undergo normal processes, such as LN shutdown. Following activation, egress of activated lymphocytes is prevented for a period of time (Cyster and Schwab, 2012). It is not clear whether or not populations of ILC are also prevented from leaving LNs during this time. Should normal LN shutdown not occur in the dLNs of CCR7$^{-/-}$ and CD80$^{-/-}$CD86$^{-/-}$ mice then this could provide further explanation for the lack of ILC accumulation detected.

6.4 ROLE OF ILC3 IN A PRIMARY CD4^{+} T CELL RESPONSE

6.4.1 ILC3-deficiency does not impair expansion of CD4^{+} T cells in a primary immune response

Lymph nodes are important for the generation of CD4 T cell responses, confining all cells required to mount a response to a defined site and maximising the opportunities for re-circulating CD4^{+} T cells to sample a large number of different antigens (von Andrian and Mempel, 2003). Data from our group has previously shown that support for populations of CD4^{+} T memory cell is impaired in mice which lack LTi cells, however the effects of these cells on CD4^{+} T cell responses in LNs was not explored (Withers et al., 2012). We have shown that ILC3 sit in regions of LNs which are exposed to large numbers of naïve CD4^{+} T cells, as well as CD4^{+} T cells taking part in an immune response. Additionally we have observed that populations of ILC can increase in a draining LN following immunisation, potentially indicative of a role in this immune response. A bone marrow chimera method was therefore used to investigate whether loss of ILC3 had any impact on primary CD4^{+} T cell responses in the skin-draining axillary and brachial LNs.

Analysis of an antigen-specific $CD4^+$ T cell response in the absence of RORγt-expressing cells following immunisation revealed that $CD4^+$ T cell numbers were similar to those in WT controls. In addition to this, no evidence of increased T cell dysregulation, in terms of the expression of markers associated with T cell activation, could be found. Whilst these data suggest that RORγt-expressing cell types, including ILC3, are not required for the mounting of a primary $CD4^+$ T cell response in peripheral LNs, this investigation has not explored other elements of a $CD4^+$ T cell response, for example the phenotype of these T effector cells. This, and other studies into the function of these cells, would benefit from more sophisticated ILC3-depletion models which have recently been developed.

6.4.2 Models to analyse ILC function

Innate lymphoid cells are a part of a fast-growing field of research and, as such, new advances are made often. The development of mouse models which enable the effective, selective targeting of these populations will revolutionise research into the functions of these cells. Up until recently most analysis of immune responses in the absence of ILC subsets has had to rely upon the use of bone marrow chimeras or studies in T cell deficient mice (Withers et al., 2012). This is largely due the similarity of ILCs to other cell types, in their expression of transcription factors and surface markers, and the subsequent difficulties in specifically targeting these cells without affecting others. Advances in the field have led to the development of elegant mouse models where populations of ILCs, or specific molecules on these cells, can be genetically deleted, either constitutively or in an inducible fashion.

$MHCII^{\Delta ILC3}$ mice, where only ILC3 lack the expression of MHCII, provide a good example of where the investigators have made use of an ILC-specific observation and Cre-Lox

recombination technology. By crossing floxed H2-Ab1 mice with those that express a Cre recombinase under the control of the *Rorc* promoter, they created a strain of mice where expression of RORγt resulted in the deletion of the gene which results in MHCII expression (Hepworth et al., 2013). This ILC3-specific targeting left MHCII expression by other APCs comparable to that in controls, and did not affect the embryonic lymphoid tissue inducing functions of cells within this group (Hepworth et al., 2013). Using these mice it would be of interest to investigate the role of ILC3-expressed MHCII in a range of different LNs, not just the mLN, and through all stages of a $CD4^+$ T cell response; from initial priming to the maintenance of and response of memory cells.

Although details of mouse models in which ILC3 are genetically and selectively deleted have not yet been published, such models exist for ILC2. Oliphant et al (2014) use an ILC2-deficient mouse in which a floxed diphtheria toxin (DT) receptor is expressed in the place of the gene for inducible T cell co-stimuator (ICOS) protein. This results in those cells which ordinarily express ICOS now expressing a receptor for DT, uptake of which results in the death of the cell. Although ICOS is also expressed by T cells, and thus ordinarily this would result in the DT-mediated deletion of both ILC2 and T cells, the authors circumvented this by including a gene for Cre recombinase expression which is activated in the event of expression of CD4; therefore those cells in which CD4 expression has been switched excise the gene for DT receptor expression and are no longer deleted upon administration of DT. As ILC2 do not express CD4, but all T cells will upregulate this marker at some stage during development (Germain, 2002) this results in a mouse model where ILC2 are selectively deficient (Oliphant et al., 2014). One of the advantages of this system is that it can be induced with the administration of the toxin, thereby allowing ILC2 to be deleted at different stages in an immune response.

The growing use of photo-convertible fluorescent proteins in mouse models, where cells can be 'tagged' and their migration analysed (Morton et al., 2014, Tomura et al., 2014), could be an effective way to study whether ILCs are recruited from the skin to the LN in our draining LN model, and whether they then leave and re-circulate to other sites. Indeed, these models have already proved a useful tool in studying ILC3 migration from the small intestine to the mLN (Mackley et al., 2015). The tagging of cells could also provide answers as to whether ILCs in LNs at different sites are in fact distinct populations, or widely re-circulating cells. The migratory capacity of these cells could also be investigated using surgical methods, such as cannulation of lymph, to determine whether CCR7-dependent entry of ILCs to LNs is as a result of trafficking through the lymph or blood. Additionally, the location of these cells near the exterior of LNs lends itself to analysis using multi-photo microscopy methods to reveal specific interactions of ILCs within the interfollicular area.

Most importantly, these methods will enable the role of ILCs in immune responses, and the specific mechanisms by which they act, to be elucidated. Discovery of whether or not $MHCII^+$ ILC3 carry out their regulation of $CD4^+$ T cell responses in the gut or in the draining mesenteric LN will fundamentally contribute to our knowledge of tolerance to commensal antigens (Hepworth et al., 2015). Expression of MHCII has been reported on human ILC3 (Hepworth et al., 2013) and found to be lower on ILC3 from patients with pediatric Crohn's Disease when compared to controls (Hepworth et al., 2015). With a better understanding of the role of these cells in tolerance and the prevention of inappropriate inflammatory responses in the gut, it is possible that these cells could become future therapeutic targets to treat immune-mediated pathologies. Given our observation of LTi-like ILC3 resistance to irradiation, therapeutically increasing the numbers of this

population could be useful in the treatment of mucositis, and it would be important to investigate whether the same phenotype is true of ILC3 within the gut. Finally, it is important that we understand the ways in which adaptive immune responses are initiated and shaped in order to be able to manipulate them beneficially ourselves.

6.5 CONCLUDING REMARKS

Within this investigation I have extensively characterised ILCs within a range of different LNs at steady state and following immunisation, which will provide the foundation for further experiments which can specifically elucidate their function within these structures. The observed enrichment of LTi-like ILC3 in mucosal tissue-draining LNs is indicative of an increased requirement for these cells in LNs which drain barrier sites, and which are regularly exposed to antigen. Our finding that the majority of ILC3 within the mLN express CCR6 and MHCII, and thus resemble those cells shown to regulate $CD4^+$ T cell responses in the gut, suggests that ILC3-mediated tolerance could take place in the mLN. Consistent with this, we show that LTi-like ILC3 entry to this tissue, like that of DCs, is dependent upon CCR7 signalling and that once within mLNs ILC3 cluster in interfollicular regions to create a microenvironment which is not detected in peripheral tissue-draining LNs. It is therefore feasible that the increased numbers of ILC3 in mucosal tissue-draining LNs serves to limit immune responses to commensal microorganisms and harmless antigens.

Although ILC populations are less numerous in peripheral LNs we show that they accumulate in these tissues following local immunisation. The observation that this accumulation was not as a result of ILC proliferation within the LN could be seen as consistent with cell trafficking, whilst the failure of all ILC subsets to accumulate in

draining LNs of CCR7-deficient mice suggests that this chemokine receptor is involved, although whether this is a cell intrinsic effect or due to extrinsic factors remains to be seen. Given that MHCII and low levels of CD80 and CD86 could be detected on the surface of some ILCs in peripheral LNs, it seems likely that the role of these cells in adaptive immune responses is dependent upon both the site and circumstances of immunisation. Nonetheless, it is not clear that these ILCs are comparable antigen-presenting cells to DCs. Given their rarity and low level expression of co-stimulatory molecules in the peripheral LNs analysed, it seems unlikely that these cells are efficient at priming naïve $CD4^+$ T cells during an immune response and, consistent with this, our data indicates that numbers of $CD4^+$ T cell cells in a primary LN response are not impaired by a deficiency in ILC3. Further experiments, using new mouse models which selectively target ILC function, are however required to fully understand the contribution of these cells to the regulation of adaptive immunity.

Papers arising from this thesis:

MACKLEY, E. C., HOUSTON, S., MARRIOTT, C. L., HALFORD, E. E., LUCAS, B., CEROVIC, V., FILBEY, K. J., MAIZELS, R. M., HEPWORTH, M. R., SONNENBERG, G. F., MILLING, S. & WITHERS, D. R. 2015. CCR7-dependent trafficking of RORγ+ ILCs creates a unique microenvironment within mucosal draining lymph nodes. *Nat Commun,* 6.

APPENDIX A **LIST OF REFERENCES**

AI, T. L., SOLOMON, B. D. & HSIEH, C.-S. 2014. T-cell selection and intestinal homeostasis. *Immunological reviews,* 259**,** 60-74.

AKIRA, S., UEMATSU, S. & TAKEUCHI, O. 2006. Pathogen recognition and innate immunity. *Cell,* 124**,** 783-801.

ANSEL, K. M., MCHEYZER-WILLIAMS, L. J., NGO, V. N., MCHEYZER-WILLIAMS, M. G. & CYSTER, J. G. 1999. In vivo-activated CD4 T cells upregulate CXC chemokine receptor 5 and reprogram their response to lymphoid chemokines. *J Exp Med,* 190**,** 1123-34.

ANSEL, K. M., NGO, V. N., HYMAN, P. L., LUTHER, S. A., FORSTER, R., SEDGWICK, J. D., BROWNING, J. L., LIPP, M. & CYSTER, J. G. 2000. A chemokine-driven positive feedback loop organizes lymphoid follicles. *Nature,* 406**,** 309-314.

ANTHONY, R. M., RUTITZKY, L. I., URBAN, J. F., STADECKER, M. J. & GAUSE, W. C. 2007. Protective immune mechanisms in helminth infection. *Nature reviews. Immunology,* 7**,** 975-987.

ARTIS, D. & SPITS, H. 2015. The biology of innate lymphoid cells. *Nature,* 517**,** 293-301.

BARLOW, J. L., BELLOSI, A., HARDMAN, C. S., DRYNAN, L. F., WONG, S. H., CRUICKSHANK, J. P. & MCKENZIE, A. N. 2012. Innate IL-13-producing nuocytes arise during allergic lung inflammation and contribute to airways hyperreactivity. *J Allergy Clin Immunol,* 129**,** 191-8 e1-4.

BARNDEN, M. J., ALLISON, J., HEATH, W. R. & CARBONE, F. R. 1998. Defective TCR expression in transgenic mice constructed using cDNA-based [agr]- and [bgr]-chain genes under the control of heterologous regulatory elements. *Immunol Cell Biol,* 76**,** 34-40.

BASSET, C., HOLTON, J., O'MAHONY, R. & ROITT, I. 2003. Innate immunity and pathogen-host interaction. *Vaccine,* 21 Suppl 2**,** S12-23.

BERNINK, JOCHEM H., KRABBENDAM, L., GERMAR, K., DE JONG, E., GRONKE, K., KOFOED-NIELSEN, M., MUNNEKE, J. M., HAZENBERG, METTE D., VILLAUDY, J., BUSKENS, CHRISTIANNE J., BEMELMAN, WILLEM A., DIEFENBACH, A., BLOM, B. & SPITS, H. 2015. Interleukin-12 and -23 Control Plasticity of CD127+ Group 1 and Group 3 Innate Lymphoid Cells in the Intestinal Lamina Propria. *Immunity,* 43**,** 146-160.

BOUSSO, P. & ROBEY, E. 2003. Dynamics of CD8+ T cell priming by dendritic cells in intact lymph nodes. *Nat Immunol,* 4**,** 579-585.

BRAUN, A., WORBS, T., MOSCHOVAKIS, G. L., HALLE, S., HOFFMANN, K., BOLTER, J., MUNK, A. & FORSTER, R. 2011. Afferent lymph-derived T cells and DCs use different chemokine receptor CCR7-dependent routes for entry into the lymph node and intranodal migration. *Nat Immunol,* 12**,** 879-887.

BRESTOFF, J. R. & ARTIS, D. 2013. Commensal bacteria at the interface of host metabolism and the immune system. *Nat Immunol,* 14**,** 676-84.

BROMLEY, S. K., THOMAS, S. Y. & LUSTER, A. D. 2005. Chemokine receptor CCR7 guides T cell exit from peripheral tissues and entry into afferent lymphatics. *Nat Immunol,* 6**,** 895-901.

BUONOCORE, S., AHERN, P. P., UHLIG, H. H., IVANOV, II, LITTMAN, D. R., MALOY, K. J. & POWRIE, F. 2010. Innate lymphoid cells drive interleukin-23-dependent innate intestinal pathology. *Nature,* 464**,** 1371-5.

BUTCHER, E. C. & PICKER, L. J. 1996. Lymphocyte homing and homeostasis. *Science,* 272**,** 60-6.

CELLA, M., FUCHS, A., VERMI, W., FACCHETTI, F., OTERO, K., LENNERZ, J. K. M., DOHERTY, J. M., MILLS, J. C. & COLONNA, M. 2009. A human natural killer cell subset provides an innate source of IL-22 for mucosal immunity. *Nature,* 457**,** 722-725.

CELLA, M., OTERO, K. & COLONNA, M. 2010. Expansion of human NK-22 cells with IL-7, IL-2, and IL-1beta reveals intrinsic functional plasticity. *Proc Natl Acad Sci U S A,* 107**,** 10961-6.

CHANG, Y. J., KIM, H. Y., ALBACKER, L. A., BAUMGARTH, N., MCKENZIE, A. N., SMITH, D. E., DEKRUYFF, R. H. & UMETSU, D. T. 2011. Innate lymphoid cells mediate influenza-induced airway hyper-reactivity independently of adaptive immunity. *Nat Immunol,* 12**,** 631-8.

CHEN, L. & FLIES, D. B. 2013. Molecular mechanisms of T cell co-stimulation and co-inhibition. *Nat Rev Immunol,* 13**,** 227-242.

CHEN, W., JIN, W., HARDEGEN, N., LEI, K.-J., LI, L., MARINOS, N., MCGRADY, G. & WAHL, S. M. 2003. Conversion of Peripheral CD4+CD25− Naive T Cells to CD4+CD25+ Regulatory T Cells by TGF-β Induction of Transcription Factor Foxp3. *The Journal of Experimental Medicine,* 198**,** 1875-1886.

COOPER, M. D. & ALDER, M. N. 2006. The Evolution of Adaptive Immune Systems. *Cell,* 124**,** 815-822.

CRELLIN, N. K., TRIFARI, S., KAPLAN, C. D., SATOH-TAKAYAMA, N., DI SANTO, J. P. & SPITS, H. 2010. Regulation of Cytokine Secretion in Human CD127+ LTi-like Innate Lymphoid Cells by Toll-like Receptor 2. *Immunity,* 33**,** 752-764.

CUPEDO, T., CRELLIN, N. K., PAPAZIAN, N., ROMBOUTS, E. J., WEIJER, K., GROGAN, J. L., FIBBE, W. E., CORNELISSEN, J. J. & SPITS, H. 2009. Human fetal lymphoid tissue-inducer cells are interleukin 17-producing precursors to RORC+ CD127+ natural killer-like cells. *Nat Immunol,* 10**,** 66-74.

CUPEDO, T., KRAAL, G. & MEBIUS, R. E. 2002. The role of CD45+CD4+CD3− cells in lymphoid organ development. *Immunological Reviews,* 189**,** 41-50.

CYSTER, J. G. & SCHWAB, S. R. 2012. Sphingosine-1-phosphate and lymphocyte egress from lymphoid organs. *Annu Rev Immunol,* 30**,** 69-94.

DEBES, G. F., ARNOLD, C. N., YOUNG, A. J., KRAUTWALD, S., LIPP, M., HAY, J. B. & BUTCHER, E. C. 2005. Chemokine receptor CCR7 required for T lymphocyte exit from peripheral tissues. *Nat Immunol,* 6**,** 889-94.

DOISNE, J.-M., BECOURT, C., AMNIAI, L., DUARTE, N., LE LUDUEC, J.-B., EBERL, G. & BENLAGHA, K. 2009. Skin and Peripheral Lymph Node Invariant NKT Cells Are Mainly Retinoic Acid Receptor-Related Orphan Receptor γt+ and Respond Preferentially under Inflammatory Conditions. *The Journal of Immunology,* 183**,** 2142-2149.

DUDAKOV, J. A., HANASH, A. M., JENQ, R. R., YOUNG, L. F., GHOSH, A., SINGER, N. V., WEST, M. L., SMITH, O. M., HOLLAND, A. M., TSAI, J. J., BOYD, R. L. & VAN DEN BRINK, M. R. M. 2012. Interleukin-22 drives endogenous thymic regeneration in mice. *Science (New York, N.Y.),* 336**,** 91-95.

EBERL, G., MARMON, S., SUNSHINE, M.-J., RENNERT, P. D., CHOI, Y. & LITTMAN, D. R. 2004. An essential function for the nuclear receptor ROR[gamma]t in the generation of fetal lymphoid tissue inducer cells. *Nat Immunol,* 5**,** 64-73.

ESPLUGUES, E., HUBER, S., GAGLIANI, N., HAUSER, A. E., TOWN, T., WAN, Y. Y., O/'CONNOR, W., RONGVAUX, A., VAN ROOIJEN, N., HABERMAN, A. M., IWAKURA, Y., KUCHROO, V. K., KOLLS, J. K., BLUESTONE, J. A., HEROLD, K. C. & FLAVELL, R. A. 2011. Control of TH17 cells occurs in the small intestine. *Nature,* 475**,** 514-518.

FINKE, D., ACHA-ORBEA, H., MATTIS, A., LIPP, M. & KRAEHENBUHL, J. P. 2002. CD4+CD3− Cells Induce Peyer's Patch Development: Role of α4β1 Integrin Activation by CXCR5. *Immunity,* 17**,** 363-373.

FORD, L., HANSELL, C. H. & NIBBS, R. B. 2013. Using Fluorescent Chemokine Uptake to Detect Chemokine Receptors by Fluorescent Activated Cell Sorting. *In:* CARDONA, A. E. & UBOGU, E. E. (eds.) *Chemokines.* Humana Press.

FORSTER, R., DAVALOS-MISSLITZ, A. C. & ROT, A. 2008. CCR7 and its ligands: balancing immunity and tolerance. *Nat Rev Immunol,* 8**,** 362-71.

FORSTER, R., SCHUBEL, A., BREITFELD, D., KREMMER, E., RENNER-MULLER, I., WOLF, E. & LIPP, M. 1999. CCR7 coordinates the primary immune response by establishing functional microenvironments in secondary lymphoid organs. *Cell,* 99**,** 23-33.

FORT, M. M., CHEUNG, J., YEN, D., LI, J., ZURAWSKI, S. M., LO, S., MENON, S., CLIFFORD, T., HUNTE, B., LESLEY, R., MUCHAMUEL, T., HURST, S. D., ZURAWSKI, G., LEACH, M. W., GORMAN, D. M. & RENNICK, D. M. 2001. IL-25 Induces IL-4, IL-5, and IL-13 and Th2-Associated Pathologies In Vivo. *Immunity,* 15**,** 985-995.

GAGLIANI, N., VESELY, M. C. A., ISEPPON, A., BROCKMANN, L., XU, H., PALM, N. W., DE ZOETE, M. R., LICONA-LIMON, P., PAIVA, R. S., CHING, T., WEAVER, C., ZI, X., PAN, X., FAN, R., GARMIRE, L. X., COTTON, M. J., DRIER, Y., BERNSTEIN, B., GEGINAT, J., STOCKINGER, B., ESPLUGUES, E., HUBER, S. & FLAVELL, R. A. 2015. Th17 cells transdifferentiate into regulatory T cells during resolution of inflammation. *Nature,* 523**,** 221-225.

GARROOD, T., LEE, L. & PITZALIS, C. 2006. Molecular mechanisms of cell recruitment to inflammatory sites: general and tissue-specific pathways. *Rheumatology,* 45**,** 250-260.

GASPAL, F. M., KIM, M. Y., MCCONNELL, F. M., RAYKUNDALIA, C., BEKIARIS, V. & LANE, P. J. 2005. Mice deficient in OX40 and CD30 signals lack memory antibody responses because of deficient CD4 T cell memory. *J Immunol,* 174**,** 3891-6.

GEREMIA, A., ARANCIBIA-CARCAMO, C. V., FLEMING, M. P., RUST, N., SINGH, B., MORTENSEN, N. J., TRAVIS, S. P. & POWRIE, F. 2011. IL-23-responsive innate lymphoid cells are increased in inflammatory bowel disease. *J Exp Med,* 208**,** 1127-33.

GERMAIN, R. N. 2002. T-cell development and the CD4-CD8 lineage decision. *Nat Rev Immunol,* 2**,** 309-322.

GIRARDI, M. 2006. Immunosurveillance and Immunoregulation by [gamma][delta] T Cells. *J Invest Dermatol,* 126**,** 25-31.

GOTO, Y., OBATA, T., KUNISAWA, J., SATO, S., IVANOV, I. I., LAMICHHANE, A., TAKEYAMA, N., KAMIOKA, M., SAKAMOTO, M., MATSUKI, T., SETOYAMA, H., IMAOKA, A., UEMATSU, S., AKIRA, S., DOMINO, S. E., KULIG, P., BECHER, B., RENAULD, J.-C., SASAKAWA, C., UMESAKI, Y., BENNO, Y. & KIYONO, H. 2014. Innate lymphoid cells regulate intestinal epithelial cell glycosylation. *Science,* 345.

GOWANS, J. L. & KNIGHT, E. J. 1964. The Route of Re-Circulation of Lymphocytes in the Rat. *Proceedings of the Royal Society of London. Series B, Biological Sciences,* 159**,** 257-282.

GRAY, E. E., FRIEND, S., SUZUKI, K., PHAN, T. G. & CYSTER, J. G. 2012. Subcapsular sinus macrophage fragmentation and CD169+ bleb acquisition by closely associated IL-17-committed innate-like lymphocytes. *PLoS One,* 7**,** e38258.

GREEN, J. M., NOEL, P. J., SPERLING, A. I., WALUNAS, T. L., GRAY, G. S., BLUESTONE, J. A. & THOMPSON, C. B. 1994. Absence of B7-dependent responses in CD28-deficient mice. *Immunity,* 1**,** 501-508.

GRIFFITH, J. W., SOKOL, C. L. & LUSTER, A. D. 2014. Chemokines and chemokine receptors: positioning cells for host defense and immunity. *Annu Rev Immunol,* 32**,** 659-702.

HALIM, TIMOTHEUS Y. F., STEER, CATHERINE A., MATHÄ, L., GOLD, MATTHEW J., MARTINEZ-GONZALEZ, I., MCNAGNY, KELLY M., MCKENZIE, ANDREW N. J. & TAKEI, F. 2014. Group 2 Innate Lymphoid Cells Are Critical for the Initiation of Adaptive T Helper 2 Cell-Mediated Allergic Lung Inflammation. *Immunity,* 40**,** 425-435.

HAMMERSCHMIDT, S. I., AHRENDT, M., BODE, U., WAHL, B., KREMMER, E., FÖRSTER, R. & PABST, O. 2008. Stromal mesenteric lymph node cells are essential for the generation of gut-homing T cells in vivo. *The Journal of Experimental Medicine,* 205**,** 2483-2490.

HARRINGTON, L. E., HATTON, R. D., MANGAN, P. R., TURNER, H., MURPHY, T. L., MURPHY, K. M. & WEAVER, C. T. 2005. Interleukin 17-producing CD4+ effector T cells develop via a lineage distinct from the T helper type 1 and 2 lineages. *Nat Immunol,* 6**,** 1123-1132.

HEATH, W. R. & CARBONE, F. R. 2013. The skin-resident and migratory immune system in steady state and memory: innate lymphocytes, dendritic cells and T cells. *Nat Immunol,* 14**,** 978-85.

HEPWORTH, M. R., FUNG, T. C., MASUR, S. H., KELSEN, J. R., MCCONNELL, F. M., DUBROT, J., WITHERS, D. R., HUGUES, S., FARRAR, M. A., REITH, W., EBERL, G., BALDASSANO, R. N., LAUFER, T. M., ELSON, C. O. & SONNENBERG, G. F. 2015. Group 3 innate lymphoid cells mediate intestinal selection of commensal bacteria–specific CD4+ T cells. *Science,* 348**,** 1031-1035.

HEPWORTH, M. R., MONTICELLI, L. A., FUNG, T. C., ZIEGLER, C. G. K., GRUNBERG, S., SINHA, R., MANTEGAZZA, A. R., MA, H.-L., CRAWFORD, A., ANGELOSANTO, J. M., WHERRY, E. J., KONI, P. A., BUSHMAN, F. D., ELSON, C. O., EBERL, G., ARTIS, D. & SONNENBERG, G. F. 2013. Innate lymphoid cells regulate CD4+ T-cell responses to intestinal commensal bacteria. *Nature,* 498**,** 113-117.

HOGQUIST, K. A., BALDWIN, T. A. & JAMESON, S. C. 2005. Central tolerance: learning self-control in the thymus. *Nat Rev Immunol,* 5**,** 772-782.

HOYLER, T., KLOSE, C. S., SOUABNI, A., TURQUETI-NEVES, A., PFEIFER, D., RAWLINS, E. L., VOEHRINGER, D., BUSSLINGER, M. & DIEFENBACH, A. 2012. The transcription factor GATA-3 controls cell fate and maintenance of type 2 innate lymphoid cells. *Immunity,* 37**,** 634-48.

HUANG, Y., GUO, L., QIU, J., CHEN, X., HU-LI, J., SIEBENLIST, U., WILLIAMSON, P. R., URBAN, J. F., JR. & PAUL, W. E. 2015. IL-25-responsive, lineage-negative KLRG1(hi) cells are multipotential 'inflammatory' type 2 innate lymphoid cells. *Nat Immunol,* 16**,** 161-9.

HURST, S. D., MUCHAMUEL, T., GORMAN, D. M., GILBERT, J. M., CLIFFORD, T., KWAN, S., MENON, S., SEYMOUR, B., JACKSON, C., KUNG, T. T., BRIELAND, J. K., ZURAWSKI, S. M., CHAPMAN, R. W., ZURAWSKI, G. & COFFMAN, R. L. 2002. New IL-17 Family

Members Promote Th1 or Th2 Responses in the Lung: In Vivo Function of the Novel Cytokine IL-25. *The Journal of Immunology,* 169**,** 443-453.

ILIEV, I. D., MILETI, E., MATTEOLI, G., CHIEPPA, M. & RESCIGNO, M. 2009. Intestinal epithelial cells promote colitis-protective regulatory T-cell differentiation through dendritic cell conditioning. *Mucosal Immunol,* 2**,** 340-50.

JIN, M. S., KIM, S. E., HEO, J. Y., LEE, M. E., KIM, H. M., PAIK, S.-G., LEE, H. & LEE, J.-O. 2007. Crystal Structure of the TLR1-TLR2 Heterodimer Induced by Binding of a Tri-Acylated Lipopeptide. *Cell,* 130**,** 1071-1082.

JUNT, T., MOSEMAN, E. A., IANNACONE, M., MASSBERG, S., LANG, P. A., BOES, M., FINK, K., HENRICKSON, S. E., SHAYAKHMETOV, D. M., DI PAOLO, N. C., VAN ROOIJEN, N., MEMPEL, T. R., WHELAN, S. P. & VON ANDRIAN, U. H. 2007. Subcapsular sinus macrophages in lymph nodes clear lymph-borne viruses and present them to antiviral B cells. *Nature,* 450**,** 110-114.

KAMADA, N., CHEN, G. Y., INOHARA, N. & NUNEZ, G. 2013. Control of pathogens and pathobionts by the gut microbiota. *Nat Immunol,* 14**,** 685-690.

KAMBAYASHI, T. & LAUFER, T. M. 2014. Atypical MHC class II-expressing antigen-presenting cells: can anything replace a dendritic cell? *Nat Rev Immunol,* 14**,** 719-30.

KASSIOTIS, G., GARCIA, S., SIMPSON, E. & STOCKINGER, B. 2002. Impairment of immunological memory in the absence of MHC despite survival of memory T cells. *Nat Immunol,* 3**,** 244-50.

KATAKAI, T., SUTO, H., SUGAI, M., GONDA, H., TOGAWA, A., SUEMATSU, S., EBISUNO, Y., KATAGIRI, K., KINASHI, T. & SHIMIZU, A. 2008. Organizer-Like Reticular Stromal Cell Layer Common to Adult Secondary Lymphoid Organs. *The Journal of Immunology,* 181**,** 6189-6200.

KELLY, K. A. & SCOLLAY, R. 1992. Seeding of neonatal lymph nodes by T cells and identification of a novel population of CD3-CD4+ cells. *Eur J Immunol,* 22**,** 329-34.

KILLAR, L., MACDONALD, G., WEST, J., WOODS, A. & BOTTOMLY, K. 1987. Cloned, Ia-restricted T cells that do not produce interleukin 4(IL 4)/B cell stimulatory factor 1(BSF-1) fail to help antigen-specific B cells. *The Journal of Immunology,* 138**,** 1674-9.

KIM, B. S., SIRACUSA, M. C., SAENZ, S. A., NOTI, M., MONTICELLI, L. A., SONNENBERG, G. F., HEPWORTH, M. R., VAN VOORHEES, A. S., COMEAU, M. R. & ARTIS, D. 2013. TSLP elicits IL-33-independent innate lymphoid cell responses to promote skin inflammation. *Sci Transl Med,* 5**,** 170ra16.

KIM, B. S., WANG, K., SIRACUSA, M. C., SAENZ, S. A., BRESTOFF, J. R., MONTICELLI, L. A., NOTI, M., WOJNO, E. D. T., FUNG, T. C., KUBO, M. & ARTIS, D. 2014. Basophils Promote Innate Lymphoid Cell Responses in Inflamed Skin. *Journal of immunology (Baltimore, Md. : 1950),* 193**,** 3717-3725.

KIM, M.-Y., ROSSI, S., WITHERS, D., MCCONNELL, F., TOELLNER, K.-M., GASPAL, F., JENKINSON, E., ANDERSON, G. & LANE, P. J. L. 2008. Heterogeneity of lymphoid tissue inducer cell populations present in embryonic and adult mouse lymphoid tissues. *Immunology,* 124**,** 166-174.

KIM, MYUNG H., TAPAROWSKY, ELIZABETH J. & KIM, CHANG H. 2015. Retinoic Acid Differentially Regulates the Migration of Innate Lymphoid Cell Subsets to the Gut. *Immunity,* 43**,** 107-119.

KIM, M. Y., ANDERSON, G., WHITE, A., JENKINSON, E., ARLT, W., MARTENSSON, I. L., ERLANDSSON, L. & LANE, P. J. 2005. OX40 ligand and CD30 ligand are expressed on adult but not neonatal CD4+CD3- inducer cells: evidence that IL-7 signals regulate CD30 ligand but not OX40 ligand expression. *J Immunol,* 174**,** 6686-91.

KIM, M. Y., GASPAL, F. M., WIGGETT, H. E., MCCONNELL, F. M., GULBRANSON-JUDGE, A., RAYKUNDALIA, C., WALKER, L. S., GOODALL, M. D. & LANE, P. J. 2003. CD4(+)CD3(-) accessory cells costimulate primed CD4 T cells through OX40 and CD30 at sites where T cells collaborate with B cells. *Immunity,* 18**,** 643-54.

KIM, M. Y., TOELLNER, K. M., WHITE, A., MCCONNELL, F. M., GASPAL, F. M., PARNELL, S. M., JENKINSON, E., ANDERSON, G. & LANE, P. J. 2006. Neonatal and adult CD4+ CD3- cells share similar gene expression profile, and neonatal cells up-regulate OX40 ligand in response to TL1A (TNFSF15). *J Immunol,* 177**,** 3074-81.

KLOSE, C. S., FLACH, M., MOHLE, L., ROGELL, L., HOYLER, T., EBERT, K., FABIUNKE, C., PFEIFER, D., SEXL, V., FONSECA-PEREIRA, D., DOMINGUES, R. G., VEIGA-FERNANDES, H., ARNOLD, S. J., BUSSLINGER, M., DUNAY, I. R., TANRIVER, Y. & DIEFENBACH, A. 2014. Differentiation of type 1 ILCs from a common progenitor to all helper-like innate lymphoid cell lineages. *Cell,* 157**,** 340-56.

KLOSE, C. S., KISS, E. A., SCHWIERZECK, V., EBERT, K., HOYLER, T., D'HARGUES, Y., GOPPERT, N., CROXFORD, A. L., WAISMAN, A., TANRIVER, Y. & DIEFENBACH, A. 2013. A T-bet gradient controls the fate and function of CCR6-RORgammat+ innate lymphoid cells. *Nature,* 494**,** 261-5.

KOOL, M., SOULLIÉ, T., VAN NIMWEGEN, M., WILLART, M. A. M., MUSKENS, F., JUNG, S., HOOGSTEDEN, H. C., HAMMAD, H. & LAMBRECHT, B. N. 2008. Alum adjuvant boosts adaptive immunity by inducing uric acid and activating inflammatory dendritic cells. *The Journal of Experimental Medicine,* 205**,** 869-882.

KORN, T., BETTELLI, E., OUKKA, M. & KUCHROO, V. K. 2009. IL-17 and Th17 Cells. *Annu Rev Immunol,* 27**,** 485-517.

KRAAL, G., SAMSOM, J. N. & MEBIUS, R. E. 2006. The importance of regional lymph nodes for mucosal tolerance. *Immunological Reviews,* 213**,** 119-130.

KURTS, C., ROBINSON, B. W. S. & KNOLLE, P. A. 2010. Cross-priming in health and disease. *Nat Rev Immunol,* 10**,** 403-414.

LANE, P. J. L., MCCONNELL, F. M., WITHERS, D., GASPAL, F., SAINI, M. & ANDERSON, G. 2009. Lymphoid tissue inducer cells: bridges between the ancient innate and the modern adaptive immune systems. *Mucosal Immunol,* 2**,** 472-477.

LANIER, L. L. 2013. Shades of grey [mdash] the blurring view of innate and adaptive immunity. *Nat Rev Immunol,* 13**,** 73-74.

LINDBLAD, E. B. 2004. Aluminium compounds for use in vaccines. *Immunol Cell Biol,* 82**,** 497-505.

LINK, A., VOGT, T. K., FAVRE, S., BRITSCHGI, M. R., ACHA-ORBEA, H., HINZ, B., CYSTER, J. G. & LUTHER, S. A. 2007. Fibroblastic reticular cells in lymph nodes regulate the homeostasis of naive T cells. *Nat Immunol,* 8**,** 1255-1265.

LISTON, A. & GRAY, D. H. D. 2014. Homeostatic control of regulatory T cell diversity. *Nat Rev Immunol,* 14**,** 154-165.

MA, C. S., DEENICK, E. K., BATTEN, M. & TANGYE, S. G. 2012. The origins, function, and regulation of T follicular helper cells. *J Exp Med,* 209**,** 1241-53.

MACKLEY, E. C., HOUSTON, S., MARRIOTT, C. L., HALFORD, E. E., LUCAS, B., CEROVIC, V., FILBEY, K. J., MAIZELS, R. M., HEPWORTH, M. R., SONNENBERG, G. F., MILLING, S.

& WITHERS, D. R. 2015. CCR7-dependent trafficking of RORγ+ ILCs creates a unique microenvironment within mucosal draining lymph nodes. *Nat Commun,* 6.
MADRENAS, J., CHAU, L. A., SMITH, J., BLUESTONE, J. A. & GERMAIN, R. N. 1997. The Efficiency of CD4 Recruitment to Ligand-engaged TCR Controls the Agonist/Partial Agonist Properties of Peptide–MHC Molecule Ligands. *The Journal of Experimental Medicine,* 185**,** 219-230.
MALHOTRA, D., FLETCHER, A. L., ASTARITA, J., LUKACS-KORNEK, V., TAYALIA, P., GONZALEZ, S. F., ELPEK, K. G., CHANG, S. K., KNOBLICH, K., HEMLER, M. E., BRENNER, M., CARROLL, M. C., MOONEY, D. J., TURLEY, S. J. & IMMUNOLOGICAL GENOME PROJECT, C. 2012. Transcriptional profiling of stroma from inflamed and resting lymph nodes defines immunological hallmarks. *Nature immunology,* 13**,** 499-510.
MARRIOTT, C. L., MACKLEY, E. C., FERREIRA, C., VELDHOEN, M., YAGITA, H. & WITHERS, D. R. 2014. OX40 controls effector CD4+ T-cell expansion, not follicular T helper cell generation in acute Listeria infection. *Eur J Immunol,* 44**,** 2437-47.
MCSORLEY, S. J., ASCH, S., COSTALONGA, M., REINHARDT, R. L. & JENKINS, M. K. 2002. Tracking Salmonella-Specific CD4 T Cells In Vivo Reveals a Local Mucosal Response to a Disseminated Infection. *Immunity,* 16**,** 365-377.
MEBIUS, R. E. 2003. Organogenesis of lymphoid tissues. *Nat Rev Immunol,* 3**,** 292-303.
MEBIUS, R. E., RENNERT, P. & WEISSMAN, I. L. 1997. Developing lymph nodes collect CD4+CD3- LTbeta+ cells that can differentiate to APC, NK cells, and follicular cells but not T or B cells. *Immunity,* 7**,** 493-504.
MIRCHANDANI, A. S., BESNARD, A. G., YIP, E., SCOTT, C., BAIN, C. C., CEROVIC, V., SALMOND, R. J. & LIEW, F. Y. 2014. Type 2 innate lymphoid cells drive CD4+ Th2 cell responses. *J Immunol,* 192**,** 2442-8.
MJOSBERG, J., BERNINK, J., GOLEBSKI, K., KARRICH, J. J., PETERS, C. P., BLOM, B., TE VELDE, A. A., FOKKENS, W. J., VAN DRUNEN, C. M. & SPITS, H. 2012. The transcription factor GATA3 is essential for the function of human type 2 innate lymphoid cells. *Immunity,* 37**,** 649-59.
MJOSBERG, J. M., TRIFARI, S., CRELLIN, N. K., PETERS, C. P., VAN DRUNEN, C. M., PIET, B., FOKKENS, W. J., CUPEDO, T. & SPITS, H. 2011. Human IL-25- and IL-33-responsive type 2 innate lymphoid cells are defined by expression of CRTH2 and CD161. *Nat Immunol,* 12**,** 1055-62.
MOGENSEN, T. H. 2009. Pathogen Recognition and Inflammatory Signaling in Innate Immune Defenses. *Clinical Microbiology Reviews,* 22**,** 240-273.
MOMBAERTS, P., IACOMINI, J., JOHNSON, R. S., HERRUP, K., TONEGAWA, S. & PAPAIOANNOU, V. E. 1992. RAG-1-deficient mice have no mature B and T lymphocytes. *Cell,* 68**,** 869-77.
MONKS, C. R., FREIBERG, B. A., KUPFER, H., SCIAKY, N. & KUPFER, A. 1998. Three-dimensional segregation of supramolecular activation clusters in T cells. *Nature,* 395**,** 82-6.
MONTICELLI, L. A., SONNENBERG, G. F., ABT, M. C., ALENGHAT, T., ZIEGLER, C. G., DOERING, T. A., ANGELOSANTO, J. M., LAIDLAW, B. J., YANG, C. Y., SATHALIYAWALA, T., KUBOTA, M., TURNER, D., DIAMOND, J. M., GOLDRATH, A. W., FARBER, D. L., COLLMAN, R. G., WHERRY, E. J. & ARTIS, D. 2011. Innate lymphoid cells promote lung-tissue homeostasis after infection with influenza virus. *Nat Immunol,* 12**,** 1045-54.

MORO, K., YAMADA, T., TANABE, M., TAKEUCHI, T., IKAWA, T., KAWAMOTO, H., FURUSAWA, J., OHTANI, M., FUJII, H. & KOYASU, S. 2010. Innate production of T(H)2 cytokines by adipose tissue-associated c-Kit(+)Sca-1(+) lymphoid cells. *Nature,* 463**,** 540-4.

MORTHA, A., CHUDNOVSKIY, A., HASHIMOTO, D., BOGUNOVIC, M., SPENCER, S. P., BELKAID, Y. & MERAD, M. 2014. Microbiota-dependent crosstalk between macrophages and ILC3 promotes intestinal homeostasis. *Science,* 343**,** 1249288.

MORTON, A. M., SEFIK, E., UPADHYAY, R., WEISSLEDER, R., BENOIST, C. & MATHIS, D. 2014. Endoscopic photoconversion reveals unexpectedly broad leukocyte trafficking to and from the gut. *Proceedings of the National Academy of Sciences,* 111**,** 6696-6701.

MOSMANN, T. R., CHERWINSKI, H., BOND, M. W., GIEDLIN, M. A. & COFFMAN, R. L. 1986. Two types of murine helper T cell clone. I. Definition according to profiles of lymphokine activities and secreted proteins. *The Journal of Immunology,* 136**,** 2348-57.

MUELLER, D. L., JENKINS, M. K. & SCHWARTZ, R. H. 1989. Clonal expansion versus functional clonal inactivation: a costimulatory signalling pathway determines the outcome of T cell antigen receptor occupancy. *Annu Rev Immunol,* 7**,** 445-80.

NEGISHI, I., MOTOYAMA, N., NAKAYAMA, K., NAKAYAMA, K., SENJU, S., HATAKEYAMA, S., ZHANG, Q., CHAN, A. C. & LOH, D. Y. 1995. Essential role for ZAP-70 in both positive and negative selection of thymocytes. *Nature,* 376**,** 435-8.

NEILL, D. R., WONG, S. H., BELLOSI, A., FLYNN, R. J., DALY, M., LANGFORD, T. K., BUCKS, C., KANE, C. M., FALLON, P. G., PANNELL, R., JOLIN, H. E. & MCKENZIE, A. N. 2010. Nuocytes represent a new innate effector leukocyte that mediates type-2 immunity. *Nature,* 464**,** 1367-70.

NISHANA, M. & RAGHAVAN, S. C. 2012. Role of recombination activating genes in the generation of antigen receptor diversity and beyond. *Immunology,* 137**,** 271-281.

OLIPHANT, CHRISTOPHER J., HWANG, YOU Y., WALKER, JENNIFER A., SALIMI, M., WONG, SEE H., BREWER, JAMES M., ENGLEZAKIS, A., BARLOW, JILLIAN L., HAMS, E., SCANLON, SETH T., OGG, GRAHAM S., FALLON, PADRAIC G. & MCKENZIE, ANDREW N. J. 2014. MHCII-Mediated Dialog between Group 2 Innate Lymphoid Cells and CD4+ T Cells Potentiates Type 2 Immunity and Promotes Parasitic Helminth Expulsion. *Immunity,* 41**,** 283-295.

ONDER, L., NARANG, P., SCANDELLA, E., CHAI, Q., IOLYEVA, M., HOORWEG, K., HALIN, C., RICHIE, E., KAYE, P., WESTERMANN, J., CUPEDO, T., COLES, M. & LUDEWIG, B. 2012. IL-7–producing stromal cells are critical for lymph node remodeling. *Blood,* 120**,** 4675-4683.

PABST, O., BERNHARDT, G. & FORSTER, R. 2007. The impact of cell-bound antigen transport on mucosal tolerance induction. *J Leukoc Biol,* 82**,** 795-800.

PABST, O. & MOWAT, A. M. 2012. Oral tolerance to food protein. *Mucosal Immunol,* 5**,** 232-239.

PANTELYUSHIN, S., HAAK, S., INGOLD, B., KULIG, P., HEPPNER, F. L., NAVARINI, A. A. & BECHER, B. 2012. Rorgammat+ innate lymphocytes and gammadelta T cells initiate psoriasiform plaque formation in mice. *J Clin Invest,* 122**,** 2252-6.

PARK, H., LI, Z., YANG, X. O., CHANG, S. H., NURIEVA, R., WANG, Y.-H., WANG, Y., HOOD, L., ZHU, Z., TIAN, Q. & DONG, C. 2005. A distinct lineage of CD4 T cells regulates tissue inflammation by producing interleukin 17. *Nat Immunol,* 6**,** 1133-1141.

PARK, J. H., YU, Q., ERMAN, B., APPELBAUM, J. S., MONTOYA-DURANGO, D., GRIMES, H. L. & SINGER, A. 2004. Suppression of IL7Ralpha transcription by IL-7 and other prosurvival cytokines: a novel mechanism for maximizing IL-7-dependent T cell survival. *Immunity,* 21**,** 289-302.

PETERSON, L. W. & ARTIS, D. 2014. Intestinal epithelial cells: regulators of barrier function and immune homeostasis. *Nat Rev Immunol,* 14**,** 141-53.

PICO, J.-L., AVILA-GARAVITO, A. & NACCACHE, P. 1998. Mucositis: Its Occurrence, Consequences, and Treatment in the Oncology Setting. *The Oncologist,* 3**,** 446-451.

PRICE, A. E., LIANG, H. E., SULLIVAN, B. M., REINHARDT, R. L., EISLEY, C. J., ERLE, D. J. & LOCKSLEY, R. M. 2010. Systemically dispersed innate IL-13-expressing cells in type 2 immunity. *Proc Natl Acad Sci U S A,* 107**,** 11489-94.

RANDOLPH, G. J., ANGELI, V. & SWARTZ, M. A. 2005. Dendritic-cell trafficking to lymph nodes through lymphatic vessels. *Nat Rev Immunol,* 5**,** 617-628.

REIF, K., EKLAND, E. H., OHL, L., NAKANO, H., LIPP, M., FORSTER, R. & CYSTER, J. G. 2002. Balanced responsiveness to chemoattractants from adjacent zones determines B-cell position. *Nature,* 416**,** 94-99.

ROEDIGER, B., KYLE, R., YIP, K. H., SUMARIA, N., GUY, T. V., KIM, B. S., MITCHELL, A. J., TAY, S. S., JAIN, R., FORBES-BLOM, E., CHEN, X., TONG, P. L., BOLTON, H. A., ARTIS, D., PAUL, W. E., DE ST GROTH, B. F., GRIMBALDESTON, M. A., LE GROS, G. & WENINGER, W. 2013. Cutaneous immunosurveillance and regulation of inflammation by group 2 innate lymphoid cells. *Nat Immunol,* 14**,** 564-573.

ROSSI, S. W., KIM, M. Y., LEIBBRANDT, A., PARNELL, S. M., JENKINSON, W. E., GLANVILLE, S. H., MCCONNELL, F. M., SCOTT, H. S., PENNINGER, J. M., JENKINSON, E. J., LANE, P. J. & ANDERSON, G. 2007. RANK signals from CD4(+)3(-) inducer cells regulate development of Aire-expressing epithelial cells in the thymic medulla. *J Exp Med,* 204**,** 1267-72.

SALIMI, M., BARLOW, J. L., SAUNDERS, S. P., XUE, L., GUTOWSKA-OWSIAK, D., WANG, X., HUANG, L.-C., JOHNSON, D., SCANLON, S. T., MCKENZIE, A. N. J., FALLON, P. G. & OGG, G. S. 2013. A role for IL-25 and IL-33–driven type-2 innate lymphoid cells in atopic dermatitis. *The Journal of Experimental Medicine,* 210**,** 2939-2950.

SALLUSTO, F. & LANZAVECCHIA, A. 1999. Mobilizing Dendritic Cells for Tolerance, Priming, and Chronic Inflammation. *The Journal of Experimental Medicine,* 189**,** 611-614.

SALLUSTO, F., SCHAERLI, P., LOETSCHER, P., SCHANIEL, C., LENIG, D., MACKAY, C. R., QIN, S. & LANZAVECCHIA, A. 1998. Rapid and coordinated switch in chemokine receptor expression during dendritic cell maturation. *Eur J Immunol,* 28**,** 2760-9.

SANOS, S. L., BUI, V. L., MORTHA, A., OBERLE, K., HENERS, C., JOHNER, C. & DIEFENBACH, A. 2009. RORgammat and commensal microflora are required for the differentiation of mucosal interleukin 22-producing NKp46+ cells. *Nat Immunol,* 10**,** 83-91.

SATOH-TAKAYAMA, N., LESJEAN-POTTIER, S., VIEIRA, P., SAWA, S., EBERL, G., VOSSHENRICH, C. A. & DI SANTO, J. P. 2010. IL-7 and IL-15 independently program the differentiation of intestinal CD3-NKp46+ cell subsets from Id2-dependent precursors. *J Exp Med,* 207**,** 273-80.

SCANDELLA, E., BOLINGER, B., LATTMANN, E., MILLER, S., FAVRE, S., LITTMAN, D. R., FINKE, D., LUTHER, S. A., JUNT, T. & LUDEWIG, B. 2008. Restoration of lymphoid

organ integrity through the interaction of lymphoid tissue-inducer cells with stroma of the T cell zone. *Nat Immunol,* 9**,** 667-675.

SCHMUTZ, S., BOSCO, N., CHAPPAZ, S., BOYMAN, O., ACHA-ORBEA, H., CEREDIG, R., ROLINK, A. G. & FINKE, D. 2009. Cutting Edge: IL-7 Regulates the Peripheral Pool of Adult RORγ+ Lymphoid Tissue Inducer Cells. *The Journal of Immunology,* 183**,** 2217-2221.

SCHWARTZ, R. H. 2003. T cell anergy. *Annu Rev Immunol,* 21**,** 305-34.

SCIUME, G., HIRAHARA, K., TAKAHASHI, H., LAURENCE, A., VILLARINO, A. V., SINGLETON, K. L., SPENCER, S. P., WILHELM, C., POHOLEK, A. C., VAHEDI, G., KANNO, Y., BELKAID, Y. & O'SHEA, J. J. 2012. Distinct requirements for T-bet in gut innate lymphoid cells. *J Exp Med,* 209**,** 2331-8.

SERAFINI, N., KLEIN WOLTERINK, R. G., SATOH-TAKAYAMA, N., XU, W., VOSSHENRICH, C. A., HENDRIKS, R. W. & DI SANTO, J. P. 2014. Gata3 drives development of RORgammat+ group 3 innate lymphoid cells. *J Exp Med,* 211**,** 199-208.

SONNENBERG, G. F., MONTICELLI, L. A., ALENGHAT, T., FUNG, T. C., HUTNICK, N. A., KUNISAWA, J., SHIBATA, N., GRUNBERG, S., SINHA, R., ZAHM, A. M., TARDIF, M. R., SATHALIYAWALA, T., KUBOTA, M., FARBER, D. L., COLLMAN, R. G., SHAKED, A., FOUSER, L. A., WEINER, D. B., TESSIER, P. A., FRIEDMAN, J. R., KIYONO, H., BUSHMAN, F. D., CHANG, K. M. & ARTIS, D. 2012. Innate lymphoid cells promote anatomical containment of lymphoid-resident commensal bacteria. *Science,* 336**,** 1321-5.

SONNENBERG, G. F., MONTICELLI, L. A., ELLOSO, M. M., FOUSER, L. A. & ARTIS, D. 2011. CD4(+) lymphoid tissue-inducer cells promote innate immunity in the gut. *Immunity,* 34**,** 122-34.

SPAHN, T. W., WEINER, H. L., RENNERT, P. D., LUGERING, N., FONTANA, A., DOMSCHKE, W. & KUCHARZIK, T. 2002. Mesenteric lymph nodes are critical for the induction of high-dose oral tolerance in the absence of Peyer's patches. *Eur J Immunol,* 32**,** 1109-13.

SPENCER, S. P., WILHELM, C., YANG, Q., HALL, J. A., BOULADOUX, N., BOYD, A., NUTMAN, T. B., URBAN, J. F., WANG, J., RAMALINGAM, T. R., BHANDOOLA, A., WYNN, T. A. & BELKAID, Y. 2014. Adaptation of Innate Lymphoid Cells to a Micronutrient Deficiency Promotes Type 2 Barrier Immunity. *Science,* 343**,** 432-437.

SPITS, H., ARTIS, D., COLONNA, M., DIEFENBACH, A., DI SANTO, J. P., EBERL, G., KOYASU, S., LOCKSLEY, R. M., MCKENZIE, A. N., MEBIUS, R. E., POWRIE, F. & VIVIER, E. 2013. Innate lymphoid cells--a proposal for uniform nomenclature. *Nat Rev Immunol,* 13**,** 145-9.

SPRENT, J. 1997. Immunological memory. *Curr Opin Immunol,* 9**,** 371-9.

SUN, Z., UNUTMAZ, D., ZOU, Y.-R., SUNSHINE, M. J., PIERANI, A., BRENNER-MORTON, S., MEBIUS, R. E. & LITTMAN, D. R. 2000. Requirement for RORγ in Thymocyte Survival and Lymphoid Organ Development. *Science,* 288**,** 2369-2373.

SWAIN, S. L., HU, H. & HUSTON, G. 1999. Class II-Independent Generation of CD4 Memory T Cells from Effectors. *Science,* 286**,** 1381-1383.

SZABO, S. J., KIM, S. T., COSTA, G. L., ZHANG, X., FATHMAN, C. G. & GLIMCHER, L. H. 2000. A novel transcription factor, T-bet, directs Th1 lineage commitment. *Cell,* 100**,** 655-69.

TAUBE, C., TERTILT, C., GYULVESZI, G., DEHZAD, N., KREYMBORG, K., SCHNEEWEISS, K., MICHEL, E., REUTER, S., RENAULD, J. C., ARNOLD-SCHILD, D., SCHILD, H., BUHL, R.

& BECHER, B. 2011. IL-22 is produced by innate lymphoid cells and limits inflammation in allergic airway disease. *PLoS One,* 6**,** e21799.

TOMURA, M., HATA, A., MATSUOKA, S., SHAND, F. H. W., NAKANISHI, Y., IKEBUCHI, R., UEHA, S., TSUTSUI, H., INABA, K., MATSUSHIMA, K., MIYAWAKI, A., KABASHIMA, K., WATANABE, T. & KANAGAWA, O. 2014. Tracking and quantification of dendritic cell migration and antigen trafficking between the skin and lymph nodes. *Scientific Reports,* 4**,** 6030.

UENO, T., SAITO, F., GRAY, D. H. D., KUSE, S., HIESHIMA, K., NAKANO, H., KAKIUCHI, T., LIPP, M., BOYD, R. L. & TAKAHAMA, Y. 2004. CCR7 Signals Are Essential for Cortex–Medulla Migration of Developing Thymocytes. *The Journal of Experimental Medicine,* 200**,** 493-505.

UMETSU, D. T., JABARA, H. H., DEKRUYFF, R. H., ABBAS, A. K., ABRAMS, J. S. & GEHA, R. S. 1988. Functional heterogeneity among human inducer T cell clones. *J Immunol,* 140**,** 4211-6.

VAN DER SLUIS, M., DE KONING, B. A., DE BRUIJN, A. C., VELCICH, A., MEIJERINK, J. P., VAN GOUDOEVER, J. B., BULLER, H. A., DEKKER, J., VAN SEUNINGEN, I., RENES, I. B. & EINERHAND, A. W. 2006. Muc2-deficient mice spontaneously develop colitis, indicating that MUC2 is critical for colonic protection. *Gastroenterology,* 131**,** 117-29.

VILLADANGOS, J. A. & SCHNORRER, P. 2007. Intrinsic and cooperative antigen-presenting functions of dendritic-cell subsets in vivo. *Nat Rev Immunol,* 7**,** 543-555.

VILLANOVA, F., FLUTTER, B., TOSI, I., GRYS, K., SREENEEBUS, H., PERERA, G. K., CHAPMAN, A., SMITH, C. H., DI MEGLIO, P. & NESTLE, F. O. 2014. Characterization of Innate Lymphoid Cells in Human Skin and Blood Demonstrates Increase of NKp44+ ILC3 in Psoriasis. *J Invest Dermatol,* 134**,** 984-991.

VINUESA, C. G., TANGYE, S. G., MOSER, B. & MACKAY, C. R. 2005. Follicular B helper T cells in antibody responses and autoimmunity. *Nat Rev Immunol,* 5**,** 853-65.

VON ANDRIAN, U. H. & MEMPEL, T. R. 2003. Homing and cellular traffic in lymph nodes. *Nat Rev Immunol,* 3**,** 867-878.

VON BURG, N., CHAPPAZ, S., BAERENWALDT, A., HORVATH, E., BOSE DASGUPTA, S., ASHOK, D., PIETERS, J., TACCHINI-COTTIER, F., ROLINK, A., ACHA-ORBEA, H. & FINKE, D. 2014. Activated group 3 innate lymphoid cells promote T-cell–mediated immune responses. *Proceedings of the National Academy of Sciences,* 111**,** 12835-12840.

VONARBOURG, C. & DIEFENBACH, A. 2012. Multifaceted roles of interleukin-7 signaling for the development and function of innate lymphoid cells. *Seminars in Immunology,* 24**,** 165-174.

VONARBOURG, C., MORTHA, A., BUI, V. L., HERNANDEZ, P. P., KISS, E. A., HOYLER, T., FLACH, M., BENGSCH, B., THIMME, R., HOLSCHER, C., HONIG, M., PANNICKE, U., SCHWARZ, K., WARE, C. F., FINKE, D. & DIEFENBACH, A. 2010. Regulated expression of nuclear receptor RORgammat confers distinct functional fates to NK cell receptor-expressing RORgammat(+) innate lymphocytes. *Immunity,* 33**,** 736-51.

VYAS, J. M., VAN DER VEEN, A. G. & PLOEGH, H. L. 2008. The known unknowns of antigen processing and presentation. *Nat Rev Immunol,* 8**,** 607-618.

WALKER, J. A., BARLOW, J. L. & MCKENZIE, A. N. 2013. Innate lymphoid cells--how did we miss them? *Nat Rev Immunol,* 13**,** 75-87.

WALKER, J. A. & MCKENZIE, A. N. J. 2013. Development and function of group 2 innate lymphoid cells. *Current Opinion in Immunology,* 25**,** 148-155.

WALKER, L. S. K. & ABBAS, A. K. 2002. The enemy within: keeping self-reactive T cells at bay in the periphery. *Nat Rev Immunol,* 2**,** 11-19.

WALSH, K. P. & MILLS, K. H. G. 2013. Dendritic cells and other innate determinants of T helper cell polarisation. *Trends in Immunology,* 34**,** 521-530.

WILLARD-MACK, C. L. 2006. Normal structure, function, and histology of lymph nodes. *Toxicol Pathol,* 34**,** 409-24.

WITHERS, D. R., GASPAL, F. M., MACKLEY, E. C., MARRIOTT, C. L., ROSS, E. A., DESANTI, G. E., ROBERTS, N. A., WHITE, A. J., FLORES-LANGARICA, A., MCCONNELL, F. M., ANDERSON, G. & LANE, P. J. L. 2012. Cutting Edge: Lymphoid Tissue Inducer Cells Maintain Memory CD4 T Cells within Secondary Lymphoid Tissue. *The Journal of Immunology,* 189**,** 2094-2098.

WOLTERINK, R. G. J. K., KLEINJAN, A., VAN NIMWEGEN, M., BERGEN, I., DE BRUIJN, M., LEVANI, Y. & HENDRIKS, R. W. 2012. Pulmonary innate lymphoid cells are major producers of IL-5 and IL-13 in murine models of allergic asthma. *European Journal of Immunology,* 42**,** 1106-1116.

WORBS, T., BODE, U., YAN, S., HOFFMANN, M. W., HINTZEN, G., BERNHARDT, G., FÖRSTER, R. & PABST, O. 2006. Oral tolerance originates in the intestinal immune system and relies on antigen carriage by dendritic cells. *The Journal of Experimental Medicine,* 203**,** 519-527.

WORBS, T., MEMPEL, T. R., BOLTER, J., VON ANDRIAN, U. H. & FORSTER, R. 2007. CCR7 ligands stimulate the intranodal motility of T lymphocytes in vivo. *J Exp Med,* 204**,** 489-95.

WUCHERPFENNIG, K. W., GAGNON, E., CALL, M. J., HUSEBY, E. S. & CALL, M. E. 2010. Structural Biology of the T-cell Receptor: Insights into Receptor Assembly, Ligand Recognition, and Initiation of Signaling. *Cold Spring Harbor Perspectives in Biology,* 2**,** a005140.

YAGI, R., ZHONG, C., NORTHRUP, D. L., YU, F., BOULADOUX, N., SPENCER, S., HU, G., BARRON, L., SHARMA, S., NAKAYAMA, T., BELKAID, Y., ZHAO, K. & ZHU, J. 2014. The transcription factor GATA3 is critical for the development of all IL-7Ralpha-expressing innate lymphoid cells. *Immunity,* 40**,** 378-88.

YANG, B. H., HAGEMANN, S., MAMARELI, P., LAUER, U., HOFFMANN, U., BECKSTETTE, M., FOHSE, L., PRINZ, I., PEZOLDT, J., SUERBAUM, S., SPARWASSER, T., HAMANN, A., FLOESS, S., HUEHN, J. & LOCHNER, M. 2015. Foxp3+ T cells expressing ROR[gamma]t represent a stable regulatory T-cell effector lineage with enhanced suppressive capacity during intestinal inflammation. *Mucosal Immunol*.

YOKOTA, Y., MANSOURI, A., MORI, S., SUGAWARA, S., ADACHI, S., NISHIKAWA, S. & GRUSS, P. 1999. Development of peripheral lymphoid organs and natural killer cells depends on the helix-loop-helix inhibitor Id2. *Nature,* 397**,** 702-6.

ZHENG, Y., VALDEZ, P. A., DANILENKO, D. M., HU, Y., SA, S. M., GONG, Q., ABBAS, A. R., MODRUSAN, Z., GHILARDI, N., DE SAUVAGE, F. J. & OUYANG, W. 2008. Interleukin-22 mediates early host defense against attaching and effacing bacterial pathogens. *Nat Med,* 14**,** 282-289.

ZHU, J., MIN, B., HU-LI, J., WATSON, C. J., GRINBERG, A., WANG, Q., KILLEEN, N., URBAN, J. F., JR., GUO, L. & PAUL, W. E. 2004. Conditional deletion of Gata3 shows its essential function in T(H)1-T(H)2 responses. *Nat Immunol,* 5**,** 1157-65.

ZHU, J., YAMANE, H. & PAUL, W. E. 2010. Differentiation of Effector CD4 T Cell Populations. *Annual Review of Immunology,* 28**,** 445-489.

ZINKERNAGEL, R. M. & DOHERTY, P. C. 1974. Restriction of in vitro T cell-mediated cytotoxicity in lymphocytic choriomeningitis within a syngeneic or semiallogeneic system. *Nature,* 248**,** 701-702.